

2007

Removal of natural organic matter through employment of anion exchange fibers impregnated with hydrous ferric and zirconium oxide nanoparticles towards reduction of disinfection by-product formation potential in water treatment

Lee Michael Blaney
Lehigh University

Follow this and additional works at: <http://preserve.lehigh.edu/etd>

Recommended Citation

Blaney, Lee Michael, "Removal of natural organic matter through employment of anion exchange fibers impregnated with hydrous ferric and zirconium oxide nanoparticles towards reduction of disinfection by-product formation potential in water treatment" (2007). *Theses and Dissertations*. Paper 967.

This Thesis is brought to you for free and open access by Lehigh Preserve. It has been accepted for inclusion in Theses and Dissertations by an authorized administrator of Lehigh Preserve. For more information, please contact preserve@lehigh.edu.

Blaney, Lee
Michael

Removal of Natural
Organic Matter
through
Employment of
Anion Exchange...

May 2007

Removal of Natural Organic Matter through Employment of Anion Exchange Fibers
Impregnated with Hydrous Ferric and Zirconium Oxide Nanoparticles towards Reduction
of Disinfection By-Product Formation Potential in Water Treatment

by

Lee Michael Blaney

A Thesis

Presented to the Graduate and Research Committee

of Lehigh University

in Candidacy for the Degree of

Master of Science

in

Civil and Environmental Engineering

Lehigh University

May, 2007

This thesis is accepted and approved in partial fulfillment of the requirements for
the Master of Science.

April 23, 2007

Date

~~Thesis~~ Advisor

Chairperson of Department

ACKNOWLEDGEMENTS

First of all, my most sincere thanks and gratitude go to Dr. Arup SenGupta, who has provided me with so many remarkable opportunities. His guidance has instigated my success on so many levels and I greatly appreciate his support and influence.

Next, I would like to acknowledge my mother. This woman is undoubtedly the strongest person I have ever met, and I want to thank her for role model and example.

Special thanks go out to my father, brothers (Dan and Jim), and grandfather, who have always been there to support and encourage me, while making life extremely funny.

Huge “thank you”s go out to John Greenleaf, Sudipta Sarkar, Pavan Puttamraju, Ping Li, Prakhar Prakash, Prasun Chatterjee, Jin Cheng Lin, Luis Cumbal, and Suna Cinar. You all have made my life so much funnier and more enjoyable; furthermore, you have always been excellent sources of knowledge, understanding, and guidance. I will miss you guys a lot

As they had to put up with me over many years, I also owe a large amount of thanks to other environmental engineering students including the following: Joe Ziemann, Sean Eggleston, Minna Kim, Paul DeSario, Shweta Tripathi, Alon Abramson, Carol Crewdson, Jackie Lanzon, Seth Donrovich, and Rene Waterman (RIP).

Thank you to the following Lehigh CEE faculty for their constant help and patience: Drs. Lennon, Wilson, Brown, Jellison, Zhang, and Pamukcu.

Finally, I would like to thank Prisca Vidanage and Cathy Miller for their enormous amount of help over the last six years and especially for all of the candy.

TABLE OF CONTENTS

<i>Section</i>	<i>Description</i>	<i>Page</i>
i	Cover.....	i
ii	Thesis Signature Sheet.....	ii
iii	Acknowledgements.....	iii
iv	Table of Contents.....	iv
v	List of Tables.....	x
vi	List of Figures.....	xii
vii	List of Acronyms/Variables.....	xvii
0.0	THESIS ABSTRACT.....	1
1.0	CHAPTER 1: INTRODUCTION.....	3
1.1	Chemistry of Natural Organic Matter.....	3
1.2	Disinfection By-Products: Compounds, Effects, Regulations.....	5
1.2.1	Disinfection By-Product Formation.....	7
1.2.2	Types of Disinfection By-Products.....	8
1.2.3	Disinfection By-Product Regulations.....	11
1.2.3.1	EPA DBPR Stage 1 Rule.....	12
1.2.3.2	EPA DBPR Stage 2 Rule.....	14
1.3	Existing Technologies for NOM Removal.....	15
1.3.1	Nonionic Macroporous Resin.....	16
1.3.2	Iron Oxides.....	17
1.3.3	Aluminum Oxides/Silicates.....	18

TABLE OF CONTENTS (cont.)

<i>Section</i>	<i>Description</i>	<i>Page</i>
1.3.4	Magnetic Ion Exchange Resin (MIEX®).....	20
1.3.5	Enhanced Coagulation.....	22
1.3.6	Other Methods.....	22
1.3.7	Summary.....	23
1.4	Towards NOM Selective Sorbent Media.....	24
1.4.1	Ferric Oxides.....	24
1.4.2	Hybrid Ion Exchanger History.....	24
1.4.2.1	Lewis Acid-Base Interaction.....	28
1.4.3	The Next Evolution.....	29
1.4.4	Application of HAIX-F Technology.....	32
1.5	Chemistry of HAIX-F and Experimental Organic Compounds.....	34
1.6	Study Objectives.....	37
2.0	CHAPTER 2: EXPERIMENTAL MATERIALS AND METHODS.....	39
2.1	Chemicals.....	39
2.2	HAIX-F Synthesis.....	40
2.2.1	HAIX-F Synthesis Protocol.....	41
2.2.1.1	HAIX-F(Fe) Synthesis Protocol.....	41
2.2.1.2	HAIX-F(Zr) Synthesis Protocol.....	42
2.2.2	Description of HAIX-F Media.....	43
2.3	Batch Studies.....	44
2.4	Column Studies.....	45

TABLE OF CONTENTS (cont.)

<i>Section</i>	<i>Description</i>	<i>Page</i>
2.4.1	Testing Protocol.....	47
2.5	Kinetic Tests.....	48
2.6	Analytical Equipment.....	51
2.6.1	Shimadzu TC/TOC Analyzer.....	52
2.6.1.1	General TOC Analyzer Protocol.....	53
2.6.2	Perkin Elmer Ion Chromatograph.....	53
2.6.2.1	General Ion Chromatograph Protocol.....	54
2.6.3	UV/VIS Spectrometer.....	55
2.6.3.1	General UV/VIS Spectrometer Protocol.....	56
3.0	CHAPTER 3: RESULTS.....	58
3.1	Initial Batch Experiments.....	58
3.2	Initial Column Experiments.....	63
3.2.1	HAIX-F(Fe) Column Run with Dilute NOM Brine.....	63
3.2.2	HAIX-F(Fe) Column Run with Oxalate Anion.....	65
3.3	Photo-oxidation Studies.....	67
3.3.1	Results from IC Analysis.....	67
3.3.2	Results from TOC Analysis.....	69
3.4	Fixed-Bed Column Experimentation with HAIX-F Media.....	70
3.4.1	Column Runs using HAIX-F(Fe).....	74
3.4.1.1	Fixed-Bed HAIX-F(Fe) Oxalate Treatment.....	74
3.4.1.2	Fixed-Bed HAIX-F(Fe) Phthalate Treatment.....	76

TABLE OF CONTENTS (cont.)

<i>Section</i>	<i>Description</i>	<i>Page</i>
3.4.1.3	Fixed-Bed HAIX-F(Fe) NOM Treatment.....	78
3.4.2	Column Runs using HAIX-F(Zr).....	79
3.4.2.1	Fixed-Bed HAIX-F(Zr) Oxalate Treatment.....	79
3.4.2.2	Fixed-Bed HAIX-F(Zr) Phthalate Treatment.....	81
3.4.2.3	Fixed-Bed HAIX-F(Zr) NOM Treatment.....	83
3.4.3	Comparison of HAIX-F(Fe) and HAIX-F(Zr).....	85
3.4.3.1	Comparison of Fixed-Bed HAIX-F Oxalate Removal Experiments.....	85
3.4.3.2	Comparison of Fixed-Bed HAIX-F Phthalate Removal Experiments.....	87
3.4.3.3	Comparison of Fixed-Bed HAIX-F NOM Removal Experiments.....	89
3.5	Kinetic Tests with HAIX-F Media.....	89
3.5.1	Kinetic Tests Employing HAIX-F(Fe).....	94
3.5.1.1	Oxalate Kinetic Test with HAIX-F(Fe).....	95
3.5.1.2	Phthalate Kinetic Test with HAIX-F(Fe).....	97
3.5.1.3	NOM Kinetic Test with HAIX-F(Fe).....	100
3.5.2	Kinetic Tests Employing HAIX-F(Zr).....	103
3.5.2.1	Oxalate Kinetic Test with HAIX-F(Zr).....	103
3.5.2.2	Phthalate Kinetic Test with HAIX-F(Zr).....	106
3.5.2.3	NOM Kinetic Test with HAIX-F(Zr).....	108
3.5.3	Comparison of Kinetic Tests Employing HAIX-F Media.....	111
3.5.3.1	Kinetics Test Comparisons for Oxalate Removal.....	112
3.5.3.2	Kinetics Test Comparisons for Phthalate Removal.....	114
3.5.3.3	Kinetics Test Comparisons for NOM Removal.....	116

TABLE OF CONTENTS (cont.)

<i>Section</i>	<i>Description</i>	<i>Page</i>
3.6	Regeneration of HAIX-F Media in Fixed-Bed Configuration.....	117
3.6.1	Regeneration of HAIX-F(Fe) Media.....	120
3.6.1.1	Regeneration of HAIX-F(Fe) Laden with Oxalate.....	121
3.6.1.2	Regeneration of HAIX-F(Fe) Laden with Phthalate.....	122
3.6.2	Regeneration of HAIX-F(Zr) Media.....	123
3.6.2.1	Regeneration of HAIX-F(Zr) Laden with Oxalate.....	124
3.6.2.2	Regeneration of HAIX-F(Zr) Laden with Phthalate.....	124
3.6.3	Comparison of Regeneration History for HAIX-F Media.....	125
3.6.3.1	Comparison of Oxalate Regeneration Runs.....	126
3.6.3.2	Comparison of Phthalate Regeneration Runs.....	127
3.7	Alternative Analysis of TOC Concentration Data.....	128
3.7.1	Ion Chromatography.....	129
3.7.2	UV/VIS Spectrometry.....	131
3.8	Modeling HAIX-F abilities for Water Treatment Facilities.....	132
4.0	CHAPTER 4: DISCUSSION.....	135
4.1	Sorption Affinity and Mechanisms.....	135
4.2	Sorption Capabilities and Effect of Donnan Co-Ion Exclusion.....	142
4.3	Enhanced Sorption Kinetics Due to Ion Exchange Support.....	147
4.4	Applicability for WTP Introduction: Regenerability.....	151
4.5	Understanding NOM Sorption.....	152
4.6	Cyclical HAIX-F Employment Process.....	154

TABLE OF CONTENTS (cont.)

<i>Section</i>	<i>Description</i>	<i>Page</i>
5.0	CHAPTER 5: CONCLUSIONS.....	158
5.1	Review of Information Contained in Previous Chapters.....	158
5.2	Conclusions on HAIX-F Ability to Remove NOM.....	159
6.0	CHAPTER 6: WORKS CITED.....	162
7.0	APPENDIX A: Disinfection By-products.....	185
8.0	APPENDIX B: Determination of Effective Diffusivity.....	188
9.0	VITA.....	194

LIST OF TABLES

<i>Number</i>	<i>Description</i>	<i>Page</i>
CHAPTER 1: INTRODUCTION		
1.1	Stage 1 D/DBP Regulatory Limits on Disinfectant Residual..... and DBP Presence	13
1.2	Stage 1 D/DBP Regulatory Limits on TOC Concentrations.....	14
1.3	Salient Properties of FIBAN A-1 Anion Exchange Fibers.....	31
1.4	Oxalate and Phthalate Speciation Data, Predominant Species,..... and Sorption Interaction Possibilities	37
CHAPTER 2: EXPERIMENTAL MATERIALS AND METHODS		
2.1	Specific Loading of Fe(III) and Zr(IV) onto HAIX-F Media.....	43
CHAPTER 3: RESULTS		
3.1	Results of Batch Tests with Oxalate.....	62
3.2	Batch Test Results with Competing Phthalate and Oxalate Species.....	62
3.3	Total and Breakthrough Capacity of HAIX-F Media for Oxalate.....	86
3.4	Total and Breakthrough Capacity of HAIX-F Media for Phthalate.....	89
3.5	Liquid Diffusivity of Oxalate and Phthalate.....	90
3.6	Effective Diffusivities of Oxalate and Phthalate for HAIX-F Media.....	112
3.7	Time (minutes) Until Specified Fractional Oxalate Uptake Capacity.....	114
3.8	Time (minutes) Until Specified Fractional Phthalate Uptake Capacity.....	115
3.9	Time (BV) Until Specified Regeneration Efficiency.....	128

LIST OF TABLES (cont.)

<i>Number</i>	<i>Description</i>	<i>Page</i>
---------------	--------------------	-------------

CHAPTER 4: DISCUSSION

4.1	Relevant Properties for Chloride/Sulfate Ion Exchange Affinity.....	136
4.2	Sorption/Desorption Mechanisms for Oxalate onto HAIX-F(Fe).....	141
4.3	Sorption/Desorption Mechanisms for Phthalate onto HAIX-F(Zr).....	142
4.4	Computer-Based Model Input/Output Streams.....	157

LIST OF FIGURES

<i>Number</i>	<i>Description</i>	<i>Page</i>
CHAPTER 1: INTRODUCTION		
1.1	Chemical Structure of Fulvic Acid.....	4
1.2	DBP Appearance and Prevalence in a Typical WTP.....	8
1.3	Possible Dichloroacetic Acid Formation Reactions.....	10
1.4	Lewis Acid-Base Interaction: Phosphate Acts as a Lewis Base,..... while Iron Oxide Surface Functional Groups Behave like Lewis Acids	18
1.5	MIEX [®] Sorption/Regeneration Mechanisms.....	21
1.6	Illustration of pH-Dependent HFO Surface Functionality.....	27
1.7	Schematic Showing Major Components and Sorptive Abilities..... of HAIX Resin	28
1.8	Lewis Acid-Base Interaction Defined via FMO Theory.....	29
1.9	Schematic Showing Concentration Gradient in HAIX Resin..... and HAIX-F Fibrous Media	30
1.10	(a) FIBAN A-1 fibers impregnated with hydrous ferric oxide..... nanoparticulates (b) FIBAN A-1 fibers loaded with hydrous zirconium oxide nanoparticulates	32
1.11	Illustration of pH-Dependent HZO Surface Functionality.....	34
1.12	Illustration of pH-Dependent Oxalate Speciation.....	35
1.13	Illustration of pH-Dependent Phthalate Speciation.....	36
1.14	Oxalate Sorption Mechanisms onto HFO Surfaces.....	36

LIST OF FIGURES (cont.)

<i>Number</i>	<i>Description</i>	<i>Page</i>
CHAPTER 2: EXPERIMENTAL MATERIALS AND METHODS		
2.1	(a) FIBAN A-1 Anion Exchange Fibers at 2000× Magnification.....	41
	(b) FIBAN A-1 Anion Exchange Fibers at 20,000× Magnification	
2.2	(a) HAIX-F(Fe) at 2000× Magnification	43
	(b) HAIX-F(Fe) at 20,000× Magnification	
2.3	Rotating Chamber for Batch Experiments	44
2.4	(a) Schematic of Fixed-Bed Column Set-Up	46
	(b) Labeled Photograph of Fixed-Bed Column Set-Up	
2.5	Schematic of Kinetic Test Set-Up.....	48
2.6	Detailed Illustration of Stirrer Assembly.....	49
2.7	Labeled Photograph of Kinetic Test Equipment.....	51
2.8	Labeled Photograph of Shimadzu TC/TOC Analyzer.....	52
2.9	Labeled Photograph of Perkin Elmer Ion Chromatograph.....	54
2.10	UV/VIS Spectrometer Analytical Equipment and Plotter.....	56
CHAPTER 3: RESULTS		
3.1	Results of Batch Tests with Diluted NOM Brine.....	59
3.2	Fulvic Acid Molecular Schematic Labeled with Reactive Sites.....	60
3.3	Arsenate and Phosphate Interaction with HFO Sorption Sites.....	61
3.4	NOM Effluent History from Fixed-Bed Column Experimentation.....	63
3.5	Various NOM Fractions and Behavior in Water Treatment Processes.....	64

LIST OF FIGURES (cont.)

<i>Number</i>	<i>Description</i>	<i>Page</i>
3.6	Oxalate Effluent History for Initial Column Run with HAIX-F(Fe).....	66
3.7	Oxalate Degradation over Time.....	68
3.8	Phthalate Degradation over Time.....	69
3.9	Oxalate and Phthalate Degradation Curves Measured as TOC.....	70
3.10	Illustration of Chromatographic Elution Effects.....	71
3.11	Effluent History for HAIX-F(Fe) Run with Oxalate.....	75
3.12	Effluent History for HAIX-F(Fe) Run with Phthalate.....	77
3.13	Effluent History for HAIX-F(Zr) Run with Oxalate.....	80
3.14	Effluent History for HAIX-F(Zr) Run with Phthalate.....	82
3.15	Effluent History for HAIX-F(Zr) Run with Dilute NOM Brine.....	84
3.16	Comparative Plot of HAIX-F(Fe) and HAIX-F(Zr) Uptake of Oxalate.....	86
3.17	Comparative Plot of HAIX-F(Fe) and HAIX-F(Zr) Uptake of Phthalate...	88
3.18	Meaning of Separation Factor Values Defined by Isotherm Plot.....	94
3.19	Kinetic Test for HAIX-F(Fe) Run with Oxalate.....	96
3.20	Kinetic Test for HAIX-F(Fe) Run with Phthalate.....	98
3.21	Kinetic Test for HAIX-F(Fe) Run with Dilute NOM Brine.....	102
3.22	Kinetic Test for HAIX-F(Zr) Run with Oxalate.....	104
3.23	Kinetic Test for HAIX-F(Zr) Run with Phthalate.....	107
3.24	Kinetic Test for HAIX-F(Zr) Run with Dilute NOM Brine.....	110
3.25	Comparison of Kinetic Test Results for HAIX-F(Fe)..... and HAIX-F(Zr) with Oxalate	113

LIST OF FIGURES (cont.)

<i>Number</i>	<i>Description</i>	<i>Page</i>
3.26	Comparison of Kinetic Test Results for HAIX-F(Fe)..... and HAIX-F(Zr) with Phthalate	115
3.27	Comparison of Kinetic Test Results for HAIX-F(Fe)..... and HAIX-F(Zr) with Dilute NOM Brine	117
3.28	(a-b) Schematic Illustrating Donnan Co-Ion Exclusion Effects.....	119
3.29	(a-b) Schematic Illustrating Regeneration of HAIX-F Media.....	120
3.30	Regeneration Effluent History for HAIX-F(Fe) Oxalate-Loaded..... Media	121
3.31	Regeneration Effluent History for HAIX-F(Fe) Phthalate-Loaded..... Media	123
3.32	Regeneration Effluent History for HAIX-F(Zr) Phthalate-Loaded..... Media	125
3.33	Regeneration Efficiency vs. Bed Volumes for Oxalate Laden..... HAIX-F(Fe) Regeneration	126
3.34	Comparison of HAIX-F Phthalate-Loaded Media Regeneration.....	128
3.35	Comparison of Kinetic Test Results for HAIX-F(Zr) and..... IC Output at 4.33 Minutes	130
3.36	Comparison of Kinetic Test Results for HAIX-F(Fe) and..... IC Output at 4.33 Minutes	131
3.37	Comparison of NOM Concentration Results Measured via..... UV/VIS Spectrometry and TOC Analyzer	132
3.38	Output Screens from C++ Based Model.....	133-4

LIST OF FIGURES (cont.)

<i>Number</i>	<i>Description</i>	<i>Page</i>
CHAPTER 4: DISCUSSION		
4.1	Illustration of Inner- and Outer-Sphere Complexation Reactions.....	137
4.2	Oxalate Sorption Mechanisms onto Hydrous Zirconium Oxide Surface....	139
4.3	Phthalate Sorption Mechanisms onto Hydrous Ferric Oxide Surface.....	140
4.4	Components and Sorption Processes within HAIX-F(Fe).....	144
4.5	Components and Sorption Processes within HAIX-F(Zr).....	144
4.6	Schematic of Rapid Kinetics due to Synergistic Effect of..... Ion Exchanger Support	148
4.7	Advancement of Anion Fronts through HAIX-F.....	150
4.8	A Stratified Plot of Normalized TOC Concentration vs..... Bed Volumes Showing Presence of Separate NOM Breakthroughs Defined by Fraction	153
4.9	Schematic of HAIX-F Process Inclusion into a Water Treatment Plant	155
4.10	Cyclical HAIX-F Process for Water Treatment Plant.....	156

LIST OF ACRONYMS/VARIABLES

The following acronyms and variables are employed throughout the text of this thesis.

<i>Acronym/Variable</i>	<i>Description</i>
α	Separation factor
β_n	Positive non-arbitrary roots of diffusion equation
ε_p	Pore volume of fiber media
ρ_A	Molecule density
ρ_f	Bulk density of fiber media
μ	Dynamic viscosity
ω	Fractional mass of contaminant in solution at equilibrium
A	Area under the curve
A_e	Area under the effluent curve
A_i	Area under the influent curve
BV	Bed Volumes
C	Concentration
C_{eq}	Equilibrium concentration
C_o	Initial concentration
C_T	Total electrolyte concentration
CSTR	Constant Stir Tank Reactor
DBP	Disinfection By-Product
DBPR	Disinfection By-Product Rule
D/DBP	Disinfectants and Disinfection By-Products
D_{eff}	Effective diffusivity of HAIX-F media
DI	Deionized Water
D_L	Liquid diffusivity
DNA	Deoxyribonucleic Acid
DOC	Dissolved Organic Carbon

LIST OF ACRONYMS/VARIABLES (cont.)

<i>Acronym/Variable</i>	<i>Description</i>
DOM	Dissolved Organic Matter
D_p	Pore diffusivity
EBCT	Empty Bed Contact Time
EPA	Environmental Protection Agency
ESWTR	Enhanced Surface Water Treatment Rule
F	Fraction of capacity achieved
FMO	Frontier Molecular Orbital
HAA	Haloacetic Acid
HAA5	Haloacetic Acids (five)
HAIX	Hybrid Anion Exchange
HAIX-F	Hybrid Anion Exchange Fiber
HAIX-F(Fe)	Hybrid Anion Exchange Fibers Loaded with Hydrous Ferric Oxide Nanoparticulates
HAIX-F(Zr)	Hybrid Anion Exchange Fibers Loaded with Hydrous Zirconium Oxide Nanoparticulates
HAN	Haloacetonitrile
HCIX	Hybrid Cation Exchange
HFO	Hydrous Ferric Oxide
HIX	Hybrid Ion Exchange
HOMO	Highest Occupied Molecular Orbital
HZO	Hydrous Zirconium Oxide
IC	Ion Chromatograph
IX-F	Ion Exchange Fiber
J	Bessel function
K	Linear equilibrium coefficient
k	Boltzmann's constant
LAB	Lewis Acid-Base

LIST OF ACRONYMS/VARIABLES (cont.)

<i>Acronym/Variable</i>	<i>Description</i>
LUMO	Lowest Unoccupied Molecular Orbital
M_{∞}	Contaminant mass on media at equilibrium
m	Mass of sorbent employed
MCL	Maximum Contaminant Level
MCLG	Maximum Contaminant Level Goal
M/DBP	Microbial and Disinfection By-Product
MIEX	Magnetic Ion Exchange Resin
MRDL	Maximum Residual Disinfectant Level
MRDLG	Maximum Residual Disinfectant Level Goal
M_t	Contaminant mass on media at given time
MW	Molecular Weight
N	Avogadro's number
NOM	Natural Organic Matter
OMO	Occupied Molecular Orbital
PZC	Point of Zero Charge
Q	Total capacity
q'	Amount of contaminant removed
q	Capacity
q_b	Breakthrough capacity
q_{eq}	Equilibrium capacity
q_t	Total capacity
R	Radius of fiber media
r	Radius of fiber media from $r=0$ to $r=R$
	Molecular radius
SDWA	Safe Drinking Water Act
SEM	Scanning Electron Microscopy
SLV	Superficial Liquid Velocity

LIST OF ACRONYMS/VARIABLES (cont.)

<i>Acronym/Variable</i>	<i>Description</i>
T	Temperature
t	Time
t₀	Start time
TC	Total Carbon
THM	Trihalomethane
TOC	Total Organic Carbon
TTHM	Total Trihalomethanes
US	United States
UV	Ultraviolet
UV/VIS	Ultraviolet - Visible
V	Volume
WTP	Water Treatment Plant
x	Fractional presence in aqueous phase
y	Fractional presence in media phase

THESIS ABSTRACT

In the recent past, details regarding toxicological impacts of disinfection by-products (DBPs) have emerged, prompting USEPA to begin regulating DBP compounds in drinking water systems. These contaminants include trihalomethanes, haloacetic acids, and haloacetonitriles; however, other halogenated compounds as well as unhalogenated compounds, including bromate and chlorite, are also of interest. Human ingestion of these contaminants results in kidney/liver cancer, cardiac malformations, neurotoxicity, cytotoxicity, and genotoxicity, among others. DBPs are produced when organic precursors, namely, natural organic matter (NOM), react with disinfection agents such as chlorine, chlorine dioxide, chloramines, or ozone, among others. Expensive, impractical post-disinfection DBP removal mandates elimination of organic precursors prior to disinfection.

Previous technologies for NOM removal are inefficient due to incomplete removal, larger sludge volumes, and longer settling times, among others. For that reason, this report sought to characterize the NOM removal abilities, sorption kinetics, and regenerability of a novel media, which is called hybrid anion exchange fiber or HAIX-F. Essentially, HAIX-F media consists of a parent anion exchange fiber material that is loaded with metal oxide nanoparticulates. The chemistry of such metal oxides allows NOM treatment through two different sorption mechanisms, namely, Coulombic and Lewis acid-base interaction. Presence of the dual-binding mechanisms allows for selective adsorption of ligands like NOM. Furthermore, the synergy enacted by fusing of anion exchange fiber support and metal oxide nanoparticulates provides the structural durability and enhanced kinetics associated with anion exchange materials with the sorption and regeneration capabilities of metal oxide nanoparticulates. Disadvantages involved with each individual component are lost when the hybrid material is formed.

The enclosed thesis report provides the results of extensive experimental studies aimed at characterizing HAIX-F ability to remove NOM and surrogate NOM compounds from surface water sources. Results dictate that HAIX-F selectively removes NOM and surrogate NOM compounds over background anions, sorbs NOM and surrogate NOM compounds at extremely fast rates, and is efficiently regenerated towards reuse in drinking water treatment applications. Furthermore, a computer generated model suggests that HAIX-F employment in the drinking water treatment industry provides exceptional ability for NOM removal and reduction of DBP formation potential.

CHAPTER 1: INTRODUCTION

1.1 Chemistry of Natural Organic Matter

Natural organic matter (NOM) is composite solid/aqueous carbon-based compounds, which are derived from plant/animal origin, present in natural water sources. Characterization of these compounds is extremely difficult due to heterogeneity and complexity of the specific components. Customarily, NOM is described as complex collections of aqueous fulvic and humic acids. These organic acids are generally composed of extensive carbon chains, hydroxyl groups, aromatic carbon rings, oxygen atoms, carboxyl groups, and nitrogen atoms. An example that illustrates the Byzantine chemical configuration of natural organic acids, especially fulvic acid, is presented in Figure 1.1. It should be noted that many chemical structures for fulvic and humic acids have been proposed; however, as each particular NOM source derives from different plant/animal origins, soil composition, and other factors, the molecular structure varies widely and so Figure 1.1 provides only a model of NOM structure.

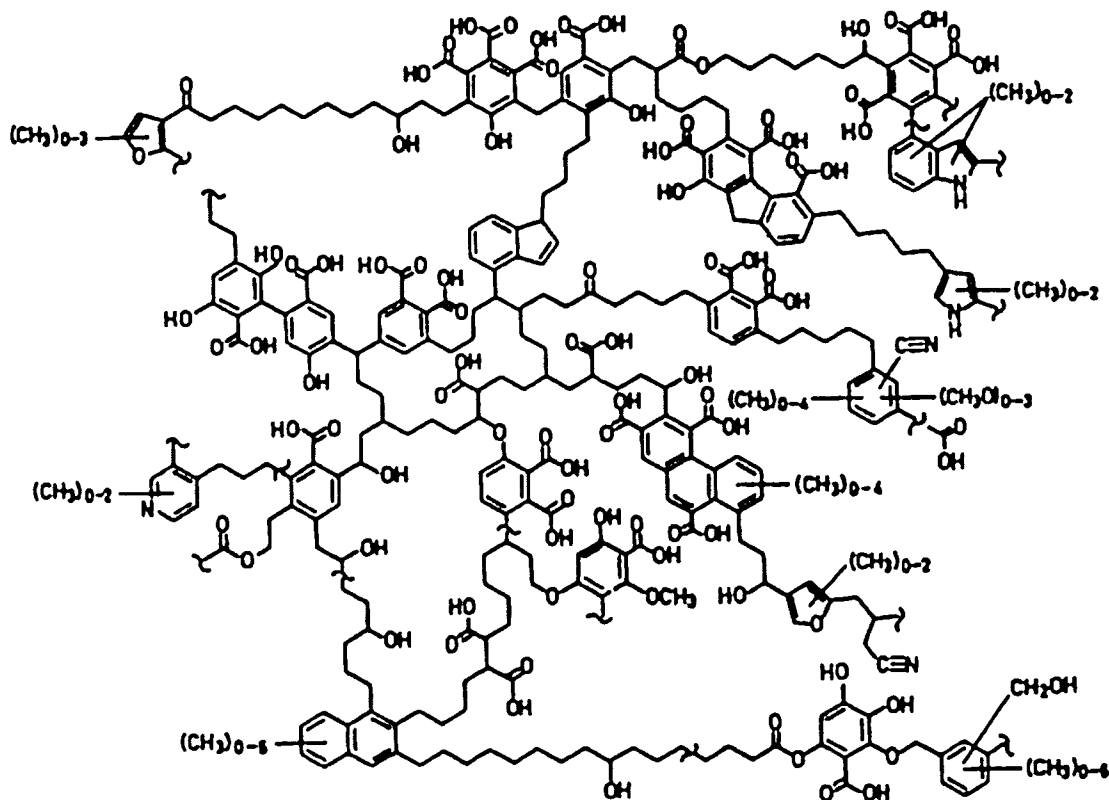


Figure 1.1 – Chemical Structure of Fulvic Acid

These organic compounds are released upon plant decomposition through both natural and animal-facilitated means, i.e., bacterial processes. Extremely activated NOM chemical compounds carry inherent negative charges, which usually allows for NOM settling through coagulation/flocculation processes in typical water treatment processes. The numerous carboxyl and hydroxyl groups, along with nitrogen and double-bonded oxygen atoms, provide high reactivity potential. For example, the fulvic acid molecular segment provided in Figure 1.1 contains approximately twenty-nine carboxyl groups, seventeen hydroxyl groups, five nitrogen atoms, and five double-bonded oxygen atoms. Upon deprotonation, resultant compounds behave as Lewis bases, or ligands, owing to the considerable amount of free electrons capable of being donated towards formation of covalent bonds with corresponding Lewis acid species.

As mentioned above, NOM components exhibiting such behavior are classified as ligands; furthermore, during coagulation/flocculation water treatment processes such compounds interact with metallic cations, specifically Fe(III) and Al(III). Essentially, coagulants (ferric chloride and alum, among others) are employed towards removal of suspended and colloidal particulates in water treatment plants. Some fraction of NOM surpasses coagulation/flocculation/settling processes and can generate public health concerns due to chemical reactions that take place during secondary treatment processes, i.e., disinfection. For that reason, the remainder of this report will explore the removal of NOM compounds prior to disinfection towards reduction of public health threats caused by compounds formed by reaction between NOM and disinfection chemicals.

The remaining sections of this chapter thoroughly describe formation of disinfection by-products and federally mandated disinfectant and disinfection by-product regulations (section 1.2), explore existing processes for NOM removal (section 1.3), detail the theory behind employment of a novel technology towards applications regarding NOM minimization (section 1.4), provide characteristic information about experimental NOM surrogate species utilized in the subsequent studies (section 1.5), and introduce the project objectives and goals (section 1.6).

1.2 Disinfection By-Products: Compounds, Effects, Regulations

The earliest recorded employment of disinfectant compounds occurred in 1850 when John Snow attempted to terminate a London cholera outbreak through chlorine dosing [Snow, 1854; Snow, 1855]. Come 1897, Sims Woodhead applied “bleach solution” to sterilize potable water distribution mains during a typhoid outbreak [Borough of Maidstone, 1898]. Throughout the early twentieth century, chlorination of water supplies was continued towards reduction of

disease outbreaks and improved public health. By 1908, Jersey City, New Jersey became the first US municipality to adopt chlorination; this technology soon spread throughout the United States and eventually waterborne diseases were practically eliminated [Mason, 1909].

Throughout the rapid boom in environmental water protection and public health technology/awareness that occurred during the remainder of the twentieth century and beginning of the twenty-first century, industrial, academic, and governmental bodies have concocted various means of ensuring the safety of water supplies. The water supply disinfection realm was not bypassed by this technological explosion; currently, there are a wide-ranging assortment of disinfectants commercially available. These disinfectants include the following compounds/technologies: chlorine (Cl_2), chlorine dioxide (ClO_2), chloramines (NH_xCl_y), ozone (O_3), potassium permanganate (KMnO_4), ultraviolet light (UV), and bromine (Br_2) [Huang et al., 1997; Shull, 1981; Farooq et al., 1977; Cleasby et al., 1974; Wolfe, 1990; Johnson and Overby, 1971]. Nonetheless, chlorine remains the most economical mainly because extremely large amounts of chlorine gas are generated as electrolysis by-products resulting from production of caustic soda [Mansfield et al., 2000]. Furthermore, some municipalities do not allow utilization of alternative disinfectants unless chlorine compounds are also employed towards establishment of a disinfectant residual, which serves to maintain water quality throughout the distribution system by preventing bacterial growth [Earth Tech Inc., 2005; USEPA, 1999a; USEPA, 1999b].

Regardless of the prevalence of multiple disinfection schemes, all currently-employed technologies encounter inherent problems through i) absence of disinfectant residuals or ii) production of disinfection by-products (DBPs) [USEPA, 1998b; Singer, 1994]. The lack of disinfectant residuals often instigates concerns that although water may be sufficiently disinfected within the specific water treatment facility, water quality may be compromised within the distribution system due to bacteria regrowth, distribution pipe fracture, or reappearance of

bacteria populations through other means. Comprehensive experimentation regarding toxicological impacts of DBP ingestion has been completed over the last few decades. Overwhelming proof that ingestion of DBPs through drinking water generates serious health impacts has been determined. The remainder of this section deals with DBP formation and classification, associated health concerns, and regulatory limits on disinfectant residual, DBP presence, and total organic carbon (TOC) concentrations, of which NOM is a significant fraction.

1.2.1 Disinfection By-Product Formation

A typical water treatment process involves collection of raw surface water, screening of larger debris, addition of coagulation compounds, rapid mixing, flocculation of suspended/colloidal particles with metal ions derived from coagulant, settling of flocs, and disinfection; subsequently, the treated water is introduced into the distribution system whereupon it is delivered to residential/commercial entities. Oftentimes, natural organic matters pass through the initial water treatment processes, which include screening, coagulation, and settling. This behavior sets the basis for DBP formation during water treatment processes.

During the disinfection stage of water treatment, NOM compounds react with disinfection agents (i.e., chlorine, ozone, chlorine dioxide, chloramines) and bromide anions (Br^-) to form DBPs [Chang et al., 2000; Nieuwenhuijsen et al., 2000; Myllykangas et al., 2005; Richardson et al., 2004]. DBP formation is influenced by common water quality factors (i.e., TOC, bromide concentration, pH, temperature, ammonia concentration, alkalinity) and treatment conditions (disinfection agent, contact time, disinfectant dosage) [Kitis et al., 2001; Huang and Yeh, 1997; Ueno et al., 2000; Elovitz et al., 2000; von Gunten, 2003a; von Gunten, 2003b; Chao, 2002; Minear and Amy, 1996; von Gunten et al., 2001]. Clearly, the process chemistry of such

reactions is incredibly complex, due to the number of variables and an indefinable natural organic matter chemical makeup. NOM compounds play the integral part in DBP formation; however, the complex chemistry makes modeling DBP formation almost impossible because so many reaction pathways are available. Regardless, empirical data has established DBP prevalence throughout water treatment plants (WTPs) similar to that provided in Figure 1.2.

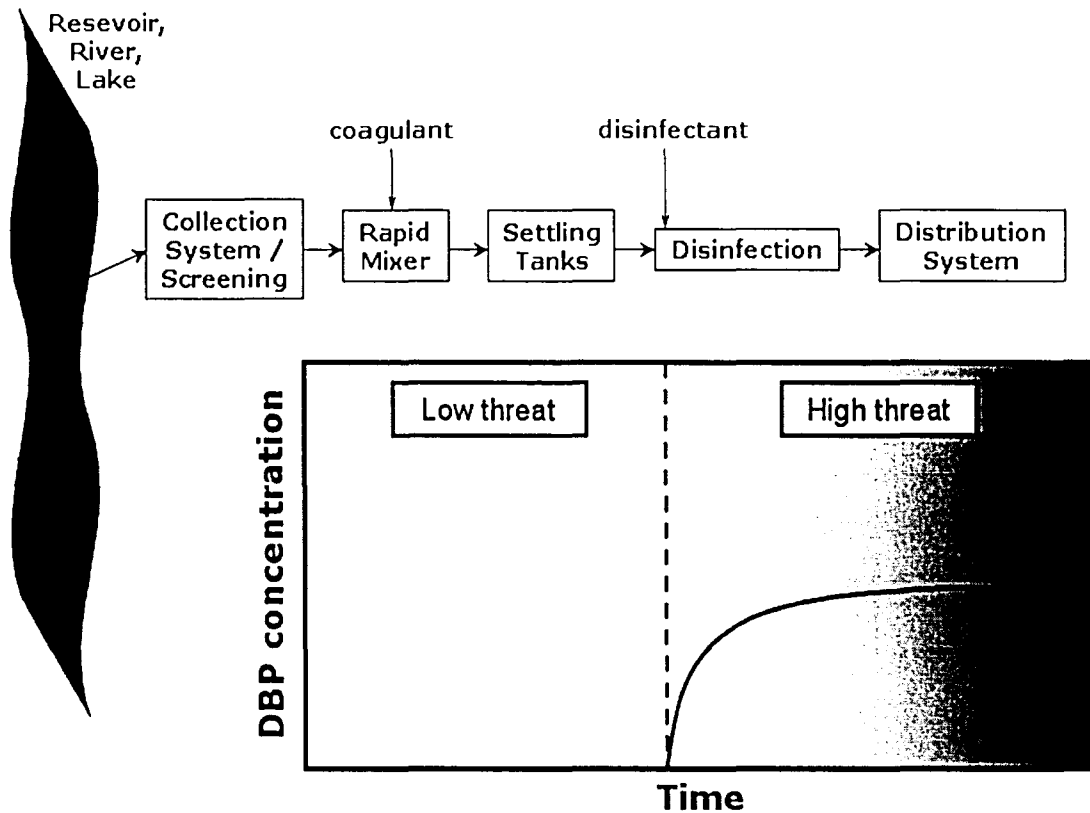


Figure 1.2 – DBP Appearance and Prevalence in a Typical WTP

1.2.2 Types of Disinfection By-Products

DBPs produced through reaction with disinfection agents vary widely. There are, however, three major groups of halogenated DBPs: trihalomethanes (THMs), haloacetic acids

(HAAs), and haloacetonitriles (HANs) [Kitis et al., 2001; Krasner et al., 1989; Richardson, 2003]. Less frequently found DBP compounds include various halo-alkanes, halo-alkenes, halo-aldehydes, halo-ketones, halo-acids, halo-alcohols, halo-nitromethanes, halo-acetates, and halo-aromatics, among others [Richardson et al., 2000]. An extensive list of halogenated DBPs identified in high-bromide waters is available in Appendix A.

As inferred above, formation of specific DBPs is heavily dependent on the disinfection agent employed. Chlorine (Cl_2) tends to generate THMs (i.e., chloroform, bromodichloromethane) and HAAs (i.e., dichloroacetic acid, trichloroacetic acid); HANs, halo-ketones, halo-aldehydes, and halo-nitromethanes are also observed, but at lesser frequency [Gallard and von Gunten, 2002; Norwood et al., 1980; Kim et al., 2002; Dalvi et al., 2000; Christman et al., 2003; Eyring et al., 2003; Richardson et al., 2003; Cancho et al., 1999; Krasner et al., 2006]. Ozone (O_3) generally produces nonhalogenated DBPs such as bromate, aldehydes (i.e., formaldehyde), keto-acids, and carboxylic acids; additionally, hypobromous acids are generated and can subsequently lead to THM production (i.e., bromoform) [USEPA, 2001; von Gunten and Hoign, 1994; Can and Gurol, 2003; Richardson et al., 1999; Xie and Reckhow, 1992; Cooper et al., 1986]. Chlorine dioxide (ClO_2) often causes formation of nonhalogenated compounds such as chlorite and chlorate [Schmidt, 2004]. Cyanogen chloride is one DBP produced through reaction of NOM compounds with chloramine (NH_2Cl) disinfectant species [Hirose et al., 1989].

In order to demonstrate typical DBP formation reactions, consider the chemical reactions described in Figure 1.3, which details production of dichloroacetic acid, an HAA [Croué et al., 2000]. Clearly, the complex structure and heterogeneity of NOM components allows for multiple DBP formation mechanisms, as mentioned above.

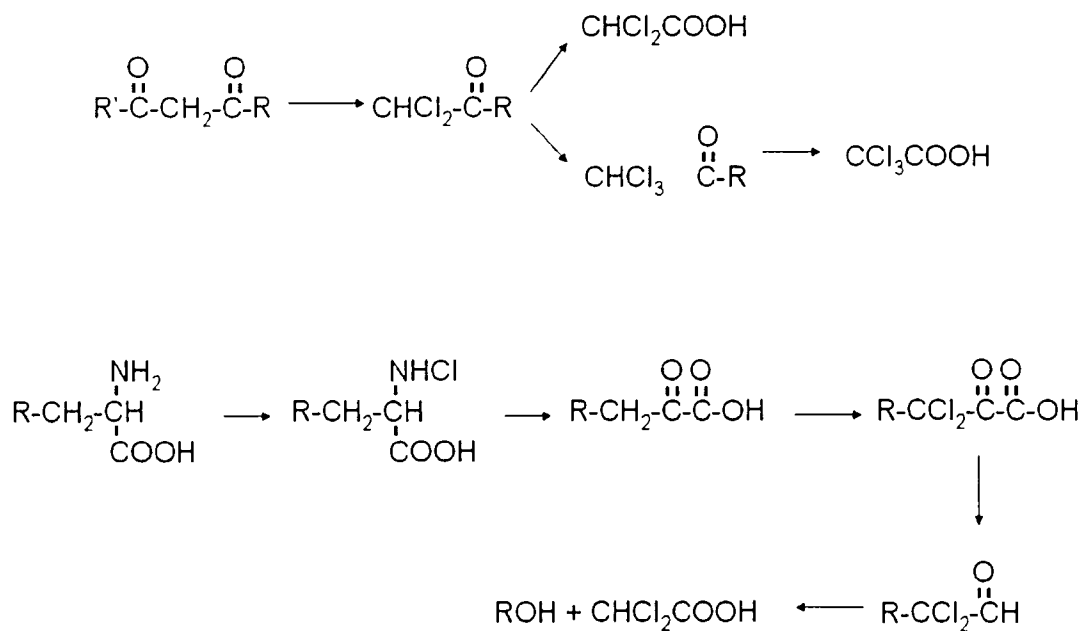


Figure 1.3 – Possible Dichloroacetic Acid Formation Reactions

Regardless of the chemical reactive pathways leading to DBP formation, the adverse health effects of DBP ingestion are extensively documented and understood. Ingestion of trihalomethanes instigate cytotoxicity in liver and kidneys; specifically, chloroform generates liver/kidney cancer, bromoform and dibromochloromethane produce tumors in the large intestine, and bromodichloromethane reduces sperm motility, causes liver/kidney cancer, and triggers large intestine tumors [Coffin et al., 2000; Lilly et al., 1997; Dunnick and Melnick, 1993; George et al., 2002; Klinefelter et al., 1995; Keegan et al., 1998; Dunnick et al., 1987]. Haloacetic acids also induce critical health effects; dichloroacetic acid acts as a neurotoxin and carcinogenic compound causing liver cancer, tumorigenic cell behavior, and cardiac malformations, trichloroacetic acid also produces tumorigenic cell behavior and cardiac malformations [Moser et al., 1999; Pereira and Phelps, 1996; Richard and Hunter, 1996; Bull, 2000; Fisher et al., 2001; Verschaeve, 2002]. Haloacetonitriles induce cell mutation and initiate tumors [Muller-Pillet et al., 2000; Lin et al., 1986]. Haloketones are often mutagenic and have clastogenic (chromosomal damage) effects

[Woo et al., 2002; Booker, 2000]. Haloaldehydes, specifically chloral hydrate, have been shown to generate hepatic necrosis, central nervous system depression, chromosomal damage and aberrations, and hepatic tumors [Daniel et al., 1992; Sing et al., 1996; Furnus et al., 1990; Eichenlaub-Ritter and Betzendahl, 1995; Klaunig et al., 1989]. Furthermore, nonhalogenated DBP compounds have considerable health effects that should be mentioned; bromate ion causes renal tubular damage, kidney, peritoneum, and thyroid tumors, genotoxic (DNA) damage, and oxidative stress to red blood cells [Kurokawa et al., 1990; Schminke and Seubert, 2004; Delker et al., 2006; Ono et al., 1994; Morgan et al., 2002]. Chlorite ingestion also demonstrates genotoxic behavior and oxidative damage to red blood cells; additionally, neurobehavioral effects have been recorded [Buschini et al., 2004; Hefferman et al., 1979; Gill et al., 2000]. It should be noted that health effects of DBP ingestion are still being studied and additional health-related problems are likely to be documented in the near future.

1.2.3 Disinfection By-Product Regulations

THMs were first determined to be DBPs in 1974 [Rook, 1974; Bellar et al., 1974]. After toxicological studies demonstrated severe health effects attributable to THM ingestion, the US Environmental Protection Agency (EPA) mandated a THM maximum contaminant level (MCL) of 0.10 mg/L in 1979 [USEPA, 1975; Federal Register, 1978]. Since that time, numerous DBPs have been recognized (Appendix A) and regulatory MCLs have been established towards maintenance of safe drinking water supplies.

The adverse health effects indicated in section 1.2.2 along with continual identification of other DBPs prompted USEPA to establish new regulations for municipal water systems. The 1996 Safe Drinking Water Act (SDWA) amendments coordinated plans towards the development

of future regulatory limits/protocol addressing the risks associated with treatment of microbial pathogens and DBP prevention [Pontius and Roberson, 1994; Pontius, 1997; Pontius, 2002]. Termed the Microbial/Disinfectants and Disinfection Byproduct (M/DBP) cluster, this new set of rules includes the Disinfectants/Disinfection By-Product (D/DBP) Rule (Stage 1), which aims to minimize risks associated with DBPs and the Enhanced Surface Water Treatment Rule (ESWTR; Stage 2), intended to strengthen microbial contamination prevention [USEPA, 1998b; National Primary Drinking Water Regulations, 2006a; National Primary Drinking Water Regulations, 2006b]. Undoubtedly, an exceptionally balanced solution is required in order to reduce both microbial pollution and DBP contamination.

1.2.3.1 EPA DBPR Stage 1 Rule

The Stage 1 Disinfectant By-Products Rule (DBPR) applies to municipal and non-transient water systems, including those serving fewer than 10,000 citizens [USEPA, 1998b]. This rule established maximum residual disinfectant level goals (MRDLGs) and maximum residual disinfectant levels (MRDLs) for chlorine, chloramine, and chlorine dioxide. Additionally, maximum contaminant level goals (MCLGs) were set for bromodichloromethane, dibromochloromethane, bromoform, dichloroacetic acid, trichloroacetic acid, chlorite, and bromate; actual MCLs were enacted for total trihalomethanes (TTHM), five haloacetic acids (HAA5), chlorite, and bromate. These regulations/regulatory goals are listed in Table 1.1 [USEPA, 1998a].

Table 1.1 – Stage 1 D/DBP Regulatory Limits on Disinfectant Residual and DBP Presence

DISINFECTANT RESIDUAL	MRDLG (mg/L)	MRDL (mg/L)	COMPLIANCE BASED ON
Chlorine	4.0 (as Cl ₂)	4.0 (as Cl ₂)	Annual Average
Chloramine	4.0 (as Cl ₂)	4.0 (as Cl ₂)	Annual Average
Chlorine Dioxide	0.8 (as ClO ₂)	0.8 (as ClO ₂)	Daily Samples
DISINFECTION BY-PRODUCTS	MCLG (mg/L)	MCL (mg/L)	COMPLIANCE BASED ON
Total trihalomethanes (TTHM)	N/A	0.08	Annual Average
- Chloroform	***		
- Bromodichloromethane	0		
- Dibromochloromethane	0.06		
- Bromoform	0		
Haloacetic acids (five) (HAA5)	N/A	0.06	Annual Average
- Dichloroacetic acid	0		
- Trichloroacetic acid	0.3		
Chlorite	0.8	1.00	Monthly Average
Bromate	0	0.01	Annual Average

In addition to setting goals regulations, Stage 1 DBPR outlined sample scheduling towards identification of regulatory violations and public exposure to DBPs; furthermore, the rule encouraged enhanced coagulation and softening processes towards reduction of DBP efflux from water treatment plants [USEPA, 1998b; National Primary Drinking Water Regulations, 2006a; National Primary Drinking Water Regulations, 2006b]. In January 2004, DBPR was established as law, and subsequently necessitated water treatment system compliance [USEPA, 1998a].

Although these regulations directly impact the problems surrounding DBP presence in drinking water systems, no definite preventative measures are taken against DBP precursors in raw waters. For that reason, if DBPs, specifically those not mentioned in Table 1.1, are present in post-treatment drinking water supplies, there are practically no guarantees against ingestion by humans; furthermore, as TTHM and HAA5 are regulated on annual bases, certain seasonal effects are essentially neglected. Stage 2 of DBPR, accordingly, considers such circumstances.

1.2.3.2 EPA DBPR Stage 2 Rule

Stage 2 regulations supplement those outlined through Stage 1 and stipulate stringent sampling protocol. Basically, D/DBP regulatory limits are mandated at each individual monitoring site, rather than via distribution system averages. Additionally, self-assessments towards identification of stagnation points within the distribution system; subsequent D/DBP sampling must then occur at those points [National Primary Drinking Water Regulations, 2006a; National Primary Drinking Water Regulations, 2006b]. Running annual averages (mean of previous twelve monthly averages) must comply with regulatory MCLs every quarter. D/DBP concentration spikes discovered throughout the distribution system must be reported to the state environmental agency. Most importantly, NOM concentrations (as TOC) are effectively enforced (Table 1.2) to ensure reduction of DBP formation potential [National Primary Drinking Water Regulations, 2006a]; essentially, such a regulation acts to prevent DBP formation as opposed to Stage 1 regulations, which define maximal occurrence levels. These USEPA directives were recently mandated (January 2006); effectively, Stage 2 rulings should increase D/DBP awareness and identification in water distribution systems towards reduction of the public's risk of exposure [National Primary Drinking Water Regulations, 2006a; National Primary Drinking Water Regulations, 2006b].

Table 1.2 – Stage 1 D/DBP Regulatory Limits on TOC Concentrations

TOC Concentration (mg/L)	Alkalinity as CaCO ₃ (mg/L)		
	0-60	60-120	>120
0.0-2.0	No action needed	No action needed	No action needed
2.0-4.0	35%	25%	15%
4.0-8.0	45%	35%	25%
>8.0	50%	40%	30%

1.3 Existing Technologies for NOM Removal

Theoretically, there are four approaches towards minimization of DBP concentrations in treated waters: (1) reduction of disinfectant dosing, (2) post-disinfection removal of DBPs, (3) employment of alternative disinfectants, such as ultraviolet light and ozone, and (4) elimination of organic matter precursors. Reducing disinfectant dosing (*option 1*) within the water treatment plant and prescribing subsequent dosing within the distribution system lessens DBP formation; however, operational difficulties and dispersed treatment centers are necessitated. Various processes for removal of DBP compounds (*option 2*) exist and could be implemented downstream of disinfection treatment; however, because a wide-ranging assortment of DBPs, which exhibit different chemical properties, are available successful employment of such technologies in an economic manner is not feasible. Application of UV disinfection systems (*option 3*) inherently eliminates generation of DBPs; however, high operating costs, nonexistent residuals, and ineffectiveness in turbid waters have restricted mass utilization of this technology [Wolfe, 1990; Hargy, 2002]. Similarly, ozone employment (*option 3*) results in the elimination of halogenated DBPs; nevertheless, nonhalogenated DBPs are formed and no residual remains in the distribution system [Boorman et al., 1999; Geldreich, 1996].

For those reasons, minimization of organic DBP precursors (*option 4*) is necessary to permit adequate microbial biocide and minimal DBP generation without necessitating major changes in standard disinfection procedures. As the majority (98%) of inorganic DBP precursors currently in use involve chlorine [chlorine gas (Cl_2), hypochlorite (OCl^-), chlorine dioxide (ClO_2), chloramines (NH_2Cl)], removal of inorganic precursors is systemically impossible, as described above [AWWA Water Quality Disinfection Committee, 1992]. Ultimately, previous efforts have concentrated on preventing NOM and synthetic organics from reaching the disinfection stage of

typical water treatment plants. Various organic matter removal technologies have been presented to the scientific community and employed in both pilot projects and actual water treatment plants. These technologies are discussed in the following subsections (sections 1.3.1-1.3.7).

1.3.1 Nonionic Macroporous Resin

This technology utilizes two nonionic macroporous resins towards NOM removal. The resins operate in series contained within separate columnar apparatuses; the primary resin, XAD-8, is comprised of acrylic ester with relatively large pore diameters and small specific surface area, the secondary resin, XAD-4, is composed of styrene divinylbenzene with smaller pore diameters and larger specific surface area. The hydrophobic organic acid fraction (i.e., aquatic fulvic/humic acids, aliphatic carboxylic acids containing 5-9 carbons, single/double ring aromatic carboxylic acids, and single/double ring phenol compounds) is removed via XAD-8 macroporous resin [Chin et al., 1994; Chin et al., 1997; Meier et al., 2004; Schwede-Thomas et al., 2005]. XAD-4 retains the transphilic, or intermediate polarity, acid fraction, which is composed of polyfunctional organic acids and aliphatic acids containing fewer than five carbons [Chin et al., 1994; Chin et al., 1997; Meier et al., 2004; Schwede-Thomas et al., 2005].

Sorbed hydrophobic/transphilic NOM acid and base components can be systematically flushed from the macroporous resin columns by introducing sodium hydroxide streams; however, hydrophobic/transphilic NOM neutral compounds cannot be removed with simple regeneration procedures [Aiken et al., 1992; Malcolm and MacCarthy, 1992]. Strictly hydrophilic NOM compounds are not significantly removed by the described system. Overall, XAD-8 and XAD-4 nonionic macroporous resins can remove between 23-58% and 7-25%, respectively, of dissolved organic carbon present in influent streams, depending on characteristic water quality [Aiken et al.,

1992; Malcolm and MacCarthy, 1992].

1.3.2 Iron Oxides

The literature is overflowing with the adsorptive capabilities and accompanying advantages of iron oxides, such as goethite (FeOOH), and hematite (Fe₂O₃), among others [Day et al., 1994; Gu et al., 1996; Gu et al., 1994; Korshin et al., 1997; Lili et al., 1997; Maurice et al., 1998; McKnight et al., 1992; Meier et al., 1999; Namjesnik-Dejanovic and Maurice, 2001; Namjesnik-Dejanovic et al., 2000; Redman et al., 2002; Tipping, 1981; Tipping and Cooke, 1982; Parfitt et al., 1977]. Major adsorption mechanisms onto mineral oxides include anion exchange through Coulombic interaction, ligand sorption via surface complexation, hydrophobic interaction, entropic effect (self aggregation of given molecules frees water molecules, providing the water molecules with high entropy, i.e., spontaneous self-aggregation), hydrogen bonding, and cation bridging [Kavanagh et al., 1977; Watson et al., 1973; Celis et al., 1999; McPhail et al., 1972; Sims and Bingham, 1968; Tipping, 1990].

Gu and coworkers determined that hydrophobic NOM fractions contained more carbon but less oxygen than hydrophilic components: this distinction marked hydrophobic compound preference by iron oxide surfaces on a carbon basis, however on an oxygen basis, hydrophobic and hydrophilic fraction adsorption were relatively comparable [Gu et al., 1995]. These experimental results indicated that the principal interaction mechanism between organic matter functional groups and iron oxide surface groups is ligand exchange, resultant of surface complexation under relatively acidic pH conditions. Ligands are loosely defined as Lewis bases; upon ligand interaction with Lewis acids (metal oxide surface functional groups) stable ligand adsorption onto active metal surface adsorption sites occurs. This behavior is demonstrated

through Figure 1.4 below, which illustrates adsorption of phosphate species, which demonstrate ligand characteristics, onto iron oxide surface sites. Another apt example is traditional coagulation processes that utilize ferric chloride compounds towards removal of suspended/colloidal particles, including NOM.

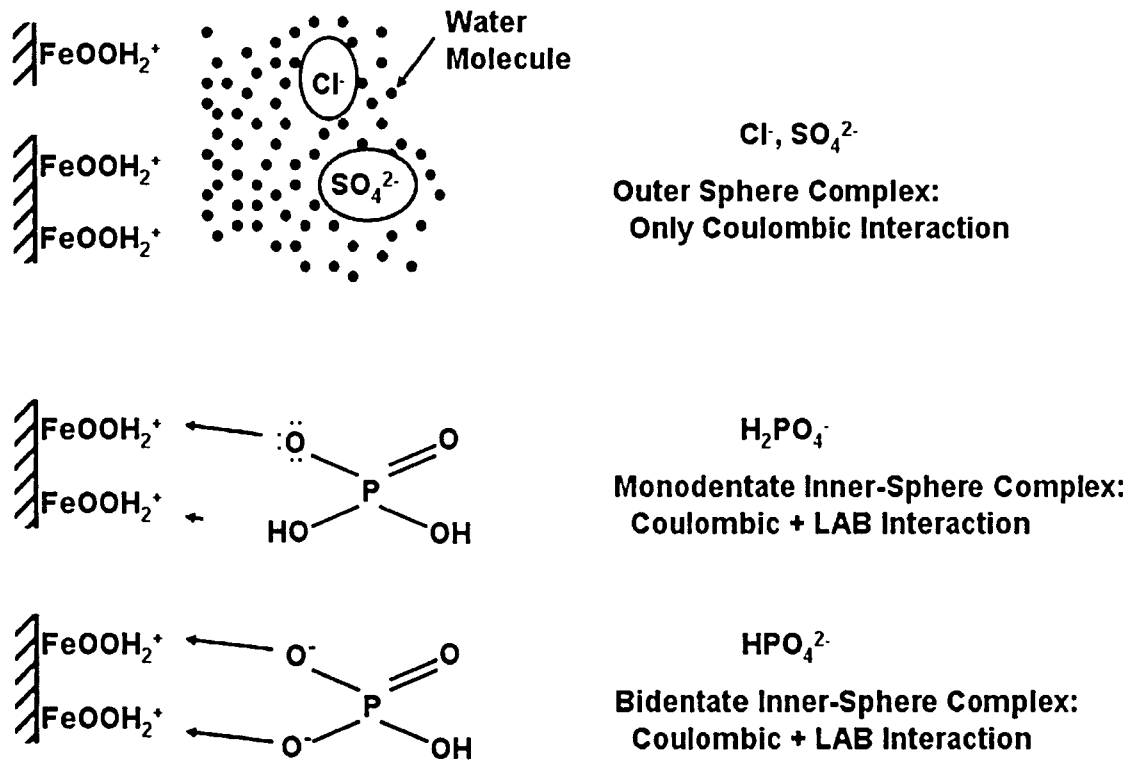


Figure 1.4 – Lewis Acid-Base Interaction: Phosphate Acts as a Lewis Base, while Iron Oxide Surface Functional Groups Behave like Lewis Acids

1.3.3 Aluminum Oxides/Silicates

Aluminum containing minerals such as alumina (Al_2O_3), kaolinite ($\text{Al}_2\text{Si}_2\text{O}_5(\text{OH})_4$), muscovite ($\text{KAl}_2(\text{AlSi}_3\text{O}_{10})(\text{F},\text{OH})_2$), gibbsite ($\text{Al}(\text{OH})_3$), imogolite ($\text{Al}_2\text{SiO}_5(\text{OH})_4$), and montmorillonite ($(\text{Na},\text{Ca})_x(\text{Al},\text{Mg})_2(\text{Si}_4\text{O}_{10})(\text{OH})_2 \cdot n\text{H}_2\text{O}$), among others have been successfully

employed towards NOM removal [Davis and Gloor, 1981; Ghabbour et al., 1998; Maurice et al., 1998; McKnight et al., 1992; Meier et al., 1999; Namjesnik-Dejanovic and Maurice, 2001; Namjesnik-Dejanovic et al., 2000; Parfitt et al., 1977; Tomaic and Zutic, 1988]. The surface and adsorption chemistry of the interaction between NOM components and aluminum oxide/silicate surface functional groups is relatively similar to that of iron oxides [Gu et al., 1994]. Again, organic acids ($pK_a \geq 10$) account for the greatest percentage of dissolved organic matter (DOM); acidic aluminum oxide functional groups behave as Lewis acids. Subsequent Lewis acid-base interaction occurs at water/oxide interfaces. This behavior can be understood through known material regarding phosphate interaction with iron/aluminum oxide surfaces as demonstrated above.

The ligand-like behavior has been observed throughout this research and in the open literature [McPhail et al., 1972; Sims and Bingham, 1968; Cabaniss and Shuman, 1988]. Copper complexation studies performed during the course of this project indicate the ability of NOM to increase copper solubility through formation of zero-valent complexes. Such capabilities allow for effective regeneration of copper loaded ion exchange media. Ability for such complexation exemplifies the ligand exchange behavior of NOM; this behavior permits successful sorption of NOM compounds onto metal oxide surfaces, as mentioned above. As a side note, such ligand behavior, coupled with the ability of concentrated NOM solutions to pass through fine and coarse sands while retaining nanofluid characteristics, allows for highly efficient ion exchange/adsorption media regeneration potential. This ability allows for sustainable utilization of organic matter waste products (recovered from water treatment plants) towards sustainable recovery of other wastes; thereby, reducing the overall waste produced and concentrating waste streams.

1.3.4 Magnetic Ion Exchange Resin (MIEX[®])

MIEX[®] resin is a specially manufactured ion exchange resin containing a magnetic core component [Orica, 2006]. Within this decade, utilization of MIEX[®] treatment towards TOC removal has been increasingly employed in numerous installations including Manchester, NH, Durham, NC, Manatee County, FL, La Verne, CA, Hackensack, NJ, Tampa, FL, Austin, TX, Indianapolis, IN, Sioux Falls, SD [Singer and Bilyk, 2002]. Basically, the resin is employed as a coagulating agent, as described above; however, the exhausted media can be easily collected via magnetic charge and regenerated. In fact, magnetization of resin particles quickens deposition of MIEX[®]-TOC flocs.

After one hour of agitation, MIEX[®] reduced THM formation potential for various US cities by 70-85% [Singer and Bilyk, 2002]. Further studies by Singer and Bilyk demonstrated that MIEX[®] resin not only efficiently removed low/medium molecular weight organics but also provided the ability to treat hydrophilic and hydrophobic components present in NOM [Singer and Bilyk, 2002]. Singer and Bilyk go on to state that MIEX[®] provides greater removal than enhanced coagulation, which is discussed in section 1.3.5 [Singer and Bilyk, 2002]. Figure 1.5, from Orica Ltd. producers of MIEX[®] resin, illustrates sorption/regeneration with MIEX[®] resin [Orica, 2006].

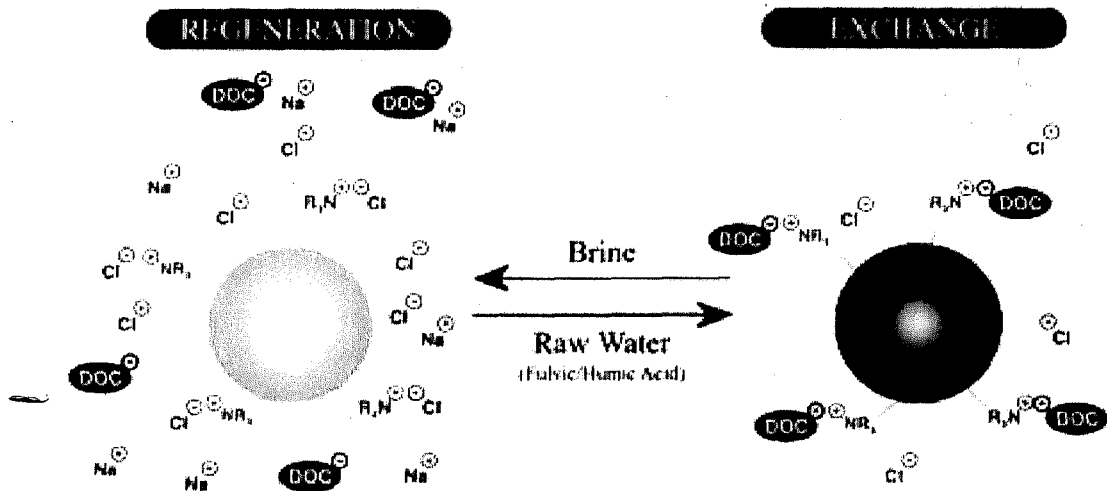


Figure 1.5 – MIEX[®] Sorption/Regeneration Mechanisms

Many advantages of pretreatment processes employing MIEX[®] have been documented throughout the literature: reduced demand of coagulation chemicals and acids/bases for pH adjustment, less waste sludge production, reduced disinfectant demand and DBP production, increased stability of disinfectant residual in distribution systems, reduced costs associated with decreased coagulant demand and waste sludge handling/disposal, and lowest potential for bacteriological re-growth during distribution [Singer and Bilyk, 2002; Drikas et al., 2003; Humbert et al., 2005; Bourke et al., 1999]. However, MIEX[®] treatment is not without disadvantages. Due to the process chemistry being controlled by surface functional groups that operate via electrostatic bonding, the MIEX[®] process is inherently not selective for NOM compounds. Furthermore, in waters with high anionic content (chloride, sulfate, bicarbonate, etc.), low NOM₂ removal efficiency is realized. Also, employment in constant stir tank reactor (CSTR), or batch, configuration denies opportunity for complete NOM removal and requires greater detention time compared with plug-flow reactor (PFR) empty bed contact times [Slunjski et al., 2000]. Furthermore, fractions of MIEX[®] resin are not collected during deposition;

therefore, regeneration does not allow for complete reusability of media [Slunjski et al., 2000; Slunjski et al., 2002].

1.3.5 Enhanced Coagulation

Due to simplicity of implementation, enhanced coagulation is probably the most utilized process for reducing TOC prior to disinfection. Furthermore, USEPA suggests municipalities employ enhanced coagulation treatment to reduce DBP formation potential [USEPA, 1998b]. Essentially, enhanced coagulation involves increasing coagulant dosage beyond normal requirements for turbidity removal, towards reduction of TOC concentrations, including particulate organics as well as dissolved organic carbon [White, et al., 1997]. The most often utilized coagulants include alum, $\text{Al}_2(\text{SO}_4)_3 \times 18\text{H}_2\text{O}$, and ferric chloride, FeCl_3 [Ndabigengesere et al., 1995; Childress et al., 1999]. Numerous studies have shown that such coagulants are very effective at removing organic DBP precursors [Fabris et al., 2003; Kastl et al., 2003; Vrijenhoek et al., 1998; Thompson et al., 1997; White et al., 1997].

While an effective means of removing organic DBP precursors due to interaction between positively charged metal ions and negatively charged NOM compounds, enhanced coagulation has many disadvantages: greater coagulant requirements and associated costs, larger waste sludge production and related handling/disposal costs, greater detention times necessary for efficient sedimentation due to high coagulant dosage, and non-selectivity for NOM compounds.

1.3.6 Other Methods

Various additional techniques have been documented in the literature as viable

technologies for efficient NOM removal. Some of these processes include flocculation, coagulation, sedimentation, filtration, granular activated carbon, membrane processes, biotreatment processes, advanced oxidation, utilization of hydrophilic aluminum oxides and hydrophobic mercury electrodes [Vilgé-Ritter et al., 1999; Lykins et al., 1988; McGuire et al., 1991; Jacangelo et al., 1995; Taylor et al., 1987; Fu et al., 1994; Hozalski and Bouwer, 1999; Miltner et al., 1992; Symons and Worley, 1995; Andrews et al., 1995; Owen et al., 1993; Ochs et al., 1994]. These technologies are not widely utilized due to inflated operating costs, complex operating protocol, additional equipment needs, low permeate flux, and an assortment of other disadvantages that can be found in the open literature.

1.3.7 Summary

Most employed NOM removal operations utilize the techniques described above due to operational simplicity and economic efficiency. The metal oxide processes are easily introduced and operationally inexpensive; the macroporous resin system is regenerable and requires no significant operational costs. Nevertheless, these technologies do contain inherent drawbacks: larger sludge volumes and incomplete removal of NOM components are the greatest disadvantages. A physico-chemical process which combines the attributes of these systems while eliminating the shortcomings would substantially reduce the presence of DBP compounds in water distribution systems and allow for sustainable waste processes.

1.4 Towards NOM Selective Sorbent Media

1.4.1 Ferric Oxides

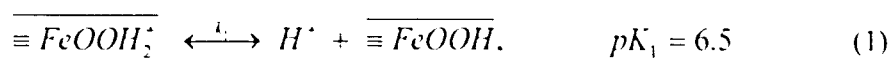
The applicability of ferric oxides towards ligand containment has been widely disseminated throughout the literature [Day et al., 1994; Gu et al., 1996; Gu et al., 1994; Korshin et al., 1997; Lili et al., 1997; Maurice et al., 1998; McKnight et al., 1992; Meier et al., 1999; Namjesnik-Dejanovic and Maurice, 2001; Namjesnik-Dejanovic et al., 2000; Redman et al., 2002; Tipping, 1981; Tipping and Cooke, 1982; Parfitt et al., 1977]. Unique surface chemistries of select metal oxides prescribe sorptive selectivity for anionic ligands at near neutral pH. This inherent characteristic can be exploited towards efficient technologies for treatment of contaminants. Utilization of metal oxide particles in fixed-bed situations causes generation of fines, which induce pressure drop. Such difficulties disallow the effective employment of ferric oxide in more efficient and manageable columnar apparatuses. This problem was overcome with the advent of hybrid ion exchange media.

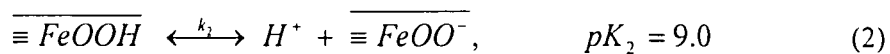
1.4.2 Hybrid Ion Exchanger History

In 2003, DeMarco and coworkers merged the beneficial adsorptive properties of ferric oxides with the structural advantages of commercial ion exchangers [DeMarco et al., 2003]. The group effectively developed a hybrid cation exchange resin, consisting of commercially available macroporous cation exchanger with polystyrene matrix and sulfonic acid (SO_3^-) functional groups impregnated with hydrous ferric oxide (HFO) nanoparticles. Coining the term “hybrid ion exchanger” (HIX), the group initiated an intense period of innovative research concentrated on

novel hybrid adsorption/ion exchange technologies, specifically concerned with arsenic removal. The novel HIX material, however, demonstrated significantly lower sorption capacity than expected. Upon scientific investigation the decreased capacity was determined to be due to Donnan co-ion exclusion effects [Cumbal and SenGupta, 2005; Puttamraju and SenGupta, 2006]. Hybrid cation exchange resins (HCIX) contain relatively high ferric oxide content due to widespread presence of negatively charged cation exchange sites. Accordingly, greater HFO particle deposition onto pore surfaces and inside gel phases was experienced; however, only HFO particles situated on pore surfaces are available for active phosphate sorption. Inside gel phases, the presence of negatively charged cation exchange sites instigates Donnan co-ion exclusion effects [Cumbal and SenGupta, 2005; Puttamraju and SenGupta, 2006]. Essentially, repulsive Donnan forces exist between negatively charged arsenic species and negatively charged sulfonic acid groups, eliminating any opportunity for arsenic sorption.

Recently, Cumbal and SenGupta overcame the difficulties encountered with HCIX technology through creation of hybrid anion ion exchange resins (HAIX), which combine the physical durability of polymeric anion exchange resins, sorptive affinity of metal (ferric and zirconium, among others) oxide nanoparticles, and enhanced permeation of anions within the gel phase due to presence of positively charged anion exchange sites [Cumbal and SenGupta, 2005; Cumbal et al., 2003; Puttamraju and SenGupta, 2006]. Therefore, even though less HFO deposition is experienced due to presence of positively charged anion exchange sites within the gel phase, significantly greater sorption capabilities are realized. Furthermore, impregnated HFO particles contain surface functional groups, which act as Lewis acids at pH less than 9.0 (equations 1-2). This advantageous characteristic allows for effective sorption of ligands through Lewis acid-base (LAB) interaction.





where $\overline{\equiv FeOOH_2^+}$, $\overline{\equiv FeOOH}$, and $\overline{\equiv FeOO^-}$ are HFO surface functional groups and pK_1 and pK_2 are the corresponding deprotonation constants [Sigg and Stumm, 1981]. Such behavior allows for selective adsorption of Lewis base contaminants at acidic and near neutral pH; furthermore, at basic pH, HFO functionality becomes negative and media is efficiently regenerated through Donnan co-ion exclusion effects. Consider Figure 1.6, which provides a graphic displaying HFO surface functionality as a function of pH. Clearly, below pH 6.5 positively charged surface groups dominate; such characteristic allows electrostatic interaction with anionic species such as NOM compounds, sulfate, and chloride, among others. From pH 6.5 to 9.0, neutral HFO surface groups abound allowing selective sorption of NOM compounds through LAB interaction (section 1.4.2.1). Above pH 9.0, negatively charged surface functionality predominates; therefore, electrostatic interaction with positively charged species (Ca^{2+} , Na^+ , etc.) could theoretically occur. However, Donnan co-ion exclusion effects due to presence of fixed positive charges ($-R_4N^+$) associated with the parent anion exchange resin, prevent any significant metal sorption abilities at such pH (as demonstrated previously with HCIX). The negative surface functionality above pH 9.0 does, however, allow for regeneration abilities as negatively charged NOM species will be expelled from the ferric oxide particulates.

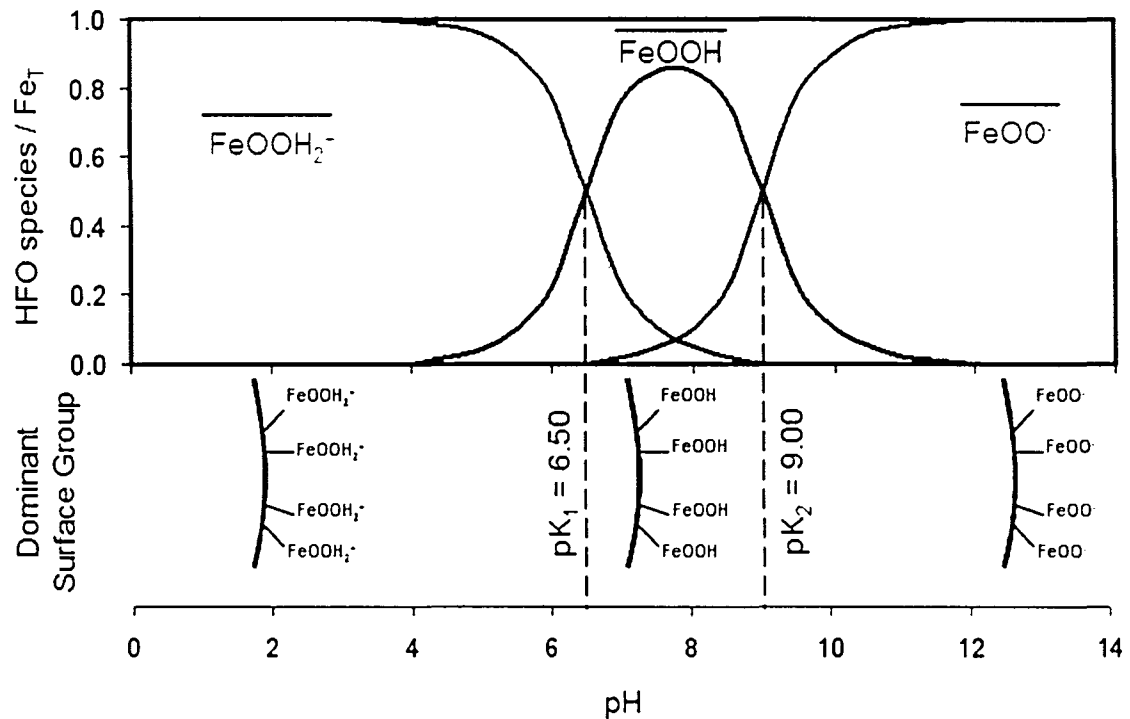


Figure 1.6 – Illustration of pH-Dependent HFO Surface Functionality

The presence of HFO groups within anion exchange resin is HAIX's major sorption mechanism. For reasons expounded in section 4.1, NOM species are selectively sorbed over typical anionic species such as chloride and sulfate. Figure 1.7 demonstrates the ability of anions to pass through HAIX media with some uptake capacity; however, the more selected anionic ligands (due to LAB interaction) are sorbed to HFO particles and are not removed until regeneration processes. Note that cations cannot enter the hybrid resin phase due to Donnan co-ion exclusion effects resultant from fixed positive charges present on the anion exchange polymer matrix.

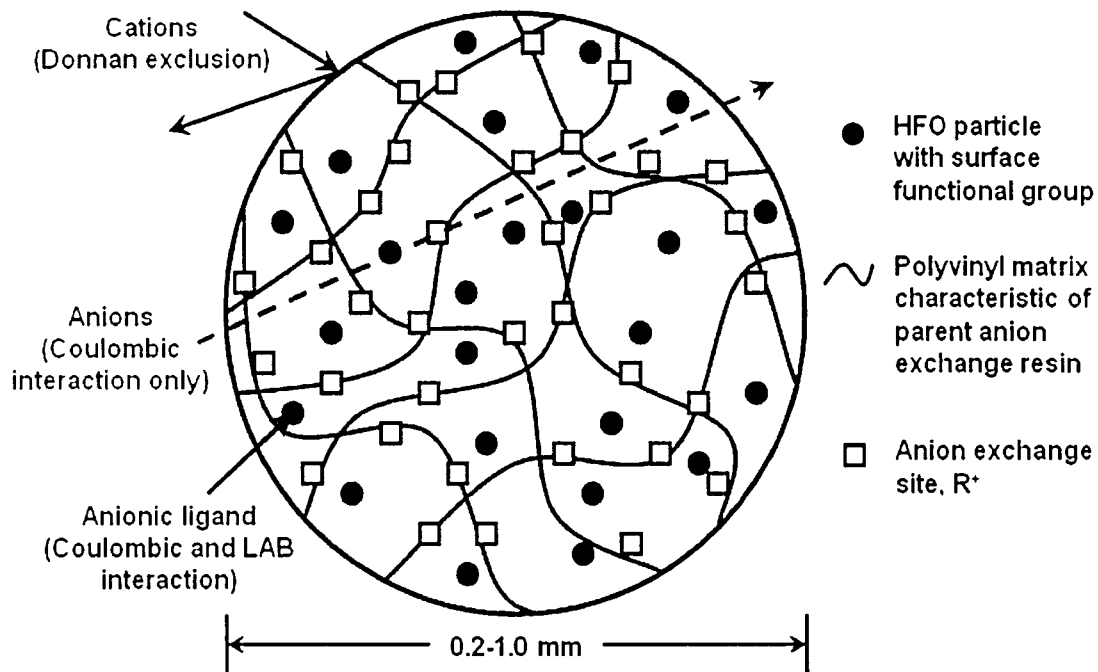


Figure 1.7 – Schematic Showing Major Components and Sorptive Abilities of HAIX Resin

1.4.2.1 Lewis Acid-Base Interaction

Lewis acid-base interaction can be defined through Lewis theory and frontier molecular orbital (FMO) theory. In Lewis theory, a Lewis acid is essentially an electron pair acceptor and a Lewis base is a species capable of donating a pair of electrons. Lewis acid-base interaction, then, is essentially inner-sphere complexation reactions that occur between species with readily available electron pairs (i.e., R-COO^- , $\text{C}_2\text{H}_3\text{O}_2^-$, H_2AsO_4^- , R-SH , R-NH_2) and species with unfilled orbitals (FeCl_3 , AlCl_3 , zeolite: $\text{AlOSi}\cdot\text{H}_2\text{O}$, SO_3). In terms of organic chemistry, the lone pair of electrons from the Lewis base will attack the Lewis acid and a two electron covalent bond will be formed.

FMO theory defines Lewis bases as species that react through the highest occupied

molecular orbital (HOMO) and Lewis acids as species which react via the lowest unoccupied molecular orbital (LUMO). Consider Figure 1.8, which shows a generic case surrounding LAB interaction as defined through FMO. Note that OMO denotes occupied molecular orbital.

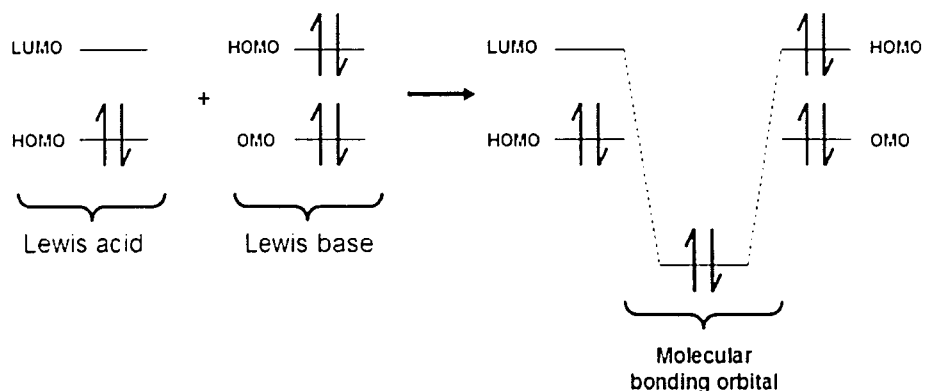


Figure 1.8 – Lewis Acid-Base Interaction Defined via FMO Theory

For chloride, sulfate, and other anions that demonstrate poor ligand characteristics LAB interaction is much weaker than for anionic ligands that can form inner-sphere complexes. These topics will be discussed in greater detail in section 4.1.

1.4.3 The Next Evolution

Experimental analysis to determine the kinetics of HAIX and similar media demonstrated intraparticle diffusion as the limiting factor in sorption capabilities [Cumbal et al., 2003; Zhao and SenGupta, 1998; Li and SenGupta, 2000]. Logically, the next chapter of the hybrid materials evolution involved increasing the kinetics. Puttamraju and SenGupta successfully accomplished this task: through loading anion exchange fibers (IX-F) with metal oxides, the two effectively produced hybrid anion exchange fibers (HAIX-F) [Puttamraju and SenGupta, 2006]. With decreased diameters, HAIX-F media operate at incredibly fast rates because intraparticle diffusive pathways are much shorter. Basic HAIX-F physico-chemical processes are identical to those of

HAIX media as shown in Figure 1.9; however, with diameters over three orders of magnitude smaller, hybrid anion exchanger fibers exhibit noticeably more rapid sorption kinetics. Note that q , C , r , t , and R represent sorption capacity, aqueous concentration, general radius, time, and specific radius.

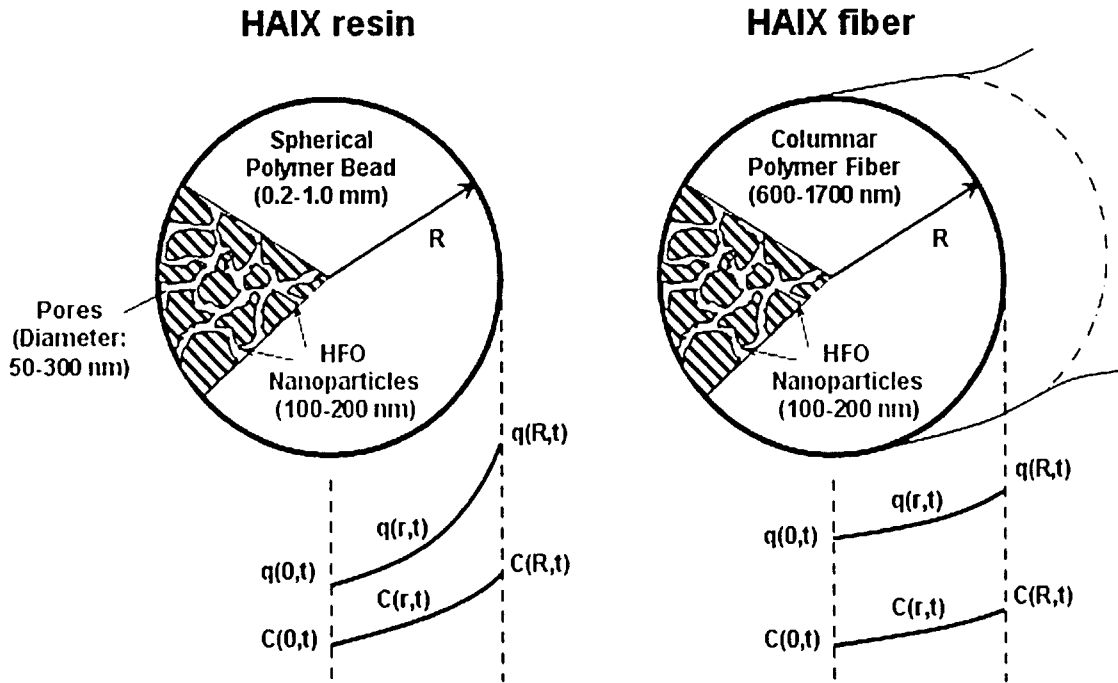


**Figure 1.9 – Schematic Showing Concentration Gradient in HAIX Resin and HAIX-F
Fibrous Media**

From Figure 1.9, it is clear that HAIX resin characteristically maintains a larger concentration gradient between bulk and resin phase. The gradient for HAIX-F fibrous media is much gentler, indicating that intraparticle kinetics are faster. Essentially, a steep concentration gradient (in terms of aqueous- or resin- phase concentration) represents slower infiltration of the given contaminant into the polymeric host. If the concentration gradient was maintained with a slope of zero, sorption kinetics would be infinitely fast, and effluent history would follow plug-flow like behavior.

Fibrous ion exchange materials are not yet commercially available on the large-scale:

however, FIBAN[®] has produced a considerable amount of literature regarding FIBAN A-1 fibers, which are essentially anion exchange media with quaternary ammonium functionality (R_4N^+) [Petruzzelli et al., 1995; Soldatov et al., 1994; Popova et al., 1991; Soldatov et al., 1999; FIBAN, 2007]. The hybrid fibers described in this study were synthesized through a unique hybridization technique (section 2.2.1) that involves FIBAN A-1 parent fibers and dissolved metal species. Salient information regarding FIBAN A-1 fibers is presented in Table 1.3.

Table 1.3 – Salient Properties of FIBAN A-1 Anion Exchange Fibers

Material	Matrix	Functional Group	Q (meq/g)	Water Uptake	Fiber diameter (μm)
FIBAN A-1	Polypropylene with polystyrene and divinylbenzene cross-linking	$-\text{CH}_2\text{N}^+(\text{CH}_3)_3$	2.5-4.0 (Cl ⁻)	0.4-1.0	30-55

The quaternary ammonium functional group [$R\text{-N}^+(\text{CH}_3)_3$] and equilibrium capacity are both typical of strong-base anion exchange resins. The polymeric matrix and water uptake are also comparable to spherical resin media. One difference is that the smaller media diameter allows for faster ion exchange kinetics and tighter packing density, which can provide advantageous effects through reactor size/design. It should be noted that coagulation, flocculation, and settling processes will have taken place before treatment for organic DBP precursors; therefore, problems related to pressure drop because of small pore space should not provide inherent dilemmas in HAIX-F treatment operation.

Section 2.2.1 discusses the metal oxide loading procedure in detail. Essentially, FIBAN A-1 anion exchange parent fibers were immersed into solution containing high concentrations of iron(III) or zirconium(IV) ion and allowed to equilibrate. Then, solution pH was quickly raised, instigating precipitation of ferric and zirconium oxide/hydroxide particulates within the polymeric phase. Upon media neutralization in dilute acid solution, metal oxide particulates stay embedded

within the polymeric media. As long as hybrid fibers are not contacted with strongly acidic solution, these metal oxides will remain in solid-phase and provide adsorbent capability. The HAIX resin schematic in Figure 1.7 is fundamentally valid for HAIX-F media. Photographs of the two HAIX-F media employed throughout the studies described in this report can be observed in Figure 1.10(a-b).

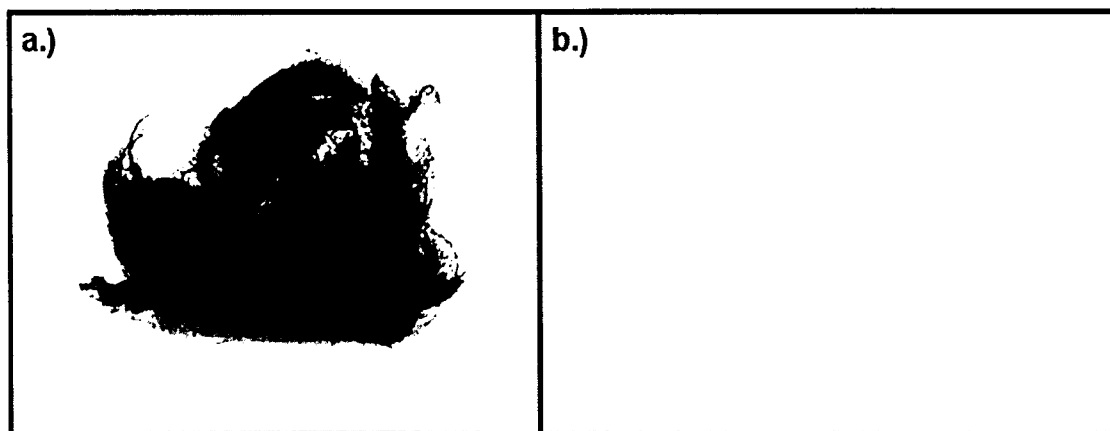


**Figure 1.10 – (a) FIBAN A-1 fibers impregnated with hydrous ferric oxide nanoparticulates
(b) FIBAN A-1 fibers loaded with hydrous zirconium oxide nanoparticulates**

1.4.4 Application of HAIX-F Technology

Resultant of the ligand-like behavior of NOM components mentioned in section 1.1 and the ligand sorption capabilities of HAIX described above, Puttamraju and SenGupta's HAIX-F media loaded with hydrous ferric oxide or hydrous zirconium oxide particulates should provide significant NOM removal abilities. Furthermore, the anticipated kinetics of such a technology will offer considerable implementation feasibility for municipal and industrial applications. As HFO nanoparticle chemistry does not change between resin and fibrous media, sustainable regeneration and concentration of NOM-loaded wastes should be possible. This process, then, can

theoretically eliminate NOM compounds before disinfection processes, permitting exceptional water quality and safety throughout the distribution system.

An additional benefit from employment of HAIX-F technology is lower disinfectant demand because NOM compounds will not interact with disinfectant species in the distribution system; therefore, disinfectant residuals will not be decreased. Similarly, disinfectant residuals will be more stable and provide better protection against bacterial contamination within water distribution systems. Obviously, the ability for DBPs to form is lessened by removal of NOM compounds before disinfection treatment.

The open literature regarding MIEX[®] technology boasts that smaller particle size allows for faster kinetics as compared to conventional resins; however, HAIX-F media has diameters over two orders of magnitude smaller than both MIEX[®] and conventional resins [Slunjski et al., 2000]. Slunjski and coworkers found that MIEX[®] treatment resulted in the lowest bacterial regrowth potential compared to alternative treatment processes; due to similarities between MIEX[®] and HAIX-F, similar characteristics regarding bacteria regrowth are expected [Slunjski et al., 2000].

Furthermore, utilization of HAIX-F technology for elimination of DBP formation potential via removal of organic DBP precursors leads to various externalities. For instance, bypassing enhanced coagulation processes, which are oft employed for meeting D/DBP regulations, permits a lesser amount of water treatment residuals to be produced. Costs associated with handling, transport, and disposal of that excess sludge can potentially offset capital costs for implementing HAIX-F treatment. Additionally, operating costs related to coagulant chemical demands will be reduced, providing further economic benefit related to HAIX-F employment.

1.5 Chemistry of HAIX-F and Experimental Organic Compounds

Throughout this research, two different HAIX-F media were utilized. One of those materials contained hydrous ferric oxide (HFO) nanoparticulates; the other media was impregnated with irremovable hydrous zirconium oxide (HZO) nanoparticulates. Doping polymeric fiber host materials with different metal oxides, results in slightly different properties due to differences in metal oxide chemistry, speciation vs. pH, and loading ability. Figure 1.6 showed HFO functional groups, or moieties, as a function of pH. Below, Figure 1.11 provides the same information for HZO-modified FIBAN A-1 fibers [HAIX-F(Zr)].

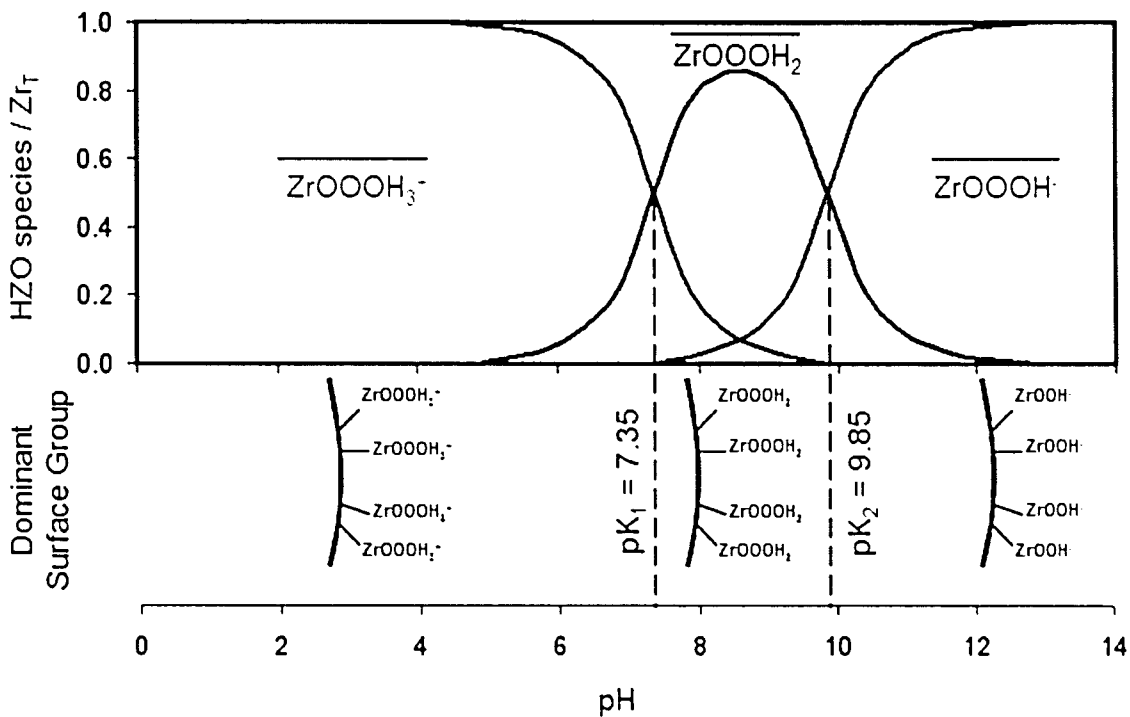


Figure 1.11 – Illustration of pH-Dependent HZO Surface Functionality

Recall that HFO deprotonation constants are 6.5 and 9.0, respectively. From Figure 1.11, pK_1 and pK_2 for HZO are 7.35 and 9.85, respectively. Thus, HFO-doped fibers [HAIX-F(Fe)] should provide more selective uptake of NOM compounds at pH 6.5-7.5, whereas HAIX-F(Zr) will

likely provide better NOM adsorption capabilities from pH 7.5-9.0. These statements are based upon the fact that HAIX-F selectivity for NOM compounds (especially monovalent and divalent species) stems from LAB interaction.

For this study, oxalate, $C_2O_4^{2-}$, and phthalate, $C_6H_4(COO)_2^-$, will be employed as synthetic organic DBP precursors and surrogate NOM compounds. Each compound has specific chemical speciation dependent upon pH. As this speciation is vital to HAIX-F selectivity considerations, consider Figures 1.12-1.13. Noticeably, in the near-neutral pH realm, oxalate and phthalate both exhibit divalent anionic characteristics; therefore, both species of interest will be capable of bidentate binuclear or monodentate mononuclear surface complexation with metal oxide nanoparticulates and divalent binuclear or monovalent mononuclear electrostatic interaction with positively charged metal oxide surface functional groups. General schematics showing these sorption mechanisms are presented in Figure 1.14.

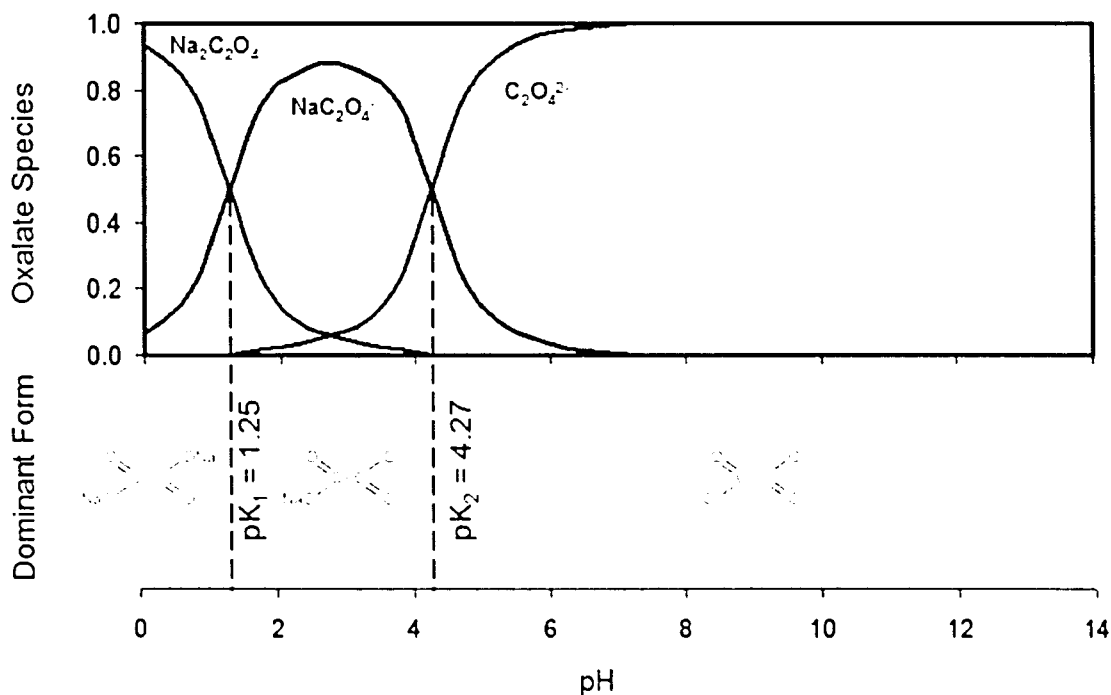


Figure 1.12 – Illustration of pH-Dependent Oxalate Speciation

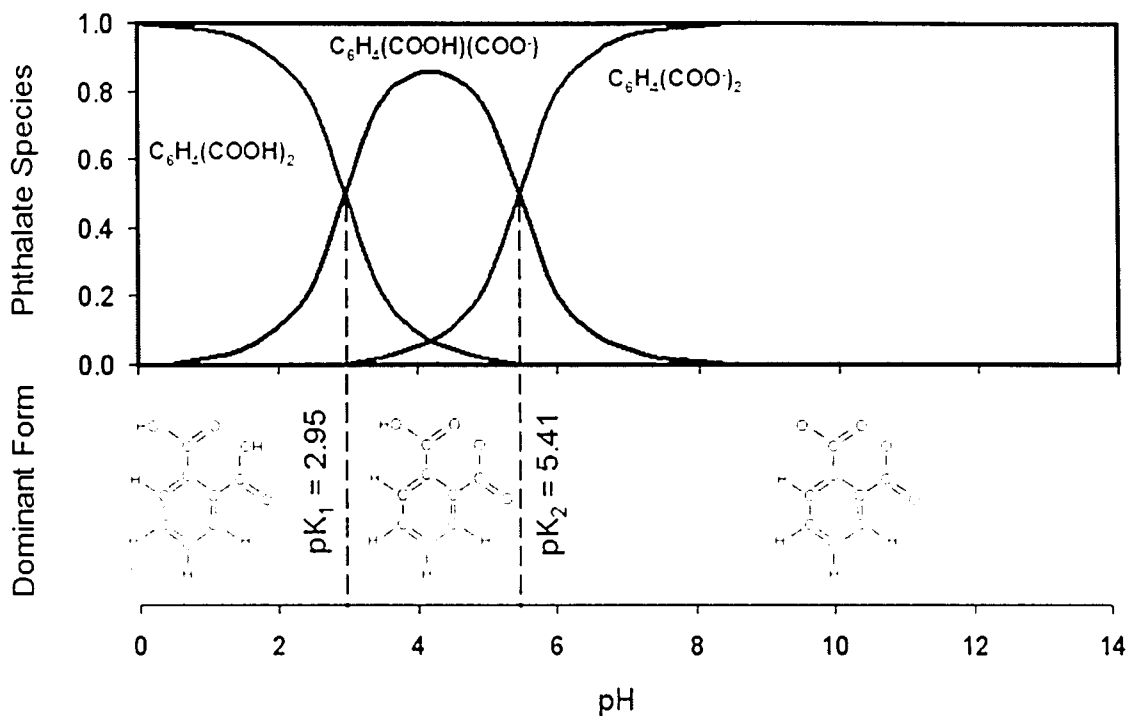


Figure 1.13 – Illustration of pH-Dependent Phthalate Speciation

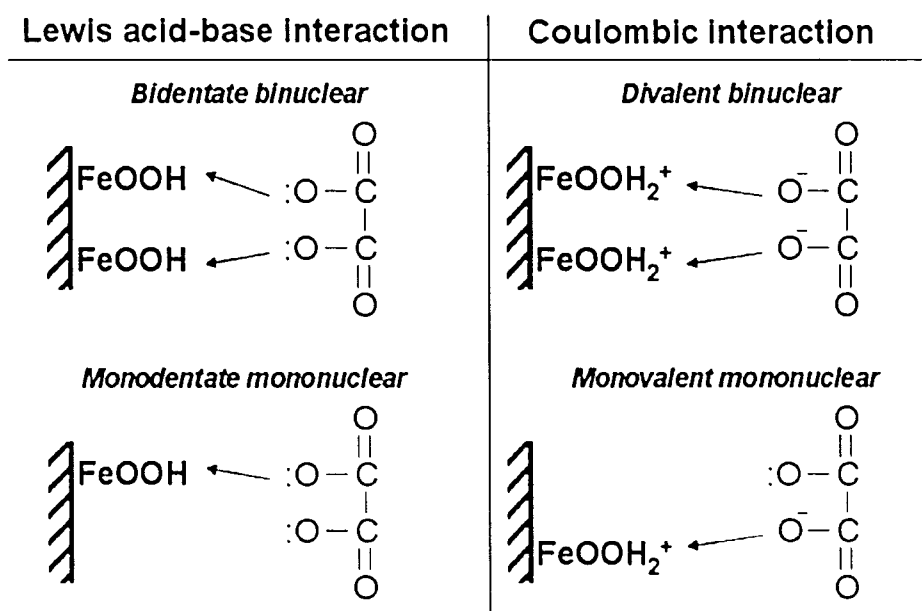


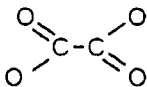
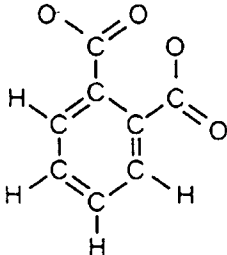
Figure 1.14 – Oxalate Sorption Mechanisms onto HFO Surfaces

In summary, metal oxide nanoparticulates exhibit positively charged and neutral functional surface groups at the near-neutral solution pH of influent drinking water streams. These groups

are capable of providing sorption of negatively charged and neutral NOM compounds through LAB and Coulombic interaction mechanisms. Furthermore, the parent anion exchange fiber media's positively charged quaternary ammonium functional groups (Table 1.3) provide enhanced anion transport. Additionally, the relatively small filament diameter allows very rapid sorption kinetics to dominate.

In summary, oxalate and phthalate characteristics of interest and sorption mechanisms regarding HAIX-F media are summarized in Table 1.4.

Table 1.4 – Oxalate and Phthalate Speciation Data, Predominant Species, and Sorption

Interaction Possibilities			
Parent Oxyacid	pK _a Values	Predominant Species at Near-Neutral pH	Sorption Interactions
$\text{Na}_2\text{C}_2\text{O}_4$	pK ₁ = 1.25 pK ₂ = 4.27		Mono/bidentate mono/binuclear surface complexation; mono/divalent electrostatic interaction
$\text{C}_6\text{H}_4(\text{COOH})_2$	pK ₁ = 2.95 pK ₂ = 5.41		Mono/bidentate mono/binuclear surface complexation; mono/divalent electrostatic interaction

1.6 Study Objectives

The adverse health effects associated with natural organic matters and disinfection processes, thoroughly described above, mandate operation of water treatment plants with consideration for both microbial and DBP contamination of water within the distribution system.

Furthermore, recent USEPA regulations regarding excessive DBP concentrations and disinfection residuals require municipalities to reduce DBP formation potential and TOC concentration while maintaining low disinfectant residual levels. The chemical composition of NOM compounds warrants ligand-like behavior, which authorizes employment of HAIX-F sorbent media towards effective removal of NOM from influent waters.

The remainder of this report describes experimental materials and methods (Chapter 2), results (Chapter 3), discussion (Chapter 4), and conclusions (Chapter 5) regarding HAIX-F applicability towards NOM removal.

CHAPTER 2: EXPERIMENTAL MATERIALS AND METHODS

The following sections describe the experimental materials, methods, protocol, and equipment utilized throughout this project. Detailed information regarding the chemicals employed, the batch, column, kinetic, and regeneration experiments run, and the analytical equipment utilized will be provided in the respective sections.

2.1 Chemicals

Throughout the course of these studies, numerous chemical compounds were utilized. Disodium oxalic acid ($\text{Na}_2\text{C}_2\text{O}_4$), phthalic acid ($\text{C}_6\text{H}_4(\text{COOH})_2$), sodium chloride (NaCl), sodium sulfate (Na_2SO_4), sodium hydroxide (NaOH), sulfuric acid (H_2SO_4), and other indirectly employed chemicals towards operation of the various analytical tools were obtained through Sigma-Aldrich or Fisher Scientific. All chemicals were analytical grade and no discrepancies between chemical labels and contents were encountered.

Oxalic acid and phthalic acid were employed towards as surrogate NOM compounds due to simple analysis and description of compound uptake via HAIX-F sorbent media. Contaminants of concern were charged oxalate ($\text{C}_2\text{O}_4^{2-}$) and phthalate ($\text{C}_6\text{H}_4(\text{COO}^-)_2$) species that result upon oxalic acid and phthalic acid dissolution in deionized water. Sodium salts, listed above, provided a source of background anions (sulfate, SO_4^{2-} ; chloride, Cl^-) towards determination of HAIX-F media affinity for organic compounds over commonly occurring anions. Sodium hydroxide (NaOH), as well as sodium chloride (NaCl), was used as regenerant for HAIX-F media; the regeneration process will be described in section 2.4. Sulfuric acid (H_2SO_4) was employed towards desorption of iron (Fe^{3+}) and zirconium (Zr^{4+}) from HAIX-F media in order to ascertain

the amount of metal ion present within the hybrid media.

Concentrated NOM brine was recovered from the regenerant stream of an NOM removal operation in New Zealand. The solution contains approximately 5200 mg/L TOC, 3300 mg/L SO_4^{2-} , and 53,000 mg/L Cl^- with a pH of 7.0. Specific dissolved organic constituents are unknown as mass spectrometry analytical equipment was not directly available to the primary investigator. HAIX-F media is expected to display ideal employment potential in waters with relatively low TOC concentration; therefore, the brine described above is about 1000× stronger than the waters this project is aimed at treating. Therefore, this solution was diluted approximately 1000× before being employed in the experiments described within this report.

Various other chemicals were utilized throughout the project's various components; such chemicals will be described during explanation of the experimental tests detailed in the following sections (sections 2.2-2.6).

2.2 HAIX-F Synthesis

Table 1.4 provided salient properties of parent anion exchange fibers utilized for synthesis of HAIX-F media towards removal of NOM and surrogate organic compounds. Scanning Electron Microscopy (SEM) imaging provided enhanced understanding of HAIX-F synthesis processes. Consider Figure 2.1(a-b), which provides SEM images of parent FIBAN A-1 fibers.

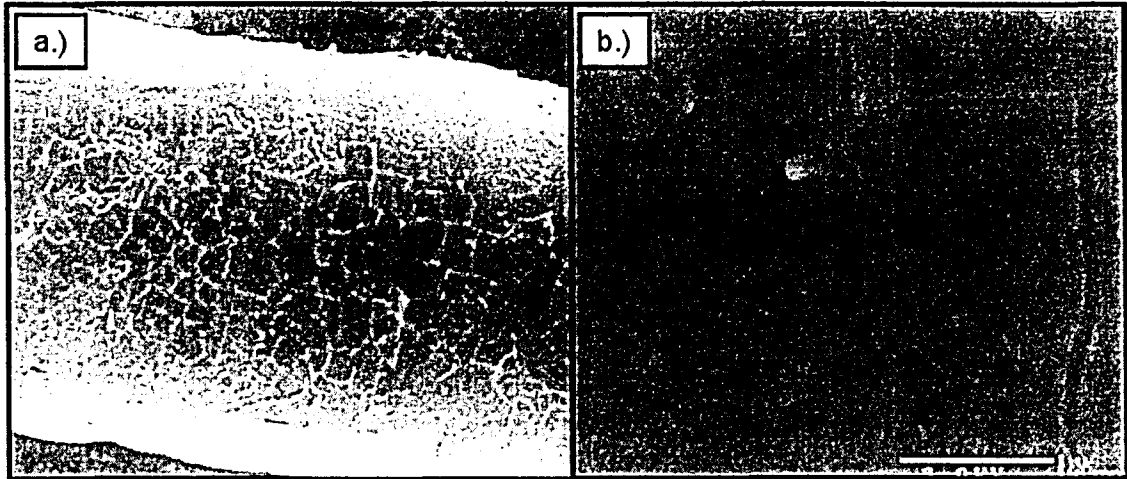


Figure 2.1 – (a) FIBAN A-1 Anion Exchange Fibers at 2000× Magnification (b) FIBAN A-1 Anion Exchange Fibers at 20,000× Magnification

Figure 2.1a demonstrates that filament surface is relatively smooth and uniform; furthermore, pore structures can be clearly identified in Figure 2.1b.

2.2.1 HAIX-F Synthesis Protocol

A simple process for embedding metal oxide nanoparticulates on anion exchange fibers was recently developed by Puttamraju and SenGupta [Puttamraju and SenGupta, 2006]. This synthesis procedure was employed towards production of HAIX-F(Fe) and HAIX-F(Zr) media. The following sections (sections 2.2.1.1-2.2.1.2) describe HAIX-F production protocol for HAIX-F(Fe) and HAIX-F(Zr), respectively.

2.2.1.1 HAIX-F(Fe) Synthesis Protocol

HAIX-F(Fe) synthesis was completed through execution of the following protocol:

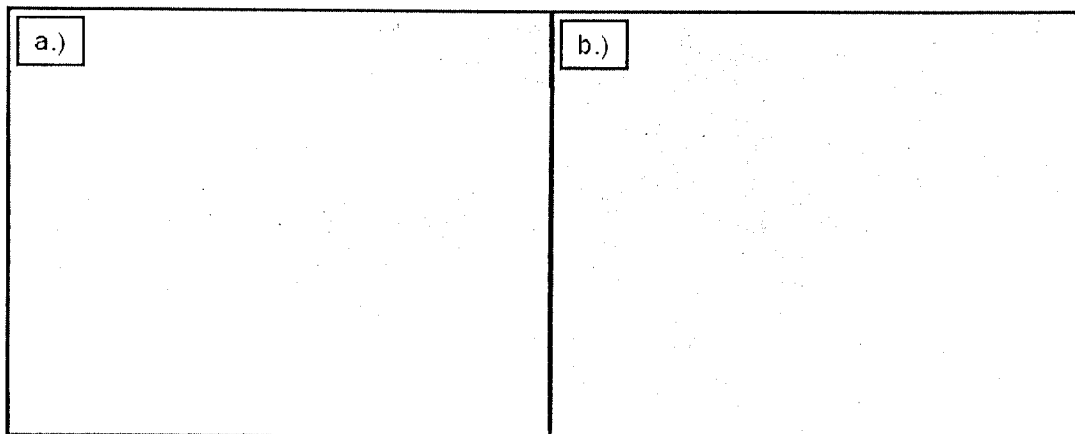


Figure 2.1 – (a) FIBAN A-1 Anion Exchange Fibers at 2000× Magnification (b) FIBAN A-1 Anion Exchange Fibers at 20,000× Magnification

Figure 2.1a demonstrates that filament surface is relatively smooth and uniform; furthermore, pore structures can be clearly identified in Figure 2.1b.

2.2.1 HAIX-F Synthesis Protocol

A simple process for embedding metal oxide nanoparticulates on anion exchange fibers was recently developed by Puttamraju and SenGupta [Puttamraju and SenGupta, 2006]. This synthesis procedure was employed towards production of HAIX-F(Fe) and HAIX-F(Zr) media. The following sections (sections 2.2.1.1-2.2.1.2) describe HAIX-F production protocol for HAIX-F(Fe) and HAIX-F(Zr), respectively.

2.2.1.1 HAIX-F(Fe) Synthesis Protocol

HAIX-F(Fe) synthesis was completed through execution of the following protocol:

1. Create 7% FeCl_3 ethanol/methanol solution; pH should be approximately 1.6
2. Add 10 grams of parent FIBAN A-1 fibers into solution
3. Allow the solid/liquid mixture to equilibrate through 6-8 hours of shaking
4. Remove fibers from ferric chloride solution
5. Place fibers into 0.5% NaOH solution and shake for 1-2 hours
6. Remove fibers from sodium hydroxide solution and rinse with deionized water
7. Let fibers dry in ambient air conditions
8. Repeat steps 1-7 for two more loading cycles

2.2.1.2 HAIX-F(Zr) Synthesis Protocol

Production of HAIX-F(Zr) media calls for an almost identical HZO loading procedure as observed below:

1. Create 7% ZrOCl_2 ethanol/methanol solution; pH should be approximately 1.7
2. Add 10 grams of parent FIBAN A-1 fibers into solution
3. Allow the solid/liquid mixture to equilibrate through 6-8 hours of shaking
4. Remove fibers from zirconium oxychloride solution
5. Place fibers into 2% NaOH solution and shake for 1-2 hours
6. Remove fibers from sodium hydroxide solution and rinse with deionized water
7. Let fibers dry in ambient air conditions
8. Repeat steps 1-7 for two more loading cycles

2.2.2 Description of HAIX-F Media

Consider SEM images of HAIX-F(Fe) [Figure 2.2(a-b)] at the same magnification levels as those photographs Figure 2.1(a-b). Differences between parent and hybrid materials are immediately evident. In Figure 2.2a, ion exchange fiber surface is noticeably rougher and less uniform compared to parent fibers shown in Figure 2.1a; furthermore, clear evidence of HFO deposition and scaling along fiber surface and pore structures is given in Figure 2.2b. No SEM photographs were taken for HAIX-F(Zr) media but HZO deposition should be very similar to that seen for HFO in Figure 2.2(a-b).

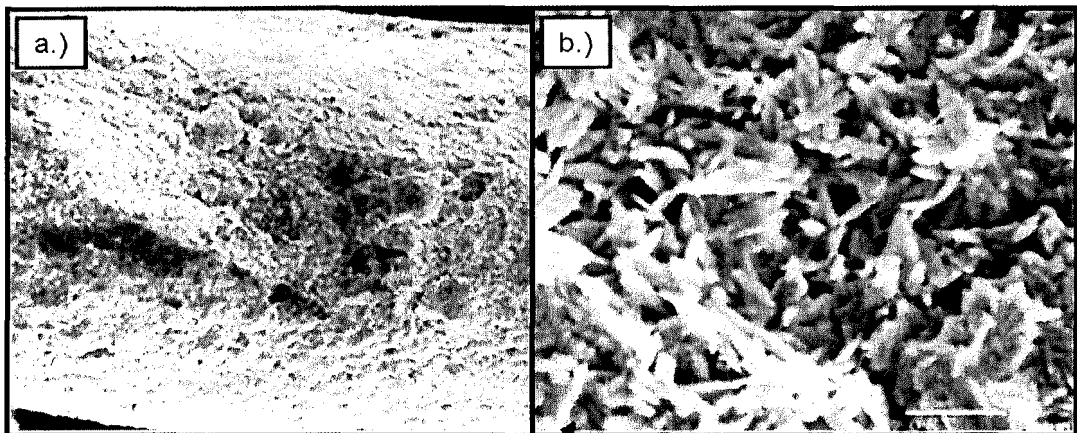


Figure 2.2 – (a) HAIX-F(Fe) at 2000× Magnification (b) HAIX-F(Fe) at 20,000× Magnification

These electron microscopy images verify metal oxide loading onto anion exchange fibers; additionally, Table 2.1 yields information regarding specific loading rates of iron(III) and zirconium(IV). Noticeably, iron loading was more efficient.

Table 2.1 – Specific Loading of Fe(III) and Zr(IV) onto HAIX-F Media

Material	Loading Rate (mg/g)	Loading Rate (mol/g)	Loading Rate (meq/g)
HAIX-F(Fe)	115.24	2.06	6.19
HAIX-F(Zr)	58.30	0.64	2.56

2.3 Batch Studies

Batch studies were employed towards determination of HAIX-F media sorptive abilities for organic matter. These experiments utilized 150 mL polymeric sample bottles, containing approximately 250 mg of HAIX-F media (impregnated with either Fe^{3+} or Zr^{4+}), with 100 mL of oxalate-, phthalate-, or NOM-dosed solution containing suitable levels of background anions. Small samples of the initial solution (before contact with HAIX-F media) were taken to record the initial concentrations of all anions present. Sample bottles containing synthetic surface waters were then positioned inside a rotating chamber, constructed by the Lehigh University lab group (Figure 2.3); sample bottles remained within this chamber for approximately 24 hours. After that period of contact time, initial and equilibrium samples were analyzed using Shimadzu TC/TOC Analyzer and Perkin Elmer Ion Chromatograph (section 2.6).

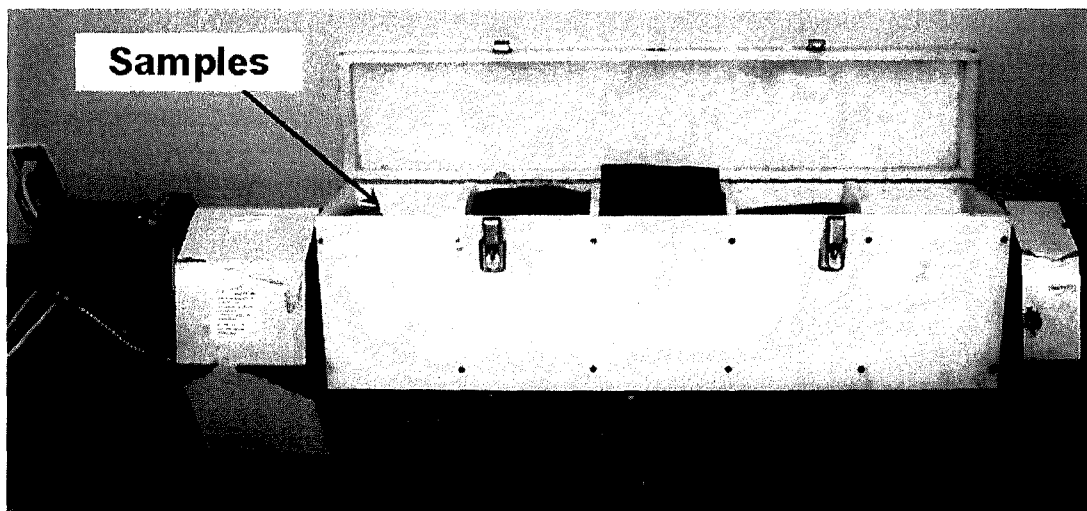


Figure 2.3 – Rotating Chamber for Batch Experiments.

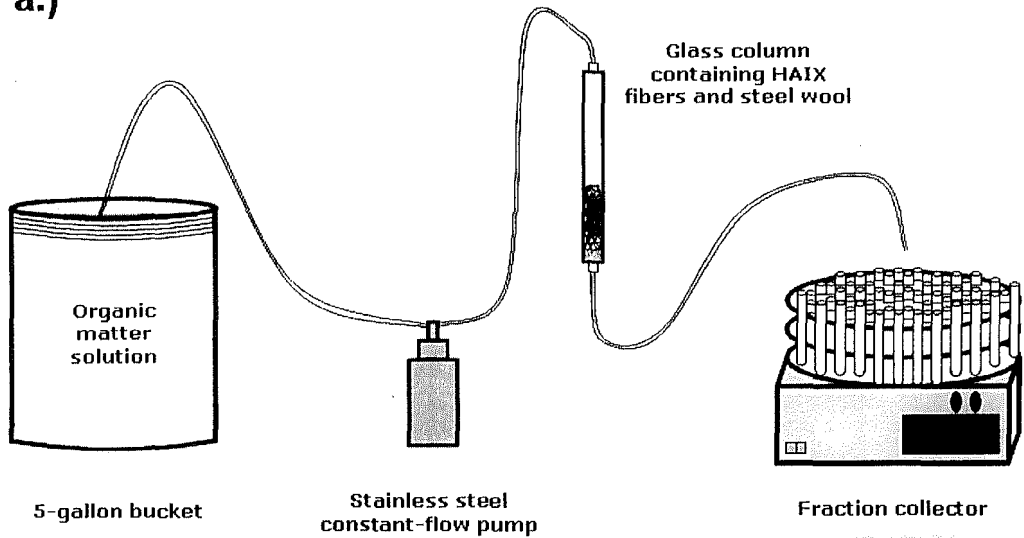
2.4 Column Studies

Fixed bed column runs were carried out using glass columns, HAIX-F media, constant-flow stainless steel pumps, synthetic surface waters contained in 5-gallon buckets, various tubing and fasteners, and Eldex fraction collectors. The synthetic surface waters (*one-three*) were composed of the following constituents:

- *One*: 2 ppm oxalate, 20 ppm sulfate, 100 ppm chloride
- *Two*: 2 ppm phthalate, 20 ppm sulfate, 100 ppm chloride
- *Three*: 10 ppm TOC (from NOM brine), 20 ppm sulfate, 100 ppm chloride

From the influent reservoir, the synthetic surface waters were pumped through tubing by the stainless steel pump. The pumped solution (~2 mL/min) was emptied into the top of the glass column, which was approximately 11 mm in diameter and 250 mm in length. At the bottom of the column (in vertical position), steel wool was placed as a support to ensure no leakage of HAIX-F media; located on top of the steel wool was a quantity (250 mg) of HAIX-F media. The fixed-bed column effluent solution was pumped through tubing and connected to the Eldex fraction collector. See Figure 2.4(a-b) for illustration and photograph of experimental setup. The fraction collector was typically programmed to rotate every ten minutes; test tubes were analyzed according to protocol listed in section 2.4.1.

a.)



b.)

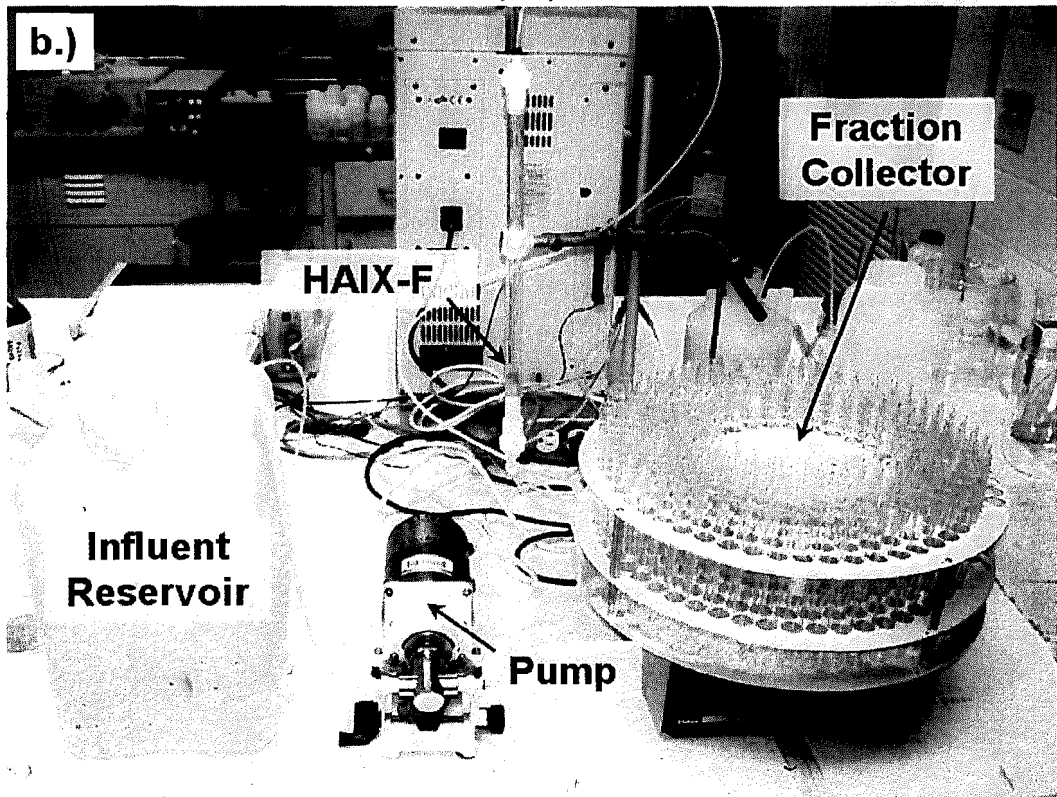


Figure 2.4 – (a) Schematic of Fixed-Bed Column Set-Up (b) Labeled Photograph of Fixed-Bed Column Set-Up

2.4.1 Testing Protocol

- Analyze tubes #2 and #5
- Analyze tube #10 and every 10 tubes afterwards until test tube #100
- Analyze tube #120 and every 20 tubes afterward
- If an interruption test is performed, multiple samples directly after that interruption may be analyzed
- Several runs demonstrate additional samples analyzed after breakthrough of compounds of interest

Flow rates for all experiments were held constant at approximately 2 mL/min; therefore, all sample test tubes contained roughly 20 mL of treated column effluent solution. Furthermore, the height of the HAIX-F media in the column was recorded in order to allow calculation of bed volume. With these values the superficial liquid velocity (SLV) and the empty bed contact time (EBCT) were determined for each column run.

Upon exhaustion, HAIX-F media were regenerated by passing a 2% NaOH and 2% NaCl solution through the exhausted media. Detailed explanation of regeneration physico-chemical concepts will be presented in section 3.6. Fibers were then rinsed and reactivated in carbon dioxide (CO₂) sparged deionized water for about 10 bed volumes. Again, samples from the actual treatment, regeneration, and rinsing were analyzed in the Perkin Elmer Ion Chromatograph or Shimadzu TC/TOC Analyzer in order to ascertain (1) when media is exhausted and (2) when regeneration is complete (i.e., the contaminant of concern has been completely expelled from exhausted media column).

In the past, experiments have been designed to determine whether or not premature leakage due to wall effects or channeling in beds consisting of ion exchange beads. With a 20:1 ratio between column diameter and IX resin particle diameter, no noticeable attributes of effluent history diagrams could be ascribed to wall effects or bed channeling. As ion exchange fibers have diameters two orders of magnitude smaller than ion exchange resins, potential for wall effects or channeling within the HAIX-F fixed-bed should be negligible.

2.5 Kinetic Tests

Experimentation towards determination of oxalate, phthalate, and NOM sorption kinetics onto HAIX-F media was undertaken using the experimental batch setup shown in Figure 2.5-2.7.

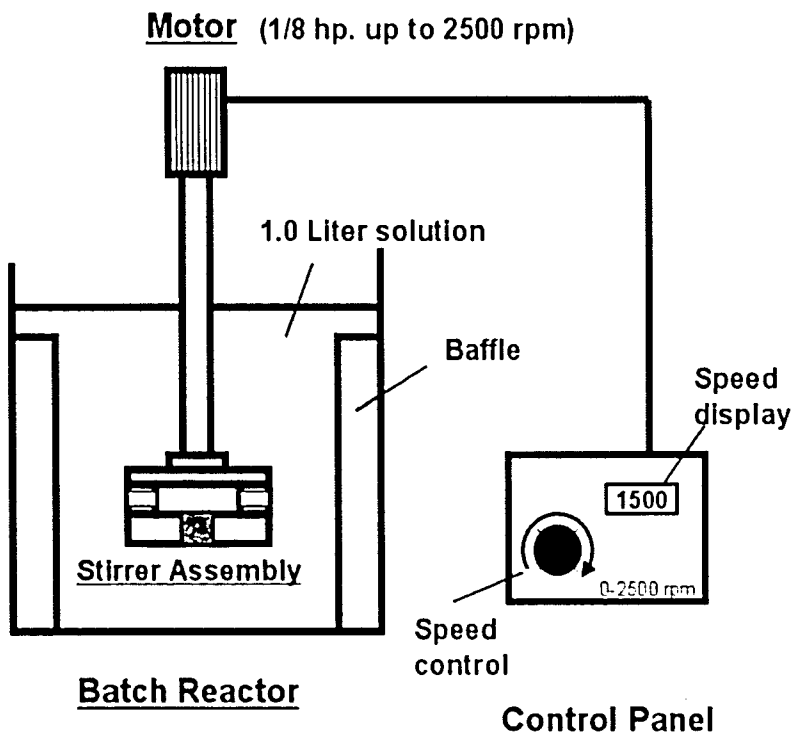


Figure 2.5 – Schematic of Kinetic Test Set-Up

Basically, a baffled container containing exactly one liter of solution (oxalate, phthalate, or NOM with background chloride and sulfate concentrations) is stirred with a device containing the active media. A motor/control panel allows for adjustable stirring speeds; these experiments typically utilized a stirrer speed of 1500 ($\pm 0.33\%$) rpm. The actual stirrer assembly is detailed more clearly in Figure 2.6.

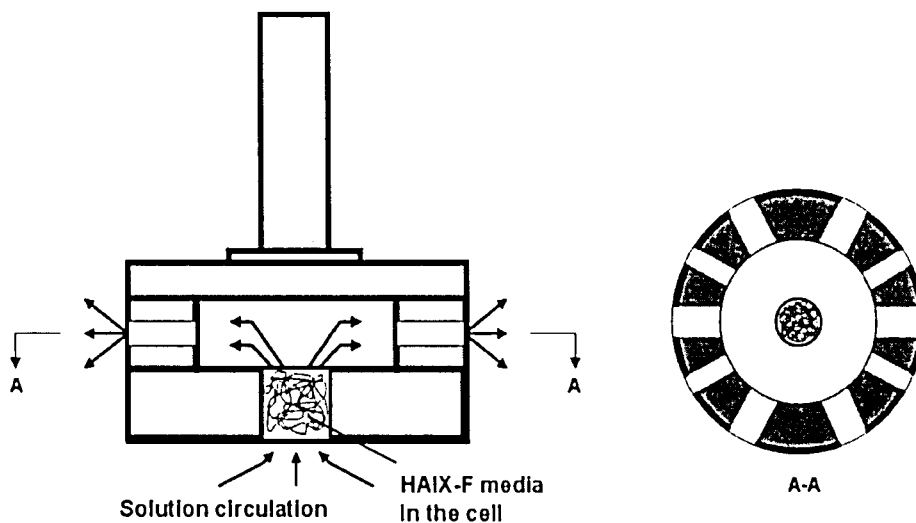


Figure 2.6 – Detailed Illustration of Stirrer Assembly

As the stirrer spins, water from the baffled container is drawn up through a mesh screen at the assembly's bottom center. This water then passes through a chamber (enclosed on top and bottom with fine mesh, enclosed on sides by plastic), containing the HAIX-F media. Clearly, sorption processes occur in this chamber. Then, as described by the flow lines in Figure 2.6, water continues into a larger chamber directly above the media-containing cell and subsequently flows out of the stirrer unit via radial holes.

The elevated stirrer speed produces strong centrifugal currents around the HAIX-F media, effectively eliminating any liquid film on the fibers. The elimination of said liquid film, allows intraparticle diffusion to be the kinetically limiting means [Li and SenGupta, 2000]. Therefore, any kinetic data will detail the migration of contaminant molecules onto the HAIX-F

media, and subsequently into the HAIX-F media. The theory involved with this experimental procedure was originally developed by Kitchener and later described by Helfferich [Helfferich, 1962].

For our purposes, the contaminant compound (oxalate, phthalate, or NOM) was present at approximately 2.0 ppm; furthermore, the background anions, chloride and sulfate, were present at approximately 100.0 ppm and 20.0 ppm, respectively. At determined time intervals, small volumes (less than 5.0 mL/sample) were extracted for analysis; compound concentrations within the solid phase (i.e., HAIX-F) were calculated from mass balance as volatilization at given pH, temperature, and pressure was not feasible. Solution pH was maintained in the range 6.0-7.0.

A photograph of the actual set-up and stirrer assembly for this experiment is shown below in Figure 2.7.

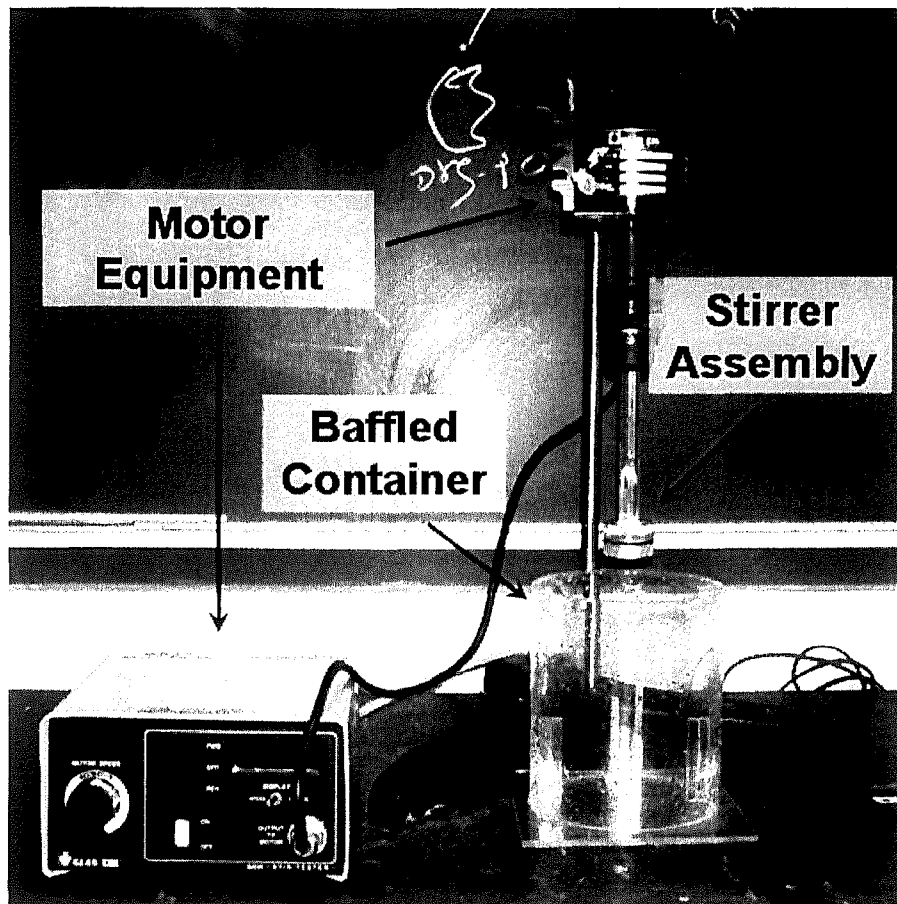


Figure 2.7 – Labeled Photograph of Kinetic Test Equipment

2.6 Analytical Equipment

The following sections describe the analytical equipment utilized for measurement of species (Cl^- , SO_4^{2-} , and TOC) involved in the experimentation reported later (Chapter 3). General protocol for each equipment is also provided.

2.6.1 Shimadzu TC/TOC Analyzer

During the course of the project, this machine was often utilized to determine the total organic carbon concentration of various samples. See Figure 2.8 for photo of unit. A detailed explanation of the analytical protocol will be avoided here for the sake of brevity; however, a general protocol is provided below. It should be noted that the NOM brine mentioned above contained 5200 mg/L DOC; in accordance with Symons and co-workers description, DOC represents a majority of TOC and can therefore be utilized as a surrogate measure of TOC [Symons et al., 2000].

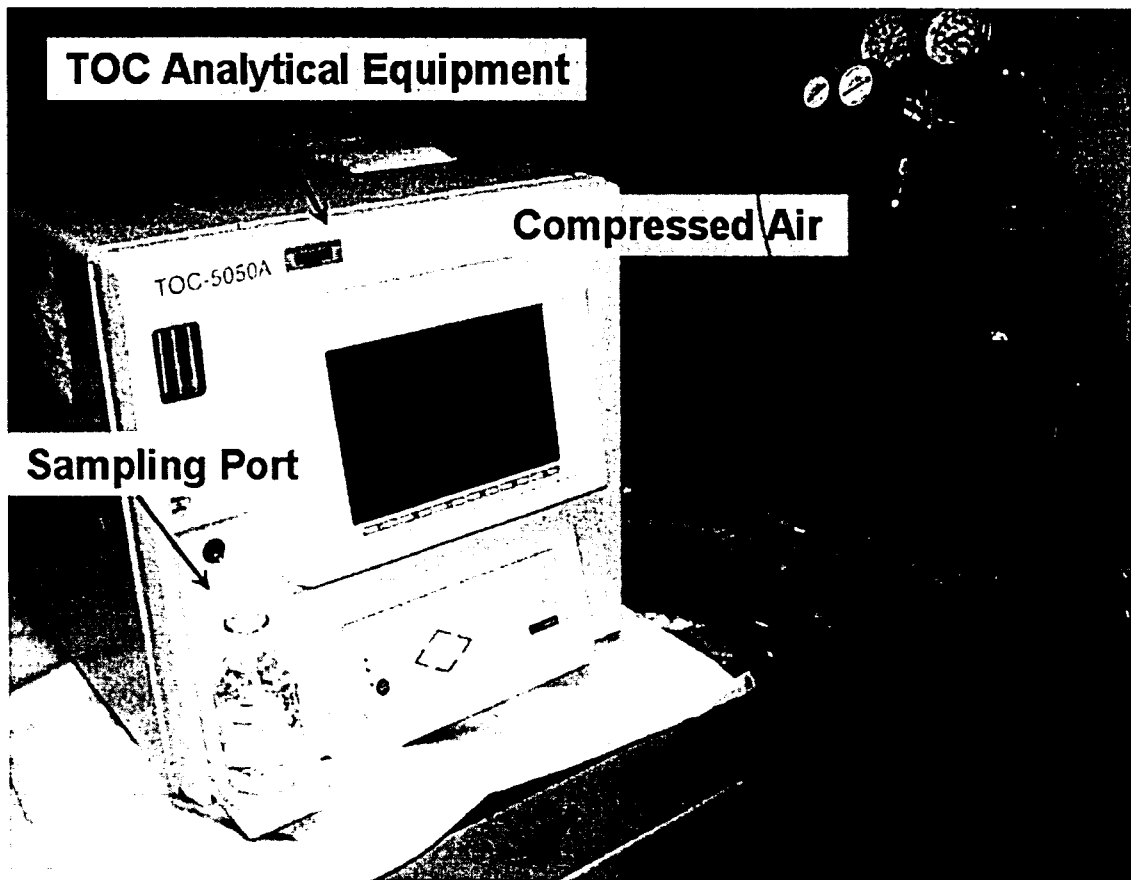


Figure 2.8 – Labeled Photograph of Shimadzu TC/TOC Analyzer

2.6.1.1 General TOC Analyzer Protocol

- Turn machine/furnace on and allow adequate warm-up time
- Condition the equipment by passing a 2N hydrochloric acid solution for multiple (10) injections
- Calibrate the machine using stock standards
 - Standards employed for these analyses include 0, 5, 10, and 100 ppm TOC.
 - A three-point calibration (0, 10, and 100 ppm TOC) was utilized for batch studies
 - A three-point calibration (0, 5, and 10 ppm TOC) was utilized for column studies
 - Three (3) injections were made for each standard to ensure accurate readings
- Analyze samples
 - Two (2) injections were made for each sample to ensure accurate readings
- Analyze a deionized water sample (two injections) to ensure accuracy of the machine
- Turn off furnace and allow a suitable cool-off time before shutting equipment down

The 2N hydrochloric acid solution was obtained from Shimadzu at the time of equipment purchase.

2.6.2 Perkin Elmer Ion Chromatograph

The Ion Chromatograph (IC) was the main analytical tool utilized for this project. All samples taken for all experiments were analyzed in this machine. Oxalate, phthalate, sulfate, and chloride are all eluted from the anionic column and can be calibrated against known standards to determine sample concentrations. See Figure 2.9 for photo of IC unit. A general protocol for the

equipment follows:

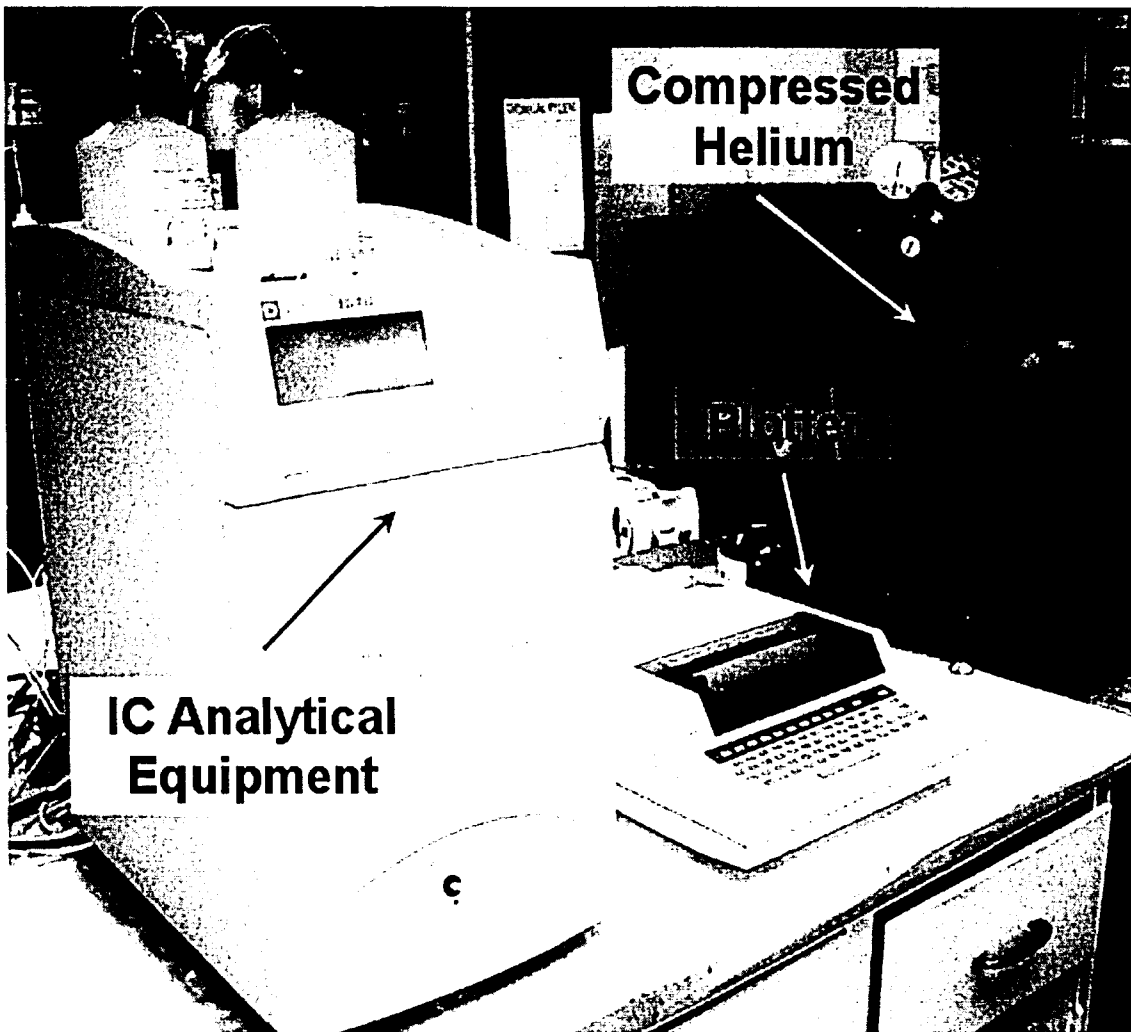


Figure 2.9 – Labeled Photograph of Perkin Elmer Ion Chromatograph

2.6.2.1 General Ion Chromatograph Protocol

- Ensure that the anion eluent reservoir is amply full
 - The anion eluent is composed of 52.5 mM Na_2CO_3 and 15 mM NaHCO_3
- Turn machine on and allow suitable warm-up time
- Inject a sample of deionized water to flush the tubing and ensure no carry-over effect

from previous runs

- Inject known standards and create a calibration curve based off of the results (area under peak) provided by the attached integrator
 - Standards employed for these analyses include:
 - One: 1 ppm oxalate, 10 ppm sulfate, 50 ppm chloride
 - Two: 3 ppm oxalate, 30 ppm sulfate, 150 ppm chloride
 - Three: 1 ppm phthalate, 10 ppm sulfate, 50 ppm chloride
 - Four: 3 ppm phthalate, 30 ppm sulfate, 150 ppm chloride
- Analyze samples and calculate the concentration from calibration curve
- Inject a sample of deionized water to flush the lines
- Turn machine off

Although timing of the ionic compound peaks could not be directly calculated, the relative timing of the peaks could be determined by relative ion exchange affinities. This theoretical determination was later verified using solutions containing only one of the above compounds (oxalate, phthalate, sulfate, or chloride) in order to find approximate elution times.

2.6.3 UV/VIS Spectrometer

Some effluent samples from fixed-bed column experimentation employing HAIX-F media towards removal of organic carbon from dilute NOM brine were analyzed using UV/VIS spectrometry on the Perkin Elmer UV/VIS Spectrometer Lambda 2. The open literature contains numerous examples of accurate analytical techniques employing UV/VIS spectrometry at a wavelength of 254 nanometers [Morran et al., 1996; Matilainen et al., 2002; Abbt-Braun and

Frimmel, 1999; Her et al., 2002]. For that reason, sample analyses were completed using UV/VIS methodology and compared to IC and TOC data for accuracy purposes. Figure 2.10 provides a photograph of the UV/VIS spectrometer used for this analysis.

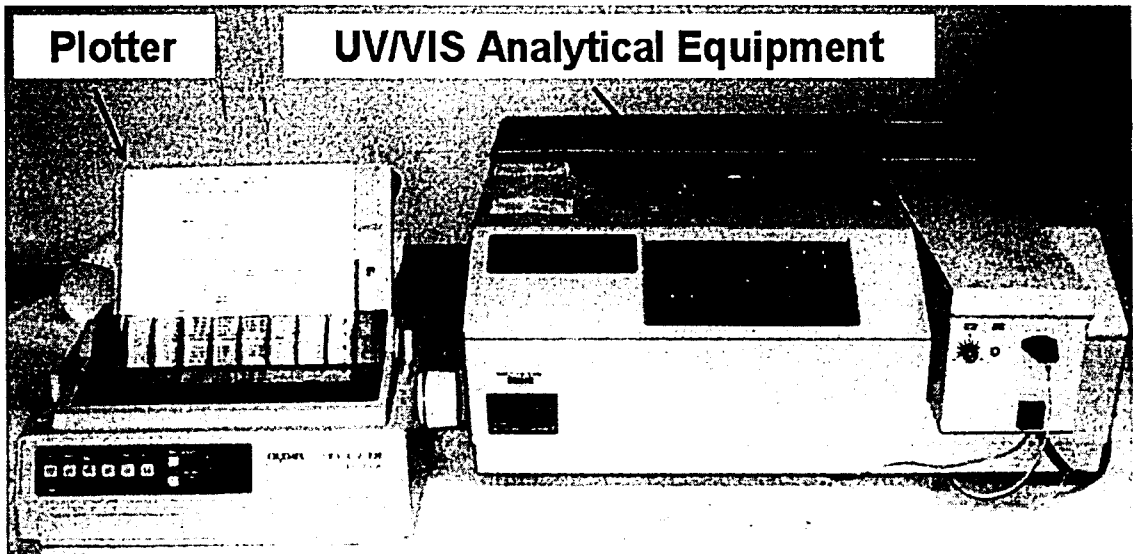


Figure 2.10 – UV/VIS Spectrometer Analytical Equipment and Plotter

2.6.3.1 General UV/VIS Spectrometer Protocol

- Turn machine on and allow suitable warm-up time
- Create a method, which allows for determination of UV/VIS absorbance at a wavelength of 254 nanometers
- Fill the measurement vial with DI water and analyze for background correction factor determination
- Analyze known standards and create a calibration curve based off of the results (area under peak) provided by the attached integrator
 - Standards employed for these analyses include:

- One: 0 ppm TOC (DI water)
 - Two: 1 ppm TOC
 - Three: 10 ppm TOC
 - Four: 25 ppm TOC
- Analyze samples and calculate concentration from calibration curve
 - Occasionally analyze DI and standards as quality check
 - Turn machine off

CHAPTER 3: RESULTS

The following section details the results of all experimental methods described in Chapter 2. Extensive detail regarding significance of findings will be provided.

3.1 Initial Batch Experiments

In order to determine an approximate capacity, batch tests were initially performed. The first test was completed using HAIX-F(Fe) media submersed in 100 mL samples dosed with NOM, sulfate, and chloride. From Figure 3.1, the NOM concentration present within the aqueous phase can be readily observed as dropping over the 24 hour test; influent conditions, as well as pH data, are present within the subset. From these data, an approximate NOM-capacity of 12.778 mg TOC/g HAIX-F(Fe), or 6.203 mg TOC/mol Fe³⁺, was found. These results provided promising information regarding the applicability of HAIX-F media utilization towards removal of NOM compounds from drinking water streams. Although a small amount of sulfate was sorbed, the relative amount compared to NOM sorption cannot compare. This negligible sulfate sorption demonstrates sorption affinity of NOM compounds over competing anions. The rise in chloride concentration is likely due to chloride ion expulsion from sorption sites (HAIX-F(Fe) media was originally in chloride form). There was also a slight rise in pH; however, as pH for all subsequent experimentation indicated gradual pH drop over time, this detail is negligible.

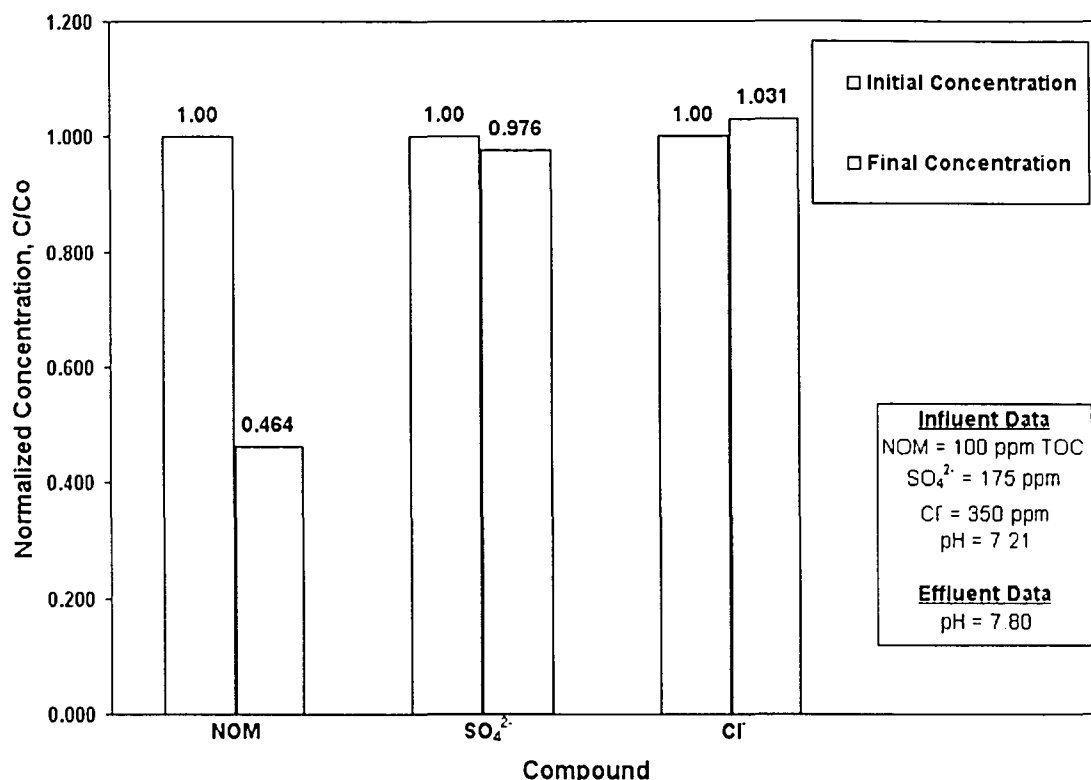


Figure 3.1 – Results of Batch Tests with Diluted NOM Brine

Consider fulvic acid, a well known natural organic matter; while there is no abiding molecular formula for fulvic acid (section 1.1), one typically utilized makeup demonstrates the properties of NOM that relate to its capability of being sorbed. Figure 3.2 presents a chemical representation of the compound, with carboxyls, hydroxyls, nitrogens, and double-bonded oxygen atoms highlighted. These chemical groups, upon deprotonation, become anionic in nature and can, therefore, be treated using media, such as HAIX-F. Such properties are what allow for coagulation using ferric or aluminum based salts. The metal cation binds with negatively charged organic matters and precipitates out. Per design, HAIX-F media contains active groups with HFO or HZO nano-scale particulates providing active sorption sites; these groups operate as Lewis acids. Therefore, the carboxylic groups present in fulvic acid (and NOM compounds, in general) can form inner-sphere complexes via LAB interaction mechanisms with Lewis acids (i.e., metal

ions). This interaction mechanism has been described in detail in section 1.4.2. It should be noted that the dominant Lewis base groups are likely carboxyl groups due to low relative pK_a values.

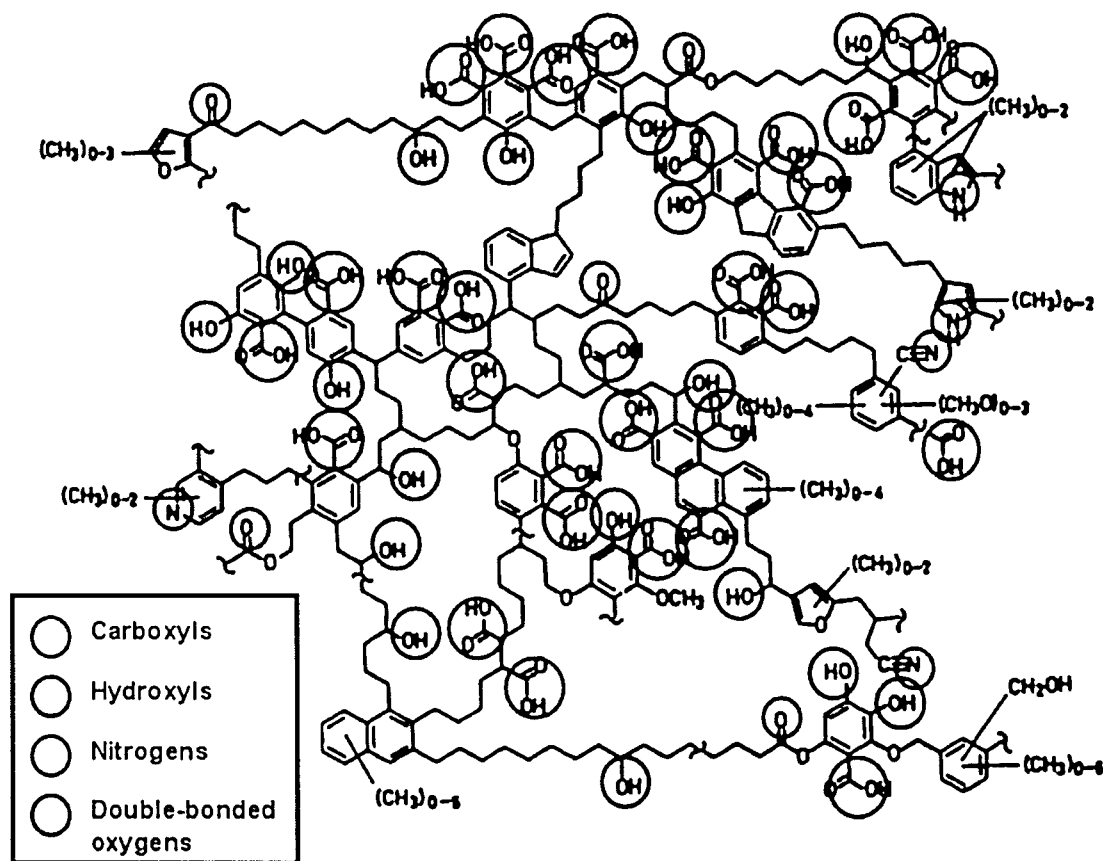


Figure 3.2 – Fulvic Acid Molecular Schematic Labeled with Reactive Sites

From earlier studies, the sorption affinity of HAIX resins for other ligands, namely, arsenic and phosphorus, has been shown to demonstrate excellent characteristics. The arsenic and phosphorus species of interest are bidentate arsenate and phosphate, which are shown in Figure 3.3 along with available binding mechanisms onto HFO sorption sites.

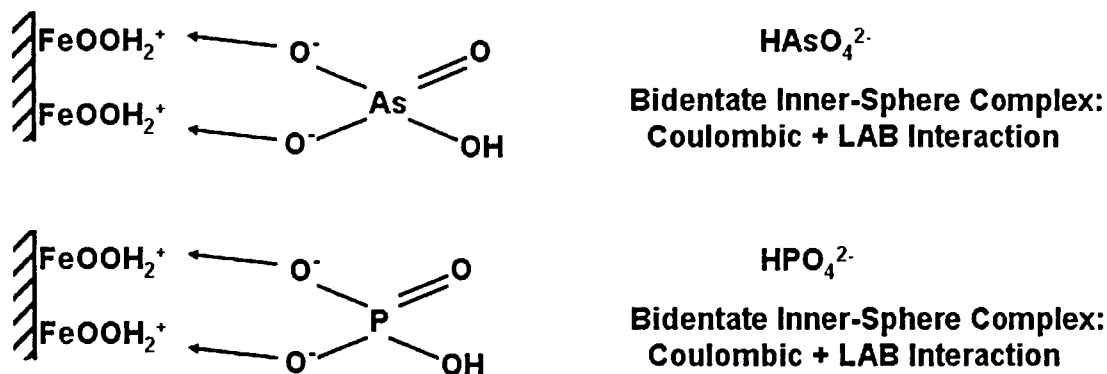


Figure 3.3 – Arsenate and Phosphate Interaction with HFO Sorption Sites

Clearly, the presence of carboxylic groups permits both Coulombic and LAB interaction to occur. Therefore, the choice to employ oxalate and phthalate as surrogate NOM species throughout this project was deemed attractive. The chemical speciation for these compounds was given in section 1.5, both compounds contain two carboxylic groups at near neutral pH; however, phthalate also contains a benzene ring.

Due to the relatively similar chemistry, hydrous zirconium oxides exhibit the same abilities as HFO particulates. In sections 1.4-1.5, these similarities were thoroughly discussed and do not require mention here.

A batch test with oxalate was performed in similar fashion as the NOM experiment described above. Approximately 250 mg of HAIX-F(Fe) or HAIX-F(Zr) was immersed in a 100 mL solution containing approximately 250 mg/L of oxalate with background concentration. The calculated uptake capacities are detailed in Table 3.1. Clearly, HAIX-F(Fe) media demonstrate greater sorption capacity than HAIX-F(Zr). Note, that *M* represents the specific metal, Fe(III) or Zr(IV). Note that the final column of Table 3.1 provides meq of oxalate removed per meq of metal ion (iron or zirconium) present in HAIX-F phase.

Table 3.1 – Results of Batch Tests with Oxalate

Material	Compound	Capacity (mg/g)	Capacity (meq/mol M⁺)	Capacity (meq/meq)
HAIX-F(Fe)	oxalate	47.838	0.528	0.176
HAIX-F(Zr)	oxalate	23.325	0.828	0.207

In order to further quantify the sorption of surrogate NOM compounds onto HAIX-F media, a batch test with solution containing both phthalate and oxalate species was undertaken. Again, 250 mg of fibers were submersed in 100 mL solution containing 250 mg/L of oxalate and phthalate with background anions. The results of this test, presented in Table 3.2, provide information regarding the preference of species. Obviously, phthalate is sorbed at a higher rate due to the presence of the benzene ring but some competition clearly takes place. It is important to note that compounds with higher carbon content experience better sorption; as surrogate NOM compounds utilized in this study are of smaller molecular weight as compared to typical NOM chemical makeup (see Figure 1.1), sorption abilities of HAIX-F in regards to oxalate and phthalate may slightly understate actual values. Again, M represents the specified metal element, Fe(III) or Zr(IV) and the final column represent meq of organic species removed per meq of metal ion present in HAIX-F media.

Table 3.2 – Batch Test Results with Competing Phthalate and Oxalate Species

Material	Compound	Capacity (mg/g)	Capacity (meq/mol M⁺)	Capacity (meq/meq)
HAIX-F(Fe)	oxalate	33.800	0.373	0.124
	phthalate	67.747	1.291	0.430
HAIX-F(Zr)	oxalate	13.848	0.153	0.038
	phthalate	81.235	1.548	0.387

3.2 Initial Column Experiments

3.2.1 HAIX-F(Fe) Column Run with Dilute NOM Brine

From the promising results presented in Tables 3.1-3.2, HAIX-F selectivity for organic compounds such as oxalate and phthalate over sulfate and chloride was determined. Furthermore, Figure 3.1 provided direct evidence of NOM sorption onto HAIX-F. In order to observe the behavior of such media in fixed-bed configuration, a column run was prepared. NOM effluent history from this fixed-bed column experiment is shown in Figure 3.4; the subset describes influent conditions as 5 ppm TOC, 100 ppm sulfate, and 100 ppm chloride.

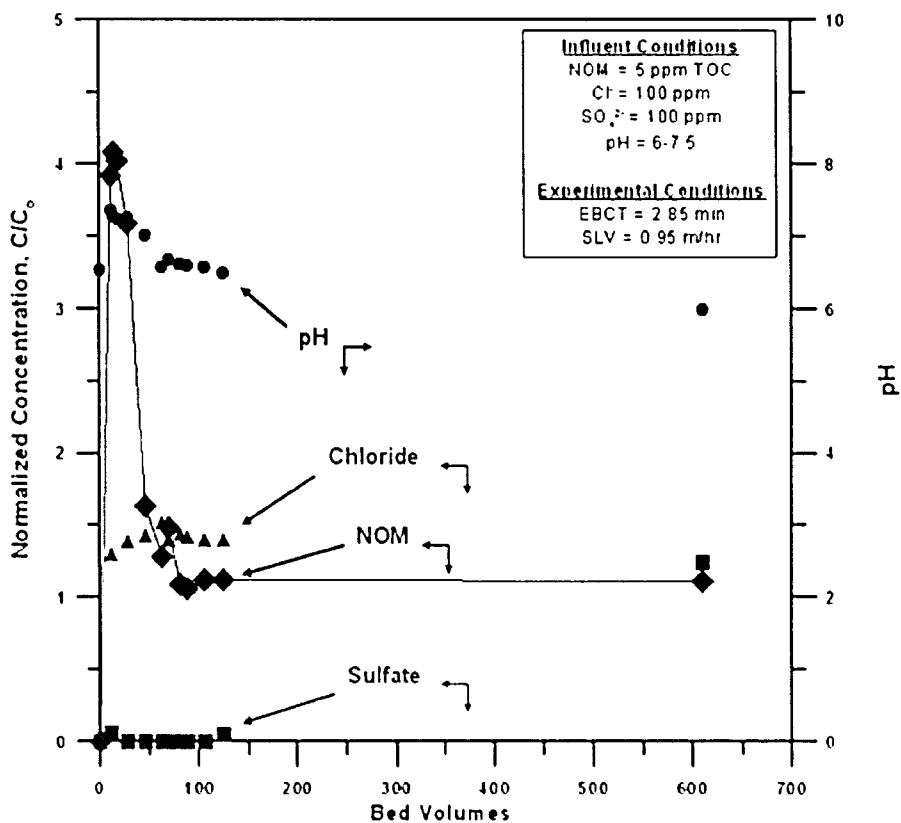


Figure 3.4 – NOM Effluent History from Fixed-Bed Column Experimentation

The results of the NOM column run provided extremely confusing results. Essentially, the effluent history curve demonstrated an initial breakthrough of NOM; later, chloride and sulfate breakthrough are observed. The pH curve follows the trends of the NOM curve. The authors can provide no definite explanations as to the odd nature of these results, provided results of the NOM batch experiment presented in Figure 3.1. The open literature recognizes that NOM contains various organic compounds, as demonstrated in Figure 3.5. One possible explanation for phenomena observed in Figure 3.4 is that hydrophilic species were overly present in the NOM brine. Another explanation could be that sulfate species are more preferred compared to organic compounds present in NOM; however, batch experiments employing HAIX-F towards NOM removal showed affinity for NOM compounds. Further analysis and discussion of the results described in Figures 3.1 & 3.4 is provided in Chapter 4.5.

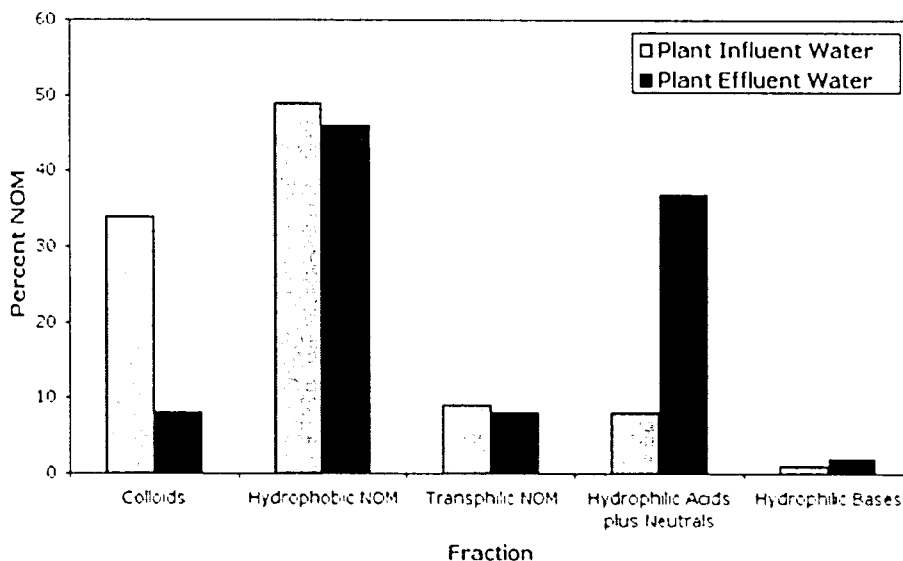


Figure 3.5 – Various NOM Fractions and Behavior in Water Treatment Processes

3.2.2 HAIX-F(Fe) Column Run with Oxalate Anion

From the NOM column run (Figure 3.4), applicability of HAIX-F media in fixed-bed scenarios towards removal of NOM and NOM surrogate compounds is in doubt. As the technology should provide ideal employment in such configuration (sections 1.4-1.5), a fixed-bed column experiment employing HAIX-F(Fe) media towards oxalate removal from aqueous solution was undertaken.

Influent conditions are as follows: 2 ppm oxalate, 20 ppm sulfate, and 100 ppm chloride at pH 7.0; operating conditions were maintained at empty bed contact time (EBCT) of 2.85 min and superficial liquid velocity (SLV) of 0.95 m/hr. The effluent history is depicted in Figure 3.6. Noticeably, results of this experiment were in accordance with data provided in Tables 3.1-3.2. The initial chromatographic elution of chloride suggests that it is the least selective compound (i.e., lowest separation factor); next, sulfate is eluted from the column. These occurrences suggest that HAIX-F exerts an affinity for oxalate over other competing species; therefore, results from Figure 3.4 need to be reassessed.

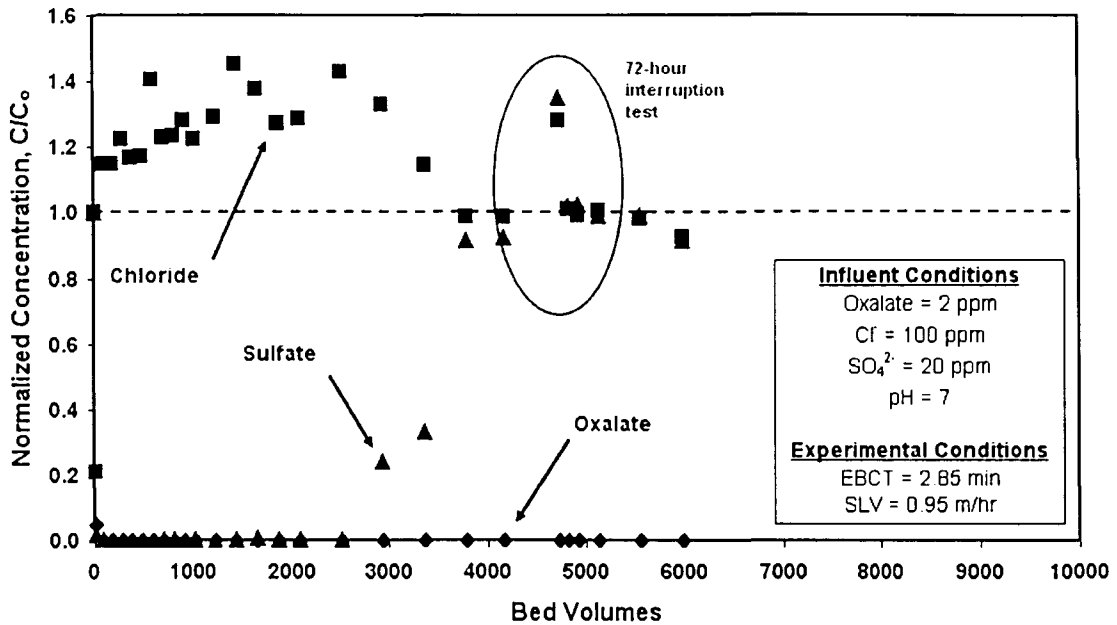


Figure 3.6 – Oxalate Effluent History for Initial Column Run with HAIX-F(Fe)

An interruption test conducted at approximately 4750 bed volumes demonstrated elution of sulfate and chloride concentrations. In less than 100 bed volumes, sulfate and chloride concentrations returned to influent levels, implying intraparticle diffusion is rate-limiting. During interruption organic species are permitted to infiltrate the media and diffuse into the fiber core; concurrently, chloride and sulfate species sorbed to inner-core HFO functional groups are expelled into solution, resulting in the observed concentration hike. Due to the gentle concentration gradient described in section 1.4.3, equilibrium is quickly achieved and sulfate and chloride concentrations rebound to influent levels. More results regarding HAIX-F sorption kinetics are provided in section 3.5.

Later data (bed volumes >6000) from the experiment described in Figure 3.6 showed that oxalate does not experience complete breakthrough. For that reason, some sort of degradation must be occurring within the experimental setup. No bacterial growth was observed in the reservoir bucket or on HAIX-F media and so consumption of organic carbon by biological

organisms is probably not the cause for oxalate degradation. As oxalate is a low-molecular weight organic compound, photo-oxidation of carbon-oxygen bonds may have occurred. It should be noted that quality checks were conducted throughout operation to ensure the stability of oxalate species in the influent reservoir. After the interruption test, quality checks revealed that oxalate concentrations in the reservoir experienced a considerable reduction. For that reason, a series of degradation tests were completed on the two surrogate NOM compounds utilized in these studies to ensure accuracy in recorded results.

3.3 Photo-oxidation Studies

Two solutions of 200 mL were prepared: (1) 50 ppm oxalate and (2) 50 ppm phthalate. These solutions were then divided into two new solutions, each of 100 mL; one of these solutions was kept at 4°C in the dark, the other remained on a laboratory bench (under artificial light conditions for normal working hours) at room temperature. After certain time periods, samples from each of the four bottles were taken and analyzed using Ion Chromatography and Total Organic Carbon Analyzer equipment.

3.3.1 Results from IC Analysis

Figure 3.7 provides results of oxalate degradation studies; note that data labeled “dark” were kept away from light sources and refrigerated, while “light” sample were kept on an open lab bench. Results offer very clear evidence that oxalate breaks down over time while exposed to artificial light sources; conversely, oxalate samples stored in the refrigerator do not exhibit any noticeable degradation. Such results demonstrate complications that arise from oxalate

employment as surrogate NOM compounds for these quantification and characterization studies; however, as many components of NOM present in surface water sources may exhibit similar qualities, experiments should be completed with oxalate species towards comprehension of complete picture of organic contaminant interaction with HAIX-F media.

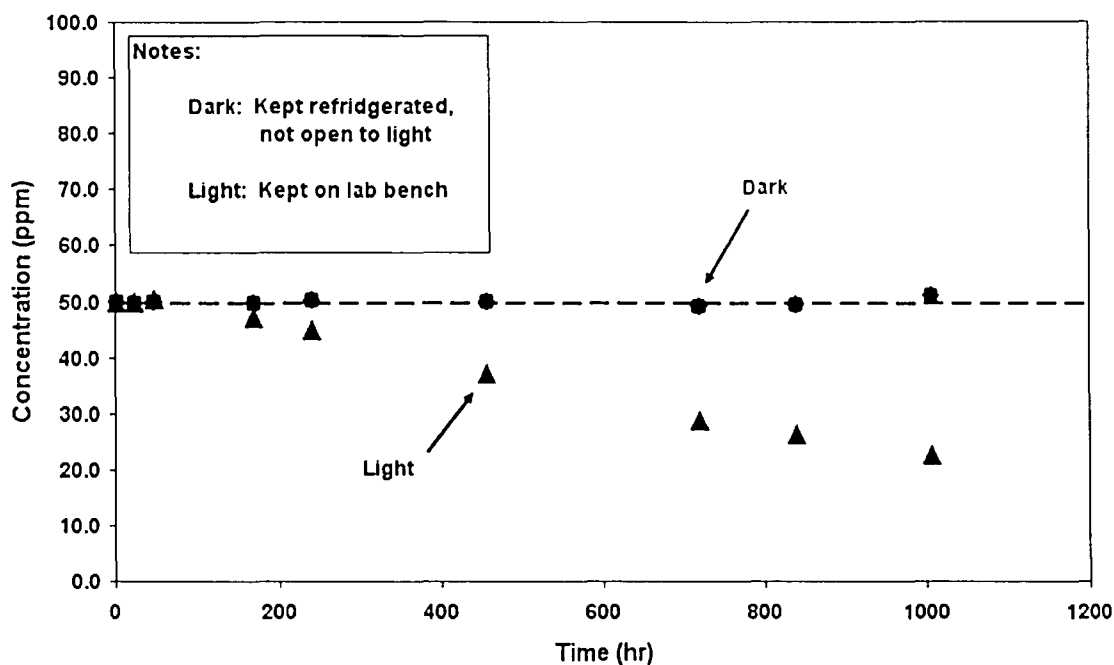


Figure 3.7 – Oxalate Degradation over Time

According to results shown in Figure 3.8, phthalate experiences much lower rates of photo-oxidation. Given that phthalate is a higher molecular weight organic compound containing an aromatic carbon ring, increased stability makes sense. Based on these results, phthalate experimentation should provide relatively accurate means of characterizing organic carbon treatment by HAIX-F. It should be noted that slight increases in phthalate concentration observed in Figure 3.8 can be attributed to experimental error.

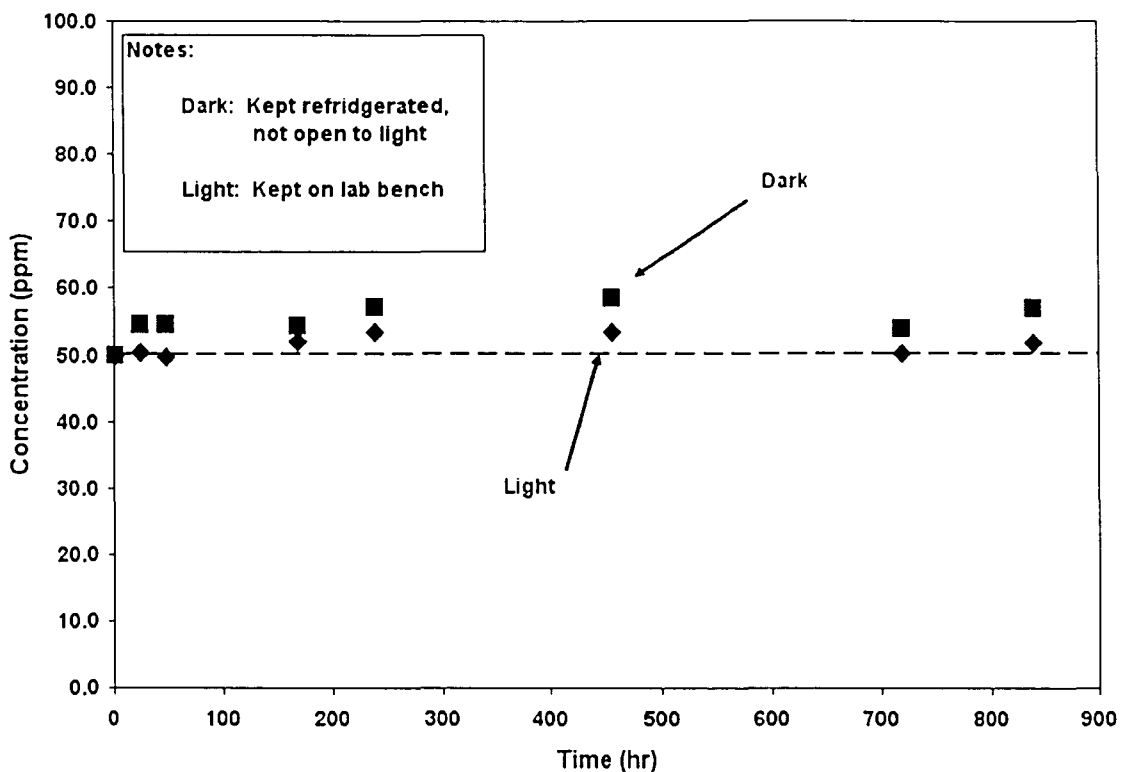


Figure 3.8 – Phthalate Degradation over Time

3.3.2 Results from TOC Analysis

Regardless of the presence/absence of oxalate oxidation, aqueous TOC concentrations should remain constant. From an enthalpy viewpoint, that oxidation reaction would not have enough energy for conversion of organic C(III) to inorganic C(IV), or $C_2O_4^{2-}$ to $2CO_2$. Therefore, some form of organic carbon should remain within the aqueous phase. Analysis of the same samples described in Figures 3.7-3.8 using Total Organic Carbon Analyzer equipment yields the results provided in Figure 3.9. Clearly, there is no loss of organic carbon for oxalate or phthalate samples; therefore, employing oxalate as a NOM-like compound should still provide meaningful results with regards to sorption of organic carbon compounds using HAIX-F. This fact provides

the motivation for continued employment of oxalate as surrogate NOM compound in subsequent experimentation. Note the precision of samples analyzed by TOC Analyzer; this subject will resurface later in the report (sections 3.5, 3.6, 3.7 & 4.5, specifically).

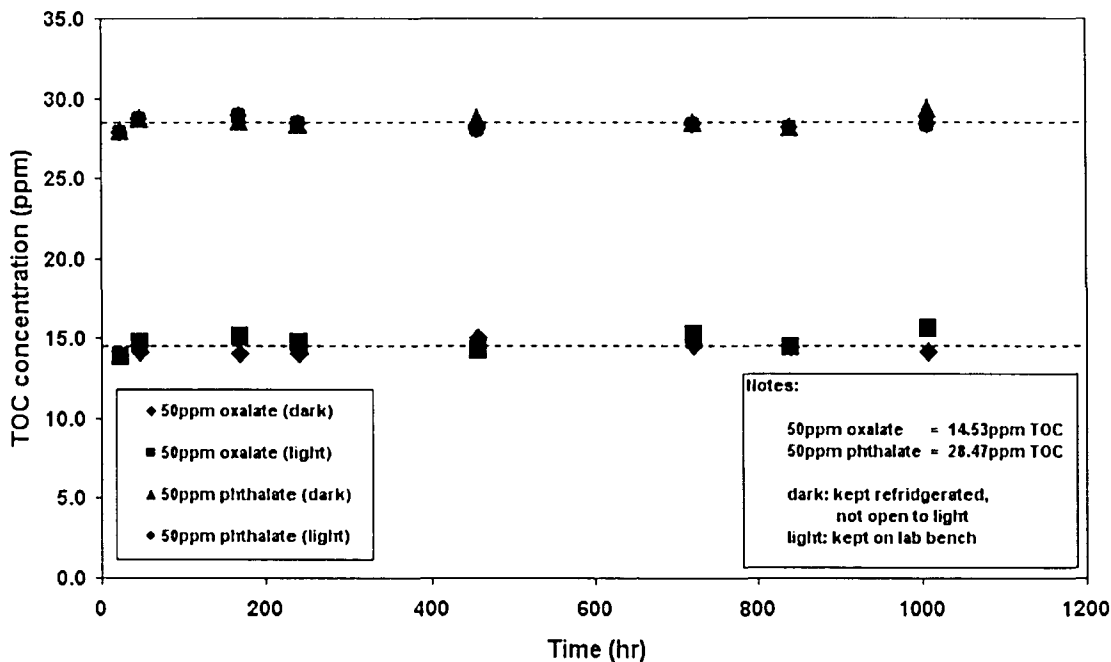


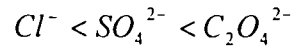
Figure 3.9 – Oxalate and Phthalate Degradation Curves Measured as TOC

3.4 Fixed-Bed Column Experimentation with HAIX-F Media

Fixed-bed column runs were completed in order to observe breakthrough patterns of oxalate, phthalate, and diluted NOM brine compared to background sulfate and chloride ions. An illustrated schematic of the plug-flow reactor setup is provided in Figure 2.4a; a photograph of the actual apparatus employed appears in Figure 2.4b. Notice that synthetic wastewaters are pumped from a five gallon bucket into the column, which contains HAIX-F; subsequently, the column's effluent is pumped into a fraction collector, allowing analysis of samples from different efflux

times/volumes.

The resultant effluent histories will provide the relative affinity of HIAX-F for the compounds mentioned above. For instance, if the relative affinity is



then, chloride will exit the column first, sulfate second, and oxalate third. Additionally, due to chromatographic elution effects, effluent chloride concentrations will surpass the influent concentration because chloride is effectively being flushed from the media. When sulfate exits, the chloride concentration will decrease; however, the concentration will still exceed the original concentration. Similarly, sulfate undergoes chromatographic elution. Finally, efflux of oxalate will cause all three compounds to return to their influent levels. Assuming instantaneous breakthrough due to plug-flow configuration, a generalized illustration of chromatographic elution concepts is provided in Figure 3.10.

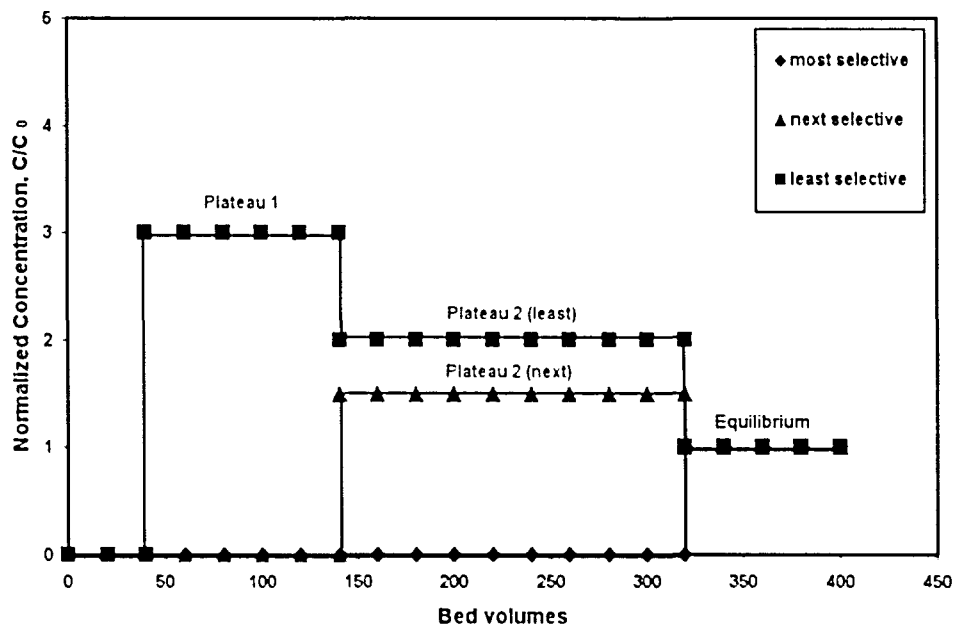


Figure 3.10 – Illustration of Chromatographic Elution Effects

Furthermore, by calculating the area between the influent history curve and the effluent history

curve, the capacity of HAIX-F for the three subject compounds can be evaluated. Consider equations 3-4,

$$A_i = \frac{1}{2} (C_{2,i} + C_{1,i}) \left(\frac{mg}{L} \right) \times (V_{2,i} - V_{1,i}) (L) \quad (3)$$

$$A_e = \frac{1}{2} (C_{2,e} + C_{1,e}) \left(\frac{mg}{L} \right) \times (V_{2,e} - V_{1,e}) (L) \quad (4)$$

where, A is area under the curve, C is concentration, V is volume of water passed, i is influent, and e is effluent. The equations described above utilize the trapezoidal method of calculating integrals. Essentially, the area under the influent curve is the amount of contaminant (i.e., oxalate, phthalate, or NOM) passed into the column. Hence, subtracting the amount of contaminant in the effluent from the amount of contaminant in the influent provides the amount of contaminant sorbed to HAIX-F media (equation 5). Of course, this method assumes that there are no other mechanisms removing the contaminant from the influent water (i.e., degradation). Then,

$$q' (mg) = A_i (mg) - A_e (mg) \quad (5)$$

where, q' is the amount of contaminant sorbed onto HAIX-F media. Utilizing this variable in coordination with the amount of HAIX-F employed, the breakthrough and total capacity of HAIX-F for a given contaminant can be calculated. For this study, breakthrough capacity is described by equation 6; total capacity (equation 7) is the amount of oxalate removed per gram of HAIX-F as calculated using the trapezoidal integration technique.

$$q_b \left(\frac{mg}{g} \right) = 0.2 \times \frac{A_i (mg) - A_e (mg)}{m (g)} \quad (6)$$

$$q_t \left(\frac{mg}{g} \right) = \frac{A_i (mg) - A_e (mg)}{m (g)} \quad (7)$$

where, q_t is the total capacity, m is the amount of HAIX-F employed, and q_b is the breakthrough

capacity.

The fixed-bed column runs, as described in section 2.4, were conducted by placing a known amount of HAIX-F into a glass column and pumping synthetic wastewater through that media. Samples were collected via fraction collector, and analysis of the effluent was completed towards construction of effluent history curves. In order to accurately compare different effluent histories, two experimental parameters must be maintained. Superficial liquid velocity (SLV) is essentially the Darcy velocity, as shown in equation 8. Empty bed contact time (EBCT) describes the amount of time it takes for flow to move through the bed (equation 9).

$$SLV = \frac{\text{Flow Rate (mL/min)}}{\text{Cross-sectional Area (cm}^2\text{)}} \quad (8)$$

$$EBCT = \frac{\text{Bed Volume (cm}^3\text{)}}{\text{Flow Rate (mL/min)}} \quad (9)$$

Clearly, low SLV allows for either (i) small flow rate or (ii) large cross-sectional area; conversely, high EBCT is witnessed when the (i) bed volume is very large or (ii) flow rate is rather small. Ideally, plug-flow reactors operate best under low SLV, high EBCT conditions because there is more contact time between the contaminant of concern and the employed media. Realistically, such operating conditions are not efficient; therefore, typical values of 2.0 cm/min and 1.0 min for SLV and EBCT are employed. The following experiments were all conducted at SLV and EBCT in this range to ensure accurate comparison of results (section 3.4.3).

During some of the fixed-bed column runs, interruption tests were performed. An interruption test is when flow to the column is shut off for a period of 24-72 hours. The effluent history curve's conduct directly after the interruption suggests the diffusion-limiting mechanism. For instance, if the curve quickly returns to its original path, intraparticle diffusion likely dominates; if a path parallel to the original occurs, kinetics are governed by liquid-film diffusion.

These concepts will be explored further in section 3.5.

3.4.1 Column Runs using HAIX-F(Fe)

The following fixed-bed runs employed HAIX-F(Fe) towards removal of organic DBP precursors, namely, oxalate, phthalate, and NOM.

3.4.1.1 Fixed-Bed HAIX-F(Fe) Oxalate Treatment

Figure 3.11 provides the normalized effluent history of a plug-flow experiment involving chloride, sulfate, and oxalate. Note that chloride and sulfate concentrations are 50 and 10 times greater than contaminant, oxalate, concentration. Clearly, HAIX-F(Fe) has the least affinity for chloride and the most selectivity for oxalate; furthermore, both chloride and sulfate undergo chromatographic elution verifying oxalate as the preferred species. Oxalate experiences breakthrough around 3000 bed volumes and slowly the effluent concentration increases until approximately $0.4C_0$. At this point, oxalate plateaus and effectively reaches equilibrium.

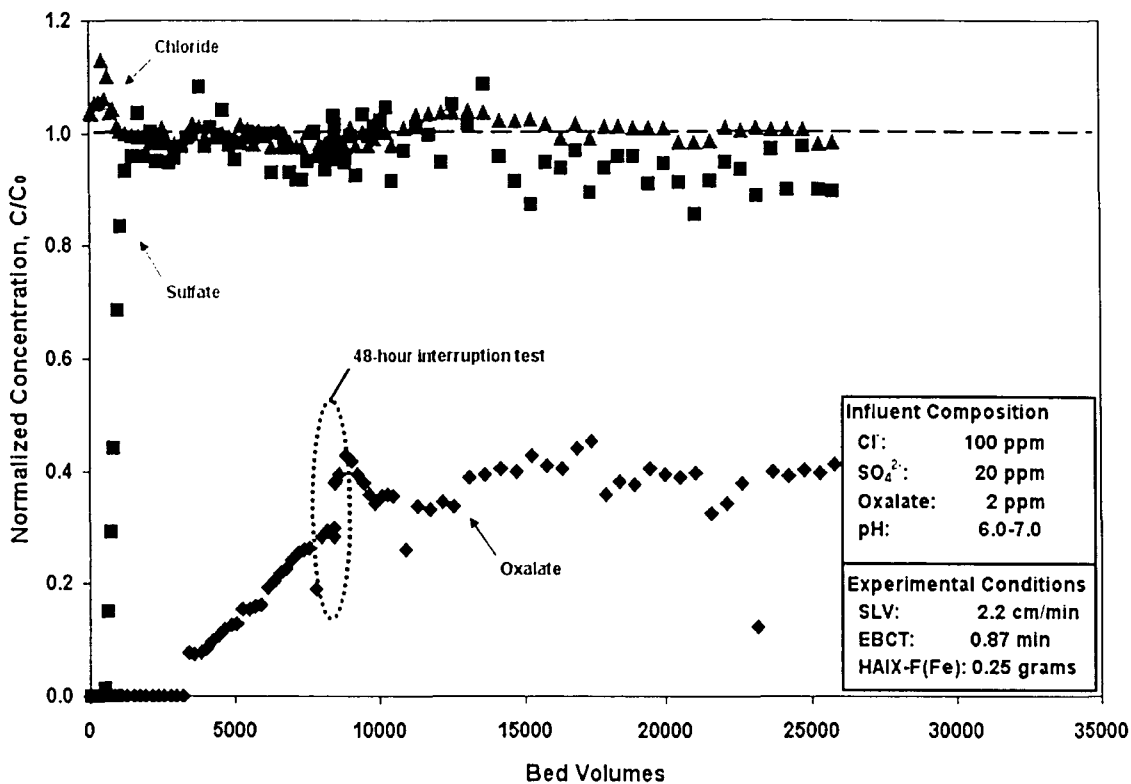


Figure 3.11 – Effluent History for HAIX-F(Fe) Run with Oxalate

Clearly, oxalate does not experience complete breakthrough. As described in sections 1.4-1.5 hydrous ferric oxide surface (and oxalate) chemistry changes with pH. At first, changes in pH were thought to be responsible for the incomplete oxalate breakthrough; however, analysis of sample pH showed no significant increase/decrease during operation. Analysis of the synthetic surface water present in the influent reservoir demonstrates that this degradation takes place before oxalate contact with HAIX-F(Fe). That finding prompted the photo-oxidation studies described in section 3.3. As these concepts have already been discussed at length, they will be neglected here.

At approximately 8400 bed volumes, a 48-hour interruption test was executed. Figure 3.11 shows that this test had almost no impact whatsoever on the effluent history curve as the path recovered in less than 10 bed volumes. Such rapid rebound describes intraparticle diffusion.

Section 3.5.1.1 will verify that intraparticle diffusion is the limiting oxalate sorption mechanism.

Finally, utilization of the trapezoidal integration technique described in equations 3-7 demonstrates that HAIX-F(Fe) demonstrates a breakthrough capacity of 16.79 mg oxalate per gram of HAIX-F(Fe) [4.58 mg TOC/g HAIX-F(Fe) or 0.185 meq/mol Fe^{3+}] and a total capacity of 23.31 mg oxalate per gram of HAIX-F(Fe) [6.36 mg TOC/g HAIX-F(Fe) or 0.257 meq/mol Fe^{3+}]. Total capacity was significantly less (% difference = 51%) than that found in Table 3.1. The total amount of oxalate removed is 11.65 mg oxalate or 3.18 mg TOC. It should be noted that capacity was calculated at the oxalate concentration peak present at ~9000 bed volumes.

3.4.1.2 Fixed-Bed HAIX-F(Fe) Phthalate Treatment

As complications arose during the oxalate fixed-bed column experiment, a second organic anion, phthalate, was utilized to determine accurate breakthrough characteristics with HAIX-F(Fe) media. The normalized effluent history of a plug-flow experiment involving HAIX-F(Fe) with synthetic surface water consisting of the anionic species chloride, sulfate, and phthalate is presented in Figure 3.12. Again, chloride and sulfate concentrations are drastically greater than the contaminant, phthalate, by 50 and 10 times, respectively. HAIX-F(Fe) has the greatest affinity for phthalate; furthermore, both chloride and sulfate undergo chromatographic elution verifying phthalate as the preferred species. Phthalate breakthrough comes at approximately 2500 bed volumes and follows a nicely-shaped “s” curve, which is a typical characteristic of plug-flow configuration, until complete breakthrough at about 6000 bed volumes. Then, phthalate concentration plateaus and effluent and influent streams reach effective equilibrium; essentially, the media is completely exhausted and maximal phthalate sorption has been achieved.

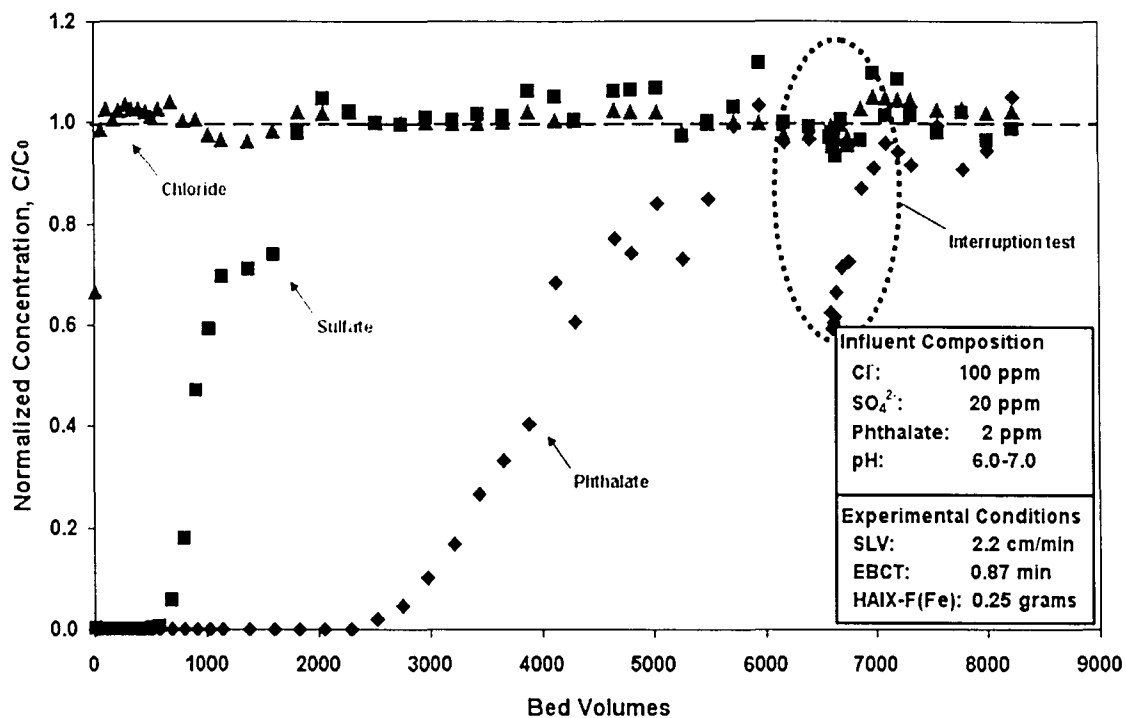


Figure 3.12 – Effluent History for HAIX-F(Fe) Run with Phthalate

Effluent pH history demonstrated no significant trends throughout the course of this experiment. However, during initial phthalate breakthrough (~2500 bed volumes) a slight drop in pH occurred and immediately after the interruption test a slight increase in pH was observed. These results are probably caused by the presence of ion pairs within the anion exchange media. Likely, during phthalate breakthrough, chloride-hydrogen or sulfate-hydrogen ion-pairs were expunged from the media, resulting in the small pH decrease upon ion separation in solution. During the interruption test, anionic species migrated into the HAIX-F(Fe) media; that diffusion probably allowed some chloride-hydrogen or sulfate-hydrogen ion-pairs to form and penetrate the media, hence the observed pH increase.

At approximately 6500 bed volumes, a 72-hour interruption test was executed towards comprehension of kinetic limitations. From Figure 3.12, the test had a clear and definite impact on phthalate effluent history; however, the curve recovered its original path after only 500 bed

volumes, suggesting intraparticle diffusion controls the sorption process. From the effluent history diagram, chloride and sulfate concentrations seem to decrease during the interruption test. Likely, HAIX-F media was able to sorb the phthalate remaining the standing liquid (i.e., solution remaining in the glass column) and sufficient sorption capacity was available for uptake of small amounts of chloride and sulfate. The chromatographic elution of chloride and sulfate immediately following the interruption verify these results. In order to obtain more reliable and quantitative data on the sorption kinetics of HAIX-F(Fe) media regarding phthalate removal, a kinetics test was completed; section 3.5.1.2 describes the results of that test.

Utilization of trapezoidal integration techniques presented in equations 3-7, allowed for calculation of HAIX-F(Fe) breakthrough capacity of 15.32 mg phthalate per gram of HAIX-F(Fe) [9.08 mg TOC/g HAIX-F(Fe) or 0.091 meq/mol Fe³⁺] and a total capacity of 19.05 mg phthalate per gram of HAIX-F(Fe) [11.29 mg TOC/g HAIX-F(Fe) or 0.113 meq/mol Fe³⁺]. The total amount of phthalate removed is 9.52 mg phthalate or 5.64 mg TOC. On a TOC basis, phthalate removal is more efficient compared to oxalate removal with HAIX-F(Fe). Given the problems associated with oxalate degradation, the TOC removal capabilities experienced with HAIX-F(Fe) treatment of phthalate contaminated water sources are considered more representative of actual capacity.

3.4.1.3 Fixed-Bed HAIX-F(Fe) NOM Treatment

Effluent history from the HAIX-F(Fe) run with dilute NOM brine is provided in Figure 3.4. As discussed above, an almost immediate chromatographic elution was experienced and then TOC concentrations dropped to approximately $C/C_0 = 1$. Such behavior is typical of poorly adsorbed species and may be explained by the fractionalization of NOM concentration as implied

in Figure 3.5.

Since no initial breakthrough or chromatographic elution effects were noted in fixed-bed experimentation with oxalate and phthalate compounds, the effects noted during the NOM column experiment must be related to NOM composition as proposed through discussion surrounding Figure 3.5. For that reason, breakthrough of various fractions of NOM (hydrophilic, transphilic, hydrophobic, etc.) probably occurs. Further comment on removal of NOM will be provided in section 3.4.2.3, which describes NOM removal via HAIX-F(Zr) fibrous media.

3.4.2 Column Runs using HAIX-F(Zr)

The following sections describe fixed-bed experiments employing HAIX-F(Zr) towards removal of surrogate NOM compounds or actual NOM recovered from New Zealand as described in section 2.1. Note that influent water properties and experimental operating conditions are similar to those employed in the preceding section, which dealt with HAIX-F(Fe) media. Furthermore, these experiments provide opportunity to compare organic carbon removal between HFO and HZO impregnated anion exchange fibers.

3.4.2.1 Fixed-Bed HAIX-F(Zr) Oxalate Treatment

Normalized results for the plug-flow experiment using HAIX-F(Zr) media towards removal of oxalate anion in the presence of background concentrations of chloride and sulfate can be found in Figure 3.13. From the legend, note that chloride and sulfate concentrations greatly exceed oxalate concentrations by 50 and 10 times, respectively. From relative breakthrough of chloride, sulfate, and oxalate species, results dictate that HAIX-F(Zr) has greatest affinity for

oxalate and least affinity for chloride; furthermore, both chloride and sulfate undergo chromatographic elution verifying oxalate as the preferred species. As with HAIX-F(Fe), oxalate experienced breakthrough at approximately 3000 bed volumes; effluent concentrations slowly rose until approximately $0.45C_0$, where oxalate concentration plateaus and effectively reaches equilibrium.

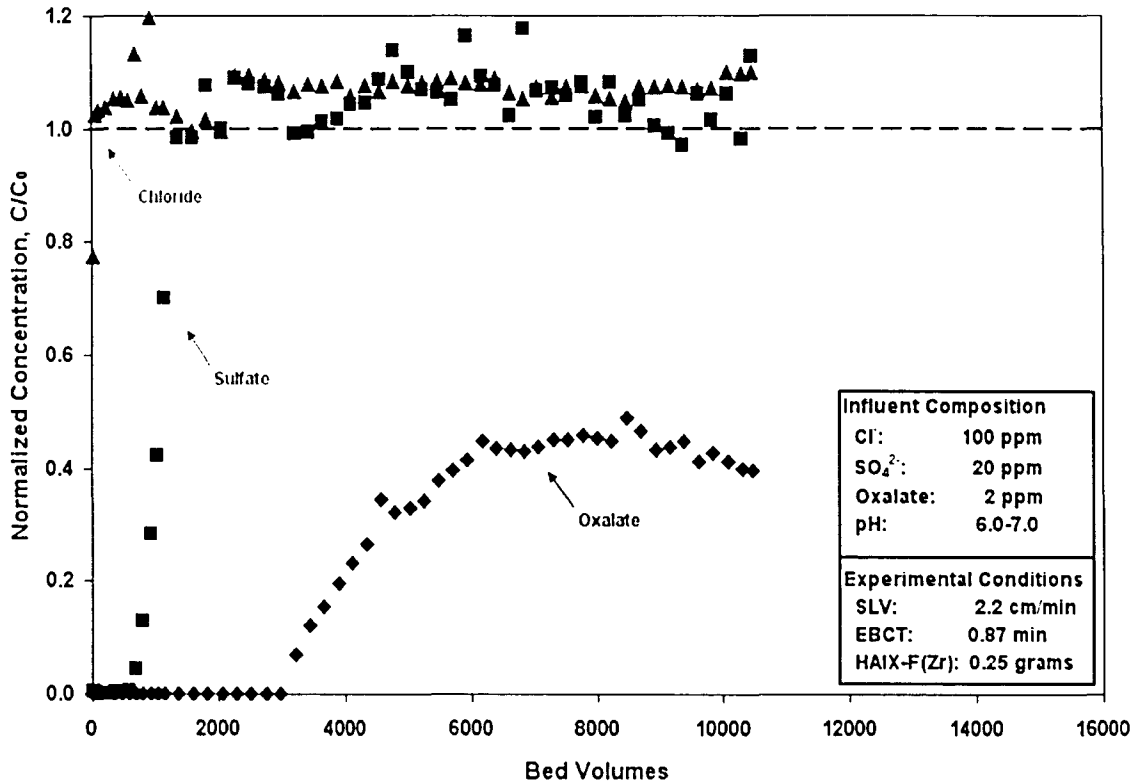


Figure 3.13 – Effluent History for HAIX-F(Zr) Run with Oxalate

Once more, oxalate does not experience complete breakthrough due to degradation of oxalate species in the influent reservoir. It should be noted that the influent reservoir was an opaque 5-gallon bucket that was capped with a lid; therefore, no extraordinary precautions were considered towards reducing light penetration as the apparatus should have exhibited such behavior in the first place. Analysis of samples demonstrated almost constant effluent pH values (~6.5) with very little variation. This fact confirms that oxalate degradation within the column is

not controlled by pH variations, which could theoretically alter HZO surface functionality or oxalate speciation as described by Figures 1.11-1.12.

For this particular experiment, no interruption tests were conducted. Effluent histories of involved anionic species follow almost identical breakthrough patterns as demonstrated by HAIX-F(Fe) media. As anion exchange fibers impregnated by HZO nanoparticulates should behave similarly to fibers doped with HFO and HAIX-F(Fe) column runs with oxalate exhibited behavior characteristic of intraparticle diffusion limited kinetics, interruption tests were not necessary for this experiment. Furthermore, previous studies with similar hybrid ion exchange media have exhibited intraparticle diffusion [Cumbal et al., 2003; Zhao and SenGupta, 1998; Li and SenGupta, 2000]. Section 3.4.2.1 provides results that verify this behavior.

Calculation of the area between influent and effluent history curves allows for determination of HAIX-F(Zr) capacity for oxalate uptake. HAIX-F(Zr) is found to exhibit a breakthrough capacity of 11.74 mg oxalate per gram of HAIX-F(Zr) [3.20 mg TOC/g HAIX-F(Zr) or 0.417 meq/mol Zr^{4+}] and a total capacity of 20.65 mg oxalate per gram of HAIX-F(Zr) [5.63 mg TOC/g HAIX-F(Zr) or 0.733 meq/mol Zr^{4+}]. Total oxalate uptake capacity was relatively similar (% difference = 11%) to that found in batch experimentation (Table 3.1). The total amount of oxalate removed is 10.32 mg oxalate or 2.82 mg TOC. Note that while HAIX-F(Fe) removes more TOC, HAIX-F(Zr) provides much better oxalate sorption on a *meq/mol M* basis. Comparisons of these results and related capacities exhibited by HAIX-F(Fe) media will be discussed in section 3.4.3.1.

3.4.2.2 Fixed-Bed HAIX-F(Zr) Phthalate Treatment

In order to better compare the capabilities and behavior of organic carbon sorption onto

HAIX-F media, a synthetic surface water consisting of phthalate, chloride, and sulfate was passed through HAIX-F(Zr) media; the results of this plug-flow experiment are provided in Figure 3.14. Observe that chloride and sulfate concentrations are an order of magnitude greater than phthalate, the contaminant of concern, concentration. Based on observations made from the effluent history diagram, it is clear that HAIX-F(Zr) prefers phthalate over background anions; chromatographic elution of chloride and sulfate verifies this observation. At approximately 2200 bed volumes, phthalate breakthrough occurred and effluent phthalate concentrations followed an “s”-shaped curve until complete breakthrough at 5000 bed volumes. At complete breakthrough, phthalate concentrations plateau at influent levels.

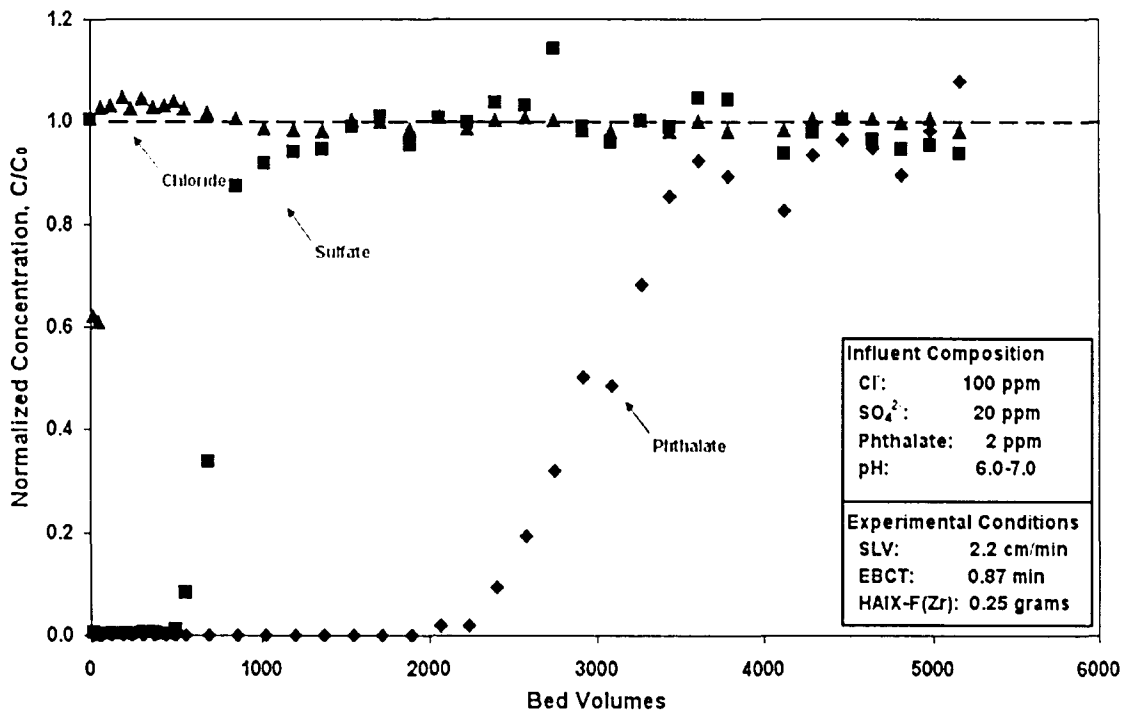


Figure 3.14 – Effluent History for HAIX-F(Zr) Run with Phthalate

Similar to results regarding phthalate uptake by HAIX-F(Fe), the fixed-bed experiment described in Figure 3.14 exhibited little variation in effluent pH. However, notable pH increases occurred at approximately 4000 and 5200 bed volumes; likewise, aqueous phthalate

concentrations experienced small reductions at the same points. The slight pH increases exhibited at these points allowed for more HZO functional groups to tend towards the point of zero charge (PZC) as mentioned earlier in Figure 1.11. Such an occurrence allows for more selective sorption of organic carbon compounds, like phthalate, due to higher prevalence of LAB interaction, which provides for selective sorption due to the inability of sulfate and chloride to form inner-sphere complexes (section 1.4.2). No definite explanation for the pH hikes can be offered; however, formation of ion-pairs and subsequent penetration into HAIX-F media may be the cause as mentioned in section 3.4.1.2.

For reasons similar to those expounded in section 3.4.2.1, no interruption tests were completed for this experimental run. Detailed information regarding the kinetics of phthalate sorption onto HAIX-F(Zr) media is provided in section 3.5.2.2.

HAIX-F(Zr) demonstrates a breakthrough capacity of 10.60 mg phthalate per gram of HAIX-F(Zr) [6.28 mg TOC/g HAIX-F(Zr) or 0.202 meq/mol Zr^{4+}] and a total capacity of 12.32 mg phthalate per gram of HAIX-F(Zr) [7.30 mg TOC/g HAIX-F(Zr) or 0.235 meq/mol Zr^{4+}]. The total amount of phthalate removed is 6.16 mg phthalate or 3.65 mg TOC. On a TOC basis, these values are slightly lower than corresponding TOC removal capacities for HAIX-F(Fe); however, it should be noted that uptake capacities are drastically greater on a *meq/mol M* basis. Comparison of HFO and HZO loaded anion exchange fibers will be discussed in section 3.4.3.2.

3.4.2.3 Fixed-Bed HAIX-F(Zr) NOM Treatment

Although, the column run employing HAIX-F(Fe) towards removal of dilute NOM solution provided in Figure 3.4 demonstrated failure based on almost immediate chromatographic elution of NOM, another experiment was completed using HAIX-F(Zr) media. This experiment

was completed using synthetic surface water solution containing 10, 20, and 100 ppm of TOC, sulfate, and chloride, respectively; effluent TOC history is provided in Figure 3.15. Due to low selectivity, chloride experiences an almost immediate breakthrough and undergoes chromatographic elution. Sulfate breakthrough occurs at approximately 300 bed volumes, which is similar to HAIX-F(Fe) results provided in Figure 3.4.

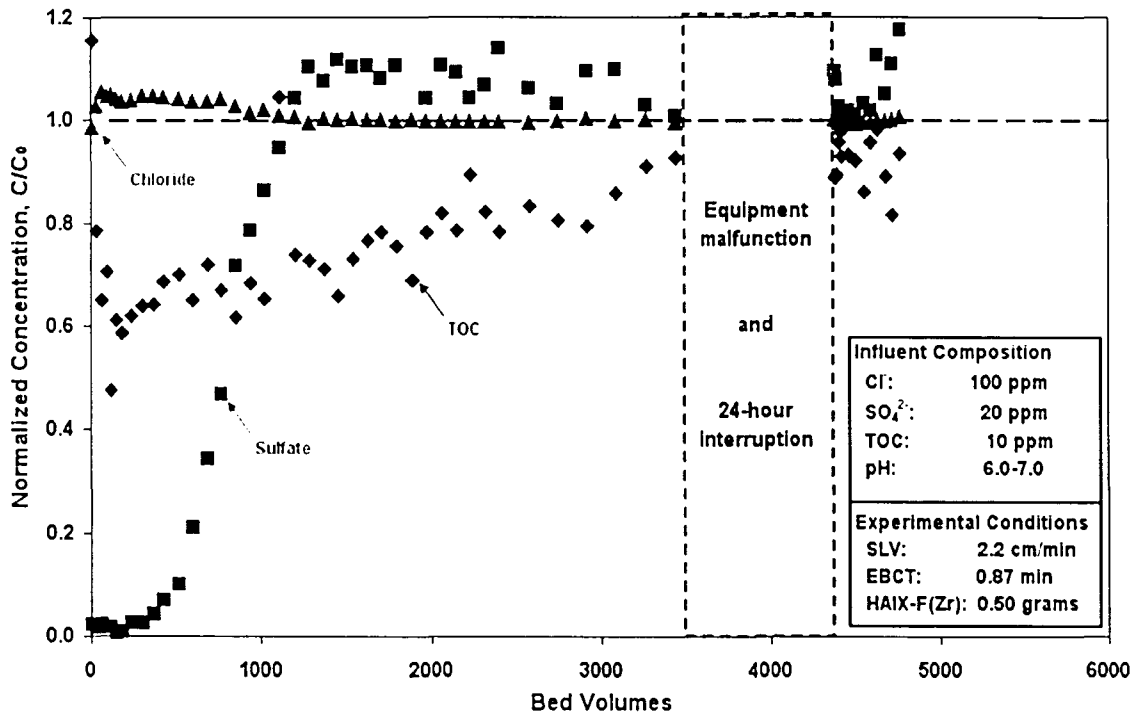


Figure 3.15 – Effluent History for HAIX-F(Zr) Run with Dilute NOM Brine

From Figure 3.15, it is clear that NOM undergoes an initial chromatographic elution; however, that elution is much shorter-lived (< 20 bed volumes) than its counterpart (~70 bed volumes), which occurred during the HAIX-F(Fe) run. Subsequent to this short chromatographic elution effect, effluent TOC concentrations drop to a minimum level and gradually rise throughout operation, which is typical of fixed-bed operation as seen from Figures 3.11-3.14. After 3500 bed volumes were passed through the HAIX-F(Zr) fixed-bed, an equipment malfunction occurred. Essentially, the wire that rotates the fraction collector apparatus sheered and the fraction collector

continued rotating about the same radial distance; therefore, samples on the outside of the test tube rack were contaminated by later effluent drops from the tubing and could not be accurately analyzed. The column was stopped for 24 hours. After column restart, some interesting phenomena occurred whereby aqueous sulfate concentration increased and aqueous TOC concentration decreased. Typically, TOC concentrations will decrease during interruption because of contaminant diffusion into the hybrid media (as seen in Figures 3.11-3.12). In this case, TOC concentration stayed constant through interruption and began decreasing after restart. Because quality checks on the influent reservoir solution did not demonstrate any degradation, no explanation can be given for these occurrences.

As opposed to oxalate and phthalate experimentation, complete TOC removal was not accomplished. Regardless, a total capacity of 33.03 mg TOC per gram HAIX-F(Zr) [51.60 mg TOC/mol Zr^{4+}] was calculated using equation 7. It should be noted that this capacity was determined from effluent history before equipment malfunction occurred. Reasons for incomplete TOC removal and initial chromatographic elution will be explained in section 4.5.

3.4.3 Comparison of HAIX-F(Fe) and HAIX-F(Zr)

3.4.3.1 Comparison of Fixed-Bed HAIX-F Oxalate Removal Experiments

Figure 3.16 provides superimposed normalized oxalate uptake (q_t/q_c) curves for HAIX-F(Fe) and HAIX-F(Zr) fixed-bed experiments: clearly, both media exhibit poor “s”-shaped curves due to the complications arising from oxalate degradation over time as discussed in sections 3.4.1.1 & 3.4.2.1. This fact means that oxalate uptake for both species exhibits poor plug-flow characteristics. Furthermore, both media exhibit almost identical curves, suggesting that oxalate

uptake abilities are pretty similar.

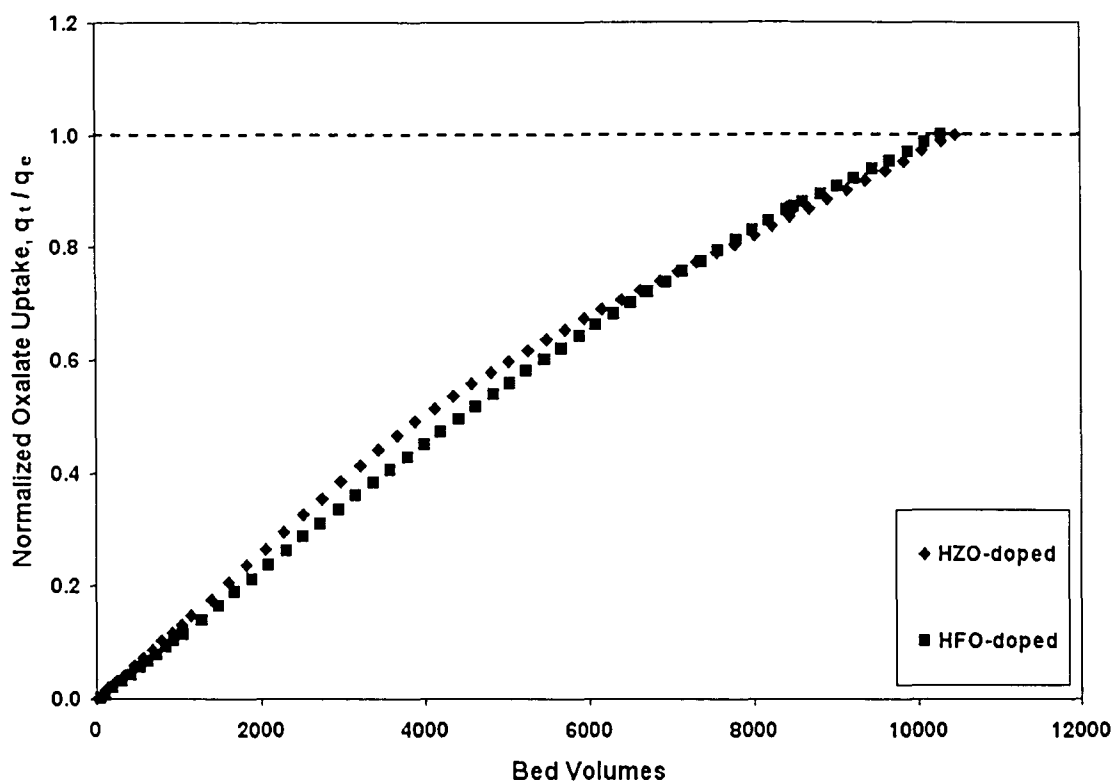


Figure 3.16 – Comparative Plot of HAIX-F(Fe) and HAIX-F(Zr) Uptake of Oxalate

Regardless of the similar curves depicted in Figure 3.16, the two media actually contain very distinct capacity for oxalate sorption. The basis of this statement lies in the amount of metal loading on HAIX-F media. Recall from Table 2.1 that 2.06 mol Fe^{3+} (6.19 meq) were loaded per gram of HAIX-F(Fe), whereas only 0.64 mol Zr^{4+} (2.56 meq) were impregnated into HAIX-F(Zr) media. Therefore, a more accurate comparison would contrast equilibrium capacity as a function of capacity (as meq/mol M^+ and meq/meq) as seen in Table 3.3.

Table 3.3 – Total and Breakthrough Capacity of HAIX-F Media for Oxalate

Material	Compound	Capacity (mg/g)	Capacity (meq/mol M^+)	Capacity (meq/meq)
HAIX-F(Fe)	oxalate	23.312	0.257	0.086
HAIX-F(Zr)	oxalate	20.648	0.733	0.183

From Table 3.3, the better capacity of HAIX-F(Zr) towards oxalate uptake can be clearly

seen. In fact, HAIX-F(Zr) exhibits over $2\times$ the capacity of HAIX-F(Fe) (on meq/meq basis). Therefore, by altering the loading process to allow more zirconium oxide presence, much more efficient oxalate (and other surrogate NOM compounds) uptake should be observed.

3.4.3.2 Comparison of Fixed-Bed HAIX-F Phthalate Removal Experiments

Normalized uptake curves for HAIX-F(Fe) and HAIX-F(Zr) treatment of phthalate are provided in Figure 3.17. In this case, both HAIX-F media display relatively good plug-flow characteristics due to the prevalent “s”-shaped curves; additionally, these plug-flow characteristics are also observed in normalized concentration curves available in Figures 3.12 & 3.14. The sharper “s” of HZO-loaded FIBAN A-1 fibers suggests that better sorption kinetics are present in HAIX-F(Zr) as compared to HAIX-F(Fe). However, both media demonstrate relatively similar breakthrough.

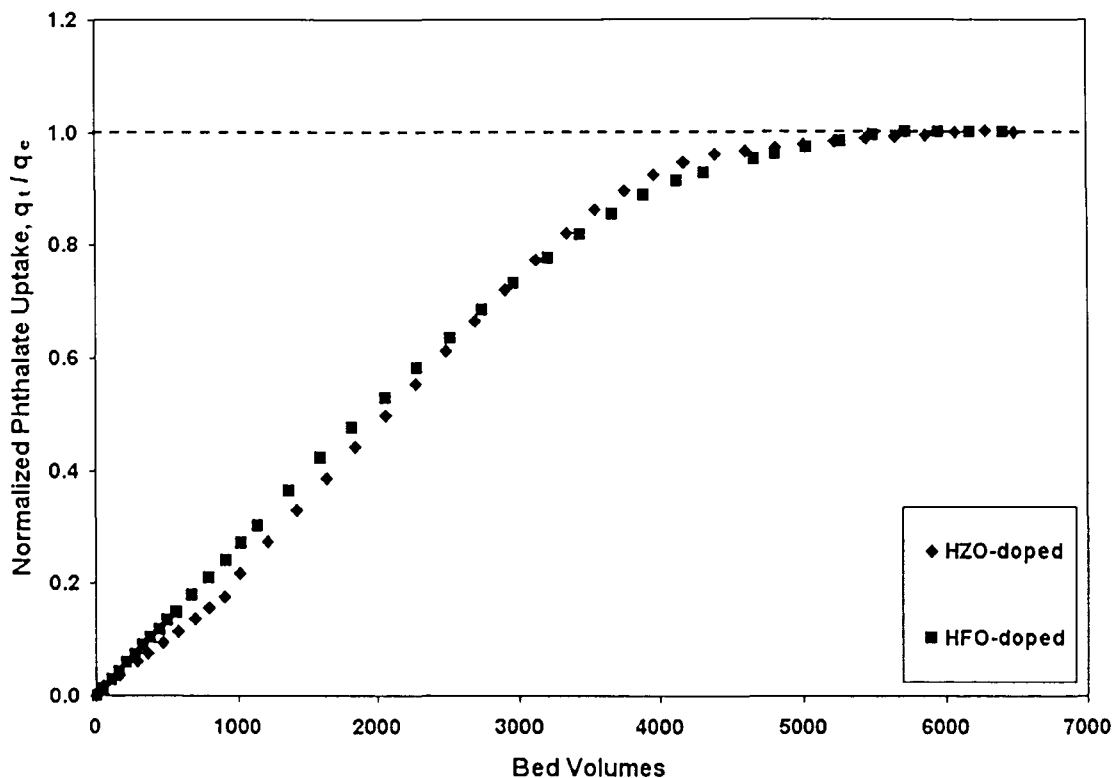


Figure 3.17 – Comparative Plot of HAIX-F(Fe) and HAIX-F(Zr) Uptake of Phthalate

Regardless of the similarity of normalized uptake curves, Table 3.4 clearly reveals that HAIX-F(Zr) media maintains a better overall capacity (as meq/mol M⁺ and meq/meq). As HAIX-F(Zr) capacity, based on milliequivalent basis, is over 1.5× that of HAIX-F(Fe), modification of the zirconium oxide nanoparticulate process should provide better overall capacity for removal of organic compounds, such as oxalate, phthalate, and NOM. The lesser zirconium loading is likely attributable to the higher oxidation state of zirconium ion, which results in increased resistance of zirconium cation penetration into parent anion exchange fibers during the loading process. Essentially, Donnan co-ion exclusion effects disallow transport of free cations into anion exchange media due to the presence of fixed positive charges (i.e., anion exchange sites); however, by overwhelming the Donnan energy, which is based in osmotic-like reasoning, zirconium can effectively enter the media and be precipitated as HZO nanoparticulates. Various

methods of extending metal oxide loading ability have recently been developed by SolmeteX[®], Inc., albeit no data has been published on these procedures as yet.

Table 3.4 – Total and Breakthrough Capacity of HAIX-F Media for Phthalate

Material	Compound	Capacity (mg/g)	Capacity (meq/mol M ⁺)	Capacity (meq/meg)
HAIX-F(Fe)	phthalate	19.047	0.113	0.038
HAIX-F(Zr)	phthalate	12.324	0.235	0.059

3.4.3.3 Comparison of Fixed-Bed HAIX-F NOM Removal Experiments

Details of NOM fixed-bed experimentation cannot be accurately compared due to the drastic inequity in run length. It should be noted, however, that both runs experienced an almost immediate chromatographic elution, and then NOM concentrations suddenly decreased. The investigator believes that inaccurate concentrations were probably obtained for the HAIX-F(Fe) experimentation and data following chromatographic elution were actually only a fraction of influent concentration, as seen with the HAIX-F(Zr) run. Again, imprecise concentration readings are explained and discussed throughout sections 3.7 & 4.5.

3.5 Kinetic Tests with HAIX-F Media

As column experiments (Figures 3.11-3.12) suggested uptake kinetics are limited by intraparticle diffusion of contaminant compounds into HAIX-F media, separate kinetics tests were conducted using the setup pictured and described in section 2.5. The following figures describe contaminant concentration history throughout kinetic test operation. Basically, reduction in the given contaminant (oxalate, phthalate, or NOM) is observed over time. Using this data, the effective diffusivity of HAIX-F media can be calculated towards comparison with other

technologies and determination of uptake-limiting mechanisms. For calculation of effective diffusivity consider equations 10-17.

In order to provide an estimation of effective NOM diffusivity into HAIX-F media, the Stokes-Einstein equation (equation 10) will be utilized. Polson determined that the Stokes-Einstein equation accurately predicts aqueous phase diffusivity of large organic molecules (molecular weight greater than 1000 Daltons) [Polson, 1950]. As the theory is rooted in molecular kinetic theory, the liquid diffusivity estimates are averages of various molecular-weight fractions of complex organics like humic acid and NOM; therefore, no impact due to NOM fractionalization (hydrophilic, transphilic, and hydrophobic components) should be realized.

$$D_l = \frac{k \cdot T}{6\pi \cdot \mu \cdot r} = \frac{k \cdot T}{6\pi \cdot \mu} \left(\frac{3}{4\pi} \cdot \frac{MW}{\rho_A N} \right)^{-\frac{1}{3}} = \frac{k \cdot T}{3 \cdot \mu} \left(6\pi^2 \cdot \frac{MW}{\rho_A N} \right)^{-\frac{1}{3}} \quad (10)$$

where k , T , μ , r , MW , N , and ρ_A represent Boltzmann's constant, temperature, dynamic viscosity, molecular radius, molecular weight, Avogadro's number, and molecule density, respectively. Cornel and coworkers determined a liquid diffusivity of humic acid value between 0.38×10^{-6} cm^2/s and 1.6×10^{-6} cm^2/s ; similarly, Tu et al. found a diffusion coefficient of 2.365×10^{-6} cm^2/s for tannic acid [Cornel et al., 1986; Tu et al., 2001]. In order to have some estimate of NOM diffusivity, the aqueous diffusivity and molecular weight properties of tannic acid will be employed towards better characterization of NOM diffusivity.

For lower molecular weight organic compounds such as oxalate and phthalate, liquid diffusivities were taken from *CRC Handbook of Chemistry and Physics* [Lide, 1998]. These values are presented in Table 3.5.

Table 3.5 – Liquid Diffusivity of Oxalate and Phthalate

Compound	D_l (cm^2/s)
oxalate	9.87×10^{-6}
phthalate	6.96×10^{-6}

Calculation of pore diffusivity (D_p) was completed through employment of equation 11. Tortuosity (τ) ranges from 0-6, where 0 indicates negligible tortuosity and 6 indicates highly torturous diffusive path. As pore diameters are relatively small compared to organic carbon molecules, the conservative value of 6 will be utilized.

$$D_p = \frac{D_L}{\tau} \quad (11)$$

The linear equilibrium coefficient was determined using equilibrium solid- and aqueous-phase concentrations as demonstrated in equation 12.

$$K = \frac{q_{eq}}{C_{eq}} \quad (12)$$

where q_{eq} , C_{eq} and K are the solid-phase equilibrium concentration (mg/g), liquid-phase equilibrium concentration (mg/L), and equilibrium coefficient (L/g), respectively.

Finally, the effective diffusivity was determined using equation 13 [Li, 1999]. Pore volume has been estimated as 30% and bulk HAIX-F density is approximately 1.4 g/mL.

$$D_{eff} = \frac{\varepsilon_p \times D_p}{\varepsilon_p + \rho_f \times K} \quad (13)$$

where D_{eff} , ε_p , and ρ_f are the effective diffusivity, porosity, and hybrid fiber density, respectively.

In order to validate effective diffusivities found using equation 13, another method for determination of effective diffusivity, which has been described in the literature, will be employed [Helfferich, 1965; Höll and Sontheimer, 1977]. Essentially, a partial differential equation that complies with cylindrical geometrical properties and contaminant diffusion into such media is utilized. The general equation is presented in equation 14.

$$\frac{\partial q}{\partial t} = D_{eff} \left(\frac{\partial^2 q}{\partial r^2} + \frac{1}{r} \frac{\partial q}{\partial r} \right) \quad (14)$$

where q , t , and r represent the concentration of contaminant in HAIX-F phase (mg/g), time, and particle cross-sectional radius, respectively [Crank, 1975].

Using the linear equilibrium relationship (equation 12) and finite volume assumption, equation 14 can be simplified to equation 15.

$$F(t) = \frac{M_t}{M_\infty} = 1 - \sum_{n=1}^{\infty} \frac{4\omega(\omega+1) \cdot \exp(-D_{\text{eff}}\beta_n^2 t/r^2)}{4 + 4\omega + \beta_n^2 \omega^2} \quad (15)$$

where $F(t)$, M_t , M_∞ , and n are the fraction of capacity achieved, mass of contaminant in HAIX-F phase at time t , mass of contaminant in HAIX-F phase at equilibrium, and the number of terms applied, respectively. The ω term represents the amount of contaminant remaining in solution at equilibrium as described by equation 16. β_n corresponds to the positive non-zero roots of equation 17.

$$\omega = \frac{VC_0}{M_\infty} - 1 \quad (16)$$

$$\omega \beta_n J_0(\beta_n) + 2 J_1(\beta_n) = 0 \quad (17)$$

where V , C_0 , $J_1(\beta_n)$ are the solution volume in kinetic test apparatus, initial concentration of contaminant, and Bessel functions of positive non-arbitrary roots of equation 15, respectively. An example of this model's utility is provided in Appendix B.

Essentially, this model provides a better overall calculation of effective dispersivity as the first method (equations 10-13) only considers equilibrium data. Therefore, while the first model will yield a rough estimate of effective dispersivity, better results should be found using the second method (equations 14-17). Utility of both methods is meant for comparison purposes and applicability assessments.

Furthermore, kinetics tests were used as equilibrium tests towards calculation of effective separation factors between contaminant of concern (i.e., oxalate or phthalate) and background

anions (i.e., sulfate and chloride). Equation 18 provides the separation factor equation of the organic/sulfate system; equation 19 gives the organic/chloride system formula.

$$\alpha_{C^{2-}/SO_4^{2-}} = \frac{[q_{C^{2-}}][C_{SO_4^{2-}}]}{[C_{C^{2-}}][q_{SO_4^{2-}}]} \quad (18)$$

$$\alpha_{C^{2-}/Cl^-} = \frac{[y_{C^{2-}}]^2[x_{Cl^-}]}{[x_{C^{2-}}]^2[y_{Cl^-}]} \times \frac{C_T}{Q} \quad (19)$$

where α , q , C , y , x , C_T , Q , and C^{2-} represent separation factor, solid-phase concentration, aqueous-phase concentration, equivalent solid-phase fraction, equivalent aqueous-phase fraction, total electrolyte concentration, total uptake capacity, and divalent organic species (i.e., oxalate or phthalate), respectively. Essentially, separation factor values provide insight into the affinity of a media for one species over another. The meaning of separation factor values regarding compound uptake onto HAIX-F media is provided below:

$\alpha_{A/B} > 1.0$... species A is preferred over species B

$\alpha_{A/B} = 1.0$... species A and B are equally preferred

$\alpha_{A/B} < 1.0$... species A is less preferred than species B

Extension of separation factor meanings to isotherm plots is demonstrated in Figure 3.18. Clearly, a separation factor greater than 1.0 indicates that species A is adsorbed over species B at all relative concentrations. For example, if species A represents 10 percent of the aqueous phase concentration, it will represent over 10% of the solid-phase concentration. By extending the above logic, meanings for other separation factor values can be ascertained. Hence, a higher separation factor yields more relative sorption of the species of concern. Similarly, a low separation factor signifies little sorption will occur; this variable is effectively exploited during regeneration of ion exchange resins in order to remove the sorbed contaminant of concern.

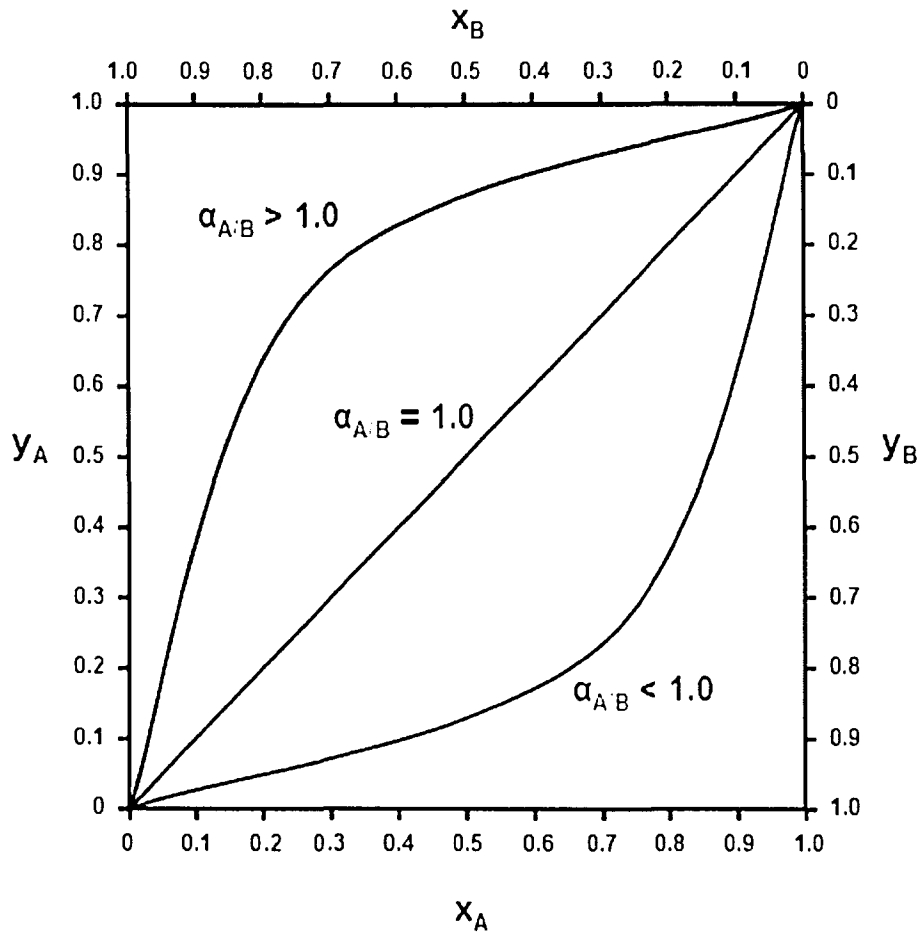


Figure 3.18 – Meaning of Separation Factor Values Defined by Isotherm Plot

The following subsections (sections 3.5.1-3.5.3) yield results of kinetic tests employing HAIX-F media towards removal of organic species (oxalate, phthalate, and NOM) in order to determine kinetic rate-limiting mechanism. Given the suggested intraparticle diffusion rate-limiting mechanism inferred from fixed-bed column experimentation, effective intraparticle diffusivities will be calculated.

3.5.1 Kinetic Tests Employing HAIX-F(Fe)

The following kinetic tests were conducted using 0.1 grams of HAIX-F(Fe) in the kinetic

test apparatus shown in Figures 2.5-2.7. As described below, the organic contaminant is the preferred species in each case.

3.5.1.1 Oxalate Kinetic Test with HAIX-F(Fe)

A one liter solution containing 3, 20, and 100 ppm of oxalate, sulfate, and chloride, respectively, was created. The stirrer device, described in section 2.5, was then contacted with solution and began rotating at 1500 rpm. At time zero (t_0), initial concentrations were witnessed; throughout operation over a 24-hour period, chloride concentrations remained constant at influent levels, sulfate concentration dropped by ~20%, and oxalate concentrations were reduced by ~60% (Figure 3.19). Clearly, the HAIX-F(Fe) media prefers oxalate over competing chloride and sulfate species as demonstrated in section 3.4.1.1. Equilibrium separation factors were calculated using equations 18-19 and are provided below. Note that the extremely high oxalate/chloride separation factor is due to almost negligible uptake of chloride ion by HAIX-F(Fe).

$$\alpha_{C_2O_4^{2-}/SO_4^{2-}} = 4.534$$

$$\alpha_{C_2O_4^{2-}/Cl^-} = > 30,000$$

Figure 3.19 also shows that equilibrium sulfate concentration is greater than minimum sulfate concentration (~240 minutes). The reason for this occurrence lies in the fact that oxalate/sulfate separation factor is greater than unity. During initial contact with synthetic surface water solution, all species are sorbed due to rate-limiting effects regarding oxalate diffusion into HAIX-F(Fe) media. However, at equilibrium, oxalate species have fully penetrated HAIX-F(Fe) media and have been sorbed on embedded HFO nanoparticulates. This occurrence causes efflux of sulfate species from HFO surface functional groups, resulting in an increase in sulfate aqueous phase

concentration.

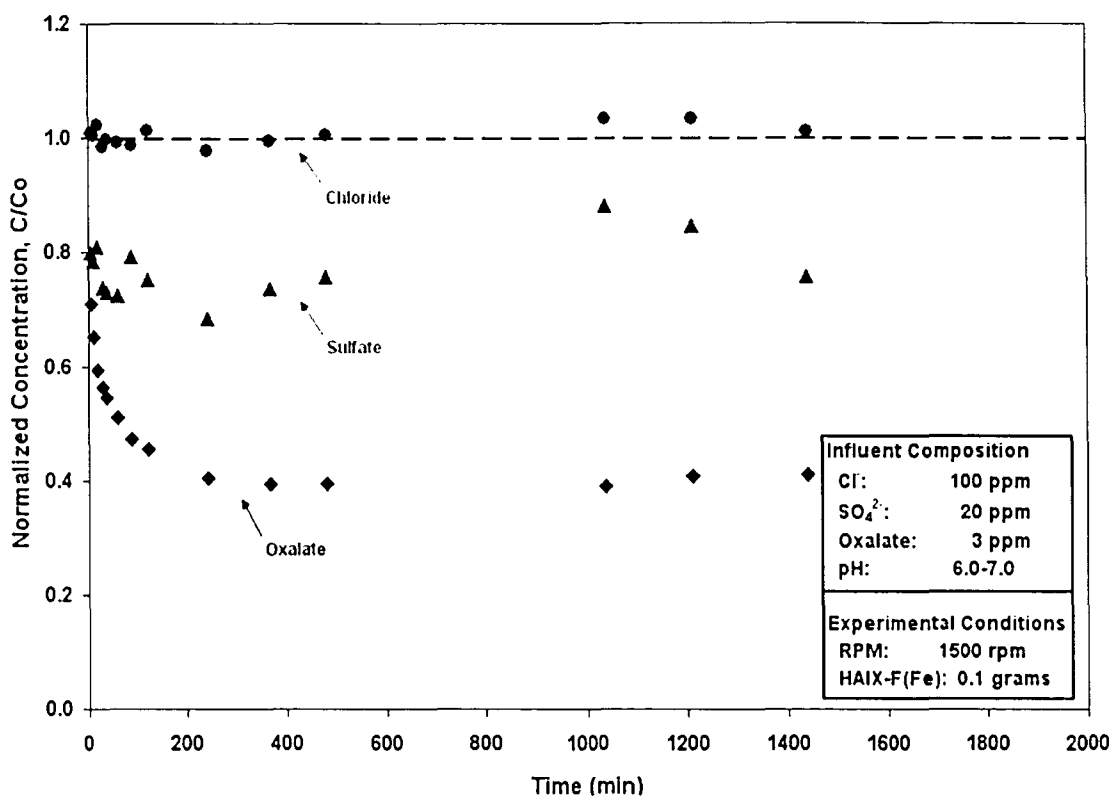


Figure 3.19 – Kinetic Test for HAIX-F(Fe) Run with Oxalate

Analysis of the 24-hour data demonstrates equilibrium solid- and aqueous-phase concentrations as follows:

$$q_{eq} \text{ (mg/g)} = 17.735$$

$$C_{eq} \text{ (mg/L)} = 1.227$$

It should be noted that the equilibrium capacity of HAIX-F(Fe) for oxalate found in this kinetic test is significantly lesser (% difference = 63%) than that provided in Table 3.1; additionally, the value is much more consistent (% difference = 24%) with the capacity found in fixed-bed experimentation presented in section 3.4.1.1.

From equation 12, the linear equilibrium coefficient (K) was calculated as

$$K \text{ (L/g)} = 14.459$$

Employment of equation 13 in association with oxalate liquid diffusivity (Table 3.5) and estimated values of pore volume ($\epsilon_p = 0.30$) and tortuosity ($\tau = 6$) allows for calculation of the effective diffusivity:

$$D_{eff}(\text{cm}^2/\text{s}) = 2.41 \times 10^{-11}$$

This value is extremely low and does not correlate with the kinetic test data. Conversely, determination of the effective diffusivity using equations 14-17 provided a more agreeable result.

$$D_{eff}(\text{cm}^2/\text{s}) = 9.35 \times 10^{-10}$$

Figure 3.25 displays the good fit of this effective diffusivity value to kinetic test data within the first sixty minutes of operation. It is important to note that the model also fits later data; however, only the first sixty minutes were shown to provide better comprehension of the period of interest. Because of better applicability of partial derivative method, the latter effective diffusivity will be utilized.

3.5.1.2 Phthalate Kinetic Test with HAlX-F(Fe)

A one liter solution containing 3, 20, and 100 ppm of phthalate, sulfate, and chloride, respectively, was produced using laboratory grade chemicals as discussed in section 2.1. The stirrer device, described in section 2.5, was contacted with solution and began rotation towards elimination of liquid film diffusion effects. At time zero (t_0), initial concentrations prevailed; over the 24-hour operational period, chloride concentrations remained relatively constant. Conversely, sulfate and phthalate concentrations dropped by ~20% and ~70%, respectively as shown in Figure 3.20. Equilibrium separation factors, calculated with equations 18-19, regarding HAlX-F(Fe) affinity for phthalate species over sulfate and chloride species are provided below. Again, phthalate/chloride separation factor is extremely high due to the small amount of chloride ion

sorption as shown in Figure 3.20.

$$\alpha_{C_6H_4(COO^-)_2 / SO_4^{2-}} = 7.051$$

$$\alpha_{C_6H_4(COO^-)_2 / Cl^-} = > 8000$$

Essentially, phthalate is preferred over sulfate by ~7.0 times, and almost infinitely preferred over chloride species. Figure 3.20 also demonstrates that near equilibrium, sulfate concentration gently increases; this occurrence is founded in the fact that phthalate/sulfate separation factor is greater than unity. Essentially, phthalate sorption is limited by intraparticle diffusion; therefore, as phthalate species diffuses through the media, sorbed sulfate species will be expelled back into aqueous phase. For that reason, normalized sulfate concentration in the aqueous phase will exhibit a slight increase.

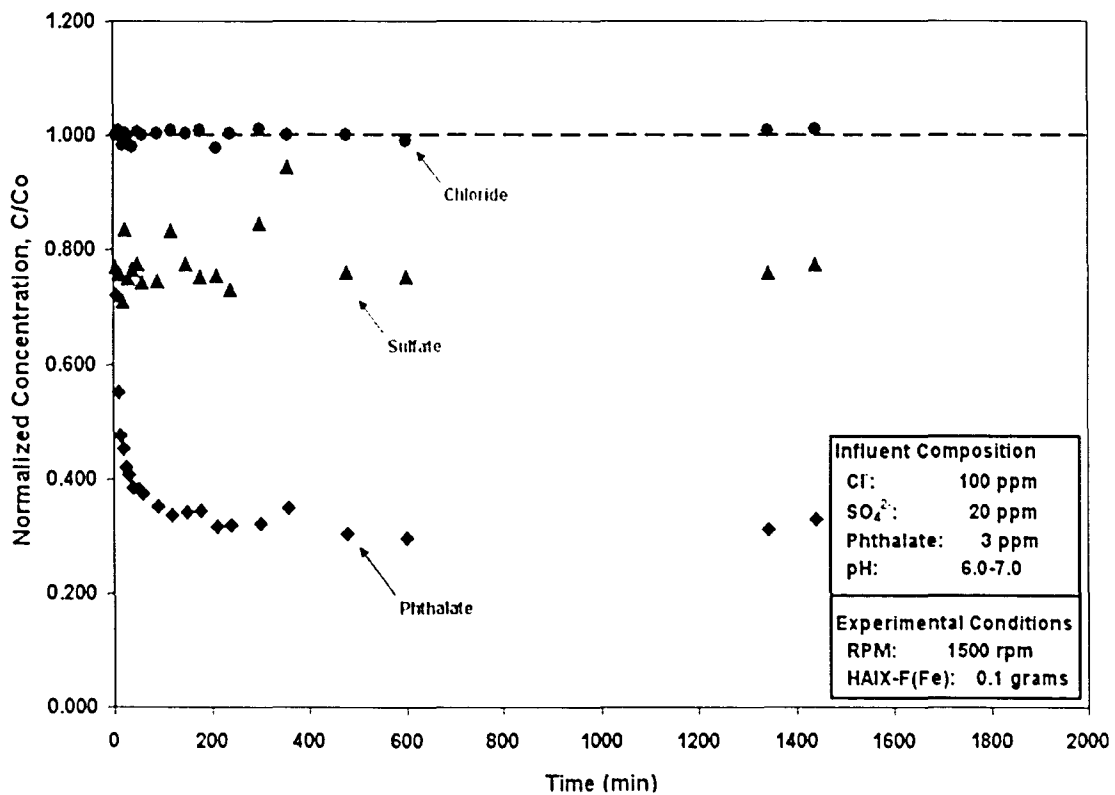


Figure 3.20 – Kinetic Test for HAIX-F(Fe) Run with Phthalate

Equilibrium solid- and aqueous-phase concentrations from the 24-hour kinetic test demonstrate the following values:

$$q_{eq} \text{ (mg/g)} = 20.323$$

$$C_{eq} \text{ (mg/L)} = 0.998$$

Comparison of the equilibrium concentration found above with that found in the fixed-bed column demonstrates 6% difference.

From equation 12, the first-order equilibrium coefficient (K) is

$$K \text{ (L/g)} = 20.363$$

Equation 13 permits calculation of the effective diffusivity. Utilizing phthalate liquid diffusivity (Table 3.5) and estimated values of pore volume ($\epsilon_p = 0.30$) and tortuosity ($\tau = 6$), the effective diffusivity can be found.

$$D_{eff} \text{ (cm}^2\text{/s)} = 1.21 \times 10^{-11}$$

Again, this is an extremely low value of effective diffusivity and does not provide good correlation with kinetic test data. Employing equations 14-17 towards calculation of effective diffusivity presents a more suitable result.

$$D_{eff} \text{ (cm}^2\text{/s)} = 9.25 \times 10^{-10}$$

This value was fitted to kinetic test data points for the first sixty minutes of operation (Figure 3.26) and demonstrated an extremely agreeable fit to the data. Again, the calculated effective diffusivity also fits later data points, but in order to show the wellness of fit for the period of interest only initial data points were plotted. Since the effective diffusivity determined through employment of the partial differential method described by Crank provided a better fit, that value will be utilized.

3.5.1.3 NOM Kinetic Test with HAIX-F(Fe)

Synthetic surface water solution containing 10, 20, and 100 ppm of TOC (from NOM brine solution), sulfate, and chloride, respectively, was utilized for the NOM kinetic test. The stirrer device, described in section 2.5, was contacted with solution and began rotation at 1500 rpm towards elimination of liquid film diffusion effects. At time zero (t_0), initial concentrations prevailed; during operation, chloride concentration increased slightly. Most likely, this slight increase is a result of chloride ion expulsion from HFO surface functional groups upon contact with sulfate and NOM species; the media was originally in chloride form. On the other hand, aqueous sulfate concentration initially dropped to $\sim 75\%C_0$ and then slowly increased until equilibrium at 24-hours. NOM concentrations (measured as TOC) showed an immediate increase in concentration, which cannot be accounted for as HAIX-F(Fe) media was not in organic form; however, aqueous-phase TOC concentrations then demonstrated negative correlation, indicating uptake by HAIX-F(Fe) media. These results can be observed in Figure 3.21.

In contrast to the well-behaved data trends observed in the previous two sections, the kinetics test concerning NOM uptake by HAIX-F(Fe) media demonstrates a much lower correlation factor. Regardless, there is a negative trend in NOM concentration, which denotes favorable uptake of NOM compounds by HFO surface groups. This observation is strengthened by the positive correlation associated with sulfate concentrations. Equilibrium separation factors regarding HAIX-F(Fe) affinity for NOM compounds over sulfate and chloride species cannot be computed. The generalized separation factor equation is provided below in equation 20.

$$\alpha_{A, B} = \frac{[y_A]^a [x_B]^b}{[x_A]^a [y_B]^b} \times \frac{[C_7]^{a-b}}{[Q]^{a-b}} \quad (20)$$

where α , y , x , C_7 , Q , A , B , a , and b represent separation factor, equivalent solid-phase fraction,

equivalent aqueous-phase fraction, total electrolyte concentration, total uptake capacity, species A , species B , valence of species A , and valence of species B , respectively. Various NOM compounds are present in the diluted NOM brine solution; furthermore, each organic compound exhibits a different valence. For these reasons, equation 20 cannot be employed because it would require inclusion of i terms, where i represents the number of organic compounds included in the bulk NOM term; additionally, the exhibited valence of each compound i would need to be known.

NOM compounds are rather large molecules (see Figure 1.1) and so diffusion through HAIX-F(Fe) media will be lower than for competing species like sulfate and chloride. Such reasoning provides insight into the details presented in Figure 3.21. Regardless, the observable correlations regarding increasing sulfate concentration over time and decreasing TOC concentration with time indicate that NOM compounds are selectively sorbed. Using simple linear regressions, an effective changeover in HAIX-F(Fe) affinity for NOM (measured as TOC) occurs at approximately 20 hours. Given constant chloride concentration and reduced NOM concentration, HAIX-F(Fe) clearly has an affinity for organic species.

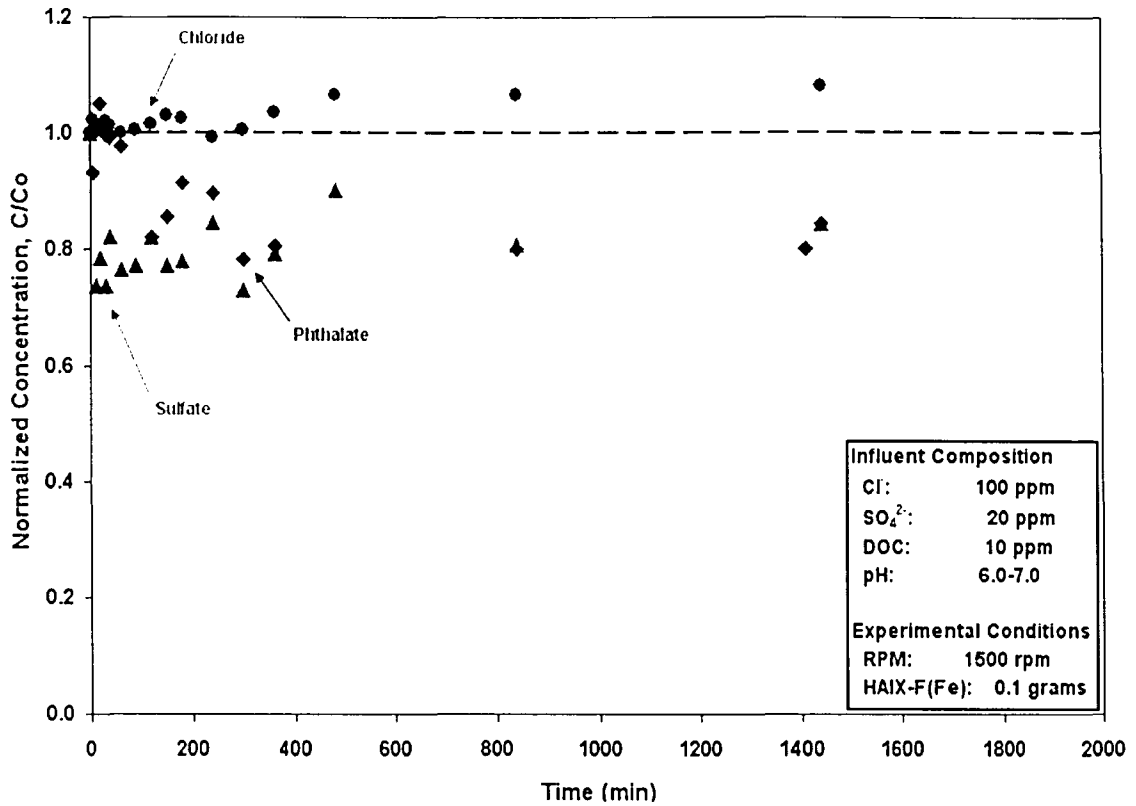


Figure 3.21 – Kinetic Test for HAIX-F(Fe) Run with Dilute NOM Brine

The 24-hour kinetic test allowed for calculation of equilibrium HAIX-F(Fe)- and aqueous-phase TOC concentrations.

$$q_{eq} \text{ (mg/g)} = 17.278$$

$$C_{eq} \text{ (mg/L)} = 9.341$$

Approximately 26% error was present between this equilibrium capacity and that found in Figure 3.1.

Using equation 12, the linear equilibrium coefficient (K) was determined:

$$K \text{ (L/g)} = 1.850$$

Normally equation 13 could be utilized towards determination of effective diffusivity; however, no way of calculating the liquid diffusivity of the employed NOM solution is available. In order to provide a rough estimate of effective diffusivity, tannic acid's liquid diffusivity of

$2.365 \times 10^{-6} \text{ cm}^2/\text{s}$ will be utilized [Tu et al., 2001]. It should be noted that the resultant value may contain a large degree of inaccuracy and is intended only for relative comparison with effective diffusivities of oxalate and phthalate for HAIX-F(Fe) and HAIX-F(Zr) media. Following the procedure described above (equation 13), an approximate effective diffusivity was found.

$$D_{eff} (\text{cm}^2/\text{s}) = 4.51 \times 10^{-11}$$

Because of the poor correlation of data points presented in Figure 3.21, calculation of effective diffusivity according to Crank's method was not possible. However, based off of the differences exhibited for oxalate and phthalate species, an actual effective diffusivity should be at least an order of magnitude greater than the value listed above.

3.5.2 Kinetic Tests Employing HAIX-F(Zr)

3.5.2.1 Oxalate Kinetic Test with HAIX-F(Zr)

A solution, identical to the one employed in section 3.5.1.1, consisting of 3, 20, and 100 ppm of oxalate, sulfate, and chloride, respectively, was created towards execution of the kinetic test. The stirrer device, described in section 2.5, was immersed into solution and rotated at 1500 rpm. At time zero (t_0), initial concentrations prevailed; during operation chloride concentrations remained relatively steady at influent levels. On the other hand, sulfate concentrations were reduced by about 10-20% through divalent electrostatic interaction with zirconium oxide functional groups. Oxalate, which was the contaminant of concern, witnessed concentration reduction of ~60%. These results are clearly depicted in Figure 3.22. HAIX-F(Zr) affinity for oxalate over competing chloride and sulfate species is clear and compatible with fixed-bed results discussed in section 3.4.2.1. Using equations 18-19, the equilibrium separation factors for oxalate

affinity over chloride and sulfate were found. Note that the excessive separation factor value for oxalate/chloride system is due to the negligible sorption of chloride species by HAIX-F(Zr).

$$\alpha_{C_2O_4^{2-}/SO_4^{2-}} = 10.594$$

$$\alpha_{C_2O_4^{2-}/Cl^-} = > 100,000$$

The latest (400-1400 minutes) sulfate concentration data points in Figure 3.22 provide clear evidence that sulfate is being expelled from the solid-phase as operating time proceeds. Such expulsion of sulfate from HAIX-F(Zr) is due to the oxalate/sulfate separation factor listed above. As mentioned earlier, a separation factor greater than unity provides for better relative sorption affinity; therefore, as oxalate diffuses into the media, sulfate is gradually effluxed, resulting in increasing aqueous phase concentration as depicted in Figure 3.22.

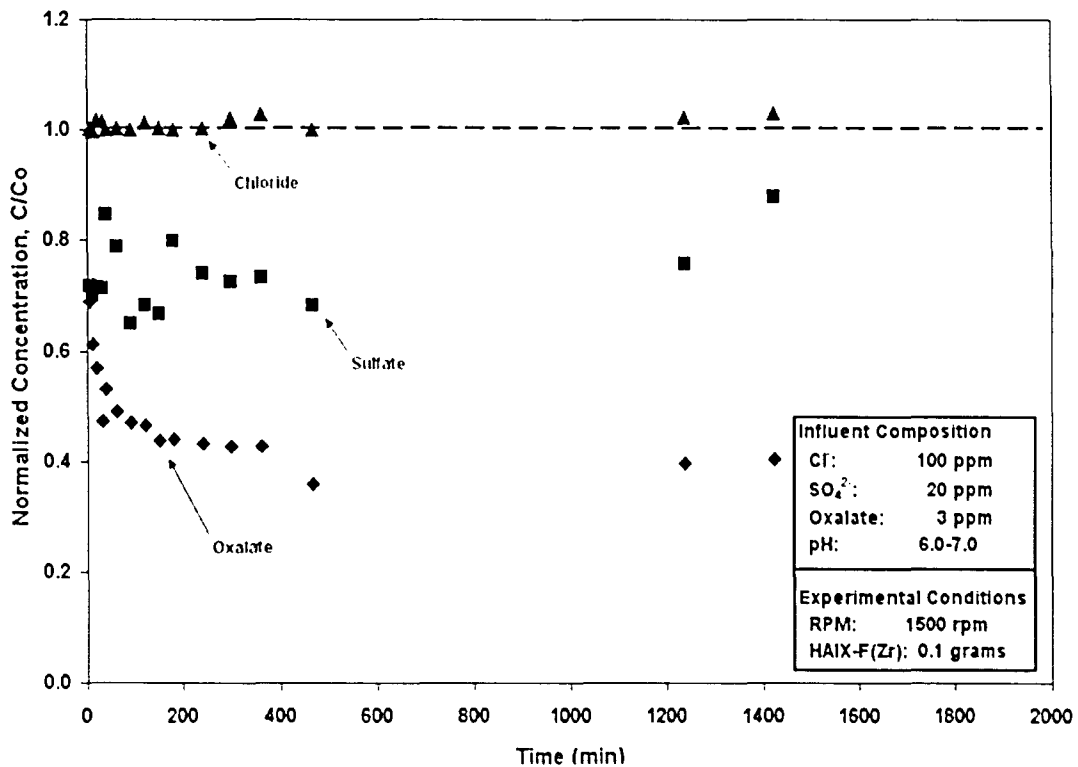


Figure 3.22 – Kinetic Test for HAIX-F(Zr) Run with Oxalate

Equilibrium data demonstrated the following solid- and aqueous-phase concentrations:

$$q_{eq} \text{ (mg/g)} = 21.124$$

$$C_{eq} \text{ (mg/L)} = 1.440$$

It should be noted that the equilibrium capacity of HAIX-F(Zr) for oxalate found in this kinetic test is relatively similar (% difference = 9%) compared to that listed in Figure 3.1 and almost identical to the capacity found during fixed-bed experimentation (% difference = 2%).

Equation 12 allows calculation of the first-order equilibrium coefficient (K):

$$K \text{ (L/g)} = 14.672$$

Using the estimated values of pore volume ($\epsilon_p = 0.3$) and tortuosity ($\tau = 6$) in accordance with the known value liquid diffusivity of oxalate (Table 3.5) allows calculation of effective diffusivity via equation 13.

$$D_{eff} \text{ (cm}^2\text{/s)} = 2.40 \times 10^{-11}$$

As in cases employing HAIX-F(Fe) media, this value of effective diffusivity is an underestimate of actual effective diffusivity based off of the poorness of fit to actual kinetic test data. Through employment of equations 14-17, a better estimate of effective diffusivity is found.

$$D_{eff} \text{ (cm}^2\text{/s)} = 5.75 \times 10^{-10}$$

By fitting this value to kinetic test data for the first sixty minutes of kinetic test operation (Figure 3.25), an extremely good fit was observed. It should be noted that the effective diffusivity found using Crank's formulas also fits later data points (i.e., after 60 minutes), but as the initial data points dictate the wellness of fit, only those data points are shown in Figure 3.25. Also, the poorness of fit observed through application of the former effective diffusivity essentially fits some latter (after 60 minutes of operation) data points but does not provide a good fit for initial data (before 60 minutes of operation), due to calculation based upon equilibrium values as mentioned above. Therefore, the effective diffusivity determined using equations 14-17 will be utilized.

3.5.2.2 Phthalate Kinetic Test with HAIX-F(Zr)

Solution containing 3, 20, and 100 ppm of phthalate, sulfate, and chloride, respectively, was produced and utilized for the kinetic test described below. A rotational stirrer (see section 2.5) was adjusted to 1500 rpm and contacted with the synthetic surface water solution in order to eliminate any effects of liquid film diffusion. Figure 3.23 displays the results of the kinetic test. Initial concentrations are signified by the dashed line that extends horizontally from $t = 0$ minutes to $t = 2000$ minutes. During the kinetic test, aqueous chloride concentration remained relatively constant, signifying that little chloride sorption onto HAIX-F(Zr) occurred. On the other hand, sulfate concentration initially dropped over 40% and then slowly increased to approximately 80% of its original concentration. Aqueous-phase phthalate concentration was reduced by about 80% during the course of operation. With the equilibrium data (concentration at 24 hours), separation factors regarding HAIX-F(Fe) affinity for phthalate species over sulfate and chloride species were found. Once more, note that phthalate/chloride separation factor is extremely high due to low chloride ion sorption.

$$\alpha_{C_6H_4(COO^-)_2 / SO_4^{2-}} = 11.835$$

$$\alpha_{C_6H_4(COO^-)_2 / Cl^-} = > 25,000$$

Essentially, HAIX-F(Zr) prefers phthalate over sulfate by a ratio of ~12; chloride competition with phthalate for sorption sites is negligible. Increasing sulfate concentrations after the early minimum aqueous-phase concentration (~90 minutes) agree with the phthalate/sulfate separation factor calculated above. Consider the following example: sulfate reaches sorption sites first due to its smaller size and greater mobility within the hybrid anion exchanger phase; later, larger organic

molecules (i.e., phthalate) diffuse into the media and expel sulfate from sorption sites. Therefore, slight increase in sulfate aqueous phase competition should occur, as displayed in Figure 3.23.

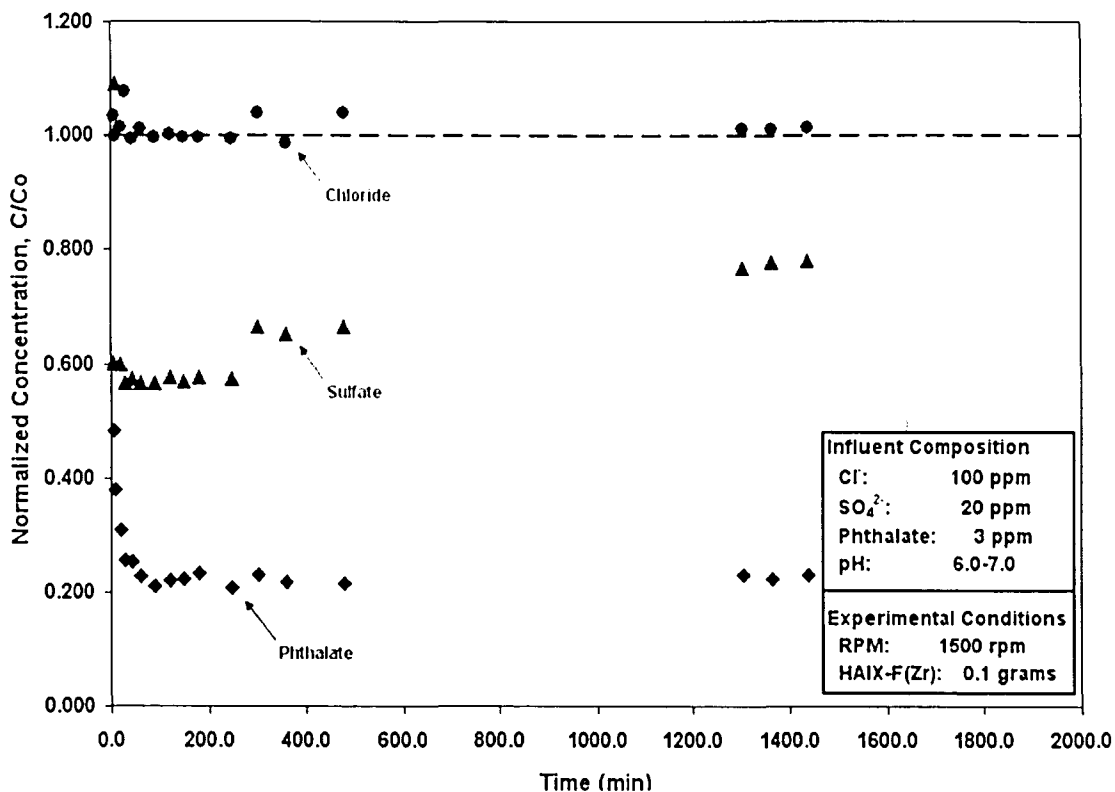


Figure 3.23 – Kinetic Test for HAIX-F(Zr) Run with Phthalate

Equilibrium solid- and aqueous-phase concentrations from the 24-hour kinetic test demonstrate the following values:

$$q_{eq} \text{ (mg/g)} = 32.697$$

$$C_{eq} \text{ (mg/L)} = 0.978$$

By comparing this equilibrium capacity to similar value determined from fixed-bed experimentation, a 62% difference was established.

From equation 12, the linear equilibrium coefficient (K) is

$$K \text{ (L/g)} = 33.433$$

Equation 13 permits calculation of the effective diffusivity. Utilizing oxalate liquid

diffusivity (Table 3.5) and estimated values of pore volume ($\epsilon_p = 0.3$) and tortuosity ($\tau = 6$), the effective diffusivity can be found.

$$D_{eff} (\text{cm}^2/\text{s}) = 7.44 \times 10^{-12}$$

This value is the lowest effective diffusivity calculated thus far and provides an extremely inaccurate fit to kinetic test data. Using equations 14-17, a better-fitting effective diffusivity was calculated through partial differential model.

$$D_{eff} (\text{cm}^2/\text{s}) = 1.95 \times 10^{-9}$$

Upon fitting this value to kinetic test data points for the first sixty minutes of operation, a very agreeable fit was realized (Figure 3.26). It is important to note this effective diffusivity value also fits later data points; however, the plot in Figure 3.26 only shows the time period where most sorption is occurring in order to demonstrate the wellness of fit. As the latter effective diffusivity (from above) demonstrates a much better fit to the kinetics test data, an effective diffusivity of $1.95 \times 10^{-9} \text{ cm}^2/\text{s}$ will be employed.

3.5.2.3 NOM Kinetic Test with HAIX-F(Zr)

The same synthetic surface water solution employed in section 3.5.1.3 was utilized for the kinetic test concerning NOM uptake onto HAIX-F(Zr) media. Aqueous concentrations were 10, 20, and 100 ppm for TOC (from NOM brine solution), sulfate, and chloride, respectively. The kinetic test stirrer device, described in section 2.5, was turned on, began rotating at 1500 rpm, and contacted with solution towards elimination of liquid film diffusion effects. Concentration history was plotted as normalized concentration (equation 21) as shown in Figure 3.24.

$$\text{Normalized concentration} = \frac{C}{C_0} \quad (21)$$

At time zero (t_0), concentration (C) was equal to the influent concentration (C_0); this condition is plotted as the horizontal dashed line presented in Figure 3.24. Throughout operation, chloride concentration was maintained at initial levels. Sulfate witnessed a large initial decrease in aqueous-phase concentration; subsequently, sulfate concentration gradually rose until equilibrium time of 24 hours. Conversely, NOM concentrations did not experience significant concentration reduction initially. As operational time went on, NOM (measured as TOC) underwent sorption onto HAIX-F(Zr) media; hence, aqueous phase concentrations dropped accordingly. By applying simple linear correlations to the data, an effective changeover in HAIX-F(Zr) affinity due to rising aqueous phase sulfate concentration and dropping aqueous phase TOC concentration took place at about 14.5 hours; this “changeover” is due to relatively slow effective diffusion.

NOM compounds are rather large molecules (see Figure 1.1) and so diffusion through HAIX-F(Zr) media will be slower than for competing species like sulfate and chloride. Regardless, observable correlations regarding increasing sulfate concentration over time and decreasing TOC concentration with time indicate that NOM compounds are selectively sorbed. Ultimately, sulfate and TOC concentrations were reduced by ~20%.

As depicted in Figure 3.24, the kinetic test results for NOM uptake by HAIX-F(Zr) media did not provide well-behaved trends or correlation. However, the general trends apparent in the data reinforce the postulate that NOM is selectively sorbed by HAIX-F(Zr) media through LAB and Coulombic interaction. Section 3.5.1.3 describes the inability of calculating separation factors for NOM tests; as sufficient detail was offered in that section, explanations will not be repeated here.

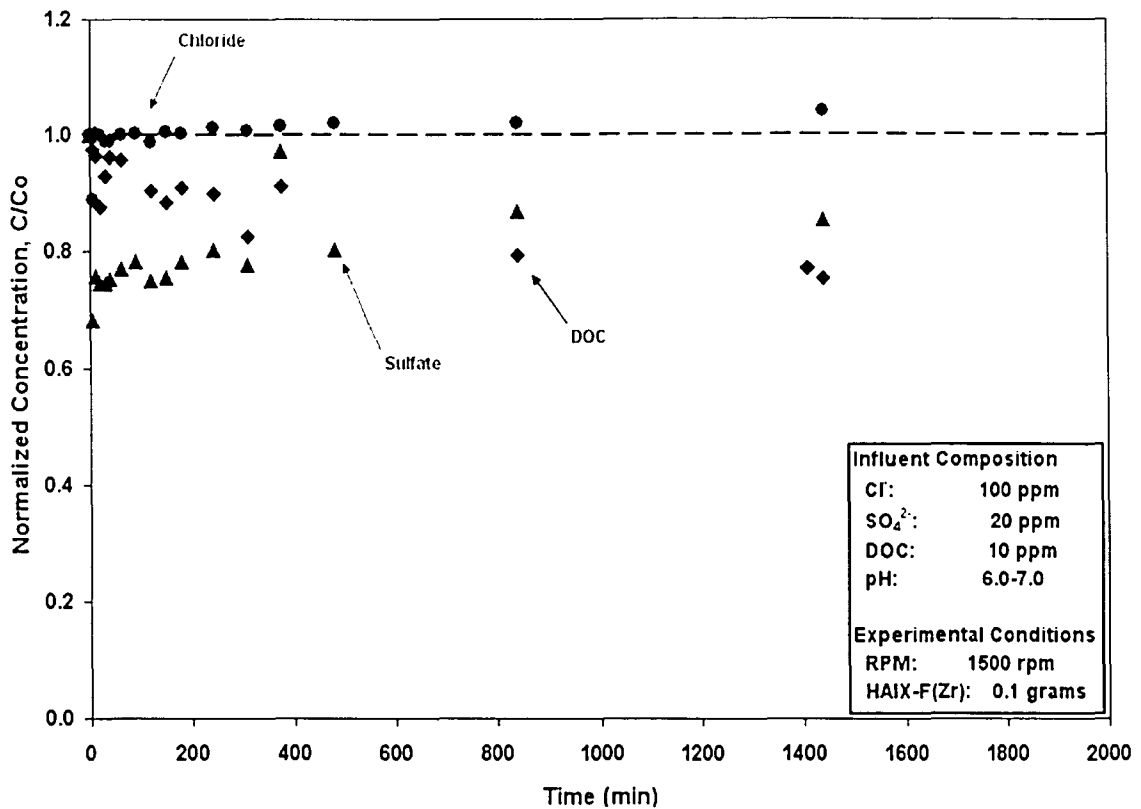


Figure 3.24 – Kinetic Test for HAIX-F(Zr) Run with Dilute NOM Brine

Equilibrium HAIX-F(Zr)- and aqueous-phase TOC concentrations were calculated using the data presented above in Figure 3.24.

$$q_{eq} \text{ (mg/g)} = 28.029$$

$$C_{eq} \text{ (mg/L)} = 8.577$$

Direct comparison of the calculated equilibrium capacity with equivalent variable found through fixed-bed experimentation demonstrates 15% error.

Using equation 12, the first-order equilibrium coefficient (K) was found:

$$K \text{ (L/g)} = 3.268$$

Normally equation 13 could be utilized towards determination of effective diffusivity; however, no way of calculating the liquid diffusivity of the employed NOM solution is available. In order to provide a rough estimate of effective diffusivity, tannic acid's liquid diffusivity of

2.365×10^{-6} cm²/s will be utilized [Tu et al., 2001]. It should be noted that the resultant value may contain a large degree of inaccuracy and is intended only for relative comparison with effective diffusivities of oxalate and phthalate for HAIX-F(Fe) and HAIX-F(Zr) media. Following the procedure described above, effective diffusivity was found using equation 13.

$$D_{eff} \text{ (cm}^2\text{/s)} = 2.59 \times 10^{-11}$$

Because of the poor correlation of data points presented in Figure 3.24, calculation of effective diffusivity according to Crank's method was not possible. Employing the effective diffusivity found above (2.59×10^{-11} cm²/s) in Crank's model, an initial kinetics data points are very much overestimated. Through attempting to fit Crank's model to the data, the need for a more complex diffusion model became apparent. Essentially, Crank's model can be utilized towards effective modeling of initial or later kinetics test data; however, both sections cannot be modeled together. Using a hybrid model where effective diffusivity is calculated for two separate regions would provide an adequate model for this data and for data presented in section 3.5.1.3. However for these purposes, an ultimate effective diffusivity approximately one order of magnitude greater than that calculated above can be assumed.

3.5.3 Comparison of Kinetic Tests Employing HAIX-F Media

A summary of the effective diffusivities found regarding the sorption kinetics of oxalate and phthalate onto HAIX-F media is provided in Table 3.6. It should be noted that HAIX-F(Fe) media yielded slightly better kinetics (defined through effective diffusivity) than HAIX-F(Zr) for oxalate sorption; however, the opposite case is true of phthalate uptake. Essentially, a greater effective diffusivity means that the contaminant of concern will diffuse into the media phase more rapidly. From the kinetics test data plots, near-complete sorption capacity is realized in one hour

or less. As contrast, ion exchange resin media with greater particle diameter and lower effective surface area exhibit near-complete realization of uptake capacity over many hours of operation; additionally, effective diffusivity of hybrid ion exchange resins typically ranges in the 10^{-11} cm²/s realm for more mobile species such as arsenate and phosphate [DeMarco et al., 2003]. Hence, HAIX-F media provides much more rapid sorption kinetics compared to conventional media. This increase in effective diffusivity provides the very rapid sorption kinetics observed in Figures 3.19-3.24 and renders hybrid filamentous media more applicable for treatment processes, which are often dependent upon flow rates and detention times.

Table 3.6 – Effective Diffusivities of Oxalate and Phthalate for HAIX-F Media

Media	Compound	D_{eff} (cm ² /s)
HAIX-F(Fe)	oxalate	9.35×10^{-10}
	phthalate	9.25×10^{-10}
HAIX-F(Zr)	oxalate	5.75×10^{-10}
	phthalate	1.95×10^{-9}

The following subsections will provide comparison of oxalate, phthalate, and NOM uptake by HAIX-F(Fe) and HAIX-F(Zr) media.

3.5.3.1 Kinetics Test Comparisons for Oxalate Removal

The data plotted in Figures 3.19 & 3.22 were manipulated towards construction of a normalized oxalate uptake (q_t/q_c) vs. time (t) plot. This allowed for direct comparison of HAIX-F(Fe) and HAIX-F(Zr) media in regards to oxalate uptake as shown in Figure 3.25. Using the effective diffusivity value calculated in sections 3.5.1.1 & 3.5.2.1, generalized curves were created to describe oxalate uptake by HAIX-F media. From these curves, effective time until certain fractions of capacity were attained was determined; such results are summarized in Table 3.7. Such a method allows for more accurate calculation of corresponding times because data

variability errors are effectively bypassed. Figure 3.25 and Table 3.7 demonstrate that HFO-loaded fibers exhibited faster oxalate sorption kinetics as described by the greater effective diffusivity value.

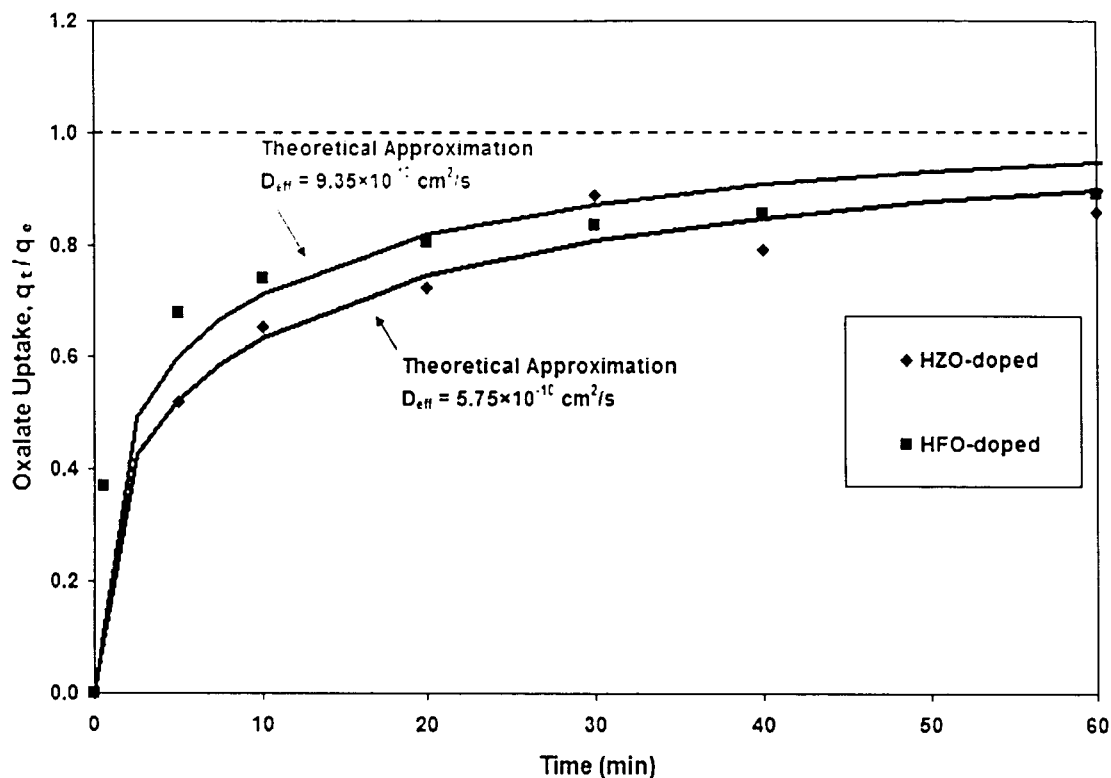


Figure 3.25 – Comparison of Kinetic Test Results for HAIX-F(Fe) and HAIX-F(Zr) with Oxalate

From Table 3.7, the exceptional kinetic capabilities of HAIX-F media can be observed. For HFO and HZO impregnated anion exchange fibers 50% capacity is reached within 5 minutes of contact time. Furthermore, 95% capacity is achieved in less than 90 minutes. Essentially, these values provide staggering evidence of the applicability of HAIX-F media towards water treatment industries and municipalities.

Table 3.7 – Time (minutes) Until Specified Fractional Oxalate Uptake Capacity

Media	q_t/q_e				
	50%	75%	90%	95%	99%
HAIX-F(Fe)	2.68	13.43	37.28	62.93	112.66
HAIX-F(Zr)	4.40	20.54	61.61	83.83	182.96

3.5.3.2 Kinetics Test Comparisons for Phthalate Removal

Phthalate kinetics experiments were undoubtedly the most accurate and well-behaved compared to oxalate and NOM. For that reason, comparison of phthalate uptake by HAIX-F media should provide the most accurate description of HAIX-F capabilities towards removal of surrogate NOM compounds and NOM. Data from Figures 3.20 & 3.23 were manipulated towards construction of a normalized phthalate uptake (q_t/q_e) vs. time (t) plot. This graph (Figure 3.26) permitted direct comparison of the two media through kinetics of phthalate removal. By employing the effective diffusivity value calculated via differential equation technique, time until a certain fraction of capacity was realized could be calculated (Table 3.8). These values along with the graphic illustration provided in Figure 3.26 demonstrate the better ability of HAIX-F(Zr) media to remove phthalate from synthetic surface water solutions.

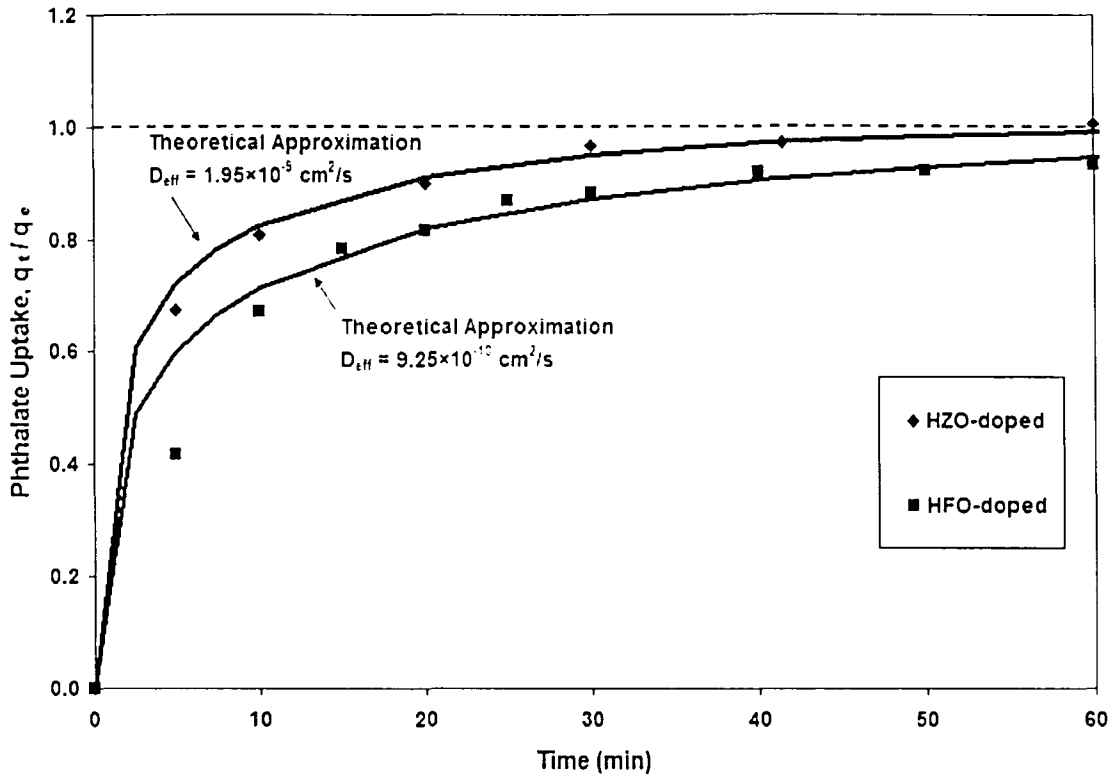


Figure 3.26 – Comparison of Kinetic Test Results for HAIX-F(Fe) and HAIX-F(Zr) with Phthalate

Both HAIX-F media demonstrated 50% exhausted capacity after less than 3 minutes of contact time with solution. Furthermore, 95% capacity achievement was experienced in about one hour for HAIX-F(Fe) and only 30 minutes for HAIX-F(Zr). In fact, HAIX-F(Zr) treated 10,000 bed volumes and successfully achieved >99% phthalate concentration reduction in less than one hour; similarly, HAIX-F(Fe) achieved 99% removal within two hours of treatment time.

Table 3.8 – Time (minutes) Until Specified Fractional Phthalate Uptake Capacity

Media	q_t/q_e				
	50%	75%	90%	95%	99%
HAIX-F(Fe)	2.72	13.58	38.49	63.64	113.93
HAIX-F(Zr)	1.71	6.17	18.74	30.05	59.71

3.5.3.3 Kinetics Test Comparisons for NOM Removal

TOC concentration histories from Figures 3.21 & 3.24 were manipulated towards construction of a normalized TOC uptake (q/q_c) vs. time (t) plot. Figure 3.27 provides the results of this reworked plot and allows for direct comparison of HAIX-F media in terms of NOM uptake. In sections 3.5.3.1-3.5.3.2 tables were established to describe the abilities of HAIX-F media in terms of treatment times towards achievement of certain percentage of total capacity. Because of the poor NOM data correlation, such tables would not provide accurate portrayals of treatment abilities; furthermore, the poor correlation of model fits due to data scatter disallows calculation of time through effective diffusivity. Several methods of curve-fitting were applied to the data with various degrees of success. Essentially, relatively accurate curves could be fitted to HAIX-F(Zr) data, but the extreme variability of HAIX-F(Fe) data did not allow for any accuracy. For that reason, no curves were provided in Figure 3.27.

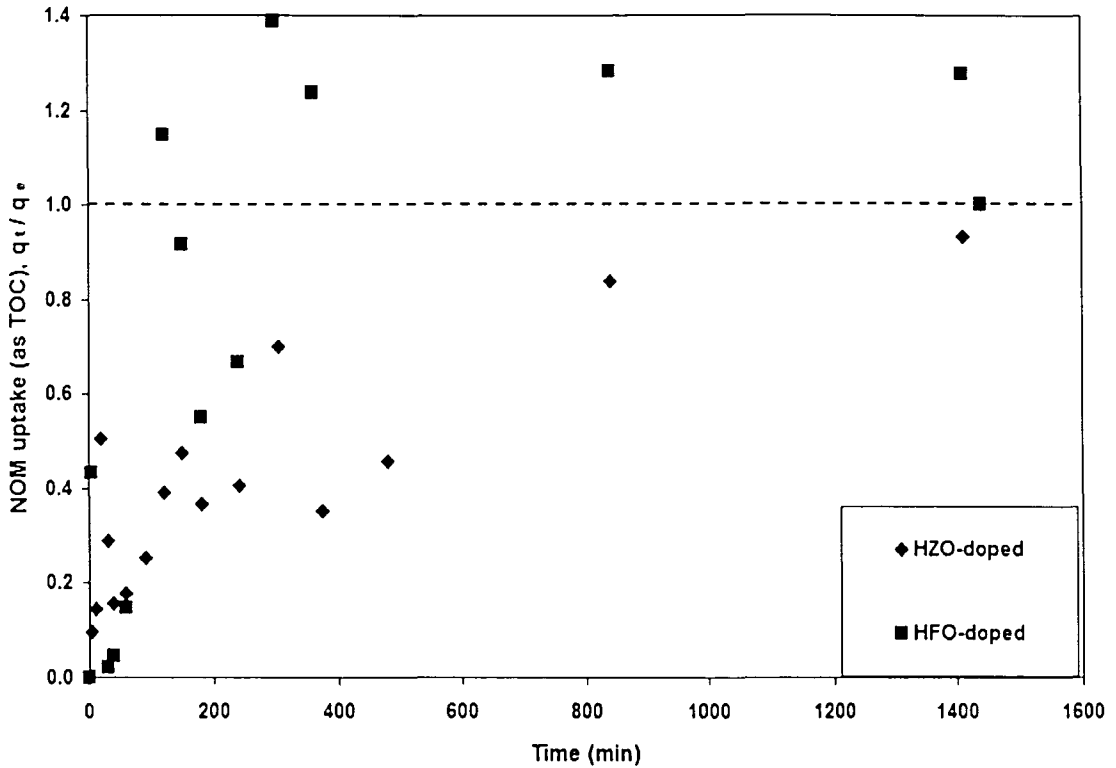


Figure 3.27 – Comparison of Kinetic Test Results for HAIX-F(Fe) and HAIX-F(Zr) with Dilute NOM Brine

It is interesting to note that HAIX-F(Fe) and HAIX-F(Zr) fibers seem to follow relatively similar trends until about 300 minutes of operation. At that time, fractional uptake capacity for HAIX-F(Fe) dramatically increases. Clearly, achievement of specific fractional uptake values occurs at later times than corresponding oxalate and phthalate experimentation. Factors affecting data precision are further discussed in section 4.5.

3.6 Regeneration of HAIX-F Media in Fixed-Bed Configuration

Due to the unique chemistry of metal oxide particulates embedded in parent anion exchange fibers, HAIX-F media is capable of simple chemical regeneration. Essentially, a

regenerant solution of 2% NaOH and 2% NaCl is contacted with the media in batch or fixed-bed reactor configuration. The regenerant solution alters the metal oxide surface functionality as defined in Figures 1.6 & 1.11. Clearly, at pH 12, or higher, both HFO and HZO surface groups deprotonate and exhibit negative functionality.

From Figures 1.6 & 1.11:

at pH >12,

>95% of HFO surface groups are present as $\overline{\equiv FeOO^-}$

>95% of HZO functional groups exist as $\overline{\equiv ZrOOOH^-}$

Presence of negative surface functionality allows for regeneration via Donnan co-ion exclusion effects. Detailed explanation of Donnan co-ion exclusion effects are presented in section 4.2. For now, consider the simple chloride/sulfate system illustrated in Figure 3.28(a-b). The proposed system has two phases, resin and aqueous, two anionic species, sulfate and chloride, and two cationic species, fixed functional groups and sodium. Consider the resin/bulk liquid boundary as a permeable membrane, then, cations and anions can freely cross from one phase to another in order to achieve electro-chemical equilibrium. However, the fixed functional groups ($-R^+$) are bound to the anion exchanger phase. Electroneutrality, then, maintains that sodium cations cannot diffuse into the resin phase because of the inability of fixed functional groups to permeate into aqueous phase. Note that anions can still permeate the resin/liquid boundary.

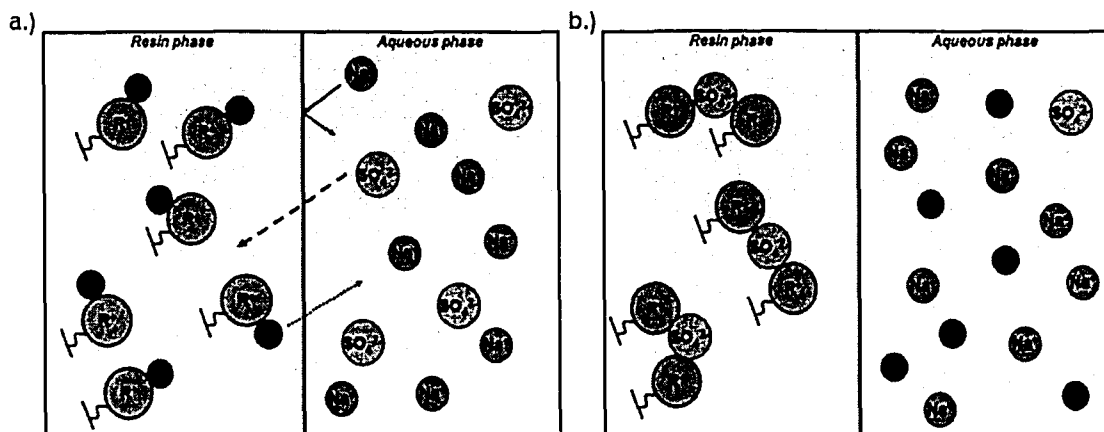


Figure 3.28(a-b) – Schematic Illustrating Donnan Co-Ion Exclusion Effects

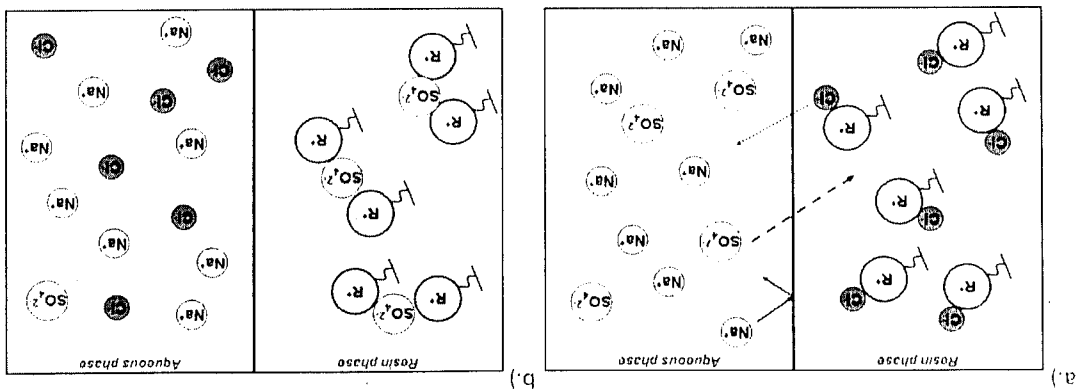
Figure 3.28a demonstrates initial conditions; the resin is in chloride form. During the exchange period, sodium cations are rejected from crossing into the resin phase, divalent sulfate anions exchange with monovalent chloride anions due to the resin's greater affinity for divalent anions. In Figure 3.28b, effective operational equilibrium has been reached.

Consider regeneration. Essentially, $-R^+$ functional groups, which are HFO and HZO nanoparticulates in this case, undergo functionality reversal (i.e., $-R^+$ surface functional groups become $-R^-$ groups due to metal oxide surface chemistry of metal oxides as discussed above. This functionality reversal causes immediate rejection of sulfate from the resin phase. These principles are illustrated in Figure 3.29(a-b). Consider HAIX-F phase reaching an effective equilibrium similar to that described in Figure 3.28b. Now, consider that HAIX-F media is contacted with regenerant solution consisting of 2%NaOH and 2% NaCl as shown in Figure 3.29a. HAIX-F surface functionality is reversed and three simultaneous events (depicted in Figure 3.29b) occur: (1) sulfate is expelled from the HAIX-F phase, (2) sodium ion is effectively sorbed by metal oxide surface functional groups, and (3) hydrogen ion is released from metal oxide surface groups, interacts with hydroxyl ion, and forms water.

nanoparticles in this case, undergo functionality reversal (i.e., $-R^-$ surface functional groups become $-R^-$ groups due to metal oxide surface chemistry of metal oxides as discussed above. This functionality reversal causes immediate rejection of sulfate from the resin phase. These principles are illustrated in Figure 3.29(a-b). Consider HAlX-F phase reaching an effective equilibrium similar to that described in Figure 3.28b. Now, consider that HAlX-F media is contacted with regenerant solution consisting of 2% NaOH and 2% NaCl as shown in Figure 3.29a. HAlX-F sulfate is expelled from the HAlX-F phase, (2) sodium ion is effectively sorbed by metal oxide surface functional groups, and (3) hydrogen ion is released from metal oxide surface groups, interacts with hydroxyl ion, and forms water.

Consider regeneration. Essentially, $-R^-$ functional groups, which are H^+ and H_2O anions, in Figure 3.28b, effective operational equilibrium has been reached. anions exchange with monovalent chloride anions due to the resin's greater affinity for divalent exchange period, sodium cations are rejected from crossing into the resin phase, divalent sulfate Figure 3.28a demonstrates initial conditions: the resin is in chloride form. During the

Figure 3.28(a-b) – Schematic Illustrating Donnan Co-Ion Exclusion Effects



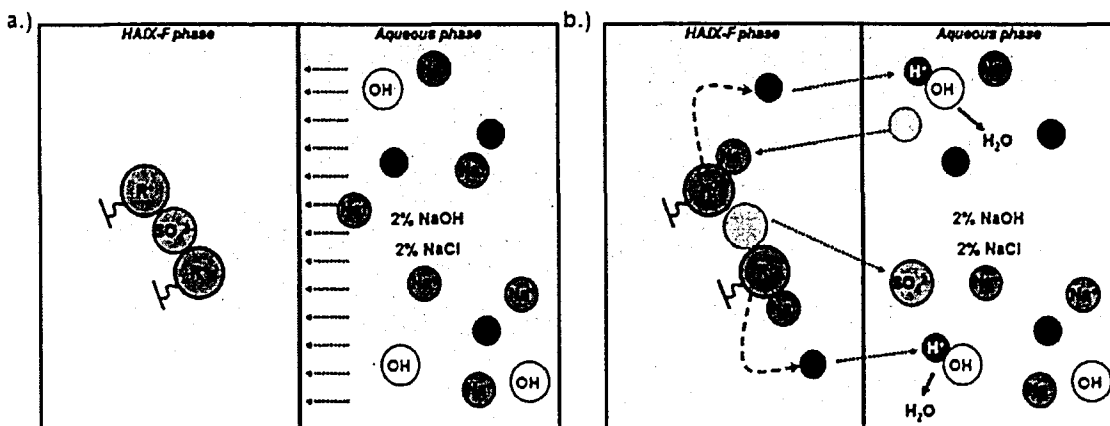


Figure 3.29(a-b) – Schematic Illustrating Regeneration of HAIX-F Media

The following subsections provide regeneration effluent histories and characterization of regeneration efficiency. It should be noted that subsequent to regeneration with caustic solution, fibers were neutralized with CO₂-sparged water in order to render HAIX-F media capable of redeployment.

3.6.1 Regeneration of HAIX-F(Fe) Media

As stated above, exhausted HAIX-F(Fe) media from the column runs detailed in Figures 3.11 & 3.12 were regenerated in fixed-bed configuration using 2% NaOH and 2% NaCl solution at pH ~13. Details regarding regeneration of oxalate and phthalate loaded fibers are provided below. It should be noted that while successful regeneration of NOM-containing HAIX-F(Fe) was completed, strict observance of the concentration history throughout regeneration was not possible due to time constraints.

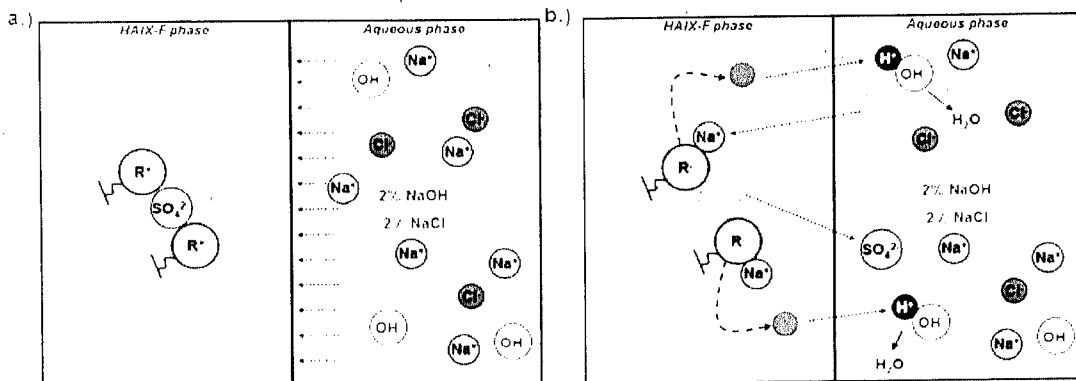


Figure 3.29(a-b) – Schematic Illustrating Regeneration of HAIX-F Media

The following subsections provide regeneration effluent histories and characterization of regeneration efficiency. It should be noted that subsequent to regeneration with caustic solution, fibers were neutralized with CO₂-sparged water in order to render HAIX-F media capable of redeployment.

3.6.1 Regeneration of HAIX-F(Fe) Media

As stated above, exhausted HAIX-F(Fe) media from the column runs detailed in Figures 3.11 & 3.12 were regenerated in fixed-bed configuration using 2% NaOH and 2% NaCl solution at pH 13. Details regarding regeneration of oxalate and phthalate loaded fibers are provided below. It should be noted that while successful regeneration of NOM-containing HAIX-F(Fe) was completed, strict observance of the concentration history throughout regeneration was not possible due to time constraints.

3.6.1.1 Regeneration of HAIX-F(Fe) Laden with Oxalate

Figure 3.30 provides the oxalate concentration effluent history for the regeneration experiment. Note that the fixed-bed column run (Figure 3.11) ran for over 3000 bed volumes before significant oxalate breakthrough occurred. Conversely, regeneration treatment lasted less than 10 operational bed volumes. Hence, time necessary for regeneration is approximately 0.30% that available for treatment. It is important to note that experimental conditions (i.e., SLV and EBCT) remained constant between the column run and regeneration experiment. Clearly, regeneration is extremely efficient due to the Donnan co-ion exclusion effects witnessed because of metal oxide surface chemistry, as described above.

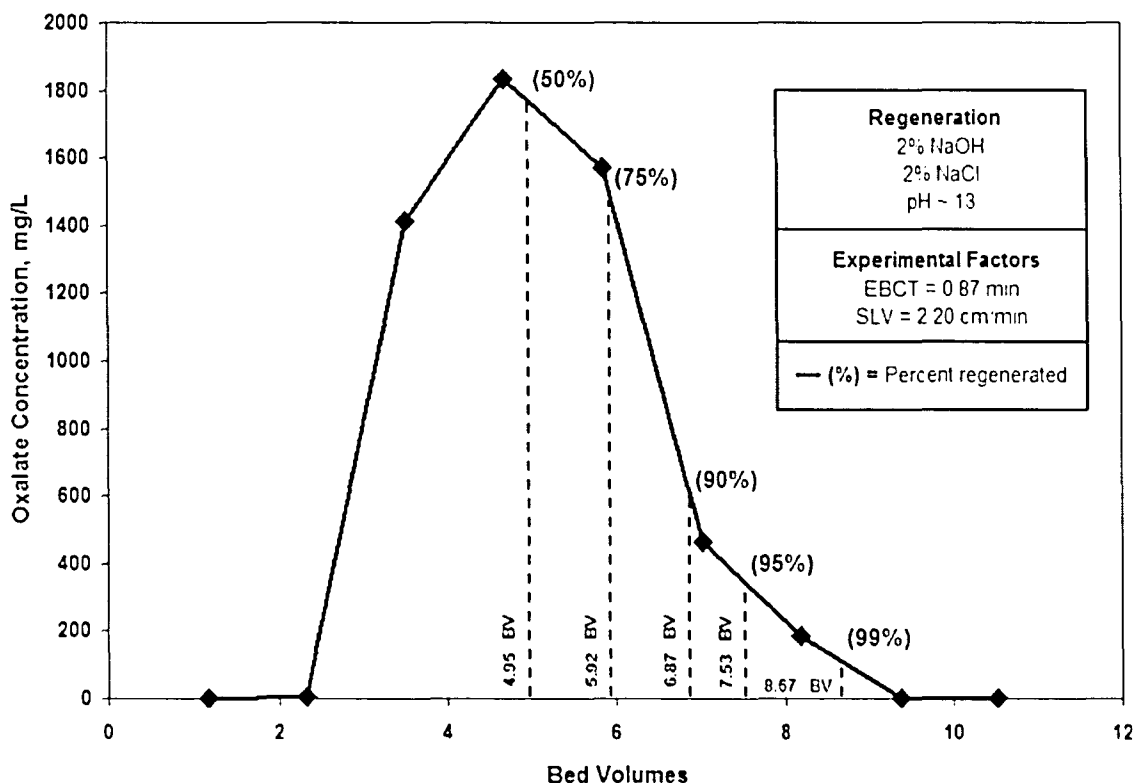


Figure 3.30 – Regeneration Effluent History for HAIX-F(Fe) Oxalate-Loaded Media

Figure 3.30 also provides stepwise regeneration efficiency values and times (as bed

volumes – BV); these values dictate that regeneration half-time occurs after less than three bed volumes, while full regeneration is experienced after only 7 bed volumes. Obviously, the viability of cyclical treatment process design is extremely applicable given the ratio of treatment to regeneration operational times.

3.6.1.2 Regeneration of HAIX-F(Fe) Laden with Phthalate

The concentration history of phthalate during regeneration is provided in Figure 3.31. While the fixed-bed column run successfully operated for over 3000 bed volumes (Figure 3.12) before phthalate breakthrough, regeneration was successfully completed in fewer than 20 bed volumes. Therefore, an operating time to regeneration time ratio of 150::1 was determined; such a large ratio demonstrates the applicability of HAIX-F(Fe) to industrial/municipal processes due to the decreased need for operational redundancy mandated by regeneration needs. Hydraulic and contact time conditions were identical to the column run described in Figure 3.12.

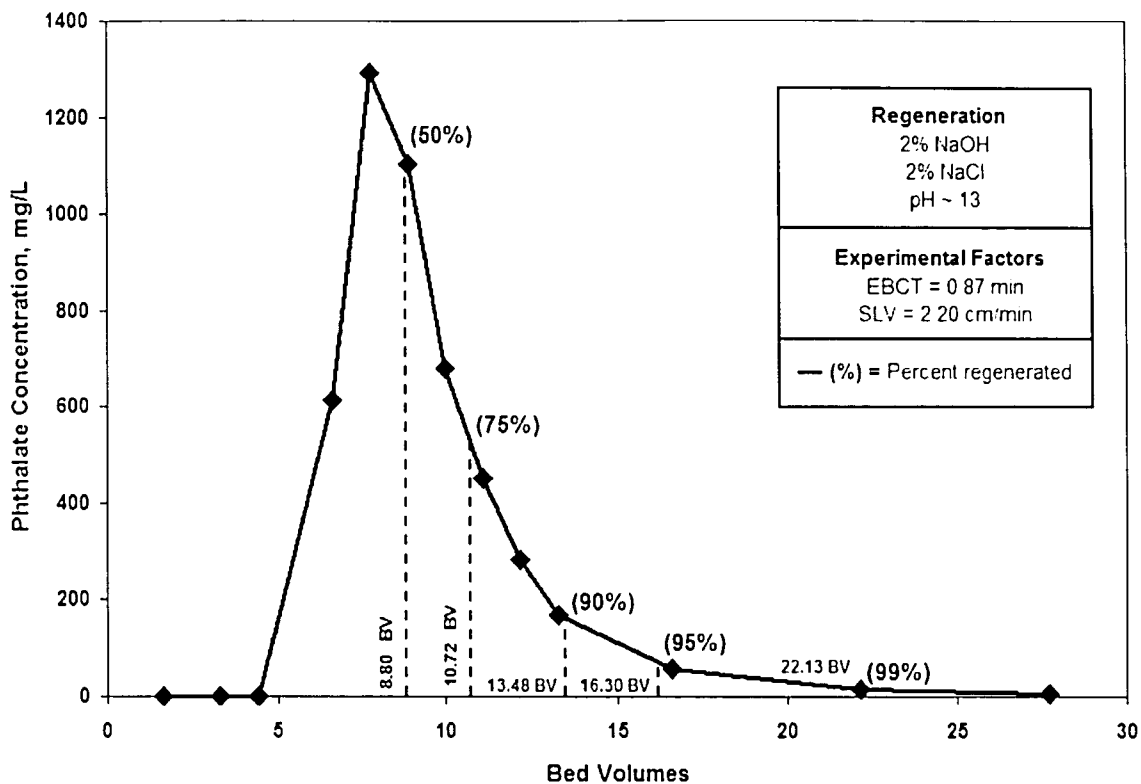


Figure 3.31 – Regeneration Effluent History for HAIX-F(Fe) Phthalate-Loaded Media

Stepwise regeneration efficiency (50%, 75%, 90%, 95%, and 99%) and effective times (as BV) are also listed in Figure 3.31. The amount of time until half and full regeneration are approximately 5 and 25 bed volumes. While these values are significantly greater than similar results from oxalate-laden HAIX-F(Fe), it should be noted that phthalate regeneration experiences a considerable regeneration “tail” as seen in Figure 3.31. Regardless, the ability of regeneration processes to enhance HAIX-F treatment technology attractiveness is extremely valid.

3.6.2 Regeneration of HAIX-F(Zr) Media

HAIX-F(Zr) media loaded with oxalate and phthalate (Figures 3.13 & 3.14) were regenerated in similar fashion as HAIX-F(Fe) media. Essentially, regenerant solution consisting

of 2% NaOH, 2% NaCl solution at pH ~13 was passed through the same fixed-bed of exhausted HAIX-F(Zr) as employed in the fixed-bed column treatment experiment. Results for these regeneration experiments are provided in the following subsections. Furthermore, measurement of TOC concentration history throughout regeneration of NOM-laden HAIX-F(Zr) could not be completed due to time constraints.

3.6.2.1 Regeneration of HAIX-F(Zr) Laden with Oxalate

The HAIX-F(Zr) oxalate-loaded media regeneration experienced equipment malfunction during operation; hence, any results could not be recorded with precision. Based off of the previous regeneration experiments and that provided below for phthalate expulsion from HAIX-F(Zr), it is expected that oxalate-laden HAIX-F(Zr) was effectively regenerated within 10-20 bed volumes.

3.6.2.2 Regeneration of HAIX-F(Zr) Laden with Phthalate

Effluent concentration history from the regeneration experiment for exhausted HAIX-F(Zr) media yielded the results presented in Figure 3.32. Previously, HAIX-F(Zr) removed phthalate for over 3000 bed volumes (Figure 3.14) before breakthrough was experienced. Regeneration demonstrated the ability to recover sorbed phthalate in approximately 12 bed volumes, providing an operation/regeneration time requirement of about 300:1. SLV and EBCT values were maintained at the same levels as employed in the phthalate treatment “loading” experiment, i.e., phthalate removal from synthetic surface water.

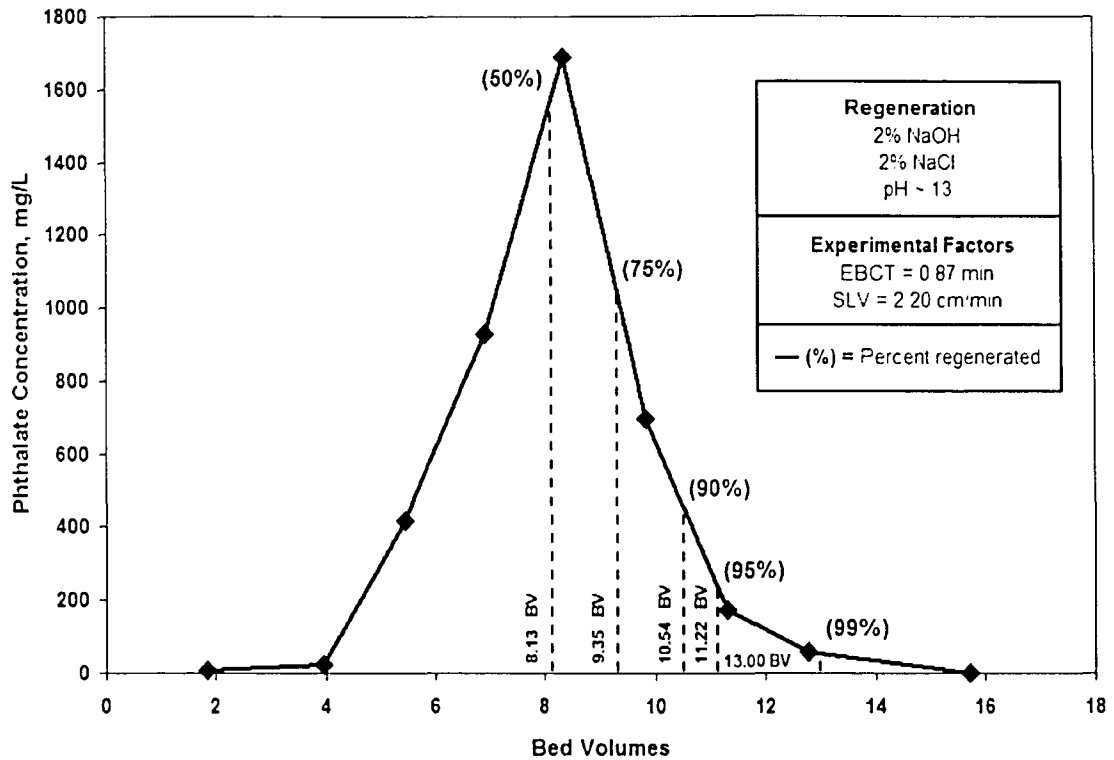


Figure 3.32 – Regeneration Effluent History for HAIX-F(Zr) Phthalate-Loaded Media

Figure 3.32 also provides the regeneration efficiency at various points. These points are indicated by dashed vertical lines with corresponding time (as BV). Noticeably, regeneration half-time is experienced after only 6 bed volumes, while full regeneration is witnessed after less than 12 bed volumes. Again, it should be reiterated that such highly effective regeneration allows for high potential of industrial/municipal adoption of the technology described throughout this report.

3.6.3 Comparison of Regeneration History for HAIX-F Media

In order to provide further explanation of regeneration processes and discussion regarding any differences between regeneration of HFO and HZO containing fiber media, consider the following sections, which compare regeneration kinetics of HAIX-F media with

regards to oxalate and phthalate.

3.6.3.1 Comparison of Oxalate Regeneration Runs

Because of the equipment malfunction that occurred during HAIX-F(Zr) oxalate-laden media regeneration, comparisons between HAIX-F media can not be made. Regardless, a modified plot of regeneration efficiency (as percent regeneration completed) vs. bed volumes for HAIX-F(Fe) regeneration is provided in Figure 3.33. Note the sharp “s”-shaped curve, which denotes almost ideal plug-flow characteristic.

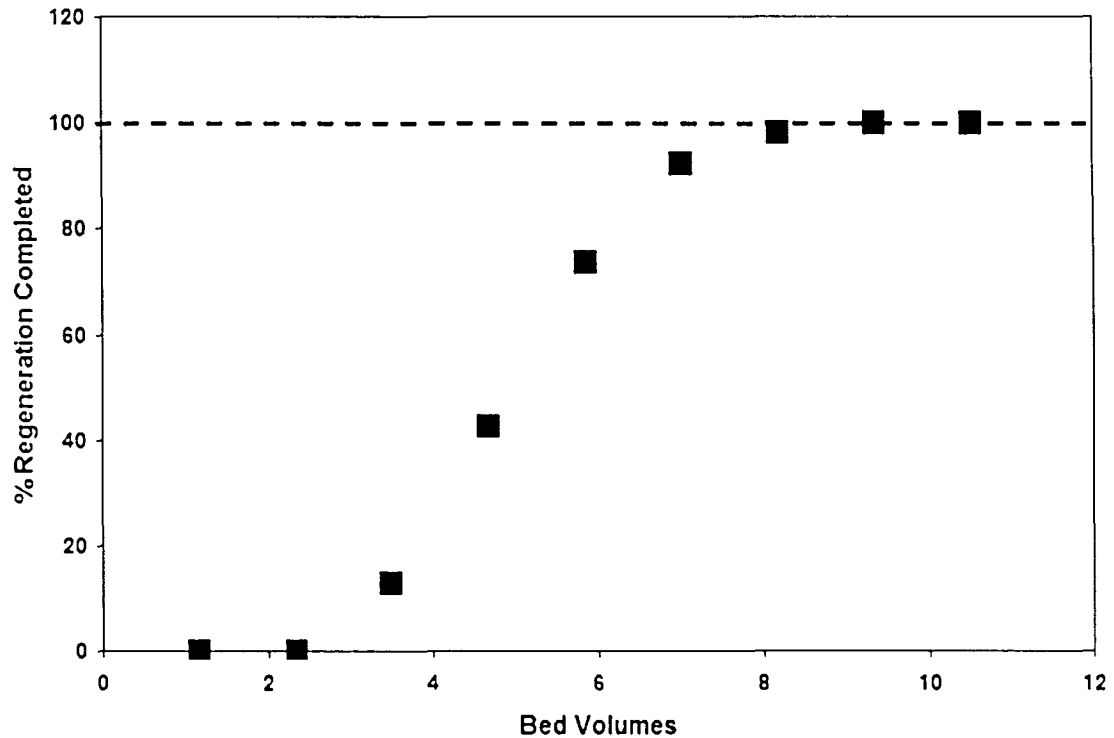


Figure 3.33 – Regeneration Efficiency vs. Bed Volumes for Oxalate Laden HAIX-F(Fe) Regeneration

Due to the consistency of regeneration processes for phthalate experiments, adequate

assessment of potential differences should be covered in the following section.

3.6.3.2 Comparison of Phthalate Regeneration Runs

Figure 3.34, below, demonstrates that HAIX-F media regeneration follow well-behaved “s”-shaped curves. It should be noted that HZO-loaded fibers provide faster regeneration kinetics as compared to HFO-loaded fibers, due to the steeper slope observed in Figure 3.34. This finding is in agreement with observed kinetic rates determined in sections 3.6.1.2 & 3.6.2.2. Obviously, zirconia nanoparticulates exhibit kinetic advantage over ferric oxide particulates during treatment and regeneration. As HFO PZC is lower than the corresponding value for HZO, the better kinetics are probably not a result of metal oxide chemistry. One possibility is that higher HFO loading and subsequent HAIX-F phase phthalate concentration (on per gram HAIX-F basis) dictate slightly slower kinetics due to expulsion of higher phthalate mass; however, as characteristics explored in treatment, kinetics, and regeneration experimentation display awesome abilities for application of HAIX-F media, these slight differences can be considered negligible.

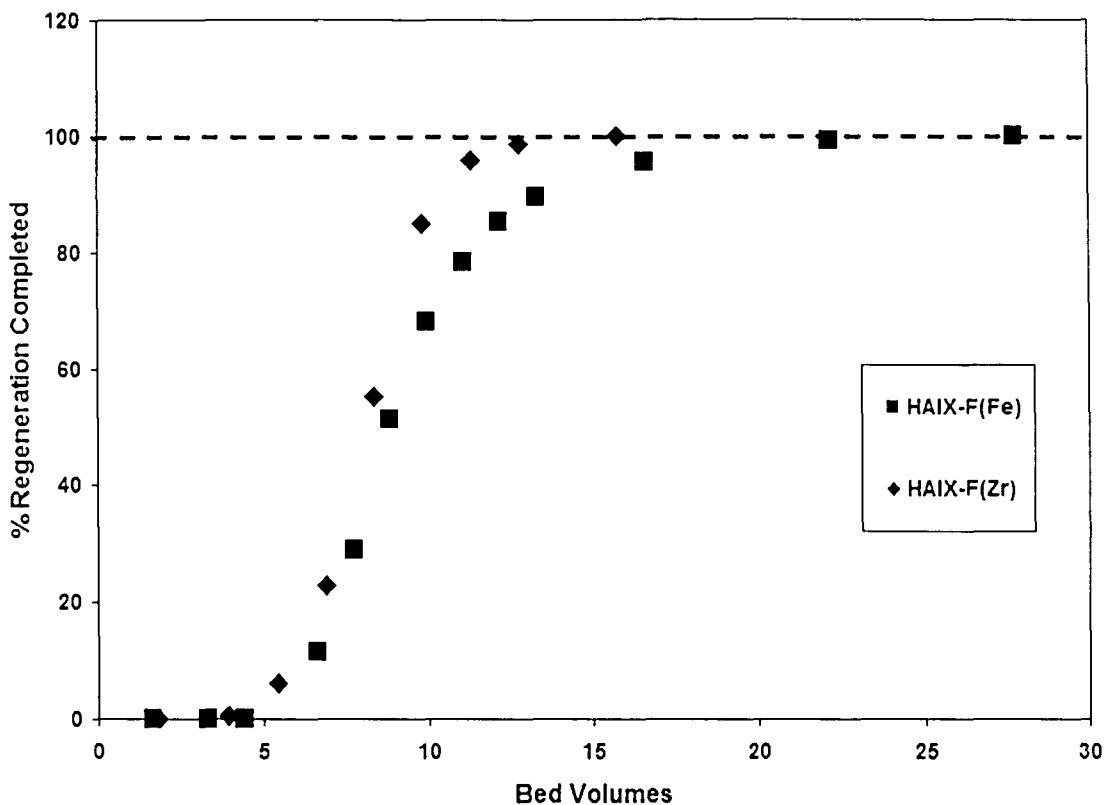


Figure 3.34 – Comparison of HAIX-F Phthalate-Loaded Media Regeneration

Table 3.9 allows comparison of effective realization of regeneration percent. Note that regeneration curves were normalized at the point where phthalate concentration first appeared in effluent samples. Obviously, there is a definite capability for highly efficient regeneration.

Table 3.9 – Time (BV) Until Specified Regeneration Efficiency

Media	Regeneration Efficiency				
	50%	75%	90%	95%	99%
HAIX-F(Fe)	4.36	6.29	9.23	11.87	17.66
HAIX-F(Zr)	4.18	5.40	6.59	7.27	9.72

3.7 Alternative Analysis of TOC Concentration Data

Due to the large amount of scatter experienced in NOM concentration (as TOC) analysis with TOC Analyzer, various other methods of measuring TOC were undertaken. The following

sections discuss applicability of ion chromatography and UV/VIS absorbance towards effective TOC measurement.

3.7.1 Ion Chromatography

During sulfate and chloride ion sample analyses on the Ion Chromatograph (section 2.6.2) from fixed-bed column and kinetics experiments, an unknown peak routinely occurred at approximately 4.33 minutes. As results from the TOC Analyzer (section 2.6.1) were highly scattered and did not adhere to the theorized breakthrough/uptake trends, any correlation that provided precise results would be appreciated, as correlation and calibration curves based on known standards could be generated. For that reason, the area under the 4.33 minute IC peak was plotted against TOC data for the HAIX-F(Zr) kinetic test (Figure 3.35). The TOC data was normalized with the 4.33 peak data at $t = 0$.

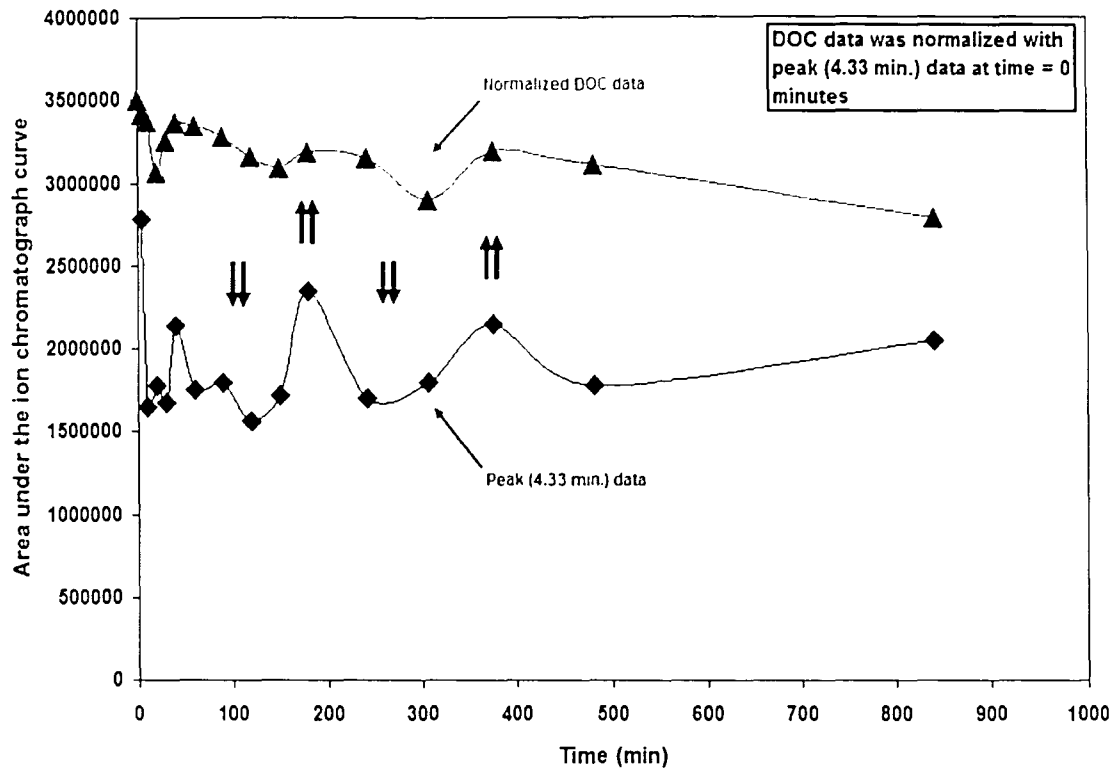


Figure 3.35 – Comparison of Kinetic Test Results for HAIX-F(Zr) and IC Output at 4.33 Minutes

Clearly, the 4.33 minute IC peak and the TOC data from the TOC Analyzer exhibit the same trends and correlations (i.e., directly related); therefore, ion chromatography may provide an alternate analysis technique for tracking TOC concentrations. Furthermore, the 4.33 minute IC peak should represent only a fraction of total NOM; since IC peak values are consistently less than normalized TOC concentration data, the fact that IC peaks represent only a fraction of total TOC is in order.

In order to validate this analysis technique, consider the same type of plot for HAIX-F(Fe) media (Figure 3.36).

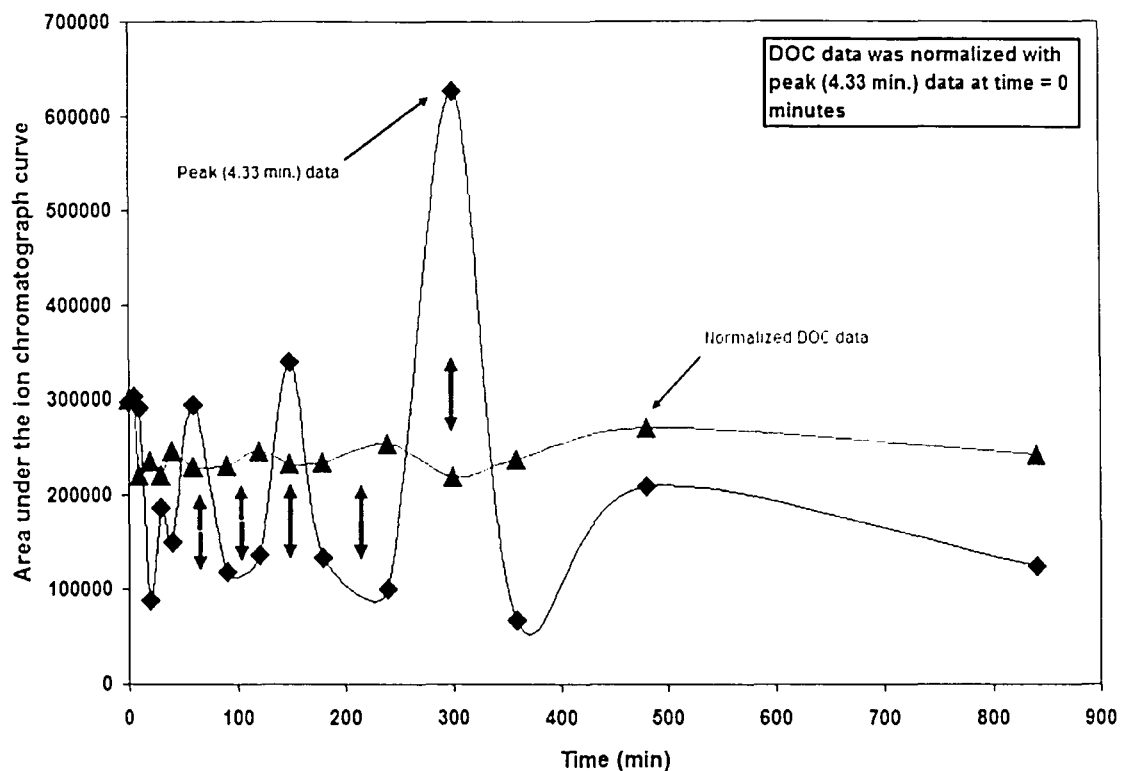


Figure 3.36 – Comparison of Kinetic Test Results for HAIX-F(Fe) and IC Output at 4.33 Minutes

Obviously, IC peaks and TOC concentrations are inversely related for HAIX-F(Fe) kinetic test data. Furthermore, peak data exceeds the normalized TOC data in at least three instances, which doesn't follow. For these reasons, TOC concentration cannot be related to 4.33 minute IC peak data and precision measurement of TOC concentrations using IC output cannot be completed.

3.7.2 UV/VIS Spectrometry

The open literature contains numerous examples of NOM analytical techniques through UV/VIS spectrometry [Morrin et al., 1996; Matilainen et al., 2002; Abbt-Braun and Frimmel,

1999; Her et al., 2002]. For that reason, data from HAIX-F(Zr) fixed-bed column run was analyzed using UV/VIS spectrometry at 254 nm as described in the literature. Results of sample analysis using this technique are compared to TOC concentrations measured by TOC Analyzer (Figure 3.37).

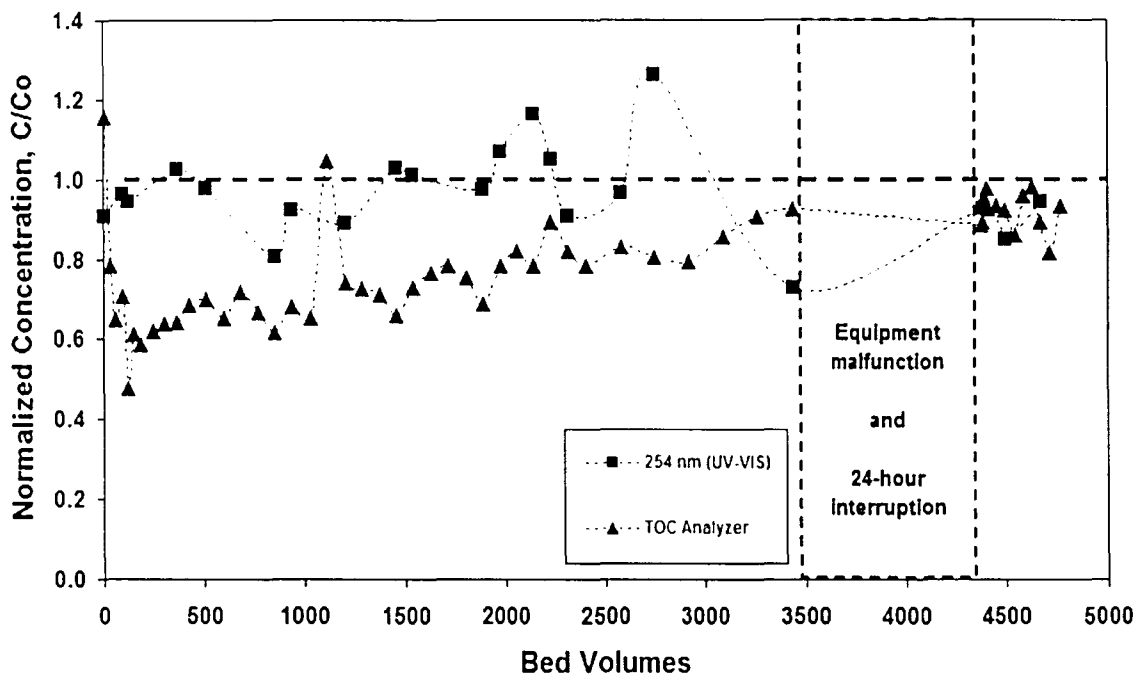


Figure 3.37 – Comparison of NOM Concentration Results Measured via UV/VIS Spectrometry and TOC Analyzer

From Figure 3.37, no clear correlation between the methods can be asserted; at some points curves are directly related and at others, curves are inversely related. Therefore, although the NOM data is not especially well-behaved, results from the TOC Analyzer provide a good idea of how TOC concentrations are changing with respect to time. The scatter of results will be discussed in further detail in section 4.5.

3.8 Modeling HAIX-F abilities for Water Treatment Facilities

In order to apply HAIX-F media to water treatment facilities for reduction of DBP formation potential through removal of NOM compounds, some modeling work was completed in order that municipalities could easily distinguish the water volumes capable of treatment before regeneration is necessary for a variety of flow configurations, including the following: constant stir tank reactor (CSTR), plug-flow reactor (PFR), bypass flow rates, redundancy, and multiple reactor employment. The model was created using C++ programming language and can be provided upon request. From the model's output, HAIX-F employment for low-medium level NOM concentrations in low-medium flow plants satisfactorily meets EPA regulations without excessive regeneration requirements. Sample output from the model can be observed in Figure 3.38. More detail about this model is provided in section 4.6.



```

c:\h:\Thesis\Program\Debug\cpp_program.exe
*****  CONSTANTS  *****
Experimental analysis has demonstrated a H1X-F breakthrough capacity
of 7.1 mg DOC / g H1X-F when operated in PFR configuration.
Experimental analysis has demonstrated that H1X-F has a total capacity
of 11.9 mg DOC / g H1X-F when operated in CSTR configuration.
The H1X-F media density has been experimentally determined to be 1.4 g/dL.
Press any key to continue . . .

c:\h:\Thesis\Program\Debug\cpp_program.exe
*****  BYPASS FLOW  *****
Do you want any bypass flow around the pretreatment units (Y/N)? n
Press any key to continue . . .

c:\h:\Thesis\Program\Debug\cpp_program.exe
*****  FLOW SCHEME  *****
Do you want to run in PFR (P) or CSTR (C) configuration? p
You have chosen to operate the NOM treatment process in PFR configuration.
How many fixed bed columns do you want to be available? 10
Out of the 10 columns being utilized, how many parallel streams do you want? 5
You want 5 parallel streams, each containing 2 columns in series.
NOTE: In order to maximize regeneration efficiency, one stream should be
'turned off' at any given time.
How many parallel streams should be simultaneously in operation? 4
Press any key to continue . . .

c:\h:\Thesis\Program\Debug\cpp_program.exe
*****  DETAILS  *****
There is no bypass stream.
You are operating in PFR configuration.
There are 10 fixed bed units, containing 500 liters of H1X.
There are 5 parallel streams, containing 2 units in series.
The flow rate to each parallel stream is 2.5 MGD.
Press any key to continue . . .

c:\h:\Thesis\Program\Debug\cpp_program.exe
*****  SOLUTIONS  *****
Approximately 1.14e+06? Liter(s) of treated water can be
treated for DEP formation potential.
- @ total of 10 MGD will pass EPA regulations.

The system can efficiently remove DEP formation potential for
approximately 14.5 hours.
Press any key to continue . . .

```

Figure 3.38 – Output Screens from C++ Based Model

CHAPTER 4: DISCUSSION

This chapter seeks to provide further detail regarding some of the processes described in preceding chapters. Essentially Chapter 4 should yield generalized discussion surrounding process chemistry of HAIX-F selective sorption of organic carbon compounds as described in the preceding experimentation.

4.1 Sorption Affinity and Mechanisms

As discussed throughout the body of this report, HAIX-F affinity is mandated by anionic valence, which affects electrostatic interaction capability, and ability for LAB interaction via formation of inner-sphere complexes. First, consider electrostatic, or Coulombic, interaction. Common characteristics known to influence ion exchange affinity for aqueous species include the following:

- Valence
- Molecular weight
- Ionic radius
- Hydrated ionic radius
- Hydration energy

It should be noted that ion exchange affinity varies directly with the absolute value of ionic valence, molecular weight, ionic radius, hydrated ionic radius, and hydration energy. Characteristic values of mentioned properties for chloride and sulfate species are provided below in Table 4.1. From Table 4.1, sulfate selectivity over chloride ion is immediately apparent due to the relationship between exchange affinity and the listed properties; such a conclusion is in

accordance with findings from sections 3.4.1, 3.4.2, 3.5.1 & 3.5.2.

Table 4.1 – Relevant Properties for Chloride/Sulfate Ion Exchange Affinity

Ion	Valence	Molecular Weight (AMU)	Ionic radius (nm)	Hydrated Ionic Radius (nm)	Hydration Energy (kJ/mol)
chloride	-1	35.45	0.181	0.347	376
sulfate	-2	96.00	0.230	0.380	1138

Chloride with a negative one (-1) valence and lower molecular weight, ionic radius, hydrated ion radius, and hydration energy is rapidly displaced from anion exchange sites by sulfate anions and dissolved organics. Sulfate's negative two (-2) ionic charge allows for a more competitive sorption mechanism compared with chloride; however, dissolved organic anions inherently have greater molecular weight, ionic radius, hydrated ionic radius, and hydration energy because of the large number of carbon atoms and carboxylic groups (among other reasons) as shown in Figure 1.1. Therefore, organic anions will experience greater electrostatic selectivity in regards to R_3N^+ anion exchange sites present in HAIX-F media. For these reasons, chloride should experience a relatively rapid breakthrough; due to the greater selectivity of sulfate ions, sulfate breakthrough will occur later. On the other hand, anionic organic species can be readily sorbed onto anion exchange sites without undergoing expulsion due to competition effects. The results present in sections 3.4.1 & 3.4.2 precisely demonstrated these principles. Such interaction between chloride, sulfate, and dissolved organic carbon (DOC) with anion exchange sites via electrostatics is termed outer sphere complexes.

Now, consider LAB bonding mechanisms. Oxalate, phthalate, and NOM are capable of forming inner-sphere complexes with metal oxide functional groups as discussed in section 1.4.2. Dissolved organic species act as Lewis bases due to electron donation potential available at carboxylic groups (among others – see equations 22-25); meanwhile, metal oxide surface functional groups fill the electron acceptor, or Lewis acid, role. When these two entities react, an

inner-sphere complex is created. Essentially, inner-sphere complexation means that the product, resulting from LAB interaction, is a single compound that is bound directly to metal oxide groups. Alternatively, chloride and sulfate can only form outer-sphere complexes whereby the product resultant from interaction is located within the outer Helmholtz plane, or Stern layer. Examples of inner- and outer-sphere complexation are available in Figure 4.1. Note that s , a , β , and d represent planes associated with surface hydroxyl groups (s), inner-sphere complexes (a), outer-sphere complexes (β), and the diffuse ion swarm (d). Essentially, the Helmholtz plane (or Stern layer) boundary exists at a .

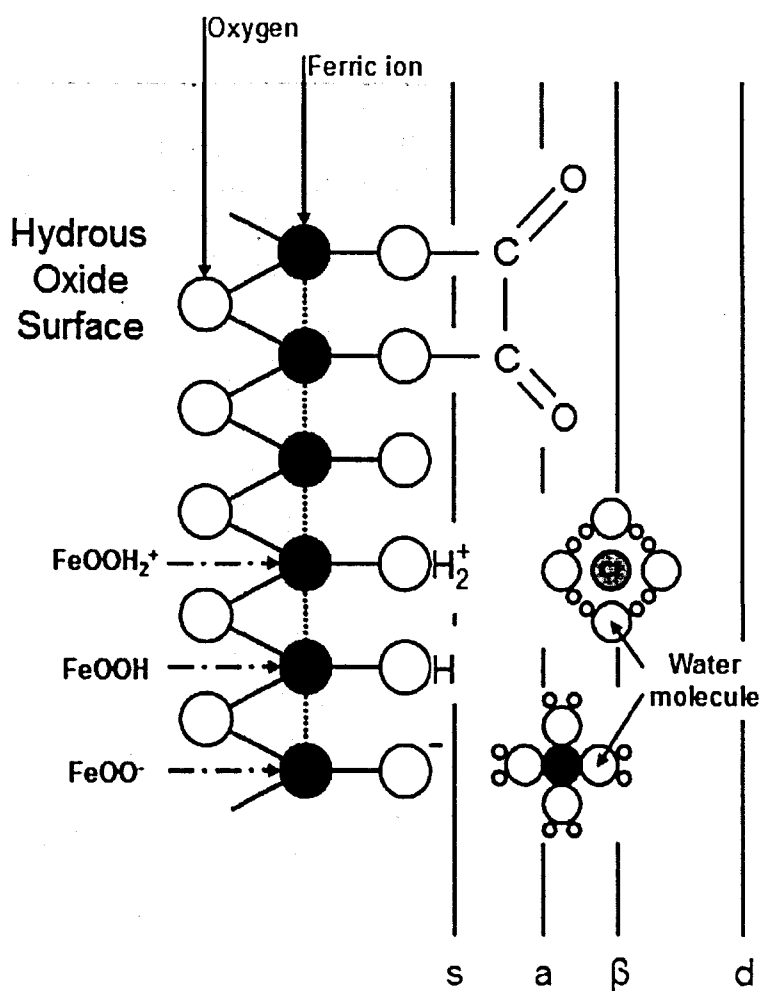
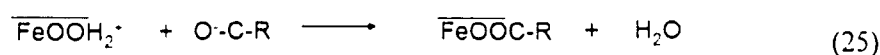
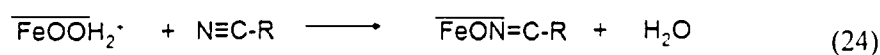
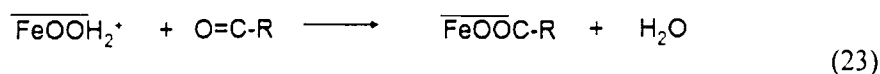
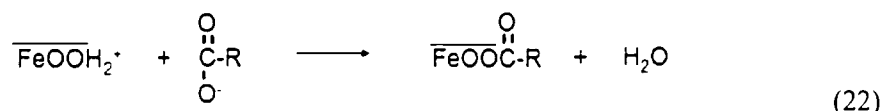


Figure 4.1 – Illustration of Inner- and Outer-Sphere Complexation Reactions

Lewis acid-base reactions can occur at carboxyl groups, hydroxyl groups, nitrogen atoms, or double bonded oxygen atoms. Consider the following equations (equations 22-25), which summarize sorption interaction for different functional groups present in NOM compounds (see Figure 3.2).



For oxalate and phthalate, LAB bonding occurs between carboxylic groups present on organic species and neutral or positively charged metal oxide surface functional groups. For NOM compounds, LAB interaction can occur between various functional groups present in NOM structure and metal oxide active groups; however, as carboxyl groups are most prevalent (Figure 3.2) and most easily deprotonated, inner-sphere complexation typically occurs here.

Figures 4.2-4.3 demonstrate sorption mechanisms for both positively charged and uncharged HZO and HFO functional groups with oxalate and phthalate, respectively. Notice that sorption occurs at the surface hydroxyl plane boundary, which indicates inner-sphere complexation as described above in Figure 4.1.

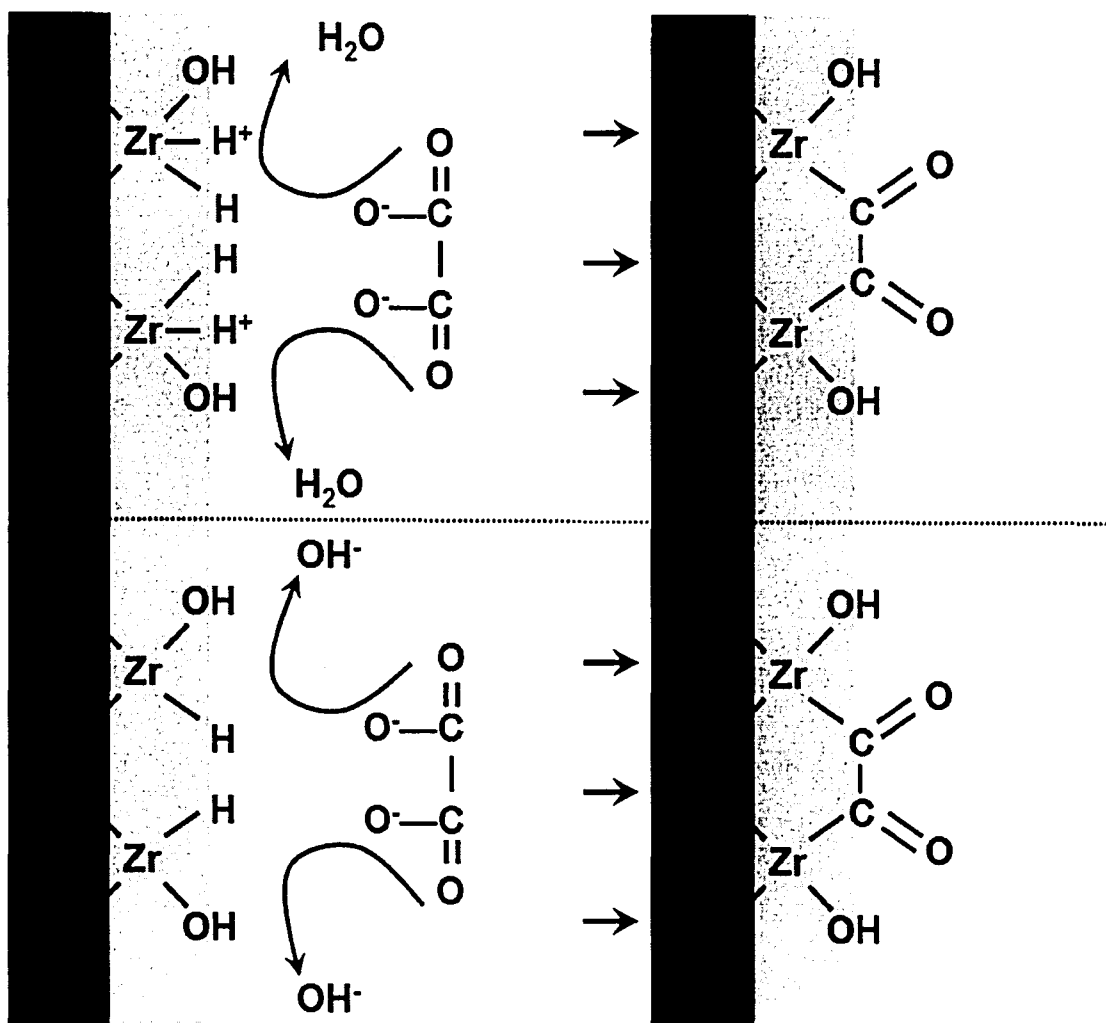


Figure 4.2 – Oxalate Sorption Mechanisms onto Hydrous Zirconium Oxide Surface

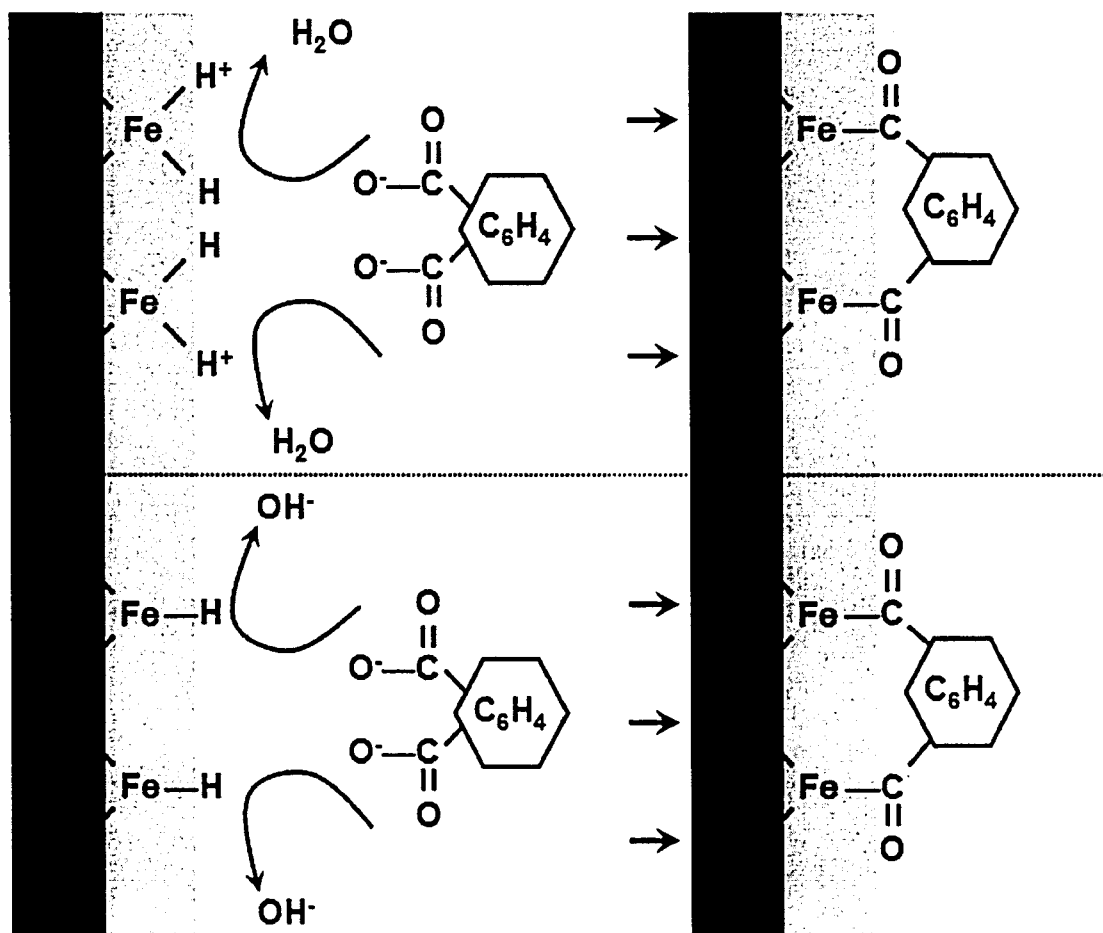


Figure 4.3 – Phthalate Sorption Mechanisms onto Hydrous Ferric Oxide Surface

In summary, chloride quickly passes through hybrid anion exchange media via diffusion along anion exchange sites where relatively unselective monovalent interaction occurs. Similarly, chloride can interact with positively charged metal oxide surface groups through monovalent Coulombic interaction; however, due to low valence, molecular weight, and hydration energy and small ionic radius and hydrated ionic radius, chloride is quickly displaced by divalent sulfate anions. Sulfate, like chloride, only forms outer-sphere complexes (see Figure 4.1) with metal oxide surface functional groups, but electrostatic interaction is slightly more selective due to existence of divalent charge. Oxalate, phthalate, and NOM are capable of selective electrostatic binding (Figures 4.2-4.3) onto embedded metal oxide nanoparticulates due to aqueous and

polyvalent characteristics. Sorption/desorption mechanisms for NOM surrogate compounds with HAIX-F media is provided in Table 4.2-4.3.

Table 4.2 – Sorption/Desorption Mechanisms for Oxalate onto HAIX-F(Fe)

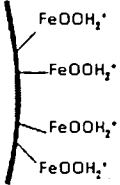
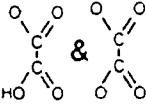
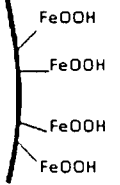
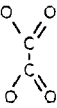
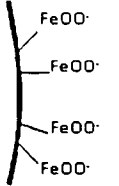
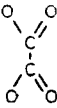
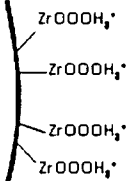
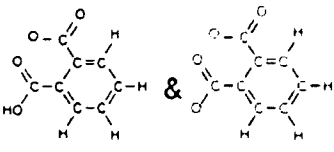
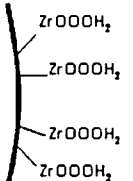
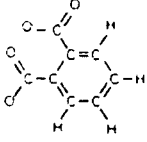
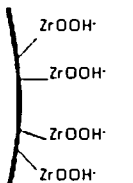
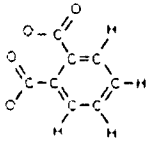
pH	Dominant Surface Functionality	Species	Sorption/Desorption Mechanisms
4.0 - 6.5			<p style="text-align: center;"><u>SORPTION</u></p> <p>Mono/bidentate inner-sphere complexation:</p> <ul style="list-style-type: none"> > Coulombic interaction > Lewis acid-base interaction
6.5 - 9.0			<p style="text-align: center;"><u>SORPTION</u></p> <p>Bidentate inner-sphere complexation:</p> <ul style="list-style-type: none"> > Lewis acid-base interaction
9.0 - 14.0			<p style="text-align: center;"><u>DESORPTION</u></p> <p>Donnan co-ion exclusion effects</p>

Table 4.3 – Sorption/Desorption Mechanisms for Phthalate onto HAIX-F(Zr)

pH	Dominant Surface Functionality	Species	Sorption/Desorption Mechanisms
4.0 – 7.35			<p style="text-align: center;"><u>SORPTION</u></p> <p>Mono/bidentate inner-sphere complexation:</p> <ul style="list-style-type: none"> > Coulombic interaction > Lewis acid-base interaction
7.35 – 9.85			<p style="text-align: center;"><u>SORPTION</u></p> <p>Bidentate inner-sphere complexation:</p> <ul style="list-style-type: none"> > Lewis acid-base interaction
9.85 - 14.0			<p style="text-align: center;"><u>DESORPTION</u></p> <p>Donnan co-ion exclusion effects</p>

Regardless of the sorption mechanism, various factors will affect applicability of HAIX-F towards TOC treatment. The next two sections (sections 4.2-4.3) examine several important details that permit HAIX-F technology to exhibit significant advantage over traditional treatments (section 1.3).

4.2 Sorption Capabilities and Effect of Donnan Co-Ion Exclusion

Chapter 3 clearly details the affinity of HAIX-F media for organic compounds over background anions during constant stir batch experiments, fixed-bed runs, and kinetics tests. Additionally, sulfate anions are more selected than chloride anions. Figures 4.4-4.5, below, demonstrate that chloride anions pass into HAIX-F media, but because of low relative affinity of anion exchange sites and metal oxide surface groups, no significant chloride removal is

experienced (illustrated with dashed lines). Sulfate, on the other hand, exhibits a slightly higher removal by anion exchange groups and charged HFO functional groups (illustrated with dotted lines), but divalent sulfate anions are displaced by NOM compounds, which display both Coulombic and Lewis acid-base interaction. It should be noted that the majority of sorption occurs at the metal oxide surface as opposed to R_4N^+ anion exchange groups. The reason for this occurrence lies in the fact that anion exchange groups provide sorption only through Coulombic mechanisms. Because of the relatively large amount of organic and background particles present in synthetic surface water solutions (per Avogadro's number), significant removal at mg/L (or ppm) concentration levels is not possible. On the other hand, a sizeable mass of metal oxide nanoparticles was effectively loaded onto parent anion exchange fibers; such mass provides adequate sorption (electrostatic and LAB) sites. Given the "rough texture" (Figure 2.2b) of loaded metal oxide particulates, full advantage of available surface functionality can be utilized. For these reasons, metal oxide particulates offer the predominant sorption mechanism. Regardless, anion exchange support material offers several distinct synergistic effects; these effects are detailed below and in section 4.3.

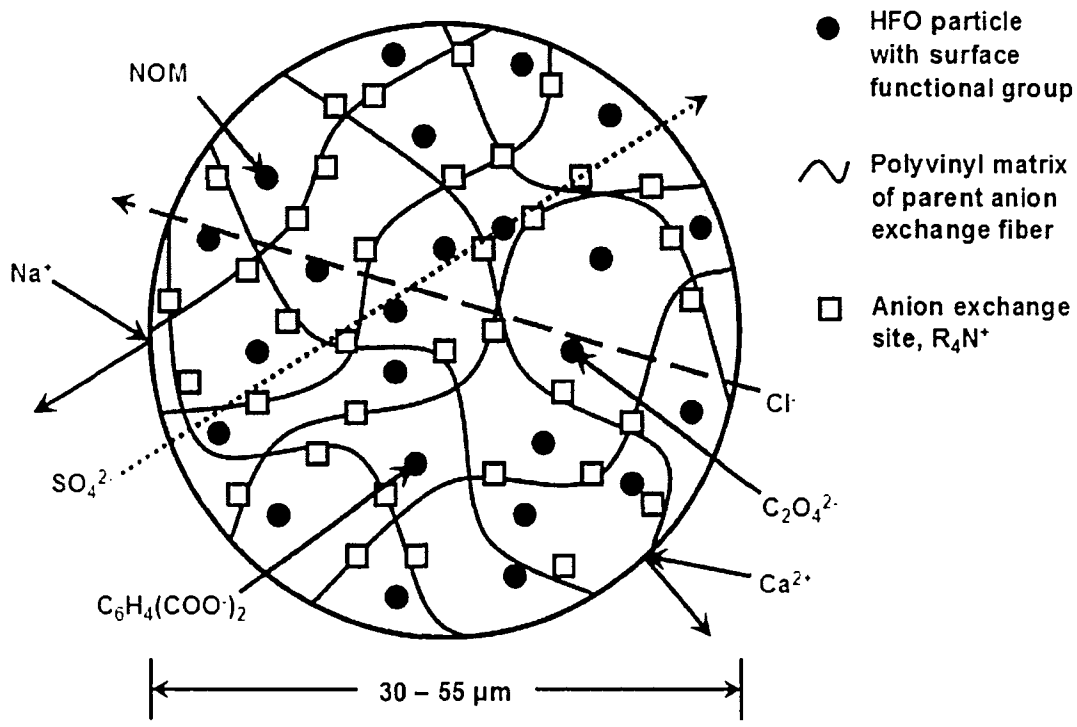


Figure 4.4 – Components and Sorption Processes within HAI-X-F(Fe)

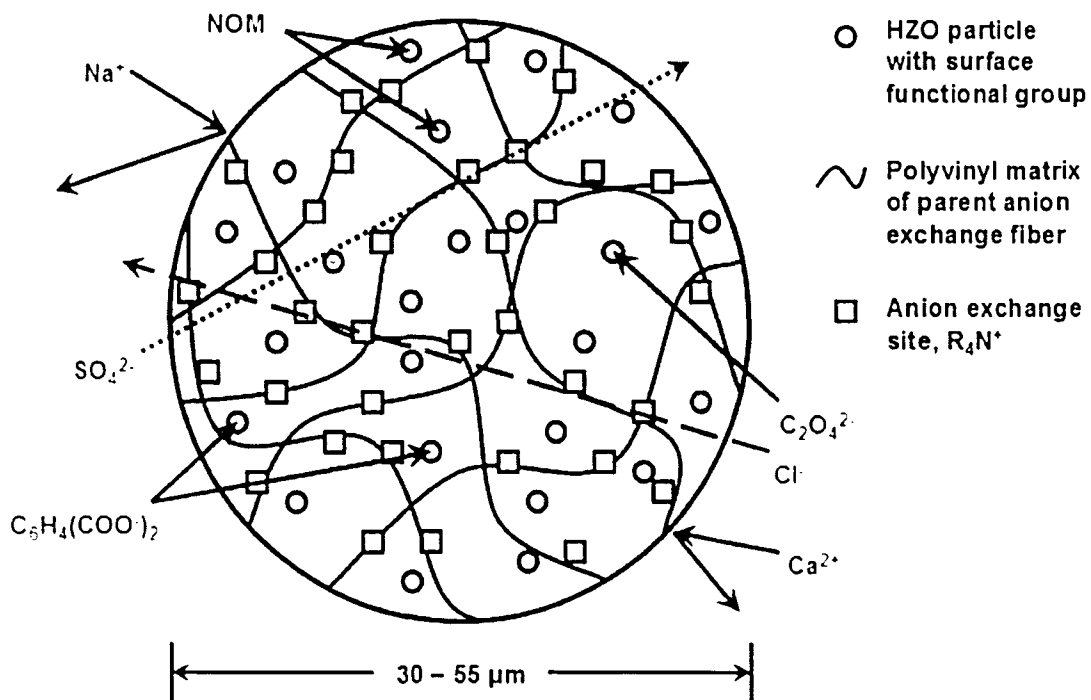
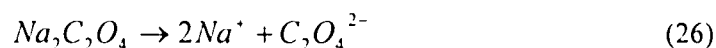


Figure 4.5 – Components and Sorption Processes within HAI-X-F(Zr)

Figures 4.4-4.5 also demonstrate that cations (Na^+ , Ca^{2+}) are rejected from entering HAIX-F media. Such rejection is referred to as Donnan co-ion exclusion; basically, anion exchange sites, R_4N^+ , prevent cations like sodium and calcium from passing through the ion exchange media. As anion exchange sites are permanently fixed to ion exchange fibers through manufacturing processes, conservation of electroneutrality mandates that other cations cannot enter. Formation of ion-pairs containing cations (even in relatively dilute solution) is the one exception to this rule; this potential was discussed in section 3.4.1.2. Essentially, uncharged ion-pairs can enter HAIX-F pores and diffuse through the media; however, such occurrences are rare and do not hold significant import.

Essentially, Donnan co-ion exclusion effects are extensions of the second law of thermodynamics; consider complete ionization of disodium oxalic acid in water (equation 26).



If the fibrous media contains no functionality, then equilibrium should exist when sodium and oxalate aqueous phase concentrations are equal within media pores and in bulk solution (equation 27).

$$[\text{Na}^+]_F^2 [\text{C}_2\text{O}_4^{2-}]_F = [\text{Na}^+]_S^2 [\text{C}_2\text{O}_4^{2-}]_S \quad (27)$$

where F and S describe electrolyte concentrations within media pore space and in bulk solution, respectively, and $[]$ represents molar concentration. Considering single solute solution containing only sodium and oxalate (as per equation 26), equilibrium conditions maintain equations 28-30. Such equations are based in uniform aqueous phase concentration, chemical electroneutrality, and osmotic pressure equilibrium conditions.

$$[\text{Na}^+]_F = [\text{C}_2\text{O}_4^{2-}]_F \quad (28)$$

$$[\text{Na}^+]_S = [\text{C}_2\text{O}_4^{2-}]_S \quad (29)$$

$$\frac{[Na^+]_F^2}{[C_2O_4^{2-}]_F} = \frac{[Na^+]_S^2}{[C_2O_4^{2-}]_S} = 1 \quad (30)$$

If fixed positive charges (i.e., anion exchange sites) are present within the hybrid fiber media, equilibrium conditions change. Consider that anion exchange sites are present at an arbitrary concentration of 1.0 M (R₄N⁺)Cl⁻ and surrogate NOM compound concentration is 0.01 M (Na⁺)₂C₂O₄²⁻. As R₄N⁺ cannot permeate out of the fiber media towards achievement of osmotic pressure and uniform dispersivity equilibrium conditions, the relative distribution between fiber and solution phases at equilibrium is skewed (equations 31-33) as compared to the aforementioned case (equations 27-30). Numerical values presented in equations 31-33 assume that a 99:1 ratio of oxalate passed into media phase (as per equilibrium conditions) compared to oxalate remaining in solution phase is valid. In reality, the extremely large oxalate/chloride separation factors observed in sections 3.5.1 & 3.5.2 render this assumption as an understatement.

$$\frac{[Na^+]_F^2}{[Na^+]_S^2} \approx \frac{1}{9800} \quad (31)$$

$$\frac{[Cl^-]_F^2}{[Cl^-]_S^2} \approx 12000 \quad (32)$$

$$\frac{[C_2O_4^{2-}]_F}{[C_2O_4^{2-}]_S} \approx 99 \quad (33)$$

Hence, the contaminant species' co-ion (i.e., sodium) is greatly rejected from passage through ion exchange filamentous media due to presence of fixed anion exchange sites and the bivalent nature of oxalate species at near-neutral pH.

Equation 33 describes higher presence of contaminant of concern in media phase due to presence of anion exchange functional groups. Typically, such characteristics allow for advantageous ion exchange capabilities due to the elevated presence of contaminant within the

anion exchanger phase. In this case, increased contaminant presence within the exchanger phase allows for increased sorption kinetics onto metal oxide functional groups.

As evidenced from equations 31-32, cations generally experience relative abundance in solution phase while anions exhibit predominant relative concentration within the media phase. For that reason, all anionic species will be present at enhanced concentration levels with the media; however, due to the affinity of HAIX-F media for organic compounds (sections 3.5.1 & 3.5.2), no problems associated with competition were encountered.

Additionally, another synergy, concerning sorption kinetics, involved with presence of anion exchange support and embedded metal oxide nanoparticulates is described in section 4.3.

4.3 Enhanced Sorption Kinetics Due to Ion Exchange Support

In sections 4.1-4.2, a synergistic role between anion exchange media and metal oxide surface chemistry was established. Consider the section of HAIX-F media shown below in Figure 4.6, which represents an inner pore on HAIX-F(Fe) fibers. Note that both HFO nanoparticulates and anion exchange groups are represented. The figure shows yet another synergy between anion exchange groups and metal oxide nanoparticulates. Essentially, anionic species are accelerated through diffusive pathways until contact with metal oxide particles. An apt analogy concerns zones of low hydraulic conductivity (K) and high conductivity in groundwater aquifers. A water particle can travel through the low K region for hundreds of years before reaching a certain destination; conversely, that particle can migrate to the high K region and reach the same destination in a much shorter time period. Similarly, chloride, sulfate, and dissolved organic carbon anions can shortcut diffusive processes by utilizing strings of anion exchange sites as “high K regions” that allow for rapid flux through ion exchange media before sorption onto HFO

nanoparticulates. This process is known as “anion jumping.”

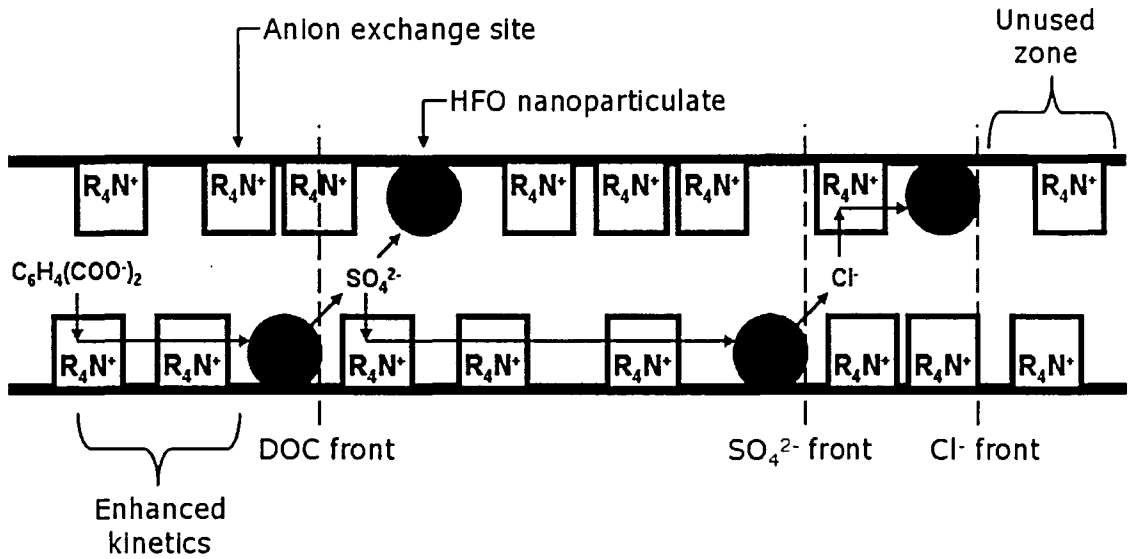


Figure 4.6 – Schematic of Rapid Kinetics due to Synergistic Effect of Ion Exchanger

Support

Now consider Figure 4.7. Imagine that the left hand side represents the outermost edge of the filament in question, and the right hand side tends towards the fiber’s core. Initially, a chloride wave front enters the given section of HAIX-F(Fe) and chloride anions are readily exchanged onto anion exchange sites, R₄N⁺. Stepwise chloride exchange along anion exchange groups allows “anion jumping” to occur and effectively transport chloride ions to metal oxide groups much faster. Upon exhaustion of available sorption sites on HFO, the wave front continues towards the particle center. When the sulfate wave commences, chloride anions are rapidly effluxed from HFO surface functional groups as described in section 3.4 & 4.1. The chloride front quickly exits the fiber and causes chromatographic elution effects in effluent samples. Similarly, sulfate anions are displaced by dissolved organic species. This synergy allows for the increased operational capacity observed by Blaney and coworkers who studied the fixed-bed capacity of granular ferric hydroxide and two hybrid ion exchange resins: HCIX and HAIX

loaded with HFO nanoparticulates [Blaney et al., 2007]. Blaney's study found that HCIX exhibited least capacity due to disadvantageous Donnan co-ion exclusion effects; furthermore, HAIX demonstrated greater (per gram Fe) capacity than GFH due to the synergistic effects generated by presence of anion exchange groups. Such results show that hybrid anion exchangers demonstrate immense advantage over parent anion exchangers and granular metal oxide media. Essentially, the structural and "anion jumping" benefits of parent anion exchange fibers are coupled with the sorption and surface chemistry properties of the metal oxide particulates; furthermore, loss of metal oxide capacity due to inaccessible area, pressure drop problems associated with metal oxide particle attrition, and low capacity caused by competition based solely on valence are not witnessed. Truly such widespread benefits demonstrate the advantages associated with HAIX-F treatment processes.

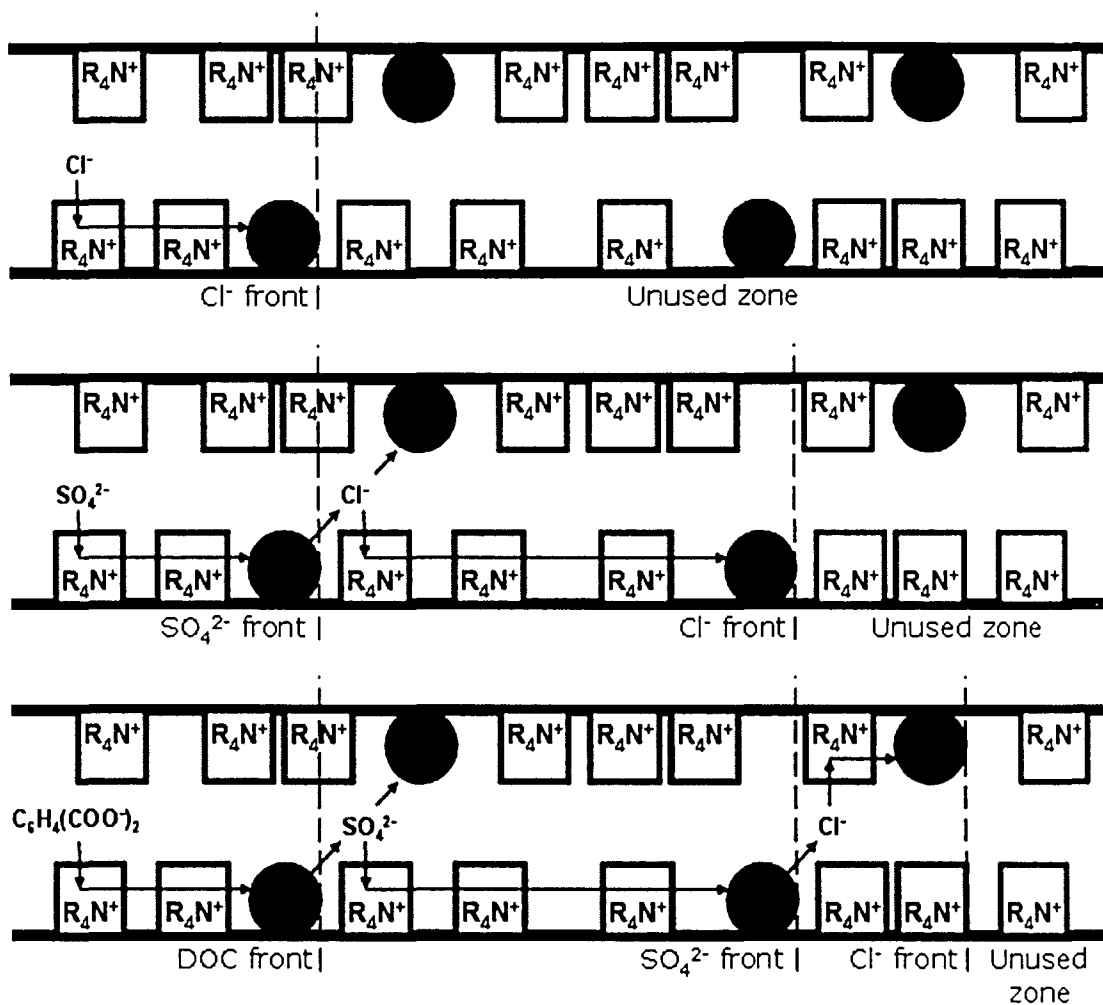


Figure 4.7 – Advancement of Anion Fronts through HAIX-F

Figure 3.26 & Table 3.8 demonstrate that HAIX-F(Zr) media demonstrated better phthalate sorption kinetics compared to HAIX-F(Fe). Likely, these more competitive kinetics are due to point of zero charge (PZC) characteristic values for HFO and HZO. Essentially PZC represents the value at which surface functionality is neutral. As evidenced in Figures 1.6 & 1.11, HFO has PZC of approximately 7.5; therefore, at near-neutral pH fewer functional groups will contain positive charge as compared to HZO, which has PZC of about 9.0. The greater presence of positively charged HZO surface groups probably allows faster interaction mechanism as compared with LAB complexation reactions.

4.4 Applicability for WTP Introduction: Regenerability

Regeneration experiments (section 3.6) demonstrated a remarkable ability for HAIX-F media to be effectively and efficiently regenerated after exhaustion. Given the time efficiencies, i.e., regeneration time (~10 bed volumes) vs. operational time (~3000 bed volumes), calculated for different experimental runs, HAIX-F introduction at municipal or industrial water treatment plants is a distinct possibility.

Recall Figures 1.6 & 1.11, HFO and HZO have PZC values at pH 7.8 and 8.8, respectively. The 2% NaOH, 2% NaCl regenerant solution has pH ~13. Therefore, HFO and HZO surface functional groups are predominately negatively charged due to deprotonation effects. Negative surface functionality expels organic carbon molecules such as oxalate, phthalate, and NOM through Donnan co-ion exclusion effects. Because pH effects rapidly penetrate HAIX-F media, the process occurs almost instantaneously. As seen in Figure 3.34, a plot of % regeneration complete vs. bed volumes demonstrates almost ideal plug-flow reactor behavior.

Furthermore, because PZC of HFO and HZO particulates is relatively high (i.e., greater than 7.0), weak acid solution can be employed towards media neutralization after regeneration with caustic solution. Essentially, carbon dioxide-sparged water is contacted with regenerated fibers for some amount of time in order to neutralize fibers before redeployment in treatment processes. From a sustainability standpoint, a water treatment plant's carbon footprint (i.e., the amount of carbon dioxide exhausted by energy needs, and other plant processes) can be reduced by diverting carbon dioxide emissions towards neutralization of regenerated media. The theory and capabilities of this process have been described in detail by Greenleaf and co-workers [Greenleaf, 2007; Greenleaf et al., 2006].

Taking into consideration the multitude of data regarding humankind's role regarding climate change and the forecasted negative effects of such change, any processes that act as carbon sequestration mechanisms provide inherent benefit. Therefore, a water treatment plant can effectively minimize its carbon output by employing carbon dioxide exhaust (direct or indirect) as regeneration chemicals. Furthermore, as multiple political entities/organizations are now enacting carbon caps and carbon trading policies, sustainable carbon-neutral or carbon-positive water treatment plants may prove a leading example of sustainable practices.

4.5 Understanding NOM Sorption

Although surrogate NOM compounds like oxalate and phthalate showed significant removal capacity and rapid sorption kinetics through HAIX-F treatment, the data provided above for experimentation with dilute NOM brine did not provide highly precise results. As mentioned in Figure 3.5, NOM consist of many different organic molecules. Some fractions are hydrophilic, others are transphilic, and still others exhibit hydrophobic properties. Obviously, these three general categories of organic molecules present in NOM will demonstrate different interaction capabilities with HAIX-F media. Consider:

- Hydrophilic, “water loving,” molecules will be poorly adsorbed.
- Transphilic, or that fraction of NOM exhibiting intermediate polarity, will be sorbed moderately well
- Hydrophobic, “water fearing,” NOM fraction will undergo better sorption.

Hence, clearly defined stratification zones between hydrophilic, transphilic, and hydrophobic NOM fraction concentration breakthroughs should be recognizable in effluent history plots. Consider Figure 4.8, which is essentially a color-coded copy of Figure 3.15; note that Figure 3.15

and Figure 4.8 represent a plot of effluent TOC history in the HAIX-F(Zr) fixed-bed column run. From Figure 4.8, one can make out several distinct “steps” in effluent concentration. The investigator believes that these “steps” are essentially breakthrough of different NOM fractions. Future work using more advanced equipment such as gas chromatograph mass spectroscopy (GC-MS) could verify this theory.

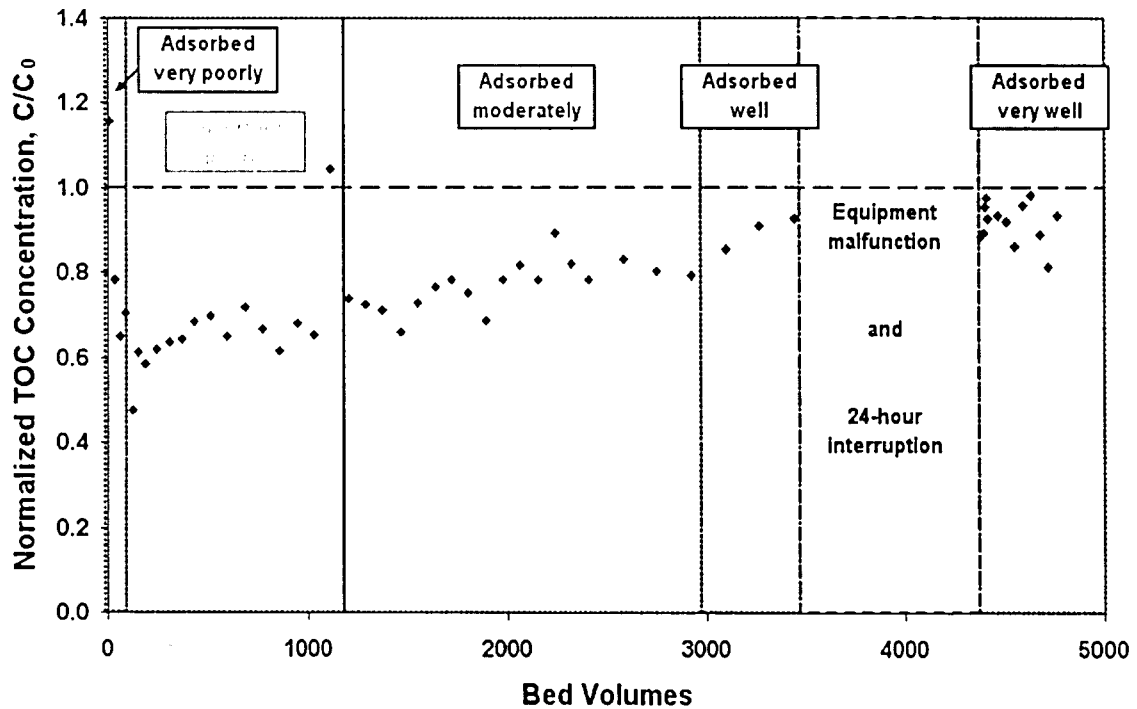


Figure 4.8 – A Stratified Plot of Normalized TOC Concentration vs. Bed Volumes Showing Presence of Separate NOM Breakthroughs Defined by Fraction

It is important to note that during degradation experimentation (section 3.3) the TOC Analyzer was employed to measure carbon concentrations. Precise and accurate results were obtained.

Section 3.7 provides detailed analysis of the same data present in Figure 4.8; however, various analytical equipment/techniques were employed. Again, a good deal of scatter in the data is noted. For these reasons, the investigator believes that scatter is inherent in the data set due to

the presence of different NOM compounds that exhibit different characteristics. After the initial chromatographic elution in Figure 4.8, the breakthrough curve follows a typical pattern. Likely, this particular NOM solution contained approximately 60% hydrophilic species that are poorly adsorbed onto HAIX-F media. The remaining 40% were successfully sorbed for the same amount of bed volumes as observed for oxalate and phthalate experimentation. Thus, HAIX-F media can remove TOC very efficiently with rapid sorption kinetics and regeneration capability; however, hydrophilic and other poorly adsorbed NOM fractions cannot be sufficiently removed. In many cases, the TOC removal abilities offered by HAIX-F should still prove vital to water treatment plants. Additionally, HAIX-F media can be implemented with another technology towards complete removal of TOC and NOM.

4.6 Cyclical HAIX-F Employment Process

For HAIX-F to be competitive with existing technologies for DBP formation potential removal, an effective employment strategy must be available. Since fixed-bed reactor, or plug flow configuration, offers maximal uptake and minimal operational complexity, PFR type reactor should be utilized. Furthermore, some operational redundancy is necessary in order to accommodate regeneration processes. For example, the simplest reactor configuration would consist of two columnar fixed-bed HAIX-F reactors with automated valve system that allows for instantaneous column turnover after breakthrough is experienced. At that point, valves for semi-treated water flow to the exhausted column will be closed and valves for regeneration solution (2% NaOH, 2%NaCl and CO₂-sparged water neutralization solution) flow to the exhausted column will be opened; similarly, valves for regeneration solution flow to the exhausted column will be closed and valves for semi-treated water flow to the regenerated column will be opened.

Such a process schematic is illustrated in Figure 4.8. For larger operations, multiple columnar units should be utilized; however, process schematics follow the same pattern as described in Figure 4.9.

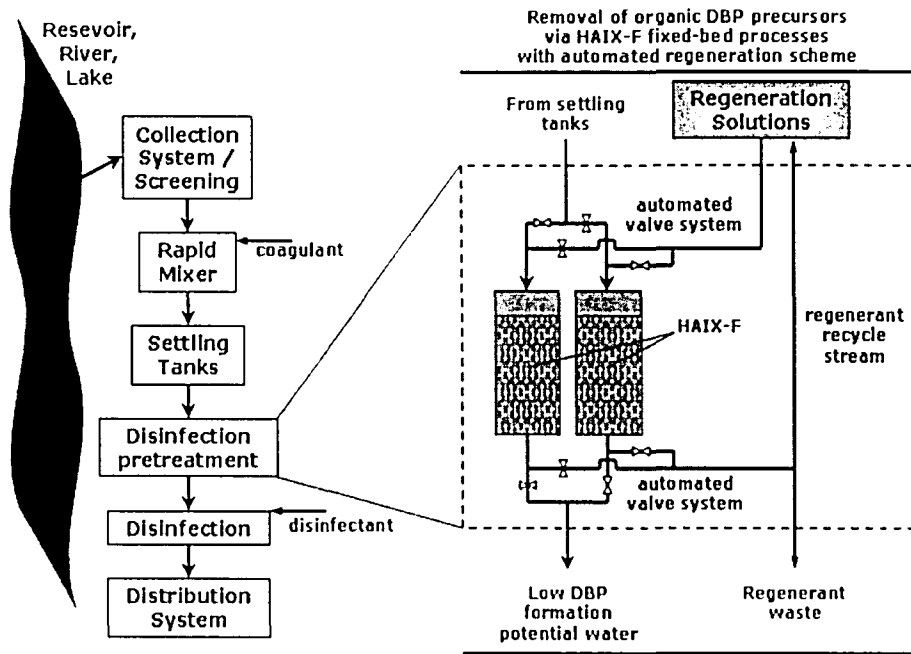


Figure 4.9 – Schematic of HAIX-F Process Inclusion into a Water Treatment Plant

Furthermore, as caustic regenerant solution is composed of 2% NaOH, 2% NaCl and a much lower concentration of dissolved organic carbon anions are being expelled from HAIX-F media during regeneration, some fraction of the passed regenerant can be reused in later regenerations. Another fraction of the regenerant stream will be disposed of as a waste product. Therefore the pretreatment scheme to remove DBP formation potential has two inputs, semi-treated water containing TOC and regenerant solutions (caustic and acidic), and two outputs, pretreated water and regenerant waste.

Complete process schematics, then, offer cyclical applicability, whereby HAIX-F media is repeatedly employed towards removal of organic DBP precursors, regenerated using 2% NaOH, 2% NaCl solution, and rinsed using carbonic acid (CO₂ sparged water) solution (Figure

4.10). Consider a water treatment plant, which utilizes 5000 L HAIX-F(Fe), which is split between 10 different PFR units, for removal of organic DBP precursors. Flow to the HAIX-F treatment system is split into 5 streams; at any given time 4 streams are operating. Furthermore, at any given time, 4000 L HAIX-F(Fe) is being employed towards TOC treatment; meanwhile, the other 1000 L is being regenerated. Influent water contains approximately 10 mg/L TOC and flow rate is 10 MGD. From above, HAIX-F(Fe) has breakthrough capacity of 9.1 mg C/g (approximately 3000 bed volumes) and density 1.40 mg/cm³. Then, 4000 L of HAIX-F(Fe) can pre-treat approximately 11.4 million liters until 2 mg/L TOC breakthrough; operating time (until regeneration) is 14.5 hours. Note that this situation is the one provided in Figure 3.38.

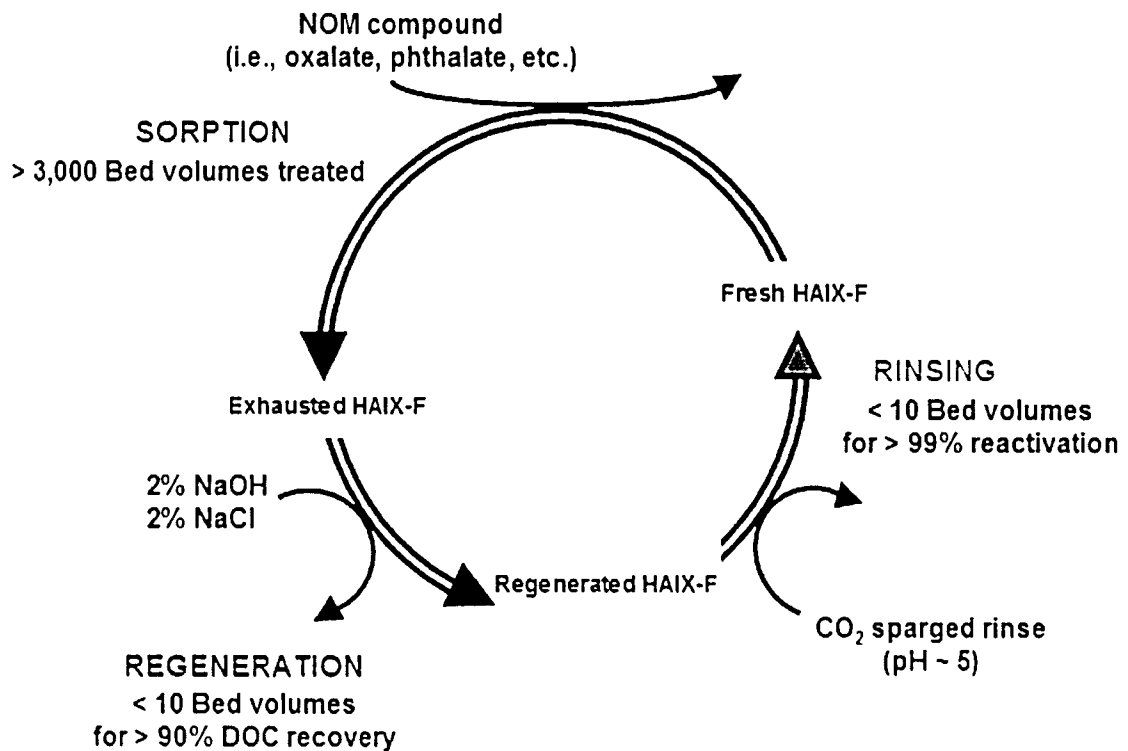


Figure 4.10 – Cyclical HAIX-F Process for Water Treatment Plant

With a conservative media addition/removal strategy mandating (1) removal of the top 5% of the bed, (2) mixing of the bed's remaining 95%, and (3) addition of 50 L of fresh media, the

input/output streams described in Table 4.4 can be expected for each regeneration cycle. Note that fresh media and regenerant streams signify the amount of HAIX-F or caustic solution necessary to maintain efficient operating conditions; furthermore, spent regenerant and exhausted media streams signify waste products.

Table 4.4 – Computer-Based Model Input/Output Streams

Substance	Remaining in system	System Inputs	Waste Products
<i>HAIX-F</i>	4750 L HAIX-F	250 L fresh HAIX-F	250 L exhausted HAIX-F
<i>Caustic Solution</i>	N/A	47500 L spent regenerant	2500 L spent regenerant
<i>Acidic Solution</i>	N/A	47500 L weak-acid rinse	2500 L weak-acid rinse
<i>Treated Water</i>	N/A	11400000 L high DBP formation potential water	11400000 L low DBP formation potential water

Basically, the bottom 4750 L HAIX-F would remain in the column during regeneration, while the top 250 L would be removed; furthermore, 2500 L of the spent regenerant solution would be disposed of as waste product, while 47500 L are recycled back into the regeneration solution storage tanks. Since regeneration processes operate via Donnan co-ion exclusion principles based in metal oxide functional group variation with pH, relatively small concentrations of organic anions in the regeneration solution should not reduce regeneration efficiency. Consequently, a product-to-waste ratio of over 1000 is realized. It should be noted that the situation described above is very conservative and realistically over-efficient. For such reason, HAIX-F media should prove extremely useful in meeting USEPA regulations regarding D/DBP and ESWTR.

CHAPTER 5: CONCLUSIONS

In this chapter, short summaries of the details contained in previous chapters will be provided; furthermore, overall conclusions of this research report are offered along with ideas for further research on this topic.

5.1 Review of Information Contained in Previous Chapters

Chapter 1 provided background information regarding a host of topics, including a history of disinfection processes, role of NOM and disinfection agents in generation of DBPs, types of DBPs formed by common disinfection agents, health impacts related to human ingestion of DBPs, US EPA regulations regarding disinfectant residual, DBP concentrations, and TOC concentrations, previous technologies for NOM removal: advantages and disadvantages, evolution of hybrid ion exchange media and conceptual description of HAIX-F media and its applicability for NOM removal processes, chemistry of surrogate NOM compounds utilized in this research, and project goals and objectives. Most importantly, the chemistry relevant to NOM removal using HAIX-F technology was detailed and deemed applicable.

In Chapter 2, the main materials and methods employed throughout experimentation and research activities were detailed. These subjects included chemicals utilized throughout experimentation, HAIX-F synthesis and description, batch study procedures, fixed-bed column experiment description, kinetics test protocol and equipment, regeneration procedure, and the analytical equipment employed and related operating protocol.

As all experimental results and discussion of those results was provided in Chapter 3, that chapter is undoubtedly the most significant. A summarized list of the topics detailed in Chapter 3

includes initial batch and column studies, photodegradation investigations, NOM and surrogate NOM compound treatment through HAIX-F fixed-bed processes, kinetics of NOM and surrogate NOM compound removal using HAIX-F media, regenerability of HAIX-F media, comparison of analytical techniques towards better understanding of NOM removal, and description of a C++ model written and employed to determine efficiency of NOM treatment in WTPs using HAIX-F.

Finally, in Chapter 4, a more generalized discussion of the results presented in Chapter 3 was undertaken. Discussion centered on the synergistic combination of ion exchange support and metal oxide sorption capabilities. For example, HAIX-F sorption capacity and mechanisms, Donnan co-ion exclusion effects and pertinence to HAIX-F treatment processes, and anion jumping effects were discussed. Furthermore, details regarding regeneration abilities and cyclical applicability of HAIX-F treatment processes in WTPs were provided. Finally, reasons for the scatter present in NOM removal data were expounded.

5.2 Conclusions on HAIX-F Ability to Remove NOM

As extensive detail regarding HAIX-F and related abilities for NOM and TOC removal has been included in the preceding report, a short list of conclusions will now be presented as summary. Consider the following points:

- NOM and surrogate NOM compounds were selectively removed over background anions as demonstrated by fixed-bed column run studies, kinetics tests, and calculated separation factors
- Surrogate NOM compounds were completely removed for approximately 3000 bed volumes before breakthrough occurred; breakthrough capacity was approximately 9.08

mg C per gram of HAIX-F(Fe), total capacity was 11.29 mg carbon per gram HAIX-F(Fe)

- HAIX-F media containing ferric oxide exhibited greater total capacity (on per gram basis); however, HAIX-F(Zr) demonstrated greater capacity on a meq/mol basis (i.e., 0.235 meq/mol Zr^{4+} vs. 0.113 meq/mol Fe^{3+})
- Sorption kinetics are limited by intraparticle diffusion and the effective diffusivity determined through experimentation is over two orders greater than that available from previous technologies
- HAIX-F(Zr) ($D_{eff} = 1.95 \times 10^{-9} \text{ cm}^2/\text{s}$) media demonstrated better sorption kinetics as compared to HAIX-F(Fe) ($D_{eff} = 9.25 \times 10^{-10} \text{ cm}^2/\text{s}$)
- Regeneration of HAIX-F media is highly efficient; 100% regeneration is typically achieved in 10 bed volumes or less
- Synergistic effects of combined presence of ion exchange support and metal oxide nanoparticulates allows for numerous advantages – specifically, selective presence of DOC at metal oxide particulates and enhanced kinetics due to anion jumping
- The ability to employ HAIX-F in municipal/industrial operations is heightened by cyclical applicability of the process as described through operation, regeneration, rinse, and reuse capabilities and modeled with the C++ program

Clearly, the media and treatment technology described throughout this report contains a very high potential for application in municipal/industrial systems that require TOC removal based on ESWTR regulations. Furthermore, the ease of operation should make the process more attractive to drinking water treatment plants. Before employment of HAIX-F media based technology in drinking water treatment plants, there are a few more sub-areas of research that

should be undertaken.

Future work in this area includes detailed analysis of NOM compounds being eluted from the fixed-bed columns, detailed analysis of NOM makeup during kinetics tests, inclusion of some media/process that can remove hydrophilic NOM fractions, better metal oxide loading on parent anion exchange fibers, detailed summary of economic considerations, and determination of any scaling effects.

In conclusion, HAIX-F technology offers so many advantages compared to traditional treatment processes. Because of HAIX-F affinity for NOM, relatively high volumes of surface water can be treated before regeneration is necessary; even then, the ability for extremely rapid regeneration allows for highly efficient HAIX-F employment. For these reasons, and those described throughout the body of the report, application of HAIX-F technology into drinking water treatment plants will undoubtedly provide an enhanced capability for meeting ESWTR regulatory limits and ensuring the absence of disinfection by-products in distribution systems. As the HAIX-F process is highly sustainable (little input variables/streams, no significant energy requirement, small treatment residual volume, and carbon-positive capabilities), it should prove to be a distinct contender in the race for meeting ESWTR guidelines over the next few decades.

Abbt-Braun G, Frimmel FH (1999). Basic characterization of Norwegian NOM samples—Similarities and differences. *Environmental International* 25(2-3), 161–180.

Aiken GR, McKnight DM, Thorn KA, Thurman EM (1992). Isolation of hydrophilic organic acids from water using nonionic macroporous resins. *Organic Geochemistry* 18(4), 567–573.

AWWA Water Quality Disinfection Committee (1992). Survey of Water Utility Disinfection Practices. *Journal of the American Water Works Association* 84(9), 121-128.

Andrews SA, Huck PM, Chute AJ, Bolton JR, Anderson WA. UV oxidation for drinking water: feasibility studies for addressing specific water quality issues. In *Proceedings, AWWA Water Quality Technology Conference, New Orleans, LA, Nov 12-16, 1995; American Water Works Association: Denver, CO, 1996.*

Bellar TA, Lichtenberg JJ, Kroner RC (1974). The occurrence of organohalides in chlorinated drinking waters. *Journal of the American Water Works Association* 66(12), 703–706.

Blaney LM, Cinar S, SenGupta AK (2007). Hybrid anion exchanger for trace phosphate removal from water and wastewater. *Water Research* 41(7), 1603-1613.

Booker SM (2000). NTP Taps disinfection by-products for study. *Environmental Health Perspectives* 108(2), A64-A66.

Boorman GA, Dellarco V, Dunnick JK, Chapin RE, Hunter S, Hauchman F, Gardner H, Cox M, Sills RC (1999). Drinking water disinfection byproducts: review and approach to toxicity evaluation. *Environmental*

Health Perspectives **107**(1), 207-217.

Borough of Maidstone (1898). Epidemic of typhoid fever 1897: report of an inquiry and appendices. HMSO, London, UK.

Bourke M, Slunjski M, O'Leary B, Smith P. Scale up of the MIEX® TOC Process for Full Scale Water Treatment Plant. Proceedings of the 18th Federal Australian Water & Wastewater Association Convention, Adelaide, Australia, 1999

Bull RJ (2000). Mode of action of liver tumor induction by trichloroethylene and its metabolites, trichloroacetate and dichloroacetate. *Environmental Health Perspectives* **108**(S2), 241-259.

Buschini A, Carboni P, Frigerio S, Furlini M, Marabini L, Monarca S, Poli P, Radice S, Rossi C (2004). Genotoxicity and cytotoxicity assessment in lake drinking water produced in a treatment plant. *Mutagenesis* **19**(5), 341-347.

Cabaniss SE, Shuman MS (1988). Copper binding by dissolved organic matter: I. Suwannee River fulvic acid equilibria. *Geochimica et Cosmochimica Acta* **52**(1), 185-193.

Can ZS, Gurol M (2003). Formaldehyde Formation During Ozonation Of Drinking Water. *Ozone: Science and Engineering* **25**(1), 41-51.

Cancho B, Ventura F, Galceran MT (1999). Behavior of Halogenated Disinfection By-Products in the Water Treatment Plant of Barcelona, Spain. *Bulletin of Environmental Contamination and Toxicology* **63**(5), 610-617.

Celis R, Hermosin MC, Cox L, Comejo J (1999). Sorption of 2,4-dichlorophenoxyacetic acid by model

particles simulating naturally occurring soil colloids. *Environmental Science and Technology* 33(8), 1200–1206.

Chang CY, Hsieh YH, Hsu SS, Hu PY, Wang KH (2000). The formation of disinfection by-products in water treated with chlorine dioxide. *Journal of Hazardous Materials* 79(1-2), 89-102.

Chao PF. Role of hydroxyl radicals and hypobromous acid reactions on bromate formation during ozonation. TOCtor of Philosophy Dissertation, Arizona State University, December 2002.

Childress AE, Vrijenhoek EM, Elimelech M, Tanaka TS (1999). Particulate and THM precursor removal with ferric chloride. *Journal of Environmental Engineering* 125(11), 1054-1061

Chin YP, Aiken G, Danielsen KM (1997). Binding of pyrene to aquatic and commercial humic substances: the role of molecular weight and humic structure. *Environmental Science and Technology* 31(6), 1630–1635.

Chin YP, Aiken G, O'Loughlin E (1994). Molecular weight, polydispersity, and spectroscopic properties of aquatic humic substances. *Environmental Science and Technology* 28(11), 1853–1858.

Christman RF, Norwood DL, Millington DS, Johnson JD, Stevens AA (1983). Identity and yields of major halogenated products of aquatic fulvic acid chlorination. *Environmental Science and Technology* 17(10), 625-628.

Cleasby JL, Baumann ER, Black CD (1974). Effectiveness of potassium permanganate for disinfection. *Journal of the American Water Works Association* 56(4), 466-474.

Coffin JC, Ge R, Yang S, Kramer PM, Tao L, Pereira MA (2000). Effect of Trihalomethanes on Cell

Proliferation and DNA Methylation in Female B6C3F1 Mouse Liver. *Toxicological Sciences* 58(2), 243-252.

Cooper WJ, Amy GL, Moore CA, Zika RG (1986). Bromoform Formation in Ozonated Groundwater Containing Bromide and Humic Substances. *Ozone: Science and Engineering* 8(1), 63-76.

Cornel P, Summers RS, Roberts PV (1986). Diffusion of Humic Acid in Dilute Aqueous Solution. *Journal of Colloid and Interface Science* 110(1), 149-164.

Crank J. *The Mathematics of Diffusion*, Second Edition, Oxford Science Publication, 1975.

Croué JP, Violleau D, Labouyrie L (2000). Disinfection by-product formation potentials of hydrophobic and hydrophilic natural organic matter fractions: A comparison between a low- and a high-humic water. In *Natural Organic Matter and disinfection by-products: Characterization and control in drinking water* (Barrett SE, Krasner SW, Amy GL eds.). American Chemical Society, Washington, DC.

Cumbal L, Greenleaf JE, Leun D, SenGupta AK (2003). Polymer supported inorganic nanoparticles: characterization and environmental applications. *Reactive and Functional Polymers* 54(1-3), 167-180.

Cumbal L, SenGupta AK (2005). Arsenic removal using polymer-supported hydrated iron(III) oxide nanoparticles: Role of Donnan Membrane effect. *Environmental Science and Technology* 39(17), 6508-6515.

Dalvi AGI, Al-Rasheed R, Javeed MA (2000). Haloacetic acids (HAAs) formation in desalination processes from disinfectants. *Desalination* 129(3), 261-271.

Daniel FB, DeAngelo AB, Stober JA, Olson GR, Page NP (1992). Hepatocarcinogenicity of Chloral

Hydrate, 2-Chloroacetaldehyde, and Dichloroacetic Acid in the Male B6C3F1 Mouse. *Toxicological Sciences* **19**(2), 159-168.

Davis JA, Gloor R (1981). Adsorption of dissolved organics in lake water by aluminum oxide: effect of molecular weight. *Environmental Science and Technology* **15**(10), 1223-1229.

Day GM, Hart BT, McKelvie ID, Beckett R (1994). Adsorption of natural organic matter onto goethite. *Colloids and surfaces. A, Physicochemical and engineering aspects* **89**(1), 1-13.

Delker D, Hatch G, Allen J, Crissman B, George M, Geter D, Kilburn S, Moore T, Nelson G, Roop B, Slade R, Swank A, Ward W, DeAngelo A (2006). Molecular biomarkers of oxidative stress associated with bromate carcinogenicity. *Toxicology* **221**(2-3), 158-165.

DeMarco MJ, SenGupta AK, Greenleaf JE (2003). Arsenic removal using a polymeric/inorganic hybrid sorbent. *Water Research* **37**(1), 164-176.

Drikas M, Chow CWK, Cook D (2003). The impact of recalcitrant organic character on disinfection stability, trihalomethane formation and bacterial regrowth: An evaluation of magnetic ion exchange resin (MIEX®) and alum coagulation. *Journal of Water Supply: Research and Technology* **52**(7), 475-487.

Dunnick JK, Eustis SL, Lilja HS (1987). Bromodichloromethane, a Trihalomethane That Produces Neoplasms in Rodents. *Cancer Research* **47**(19), 5189-5193.

Dunnick JK, Melnick RL (1993). Assessment of the Carcinogenic Potential of Chlorinated Water: Experimental Studies of Chlorine, Chloramine, and Trihalomethanes. *Journal of the National Cancer Institute* **85**(10), 817-822.

Earth Tech (Canada) Inc. Chlorine and alternative disinfectants guidance manual. Manitoba Water Stewardship, March 2005 [Online]

http://www.gov.mb.ca/waterstewardship/odw/reg-info/approvals/odw_chlorine_and_alternative_disinfectants.pdf

Eichenlaub-Ritter U, Betzendahl I (1995). Chloral hydrate induced spindle aberrations, metaphase I arrest and aneuploidy in mouse oocytes. *Mutagenesis* 10(6), 477-486.

Elovitz MS, von Gunten U, Kaiser HP (2000). Hydroxyl radical/ozone ratios during ozonation processes. II. The effect of temperature, pH, alkalinity, and DOM properties. *Ozone: Science and Engineering* 22(2), 123-150.

Eyring A, Intenzo M, Peterkin E. Natural organic matter in Philadelphia's source waters: composition and reactivity with chlorine. 2003 Water Quality Technology Conference: Stewardship of Drinking Water Quality; Philadelphia, PA; USA; 2-6 Nov. 2003.

Fabris R, Chow C, Drikas M (2003). The Impact of Coagulant Type on NOM Removal. In: *OZWATER Convention and Exhibition*, Perth, Australia, 6-10 April, CD-ROM.

Farooq S, Chian ESK, Engelbrecht RS (1977). Basic concepts in disinfection with ozone. *Journal Water Pollution Control Federation* 49(8), 1819-1831.

Federal Register (1978). Interim primary drinking water regulations. Control of organic chemical contaminants in drinking water. United States Environmental Protection Agency. Federal Register 43:5756-5779

FIBAN[®]. Commercial website. <http://ifoch.bas-net.by/S_eng.htm> Accessed April 2007.

Fisher JW, Channel SR, Eggers JS, Johnson PD, MacMahon KL, Goodyear CD, Sudberry GL, Warren DA, Latendresse JR, Graeter LJ (2001). Trichloroethylene, Trichloroacetic Acid, and Dichloroacetic Acid: Do They Affect Fetal Rat Heart Development? *International Journal of Toxicology* 20(5), 257-267.

Fu P, Ruiz H, Thompson K, Spangenberg C (1994). Selecting membranes for removing NOM and DBP precursors. *Journal of the American Water Works Association* 86(12), 55-72.

Furnus CC, Ulrich MA, Terreros MC, Dulout FN (1990). The induction of aneuploidy in cultured Chinese hamster cells by propionaldehyde and chloral hydrate. *Mutagenesis* 5(4), 323-326.

Gallard H, von Gunten U (2002). Chlorination of natural organic matter: kinetics of chlorination and of THM formation. *Water Research* 36(1), 65-74.

Geldreich EE (1996). Microbial quality of water supply in distribution systems. Lewis Publishers, Boca Raton, Fla.

George MH, Olson GR, Doerfler D, Moore T, Kilburn S, DeAngelo AB (2002). Carcinogenicity of Bromodichloromethane Administered in Drinking Water to Male F344/N Rats and B6C3F₁ Mice. *International Journal of Toxicology* 21(3), 219-230.

Ghabbour EA, Davies G, O'Donoghue K, Smith TL, Goodwillie ME (1998). Adsorption of humic acids on clays and minerals. 1. Adsorption of peat-plant- and soil-derived humic acids on kaolinite. *216th ACS National Meeting* Boston, MA.

Gill MW, Swanson MS, Murphy SR, Bailey GP (2000). Two-generation reproduction and developmental neurotoxicity study with sodium chlorite in the rat. *Journal of Applied Toxicology* 20(4), 291-303.

Greenleaf JE. Development and Characterization of Two Sustainable Environmental Separation Processes Using Ion Exchange Fibers. Doctoral Dissertation, Lehigh University, 2007.

Greenleaf JE, Lin J, SenGupta AK (2006). Two novel applications of ion exchange fibers: Arsenic removal and chemical-free softening of hard water. *Environmental Progress* 25(4), 300-311.

Gu B, Mehlhorn TL, Liang L, McCarthy JF (1996). Competitive adsorption, displacement, and transport of organic matter on iron oxide: I. Competitive adsorption. *Geochimica et Cosmochimica Acta* 60(16), 1943-1950.

Gu B, Schmitt J, Chen Z, Liang L, McCarthy JF (1994). Adsorption and desorption of natural organic matter on iron oxide: mechanisms and models. *Environmental Science and Technology* 28(1), 38-48.

Gu B, Schmitt J, Chen Z, Liang L, McCarthy JF (1995). Adsorption and desorption of different organic matter fractions on iron oxide. *Geochimica et Cosmochimica Acta* 59(2), 219-229.

Hargy TM (2002). Status of UV Disinfection of Municipal Drinking Water Systems in North America. *Water Conditioning & Purification* 44(6), 30-34.

Hefferman WP, Guion C, Bull RJ (1979). Oxidative damage to the erythrocyte induced by sodium chlorite, in vivo. *Journal of Environmental Pathology and Toxicology* 2(6), 1487-1499.

Helferich F. Ion Exchange. McGraw-Hill, New York, New York, 1962.

Helferich F (1965). Ion Exchange Kinetics: V. Ion Exchange Accompanied by Chemical Reactions. *The Journal of Physical Chemistry* 69(4), 1178-1187.

Her N, Amy G, Foss D, Cho J, Yoon Y, Kosenka P (2002). Optimization of method for detecting and characterizing NOM by HPLC-size exclusion chromatography with UV and on-line TOC detection. *Environmental Science and Technology* 36(5), 1069-1076.

Hirose, Y; Maeda, N; Ohya, T; Nojima, K; Kanno, S (1989). Formation of cyanogen chloride by the reaction of peptides and proteins with hypochlorous acid in the presence of ammonium ion. *Chemosphere* 18(11-12), 2101-2108.

Höll WH, Sontheimer H (1977). Kinetics of the Protonation of Weak-Acid Ion Exchange Resins. *Chemical Engineering and Science* 32(7), 755-762.

Hozalski RM, Bouwer EJ. Biofiltration for removal of natural organic matter. In *Formation and Control of Disinfection By-products in drinking water*; Singer PC, Ed.; American Water Works Association: Denver, CO, 1999.

Huang J, Wang L, Ren N, Li LX, Fun SR, Yang G (1997). Disinfection effect of chlorine dioxide on viruses, algae and animal planktons in water. *Water Research* 31(3), 455-460.

Huang WJ, Yeh HH (1997). The effect of organic characteristics and bromide on disinfection by-products formation by chlorination. *Journal of Environmental Science and Health. Part A. Environmental Science and Engineering & Toxic and Hazardous Substance Control* 32A(8), 2311-2336.

Humbert H, Gallard H, Suty H, Croué JP (2005). Performance of selected anion exchange resins for the treatment of a high TOC content surface water. *Water Research* 39(9), 1699-1708.

Jacangelo JG, DeMarco J, Owen DM, Randtke EM (1995). Selected processes for removing NOM: An

overview. *Journal of the American Water Works Association* 87(1), 64-77.

Johnson JD, Overby R (1971). Bromine and Bromamine Disinfection Chemistry. *Journal of the Sanitary Engineering Division* 97(5), 617-628.

Kastl G, Fisher I, Sathasivan A, Chen P, van Leeuwen J (2003). Optimisation of TOC Removal by Enhanced Coagulation to Deliver Target TTHM in Chlorinated Systems. In: *OZWATER Convention and Exhibition*, Perth, Australia, 6-10 April, CD-ROM.

Kavanagh BV, Posner AM, Quirk JP (1977). The adsorption phenoxyacetic acid herbicides on goethite. *Journal of Colloid and Interface Science* 61(3), 545-553.

Keegan TE, Simmons JE, Pegram RA (1998). Noael and loael determinations of acute hepatotoxicity for chloroform and bromodichloromethane delivered in an aqueous vehicle to F344 rats. *Journal of Toxicology and Environmental Health Part A* 55(1), 65-75.

Kim H, Shim J, Lee S (2002). Formation of disinfection by-products in chlorinated swimming pool water. *Chemosphere* 46(1), 123-130.

Kitis M, Karanfil T, Kilduff JE, Wigton A (2001). The reactivity of natural organic matter to disinfection byproducts formation and its relation to specific ultraviolet absorbance. *Water Science and Technology* 43(2), 9-16.

Kitis M, Kilduff JE, Karanfil T (2001). Isolation of dissolved organic matter (DOM) from surface waters using reverse osmosis and its impact on the reactivity of DOM to formation and speciation of disinfection by-products. *Water Research* 35(9), 2225-2234.

Klaunig JE, Ruch RJ, Lin EL (1989). Effects of trichloroethylene and its metabolites on rodent hepatocyte intercellular communication. *Toxicology and Applied Pharmacology* 99(3), 454-465.

Klinefelter GR, Suarez JD, Roberts NL, DeAngelo AB (1995). Preliminary screening for the potential of drinking water disinfection byproducts to alter male reproduction. *Reproductive Toxicology* 9(6), 571-578.

Korshin GV, Benjamin MM, Sletten RS (1997). Adsorption of natural organic matter (NOM) on iron oxide: Effects on NOM composition and formation of organo-halide compounds during chlorination. *Water Research* 31(7), 1643-1650.

Krasner SW, McGuire MJ, Jacangelo JJ, Patania NL, Reagan KM, Aieta EM (1989). The Occurrence of Disinfection By-Products in US Drinking Water. *Journal of the American Water Works Association* 81(8), 41-53.

Krasner SW, Weinberg HS, Richardson SD, Pastor SJ, Chinn R, Scilimenti MJ, Onstad GD, Thruston AD (2006). Occurrence of a new generation of disinfection byproducts. *Environmental Science and Technology* 40(23), 7175-7185.

Kurokawa Y, Maekawa A, Takahashi M, Hayashi Y (1990). Toxicity and carcinogenicity of potassium bromate – a new renal carcinogen. *Environmental Health Perspectives* 87(1), 309-335.

Li P. Sorption of synthetic aromatic anions onto polymeric ion exchangers: Genesis of selectivity and effects of equilibrium process variables on sorption kinetics. TOCtoral Dissertation, Lehigh University, 1999.

Li P, SenGupta AK (2000). Intraparticle diffusion during selective ion exchange with a macroporous exchanger. *Reactive and Functional Polymers* 44(3), 273-287.

Lide D (Editor). *CRC handbook of chemistry and physics* (79th edition). CRC Press, Cleveland, Ohio, 1998.

Lili W, Chin YP, Traina SJ (1997). Adsorption of (poly)maleic acid and aquatic fulvic acid by goethite. *Geochimica et Cosmochimica Acta* **61**(24), 5313–5324.

Lilly PD, Ross TM, Pegramt RA (1997). Trihalomethane Comparative Toxicity: Acute Renal and Hepatic Toxicity of Chloroform and Bromodichloromethane Following Aqueous Gavage. *Toxicological Sciences* **40**(1), 101-110.

Lin ELC, Daniel FB, Herren-Freund SL, Pereira MA (1986). Haloacetonitriles: metabolism, genotoxicity, and tumor-initiating activity. *Environmental Health Perspectives* **69**(1), 67-71.

Lykins BW, Clark RM, Adams JQ (1988). Granular activated carbon for controlling THMs. *Journal of the American Water Works Association* **80**(5), 85-92.

Malcolm RL, MacCarthy P (1992). Quantitative evaluation of XAD-8 and XAD-4 resins used in tandem for removing organic solutes from water. *Environment International* **18**(6), 597-607.

Mansfield CA, Depro BM, Perry VA. The chlorine industry: a profile draft report. USEPA Office of Air Quality Planning and Standards, Air Quality Strategies and Standards Division. August 2000.

Mason WP (1909). The purification of water supplies by the use of hypochlorites. *Proceedings of the American Philosophical Society* **48**(191), 67-68.

Matilainen A, Lindqvist N, Korhonen S, Tuhkanen T (2002). Removal of NOM in the different stages of the water treatment process. *Environmental International*, **28**(6), 457–465.

Maurice PA, Namjesnik-Dejanovic K, Lower SK, Pullin MJ, Chin YP, Aiken GR (1998). Sorption and fractionation of natural organic matter on kaolinite and goethite. In: Arehart M. and Hulston N., Editors, 1998. *Water-Rock Interaction IX*, Balkema, 109–113.

McGuire MJ, Davis MK, Tate CH, Aeita EM, Howe EW, Crittenden JC (1991). Evaluating GAC for Trihalomethane Control. *Journal of the American Water Works Association* **83**(1), 38-48.

McKnight DM, Bencala KE, Zellweger GW, Aiken GR, Feder GL, Thorn KA (1992). Sorption of dissolved organic carbon by hydrous aluminum and iron oxides occurring at the confluence of Deer Creek with the Snake River, Summit County, Colorado. *Environmental Science and Technology* **26**(7), 1388–1396.

McPhail M, Page AL, Bingham FT (1972). Adsorption interactions of monosilicic and boric acid on hydrous oxides of iron and aluminum. *Soil Science Society of America Proceedings* **36**, 510-514.

Meier M, Chin YP, Maurice P (2004). Variations in the composition and adsorption behavior of dissolved organic matter at a small, forested watershed. *Biogeochemistry* **67**(1), 39-56.

Meier M, Namjesnik-Dejanovic K, Maurice PA, Chin YP, Aiken GR (1999). Fractionation of aquatic natural organic matter upon sorption to goethite and kaolinite. *Chemical Geology* **157**(3), 275–284.

Miltner RJ, Shukairy HM, Summers RS (1992). Disinfection by-product formation and control by ozonation and biotreatment. *Journal of the American Water Works Association* **84**(11), 53-62.

Miner RA, Amy GL (eds.). 1996. Disinfection by-products in water treatment: the chemistry of their formation and control. New York: Lewis Publishers.

Morgan KT, Ni H, Brown HR, Yoon L, Qualls CW, Crosby LM, Reynolds R, Gaskill B, Anderson SP, Kepler TB, Brainard T, Liv N, Easton M, Merrill C, Creech D, Sprenger D, Conner G, Johnson PR, Fox T, Sartor M, Richard E, Kuruvilla S, Casey W, Benavides G (2002). Application of cDNA Microarray Technology to In Vitro Toxicology and the Selection of Genes for a Real-Time RT-PCR-Based Screen for Oxidative Stress in Hep-G2 Cells. *Toxicologic Pathology* 30(4), 435-451.

Morran JY, Bursill DB, Drikas M, Nguyen H (1996). A new technique for the removal of natural organic matter. In Proceedings of the Australian Water and Wastewater Association WATERTECH Conference, Sydney, Australia, pp. 428-432.

Moser VC, Phillips PM, McDaniel KL, MacPhail RC (1999). Behavioral evaluation of the neurotoxicity produced by dichloroacetic acid in rats. *Neurotoxicology and Teratology* 21(6), 719-731.

Muller-Pillet V, Joyeux M, Ambroise D, Hartemann P (2000). Genotoxic activity of five haloacetonitriles: comparative investigations in the single cell gel electrophoresis (comet) assay and the Ames-fluctuation test. *Environmental and Molecular Mutagenesis* 36(1), 52-58.

Myllykangas T, Nissinen TK, Hirvonen A, Rantakokko P, Vartiainen T (2005). The evaluation of ozonation and chlorination on disinfection by-product formation for a high-bromide water. *Ozone: Science and Engineering* 27(1), 19-26.

Namjesnik-Dejanovic K, Maurice PA (2001). Conformations and aggregate structures of sorbed natural organic matter on muscovite and hematite. *Geochimica et Cosmochimica Acta* 65(7), 1047-1057.

Namjesnik-Dejanovic K, Maurice PA, Aiken GR, Cabaniss S, Chin YP, Pullin MJ (2000). Adsorption and fractionation of a muck fulvic acid on kaolinite and goethite at pH 3.7, 6, and 8. *Soil Science* 165(7), 545-

National Primary Drinking Water Regulations (2006a). Stage 2 Disinfectants and Disinfection Byproducts Rule. January 4, 2006 (71 FR 388).

National Primary Drinking Water Regulations (2006b). Long Term 2 Enhanced Surface Water Treatment Rule. January 5, 2006 (71 FR 654).

Ndabigengesere A, Narasiah KS, Talbot BG (1995). Active agents and mechanism of coagulation of turbid waters using moringa oleifera. *Water Research* **29**(2), 703-710.

Nieuwenhuijsen MJ, Toledano MB, Eaton NE, Fawell J, Elliot P (2000). Chlorination disinfection byproducts in water and their association with adverse reproductive outcomes: a review. *Journal of Occupational and Environmental Medicine* **57**(2), 73-85.

Norwood DL, Johnson DJ, Christman RF, Hass JR, Bobenrieth MJ (1980). Reactions of chlorine with selected aromatic models of aquatic humic material. *Environmental Science and Technology* **14**(2), 187-189.

Ochs M, Cosovic B, Stumm W (1994). Coordinative and hydrophobic interactions of humic substances with hydrophilic Al₂O₃ and hydrophobic mercury surfaces. *Geochimica et Cosmochimica Acta* **58**(2), 639-650.

Ono Y, Somiya I, Mohri S (1994). Evaluation of genotoxicity of bromate ion produced during ozonation. *Ozone: Science and Engineering* **16**(5), 443-453.

Orica Ltd (2006). Watercare. [online] www.miexresin.com.

Owen DM, Amy GL, Chowdhury ZK. Characterization of natural organic matter and its relationship to treatability; AWWARF and AWWA: Denver, CO, 1993.

Parfitt RL, Fraser AR, Farmer VC (1977). Adsorption on hydrous oxides. III. Fulvic acid and humic acid on goethite, gibbsite and imogolite. *Soil Science Society of America Journal* **28**, 289-296.

Pereira MA, Phelps JB (1996). Promotion by dichloroacetic acid and trichloroacetic acid of N-methyl-N-nitrosourea-initiated cancer in the liver of female B6C3F1 mice. *Cancer Letters* **102**(1-2), 133-141.

Petruzzelli D, Kalinitchev A, Soldatov VS, Tiravanti (1995). Chloride/sulfate ion exchange kinetics on fibrous resins. Two independent models for film diffusion control. *Industrial & Engineering Chemistry Research* **34**(8), 2618-2624.

Polson AJ (1950). Some aspects of diffusion in solution and a definition of a colloidal particle. *Journal of Physical and Colloidal Chemistry* **54**(5), 649-652.

Pontius FW (1997). Implementing the 1996 SDWA amendments. *Journal of the American Water Works Association* **89**(33), 18-36.

Pontius FW (2002). Regulatory compliance planning to ensure water supply safety. *Journal of the American Water Works Association* **94**(1), 52-64.

Pontius FW, Roberson JA (1994). The current regulatory agenda: an update. *Journal of the American Water Works Association* **86**(22), 54-63.

Popova OP, Shunkevich AA, Prokopchuk NR, Soldatov VS (1991). Effect of a cross-linking agent on the

physical-mechanical and exchange properties of strongly basic FIBAN A-1 fibers. *Journal of Applied Chemistry of the USSR* **64**(6), 1131-1135.

Puttamraju P, SenGupta AK (2006). Evidence of tunable on-off sorption behaviors of metal oxide nanoparticles: Role of ion exchanger support. *Industrial & Engineering Chemistry Research* **45**(22), 7737-7742.

Redman AD, Macalady DL, Ahmann D (2002). Natural organic matter affects arsenic speciation and sorption onto hematite. *Environmental Science and Technology* **36**(13), 2889-2896.

Richard AM, Hunter ES (1996). Quantitative structure-activity relationships for the developmental toxicity of haloacetic acids in mammalian whole embryo culture. *Teratology* **53**(6), 352-360.

Richardson SD (2003). Disinfection by-products and other emerging contaminants in drinking water. *Trends in Analytical Chemistry* **22**(10), 666-684.

Richardson SD, Thruston AD, Caughran TV, Chen PH, Collette TW, Floyd TL, Schenck KM, Lykins BW (2000). Identification of new drinking water disinfection by-products formed in the presence of bromide. In *Natural Organic Matter and disinfection by-products: Characterization and control in drinking water* (Barrett SE, Krasner SW, Amy GL eds.). American Chemical Society, Washington, DC.

Richardson SD, Thruston AD, Caughran TV, Chen PH, Collette TW, Floyd TL, Schenck KM, Lykins BW, Sun GS, Majetich G (1999). Identification of new ozone disinfection byproducts in drinking water. *Environmental Science and Technology* **33**(19), 3368 -3377.

Richardson SD, Thruston AD, Caughran TV, Chen PH, Collette TW, Schenck KM, Lykins BW, Rav-Acha C, Glezer V (2004). Identification of New Drinking Water Disinfection by - Products from Ozone.

Chlorine Dioxide, Chloramine, and Chlorine. *Water, Air, & Soil Pollution* **123**(1-4), 95-102.

Rook JJ (1974). Formation of haloforms during chlorination of natural waters. *Journal of Water Treatment and Examination* **23**(2), 234–243.

Schmidt W (2004). Using Chlorine Dioxide for Drinking Water Disinfection by the Application of the Chlorite/Chlorine Process. *Acta Hydrochimica et Hydrobiologica* **32**(1), 48-60.

Schminke G, Seubert A (2004). Comparison of ion chromatographic methods based on conductivity detection, post-column-reaction and on-line-coupling IC-ICP-MS for the determination of bromate. *Fresenius' Journal of Analytical Chemistry* **366**(4), 387-391.

Schwede-Thomas SB, Chin YP, Dria KJ, Hatcher P, Kaiser E, Sulzberger B (2005). Characterizing the properties of dissolved organic matter isolated by XAD and C-18 solid phase extraction and ultrafiltration. *Aquatic Sciences – Research Across Boundaries* **67**(1), 61-71.

Shull KE (1981). Experience with Chloramines as Primary Disinfectants. *Journal of the American Water Works Association* **73**(2), 101-104.

Sigg L, Stumm W (1981). The interactions of anions and weak acids with the hydrous goethite (α -FeOOH) surface. *Colloids and Surfaces* **2**(2), 101-107.

Sims JR, Bingham FT (1968). Retention of boron by layer silicates, sesquioxides, and soil materials: II. Sesquioxides. *Soil Science Society of America Proceedings* **32**, 364-369.

Sing K, Erickson T, Amitai Y, Hryhorczuk D (1996). Chloral hydrate toxicity from oral and intravenous administration. *Journal of Toxicology - Clinical Toxicology* **34**(1), 101-106.

Singer PC (1994). Control of disinfection by-products in drinking water. *Journal of Environmental Engineering* 120(4), 727-744.

Singer PC, Bilyk K (2002). Enhanced coagulation using a magnetic ion exchange resin. *Water Research* 36(16), 4009-4022.

Slunjski M, Bourke M, O'Leary B (2000). MIEX® process for removal of humics in water treatment. International Humic Substances Society – Australian Branch Symposium. Monash University, Melbourne, Australia.

Slunjski M, Nguyen H, Ballard M, Eldridge R, Morran J, Drikas M, O'Leary B, Smith P (2002). MIEX® - Good research commercialized. *Water* 29(2), 42-47.

Snow J (1854). On the communication of cholera by impure Thames water. *Medical Times and Gazette* 9, 247-248.

Snow J. On the mode of communication of cholera. 2nd Ed., John Churchill, London, 1855.

Soldatov VS, Popova OP, Sunkevich AA (1994). The kinetics of exchanging chloride for organic anions on a FIBAN A-1 high-basicity fibrous ion exchanger. *Russian Journal of Physical Chemistry* 68(4), 686-688.

Soldatov VS, Shunkevich AA, Elinson IS, Johann J, Iraushek H (1999). Chemically active textile materials as efficient means for water purification. *Desalination* 124(1-3), 181-192.

Symons JM, Bradley LC, Cleveland TC (2000). The Drinking Water Dictionary (Editors). American Water Works Association. Denver, AWWA.

Symons JM, Worley KL (1995). An advanced oxidation process for DBP control. *Journal of the American Water Works Association* 87(11), 66-75.

Taylor JS, Thompson DM, Carswell JK (1987). Applying membrane processes to groundwater sources for trihalomethane precursor control. *Journal of the American Water Works Association* 79(8), 72-82.

Thompson JD, White MC, Harrington GW, Singer PC (1997). Enhanced Softening: Factors Influencing DBP Precursor Removal. *Journal of the American Water Works Association* 89(6), 94-105.

Tipping E (1990). Interactions of organic acids with inorganic and organic surfaces. In *Organic Acids in Aquatic Ecosystems* (Perdue EM, Gjessing ET, eds.). Life Sciences Research Reports, Wiley, Chichester, 209-221.

Tipping E (1981). The adsorption of aquatic humic substances by iron oxides. *Geochimica et Cosmochimica Acta* 45(2), 191-199.

Tipping E, Cooke D (1982). The effects of adsorbed humic substances on the surface charge of goethite (α -FeOOH) in freshwaters. *Geochimica et Cosmochimica Acta* 46(1), 75-80.

Tomaic J, Zutic V (1988). Humic material polydispersity in adsorption at hydrous alumina/seawater interface. *Journal of Colloid and Interface Science* 126(2), 482-492.

Tu S-C, Ravindran V, Den W, Pirbazari M (2001). Predictive membrane transport model for nanofiltration processes in water treatment. *American Institute of Chemical Engineering Journal* 47(6), 1346-1362.

Ueno H, Oishi K, Savato Y, Nakamuro K (2000). Oxidative Cell Damage in Kat-Sod Assay of Oxyhalides

as Inorganic Disinfection By-Products and Their Occurrence by Ozonation. *Archives of Environmental Contamination and Toxicology* **38**(1), 1-6.

USEPA (1975). Preliminary assessment of suspected carcinogens in drinking water — Interim report to congress. US EPA, Washington, DC

USEPA (1998a). Fact sheet: Stage 1 Disinfectants and Disinfection Byproducts Rule. EPA 815-F-98-010.

USEPA (1998b). Stage 1 Disinfectants and Disinfection Byproducts Rule. EPA 815-F-98-010. [Online.] <http://www.epa.gov/OGWDW/mdbp/dbp1.html>

USEPA (1999a). Alternative Disinfectants and Oxidants Guidance Manual, Chapter 3: Ozone. EPA 815-R-99-014.

USEPA (1999b). Alternative Disinfectants and Oxidants Guidance Manual, Chapter 8: Ultraviolet Radiation. EPA 815-R-99-014.

USEPA (2001). Controlling Disinfection Byproducts and Microbial Contaminants in Drinking Water. Chapter 6: Alternative Disinfectants. EPA 600-R-01-110.

Verschaeve L (2002). Genotoxicity Studies in Groundwater, Surface Waters, and Contaminated Soil. *The Scientific World Journal* **2**(1), 1247-1253.

Vilg -Ritter A, Maison A, Boulange T, Rybacki D, Bottero JY (1999). Removal of Natural Organic Matter by Coagulation-Flocculation: A Pyrolysis-GC-MS Study. *Environmental Science and Technology* **15**(4), 463-466.

von Gunten U (2003a). Ozonation of drinking water: Part I Oxidation kinetics and product formation. *Water Research* 37(7), 1443–1467.

von Gunten U (2003b). Ozonation of drinking water: Part II. Disinfection and by-product formation in presence of bromide, iodide or chlorine. *Water Research* 37(7), 1469-1487.

von Gunten U, Driedger A, Gallard H, Salhi E (2001). By-products formation during drinking water disinfection: a tool to assess disinfection efficiency? *Water Research* 35(8), 2095-2099.

von Gunten U, Hoign J (1994). Bromate Formation during Ozonation of Bromide-Containing Waters: Interaction of Ozone and Hydroxyl Radical Reactions. *Environmental Science and Technology* 28(7), 1234-1242.

Vrijenhoek EM, Childress AE, Elimelech M, Tanaka TS, Beuhler MD (1998). Removing Particles and THM Precursors by Enhanced Coagulation. *Journal of the American Water Works Association* 90(4), 139-150.

Watson JR, Posner AM, Quirk JP (1973). Adsorption of the herbicide 2,4-D on goethite. *European Journal of Soil Science* 24(4), 503–511.

White MC, Thompson JD, Harrington GW, Singer PC (1997). Evaluation criteria for enhanced coagulation compliance. *Journal of the American Water Works Association* 89(5), 64-77.

Wolfe RL (1990). Ultraviolet disinfection of potable water. *Environmental Science and Technology* 24(6), 768.

Woo YT, Lai D, McLain JL, Manibusan MK, Dellarco V (2002). Use of Mechanism-Based Structure-

Activity Relationships Analysis in Carcinogenic Potential Ranking for Drinking Water Disinfection By-Products. *Environmental Health Perspectives* 110(S1), 75-87.

Xie Y, Reckhow DA (1992). Formation of Ketoacids in Ozonated Drinking Water. *Ozone: Science and Engineering* 14(3), 269-275.

Zhao D, SenGupta AK (1998). Ultimate removal of phosphate using a new class of anion exchanger. *Water Research* 32(5), 1613-1625.

Halo-alkanes/alkenes

Bromochloromethane

Dibromomethane

Bromodichloromethane

Dibromochloromethane

Chloroform

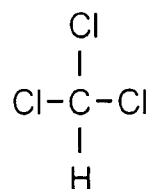
Bromoform

Bromochloroiodomethane

Tribromochloromethane

1,1-dibromopropane

2,4-dibromo-1-butene



Example: Chloroform

Halo-aldehydes

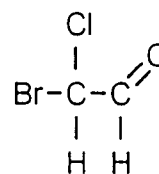
Bromochloroacetaldehyde

Tribromoacetaldehyde (bromal hydrate)

2-bromo-2-methylpropanal

3-bromo-4-hydroxy-5-methoxy

benzaldehyde

Example:
Bromochloroacetaldehyde**Halo-ketones**

1-bromopropanone

1,1-dibromopropanone

1,1,1-trichloropropanone

1,1-dibromo-3-chloropropanone

1,1,1-tribromopropanone

1,1,3-tribromopropanone

1,1,3,3-tetrachloropropanone

1,1-dibromo-3,3-dichloropropanone

1,3-dibromo-1,3-dichloropropanone

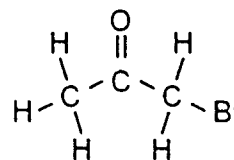
1,1,3-tribromo-3-chloropropanone

1,1,3,3-tetrabromopropanone

1,1,1,3,3-pentachloropropanone

1,1,1,3-tetrabromo-3-chloropropanone

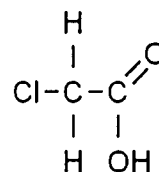
1,1,1,3,3-pentabromo-3-chloropropanone

Example
1-Bromopropanone

5-bromo-2-pentanone

Halo-acids

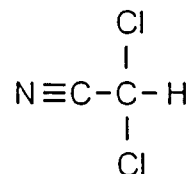
Chloroacetic acid
Bromoacetic acid
dichloroacetic acid
bromochloroacetic acid
dibromoacetic acid
trichloroacetic acid
dibromochloroacetic acid
tribromoacetic acid



Example Chloroacetic acid

Halo-acetonitriles

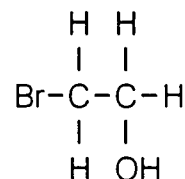
dichloroacetonitrile
bromochloroacetonitrile
dibromoacetonitrile
tribromoacetonitrile



Example: Dichloroacetonitrile

Halo-alcohols

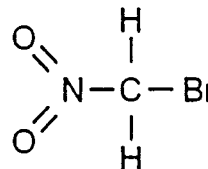
2-bromoethanol
3-chloro-2-butanol



Example: 2-Bromoethanol

Halo-nitromethanes

Bromonitromethane
Dibromonitromethane
Tribromonitromethane (bromopicrin)

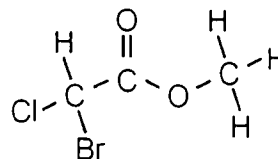


Example: Bromonitromethane

Halo-acetates

Methyl bromochloroacetate

Methyl dibromoacetate



Example:
Methyl bromochloroacetate

Halo-aromatics

Chloromethyl benzene

2,4-dibromophenol

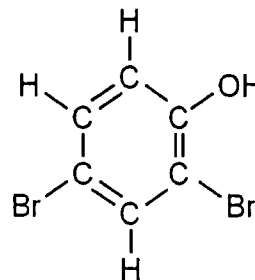
2,6-dibromophenol

2,6-dibromo-4-methyl phenol

2,4,6-tribromophenol

4-chloro-2,6-di-*tert*-butyl-phenol

4-bromo-2,6-di-*tert*-butyl-phenol

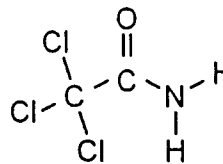


Example:
2,4-dibromophenol

Other Halogenated DBPs

2,2,2-trichloroacetamide

2,4,6-tribromobenzeneamine



Example:
2,2,2-trichloroacetamide

8.0 APPENDIX B: Determination of Effective Diffusivity

Directions for using the effective diffusivity curve-fitting program are provided below. Note that values utilized above may not appear in the provided screenshots.

Using Spreadsheet to Identify D_{eff}

1. Parameter Input:

- a) Time unit, row 3 in worksheet "Curve-X": If time unit is second, input 0; if time unit is minute, input 1; if time unit is hour, input 2.

The screenshot shows an Excel spreadsheet titled "Intraparticlemodel 2.xls". The spreadsheet is divided into two main sections: "1. DATA INPUT:" and "2. CALCULATION:".

1. DATA INPUT:

- Row 2: Time unit = second, input 0;
- Row 3: Time unit = minute, input 1; (The value '1' in cell F3 is circled in red with an arrow pointing to it from the left.)
- Row 4: Time unit = hour, input 2.
- Row 6: Input Radius of Beads → 0.005
- Row 8: Omega Value → 1.147
- Row 10: Beta Values → 3.68656 6.64762 9.68911 12.7715 15.8748 18.9899
- Row 12: Input Effective Diffusivity (cm²/sec) → 1.95E-09

2. CALCULATION:

TIME (Min)	F=1-SUM	SUM	TERM 1	TERM 2	TERM 3	TERM 4	TERM 5	TERM 6	TERM 7	TERM 8	TERM 9
0	5.68E-02	9.43E-01	3.97E-01	1.91E-01	1.03E-01	6.32E-02	4.21E-02	2.99E-02	2.23E-02	1.72E-02	1.37E-02
2.5	5.01E-01	4.99E-01	3.39E-01	1.14E-01	3.45E-02	9.37E-03	2.21E-03	4.40E-04	7.33E-05	1.00E-05	1.12E-06
5	6.30E-01	3.70E-01	2.89E-01	6.78E-02	1.15E-02	1.39E-03	1.16E-04	6.48E-06	2.41E-07	5.82E-09	9.12E-11
7.5	7.09E-01	2.91E-01	2.46E-01	4.04E-02	3.83E-03	2.06E-04	6.06E-06	9.53E-08	7.90E-10	3.38E-12	7.44E-14
10	7.64E-01	2.36E-01	2.10E-01	2.41E-02	1.28E-03	3.06E-05	3.18E-07	1.40E-09	2.59E-12	1.96E-15	6.07E-18
20	8.86E-01	1.14E-01	1.11E-01	3.05E-03	1.58E-05	1.48E-08	2.40E-12	6.56E-17	3.02E-22	2.23E-28	2.68E-34
30	9.41E-01	5.93E-02	5.89E-02	3.85E-04	1.95E-07	7.16E-12	1.81E-17	3.07E-24	3.51E-32	2.54E-41	1.19E-49
40	9.69E-01	3.12E-02	3.12E-02	4.87E-05	2.41E-09	3.46E-15	1.37E-22	1.44E-31	4.08E-42	2.90E-54	5.26E-66
50	9.83E-01	1.65E-02	1.65E-02	6.16E-06	2.98E-11	1.68E-18	1.03E-27	6.74E-39	4.74E-52	3.30E-67	2.33E-81
60	9.91E-01	8.74E-03	8.74E-03	7.79E-07	3.68E-13	8.11E-22	7.80E-33	3.15E-46	5.51E-62	3.75E-80	1.03E-100
70	9.95E-01	4.63E-03	4.63E-03	9.85E-08	4.55E-15	3.92E-25	5.88E-38	1.48E-53	6.41E-72	4.27E-93	4.55E-114
80	9.98E-01	2.45E-03	2.45E-03	1.24E-08	5.62E-17	1.90E-28	4.44E-43	6.92E-61			
90	9.99E-01	1.30E-03	1.30E-03	1.57E-09	6.95E-19	9.19E-32	3.35E-48	3.24E-68			
100	9.99E-01	6.87E-04	6.87E-04	1.99E-10	8.59E-21	4.45E-35	2.53E-53	1.52E-75			

b) Radius of fibers (unit = cm), row 6 in worksheet "Curve-X"

The screenshot shows a Microsoft Excel spreadsheet titled "Intraparticlemodel 2.xls". The spreadsheet is divided into two sections: "1. DATA INPUT:" and "2. CALCULATION:".

1. DATA INPUT:

- Row 2: Time unit = second, input 0;
- Row 3: Time unit = minute, input 1;
- Row 4: Time unit = hour, input 2.
- Row 6: Input Radius of Beads (0.005) - circled in black with an arrow pointing to it.
- Row 8: Omega Value (1.147) - circled in black with an arrow pointing to it.
- Row 10: Beta Values (3.68656, 6.64762, 9.68911, 12.7715, 15.8748, 18.9899, 22.1084, 25.2356, 28.366, 31.4985)
- Row 12: Input Effective Diffusivity (cm²/sec) (1.95E-09)

2. CALCULATION:

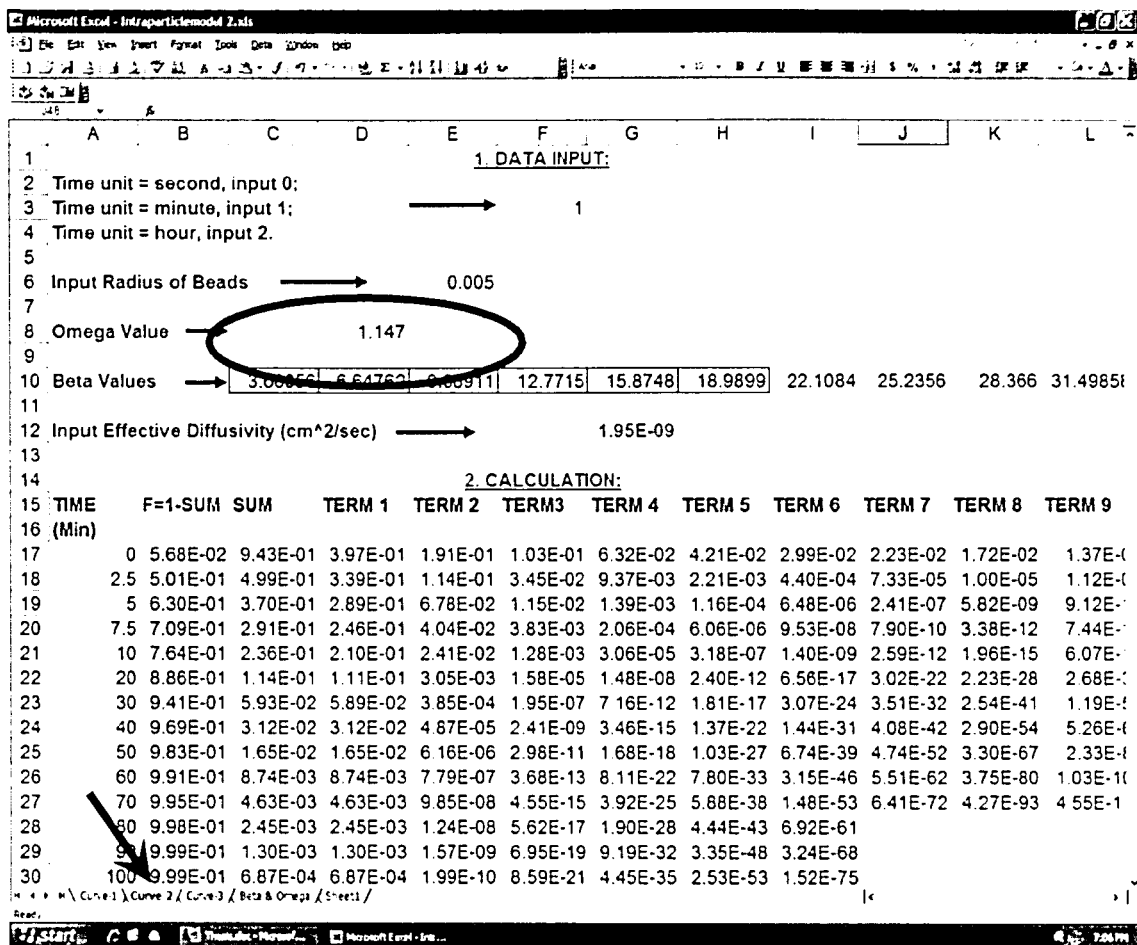
TIME (Min)	F=1-SUM	SUM	TERM 1	TERM 2	TERM 3	TERM 4	TERM 5	TERM 6	TERM 7	TERM 8	TERM 9
0	5.68E-02	9.43E-01	3.97E-01	1.91E-01	1.03E-01	6.32E-02	4.21E-02	2.99E-02	2.23E-02	1.72E-02	1.37E-02
2.5	5.01E-01	4.99E-01	3.39E-01	1.14E-01	3.45E-02	9.37E-03	2.21E-03	4.40E-04	7.33E-05	1.00E-05	1.12E-06
5	6.30E-01	3.70E-01	2.89E-01	6.78E-02	1.15E-02	1.39E-03	1.16E-04	6.48E-06	2.41E-07	5.82E-09	9.12E-11
7.5	7.09E-01	2.91E-01	2.46E-01	4.04E-02	3.83E-03	2.06E-04	6.06E-06	9.53E-08	7.90E-10	3.38E-12	7.44E-14
10	7.64E-01	2.36E-01	2.10E-01	2.41E-02	1.28E-03	3.06E-05	3.18E-07	1.40E-09	2.59E-12	1.96E-15	6.07E-17
20	8.86E-01	1.14E-01	1.11E-01	3.05E-03	1.58E-05	1.48E-08	2.40E-12	6.56E-17	3.02E-22	2.23E-28	2.68E-34
30	9.41E-01	5.93E-02	5.89E-02	3.85E-04	1.95E-07	7.16E-12	1.81E-17	3.07E-24	3.51E-32	2.54E-41	1.19E-50
40	9.69E-01	3.12E-02	3.12E-02	4.87E-05	2.41E-09	3.46E-15	1.37E-22	1.44E-31	4.08E-42	2.90E-54	5.26E-67
50	9.83E-01	1.65E-02	1.65E-02	6.16E-06	2.98E-11	1.68E-18	1.03E-27	6.74E-39	4.74E-52	3.30E-67	2.33E-84
60	9.91E-01	8.74E-03	8.74E-03	7.79E-07	3.68E-13	8.11E-22	7.80E-33	3.15E-46	5.51E-62	3.75E-80	1.03E-100
70	9.95E-01	4.63E-03	4.63E-03	9.85E-08	4.55E-15	3.92E-25	5.88E-38	1.48E-53	6.41E-72	4.27E-93	4.55E-117
80	9.98E-01	2.45E-03	2.45E-03	1.24E-08	5.62E-17	1.90E-28	4.44E-43	6.92E-61			
90	9.99E-01	1.30E-03	1.30E-03	1.57E-09	6.95E-19	9.19E-32	3.35E-48	3.24E-68			
100	9.99E-01	6.87E-04	6.87E-04	1.99E-10	8.59E-21	4.45E-35	2.53E-53	1.52E-75			

c) ω value, row 8 in worksheet "Curve-X":

It is calculated from

$$\omega = \frac{VC_0}{M_r} - 1$$

where V is the solution volume in the batch reactor, C_0 is initial concentration of the solution, M_r is the mass in the fiber phase at equilibrium.



d) β values, row 10 in worksheet "Curve-X"

i) Go to worksheet "Beta & Omega". The top of the worksheet is the table of listed β values corresponding to certain ω values. Below the table, it is the interpolation calculation. Copy two rows of listed values in the table to "upper beta values" (row 18) and "lower beta values" (row 20), then input ω value calculated from data of your kinetic test into the row "interpolation" (row 23, column D). Six β values are automatically obtained in the same row. Copy these six β values to the yellow area of row 10 in worksheet "Curve-X"

Microsoft Excel - Intraparticlemodel 2.xls

File Edit View Insert Format Tools Data Window Help

129

	A	B	C	E	F	G	H	I	J	K	L	M
			Omega		Beta 1	Beta 2	Beta 3	Beta 4	Beta 5	Beta 6		
1			Infinte		3 1416	6 2832	9 4248	12 5664	15 708	18 8496		
2					3 241	6 3353	9 4599	12 5928	15 7292	18 8671		
3			9		3 3485	6 3979	9 5029	12 6254	15 7554	18 8891		
4			4		3 465	6 4736	9 5567	12 6668	15 7888	18 9172		
5			2.3333		3 5909	6 5665	9 6255	12 7205	15 8326	18 9541		
6			1.5		3 7264	6 6814	9 7156	12 7928	15 8924	19 0048		
7			1		3 8711	6 8246	9 8369	12 894	15 9779	19 0784		
8			0.6667		3 2645	6 1407	9 1156	12 1529	15 2255	18 3188		
9			0.4286		3 4455	6 371	9 3397	12 3543	15 4031	18 4754		
10			0.25		4 3359	7 4645	10 5437	13 6133	16 6831	19 7564		
11			0.1111		4 4934	7 7253	10 9041	14 0662	17 2208	20 3713		
12			0									
13												
14												
15												
16			Omega		Beta 1	Beta 2	Beta 3	Beta 4	Beta 5	Beta 6		
17												
18	Upper Beta Values	→	1.5		3 5909	6 5665	9 6255	12 7205	15 8326	18 9541		
19	Lower Beta Values	→	1		3 7264	6 6814	9 7156	12 7928	15 8924	19 0048		
20												
21												
22												
23	Interpolation	→	1.147		3 68655	6 64762	9 68911	12 7715	15 8748	18 9899		
24												
25												
26												
27												
28												
29												
30												
31												
32												
33												

Ready

ii) More β values should be calculated, since six terms are not enough for some cases.

Calculate β values by using MathCAD to solve the following equation:

$$\omega \beta_n J_0(\beta_n) + 2 J_1(\beta_n) = 0$$

Then, input calculated β values into the blue area of row 10 in worksheet "Curve-X".

Microsoft Excel - Intraparticlemodel 2.xls

File Edit View Insert Format Tools Data Window Help

1 DATA INPUT

2 Time unit = second, input 0: → 1

3 Time unit = minute, input 1:

4 Time unit = hour, input 2:

5

6 Input Radius of Beads → 0.005

7

8 Omega Value → 1.147

9

10 Beta Values → 3.688563 6.647619 9.689111 12.77154 15.87421 18.98989 22.10843 25.23564 28.36599 31.496587 34.63254 37.76798 40.90447 44.04143

11 Input Effective Diffusivity (cm²/sec) → 1.95E-09

12

13

14 2 CALCULATION

15 TIME (Min)	F=1-SUM	SUM	TERM 1	TERM 2	TERM 3	TERM 4	TERM 5	TERM 6	TERM 7	TERM 8	TERM 9	TERM 10	TERM 11	TERM 12	TERM 13	TERM 14
17 0	5.68E-02	9.45E-01	3.97E-01	1.91E-01	1.03E-01	6.32E-02	4.21E-02	2.99E-02	2.22E-02	1.72E-02	1.37E-02	1.12E-02	9.25E-03	7.79E-03	6.65E-03	5.71E-03
18 2.5	5.01E-01	4.99E-01	3.39E-01	1.14E-01	3.45E-02	9.37E-03	2.21E-03	4.40E-04	7.33E-05	1.00E-05	1.12E-06	1.01E-07	7.44E-09	4.40E-10	2.10E-11	8.07E-13
19 5	6.33E-01	3.70E-01	2.89E-01	6.76E-02	1.15E-02	1.39E-03	1.15E-04	6.48E-06	2.41E-07	5.82E-09	9.12E-11	9.22E-13	5.99E-15	2.49E-17	6.60E-20	1.11E-22
20 7.5	7.05E-01	2.91E-01	2.46E-01	4.04E-02	3.63E-03	2.06E-04	6.06E-06	9.53E-08	7.92E-10	3.38E-12	7.44E-15	8.38E-18	4.61E-21	1.41E-24	2.06E-28	1.54E-31
21 10	7.64E-01	2.30E-01	2.10E-01	2.41E-02	1.26E-03	3.02E-05	3.16E-07	1.40E-09	2.55E-12	1.96E-15	6.07E-19	7.62E-23	3.67E-27	7.94E-32	6.54E-37	2.11E-41
22 20	8.85E-01	1.14E-01	1.11E-01	3.05E-03	1.58E-05	1.46E-08	2.40E-12	6.56E-17	3.02E-22	2.23E-28	2.68E-35	5.20E-43	1.62E-51	8.09E-61	6.44E-71	8.91E-81
23 30	9.41E-01	5.93E-02	5.89E-02	3.65E-04	1.65E-07	7.16E-12	1.81E-17	3.07E-24	3.51E-32	2.64E-41	1.19E-51	3.55E-63	6.79E-76	8.24E-90	6.33E-105	3.05E-121
24 40	9.69E-01	3.12E-02	3.12E-02	4.87E-05	2.41E-09	3.48E-15	1.37E-22	1.44E-31	4.05E-42	2.90E-54	5.26E-68	2.43E-83	2.84E-100	8.39E-119	6.22E-139	1.16E-161
25 50	9.83E-01	1.65E-02	1.65E-02	6.16E-06	2.98E-11	1.68E-18	1.03E-27	6.74E-39	4.74E-52	3.30E-67	2.33E-84	1.66E-103	1.19E-124	8.55E-148	6.12E-173	4.39E-201
26 60	9.91E-01	6.74E-03	6.74E-03	7.79E-07	3.68E-13	8.11E-22	7.80E-33	3.15E-45	5.51E-62	3.75E-80	1.03E-100	1.13E-123	4.96E-149	8.71E-177	6.02E-207	1.66E-241
27 70	9.95E-01	4.63E-03	4.63E-03	9.65E-08	4.55E-15	3.92E-25	5.86E-38	1.46E-53	6.41E-72	4.27E-93	4.65E-117	7.72E-144	2.06E-173	8.87E-206	5.92E-241	5.26E-281
28 80	9.98E-01	2.45E-03	2.45E-03	1.24E-08	5.62E-17	1.90E-28	4.44E-43	6.92E-61	3.55E-81	2.24E-103	1.19E-124	8.55E-148	6.12E-173	4.39E-201	3.05E-231	2.11E-261
29 90	9.99E-01	1.30E-03	1.30E-03	1.57E-09	6.95E-19	9.19E-32	3.35E-49	3.24E-68	1.66E-89	8.09E-111	4.05E-134	2.06E-158	1.03E-182	5.26E-206	2.84E-231	1.66E-256
30 100	9.99E-01	6.87E-04	6.87E-04	1.99E-10	8.59E-21	4.45E-35	2.63E-53	1.52E-75	7.94E-97	4.27E-121	2.23E-148	1.19E-173	6.12E-197	3.05E-221	1.66E-241	9.41E-261
31 110	1.00E+00	3.63E-04	3.63E-04	2.51E-11	1.06E-22	2.15E-38	1.91E-58	7.10E-83	3.55E-107	1.66E-134	8.09E-161	4.05E-184	2.06E-206	1.03E-226	5.26E-241	2.84E-256
32 120	1.00E+00	1.92E-04	1.92E-04	3.18E-12	1.31E-24	1.04E-41	1.44E-63	3.33E-90	1.66E-111	8.09E-134	4.05E-158	2.06E-182	1.03E-206	5.26E-226	2.84E-241	1.66E-256
33 130	1.00E+00	1.02E-04	1.02E-04	4.02E-13	1.62E-26	5.04E-45	1.09E-68	1.56E-97	7.94E-121	4.27E-148	2.23E-173	1.19E-197	6.12E-221	3.05E-241	1.66E-256	9.41E-261
34 140	1.00E+00	5.39E-05	5.39E-05	5.08E-14	2.00E-28	2.44E-48	8.72E-74	7.29E-105	4.27E-121	2.23E-148	1.19E-173	6.12E-197	3.05E-221	1.66E-241	9.41E-261	5.26E-281
35 150	1.00E+00	2.85E-05	2.85E-05	6.42E-15	2.47E-30	1.18E-51	6.21E-79	3.41E-112	1.66E-134	8.09E-161	4.05E-184	2.06E-206	1.03E-226	5.26E-241	2.84E-256	1.66E-261
36 160	1.00E+00	1.51E-05	1.51E-05	8.12E-16	3.06E-32	5.71E-55	4.65E-84	1.60E-119	7.94E-141	4.27E-161	2.23E-184	1.19E-206	6.12E-221	3.05E-241	1.66E-256	9.41E-261
37 170	1.00E+00	8.00E-06	8.00E-06	1.03E-16	3.76E-34	2.70E-58	3.54E-89	7.49E-127	3.55E-151	1.66E-173	8.09E-197	4.05E-221	2.06E-241	1.03E-256	5.26E-261	2.84E-271
38 180	1.00E+00	4.23E-06	4.23E-06	1.30E-17	4.87E-36	1.34E-61	2.67E-94	3.61E-134	1.66E-151	8.09E-173	4.05E-197	2.06E-221	1.03E-241	5.26E-256	2.84E-261	1.66E-271
39 190	1.00E+00	2.24E-06	2.24E-06	1.64E-18	5.77E-38	6.47E-65	2.02E-99	1.64E-141	7.94E-161	4.27E-184	2.23E-206	1.19E-221	6.12E-241	3.05E-256	1.66E-261	9.41E-271
40 200	1.00E+00	1.19E-06	1.19E-06	2.07E-19	7.13E-40	3.13E-68	1.52E-104	7.69E-149	3.55E-173	1.66E-197	8.09E-221	4.05E-241	2.06E-256	1.03E-261	5.26E-271	2.84E-281
41 210	1.00E+00	6.28E-07	6.28E-07	2.62E-20	8.61E-42	1.51E-71	1.15E-109	3.60E-155	1.66E-173	8.09E-197	4.05E-221	2.06E-241	1.03E-256	5.26E-261	2.84E-271	1.66E-281

16

17

18

19

20

21

22

23

24

25

26

27

28

29

30

31

32

33

34

35

36

37

38

39

40

41

210

Curve 1 \ Curve 2 \ Curve 3 \ Beta & Omega \ Sheet1 /

c) Effective diffusivity, \bar{D}_{eff} :

Input an estimated \bar{D}_{eff} value into row 11. The \bar{D}_{eff} value is in the format of "x.xxEx".

Several \bar{D}_{eff} values may need to be tried until the best-fit curve is found.

Microsoft Excel - Intraparticlemodel.xls

File Edit View Insert Format Tools Data Window Help

1. DATA INPUT:

2 Time unit = second, input 0;

3 Time unit = minute, input 1; → 1

4 Time unit = hour, input 2.

5

6 Input Radius of Beads → 0.005

7

8 Omega Value → 1.147

9

10 Beta Values → 3.68656 6.64762 9.68911 12.7715 16.8748 18.9899 22.1084 25.2356 28.366 31.49851

11

12 Input Effective Diffusivity (cm²/sec) → 1.95E-09

13

14 2. CALCULATION:

15 TIME (Min)	F=1-SUM	SUM	TERM 1	TERM 2	TERM 3	TERM 4	TERM 5	TERM 6	TERM 7	TERM 8	TERM 9
17 0	5.68E-02	9.43E-01	3.97E-01	1.91E-01	1.03E-01	6.32E-02	4.21E-02	2.99E-02	2.23E-02	1.72E-02	1.37E-02
18 2.5	5.01E-01	4.99E-01	3.39E-01	1.14E-01	3.45E-02	9.37E-03	2.21E-03	4.40E-04	7.33E-05	1.00E-05	1.12E-06
19 5	6.30E-01	3.70E-01	2.89E-01	6.78E-02	1.15E-02	1.39E-03	1.16E-04	6.48E-06	2.41E-07	5.82E-09	9.12E-11
20 7.5	7.09E-01	2.91E-01	2.46E-01	4.04E-02	3.83E-03	2.06E-04	6.06E-06	9.53E-08	7.90E-10	3.38E-12	7.44E-14
21 10	7.64E-01	2.36E-01	2.10E-01	2.41E-02	1.28E-03	3.06E-05	3.18E-07	1.40E-09	2.59E-12	1.96E-15	6.07E-18
22 20	8.86E-01	1.14E-01	1.11E-01	3.05E-03	1.58E-05	1.48E-08	2.40E-12	6.56E-17	3.02E-22	2.23E-28	2.68E-34
23 30	9.41E-01	5.93E-02	5.89E-02	3.85E-04	1.95E-07	7.16E-12	1.81E-17	3.07E-24	3.51E-32	2.54E-41	1.19E-50
24 40	9.69E-01	3.12E-02	3.12E-02	4.87E-05	2.41E-09	3.46E-15	1.37E-22	1.44E-31	4.08E-42	2.90E-54	5.26E-67
25 50	9.83E-01	1.65E-02	1.65E-02	6.16E-06	2.98E-11	1.68E-18	1.03E-27	6.74E-39	4.74E-52	3.30E-67	2.33E-83
26 60	9.91E-01	8.74E-03	8.74E-03	7.79E-07	3.68E-13	8.11E-22	7.80E-33	3.15E-46	5.51E-62	3.75E-80	1.03E-100
27 70	9.95E-01	4.63E-03	4.63E-03	9.85E-08	4.55E-15	3.92E-25	5.88E-38	1.48E-53	6.41E-72	4.27E-93	4.55E-117
28 80	9.98E-01	2.45E-03	2.45E-03	1.24E-08	5.62E-17	1.90E-28	4.44E-43	6.92E-61			
29 90	9.99E-01	1.30E-03	1.30E-03	1.57E-09	6.95E-19	9.19E-32	3.35E-48	3.24E-68			
30 100	9.99E-01	6.87E-04	6.87E-04	1.99E-10	8.59E-21	4.45E-35	2.53E-53	1.52E-75			

React

2. Calculation

When parameter input is finished, the calculation will automatically be completed. Now, two columns of data (Columns A and B) will give an estimated kinetic profile (F versus t).

Plot the theoretical kinetic curves by extracting data in Columns A and B.

Lee Michael Blaney was born in Frankford Hospital (Philadelphia, PA) on May 11, 1983 to James Edward Blaney and Joann Catherine Blaney (maiden: Kosmalski). He attended high school at Father Judge High School (Philadelphia, PA) where he graduated in June 2001. After that milestone, Lee decided to attend Lehigh University as an incoming freshman enrolled in Civil Engineering. During his sophomore year, Lee met Dr. Arup K. SenGupta and changed his major to Environmental Engineering. Two years later in May 2005, Lee graduated from Lehigh University with a Bachelor of Science degree in Environmental Engineering. After receiving his Master of Science degree from Lehigh University in May 2007, Lee will spend the summer in Beijing, China as an NSF EAPSI fellow. Then in August 2007, he will commence studies at the University of Texas at Austin towards attainment of a Doctor of Philosophy degree in Environmental Engineering under the financial assistance of an NSF graduate research fellowship awarded to him in March 2006. Ultimately, Lee plans to pursue a career in academia.

END OF TITLE